"Analysis of Antioxidant Behaviour in Lubricating Oils"

by

David Jonathan Rose

Submitted in accordance with the requirements for the degree of Doctor of Philosophy.

THE UNIVERSITY OF LEEDS

School of Chemistry

March 1991

ABSTRACT

Lubricating oils subjected to the operating conditions in an automobile engine degrade by many routes. The most important of these routes is oxidation, which at room temperature and atmospheric pressure is almost immeasurably slow. The performance of a new oil formulation is ultimately assessed by the use of a standard engine test. Such engine tests are very expensive and time consuming, which makes the use of an initial screening test a necessity. Screening tests are used to eliminate any oils that would fail the full engine test, thereby saving considerable amounts of time and money. In the present research the concern has been to compare two screening tests for the analysis of antioxidants based on differential scanning calorimetry (DSC) and cyclic voltammetry (CV). The two techniques have been applied to the analysis the of the antioxidants, dioctyldiphenyl amine (DODPA) and Topanol 'O' in three base oils.

DSC is a commonly used technique in which the time to oxidation is measured when the sample is maintained at a constant temperature in a high pressure atmosphere of oxygen. CV has not been used widely to examine lubricating oils and the present work has included the development of reliable experimental techniques for the two types of antioxidants. The results obtained for both freshly prepared oil formulations and those partially oxidised clearly reveal the different nature of the tests. DSC is a non specific technique with respect to the antioxidant and leads to an indication of the overall oxidative stability of the oil blend, whereas the voltammogram obtained in CV is specific to certain groups of antioxidant. The value of the current flowing through the circuit reaches a maximum value at a potential specific to and dependant on the concentration of the additive being analysed.

A kinetic analysis of an antioxidant by CV leads to information about the diffusion coefficient of the molecule and the rate of electron transfer at the electrode surface. It was found that the electrochemically oxidised species of the amine antioxidant underwent a chemical reaction to produce an electro-inactive species over the potential range studied. The kinetic data for this reaction was obtained but their relevance to the oxidation of an oil in an engine environment is doubtful, whereas the results obtained by DSC are probably more applicable. The kinetic data obtained from isothermal DSC curves were employed in a combined kinetic scheme to model the shapes of DSC curves.

CONTENTS

List of Headings		Page
CHAPTER 1	Introduction	1
1.1	The Aim of This Work	2
1.2	The Degradation of Lubricating Oils	2
1.3	The Composition of the Basestock	5
1.4	The Mechanisms of Hydrocarbon Oxidation	8
1.4.1	Initiation	9
1.4.2	Propagation and Degenerate Branching	9
1.4.3	Termination	12
1.4.4	Inhibition	12
1.4.5	Catalysis	13
1.5	Additives: Their Mode Of Action And Effect	13
1.6	The Need for Standard Tests	21
1.7	The Measurement of Oil Quality	21
1.8	Materials	24
	References	27
CHAPTER 2	Thermal Analysis	30
2.1	Introduction	31
2.2	Description of the Du-Pont Apparatus	35
2.2.1	The DSC Cell	35
2.2.2	The 990 Programmer-Controller	37
2.2.3	The 910 Cell Base	38
2.3	An Investigation of a Disk Type DSC Cell	38
2.4	The Need for High Pressures	43
2.5	The High Pressure Apparatus	44
2.6	Chemical Calibration	45
2.7	Experimental Variables	48
2.7.1	Introduction	48
2.7.2	Instrumental Variables	48
2.7.3	Sample Variables	53
	References	57

CHAPTER 3 Cyclic Voltammetry 59
3.1 The Basic Principles 60
3.1.1 The Electrochemical Cell 60
3.1.2 Energy Levels at the Electrode Electrolyte Interface 61
3.1.3 A Kinetic Model Based on Electrochemical Potentials 67
3.1.4 The Current Potential Relationship 68
3.1.5 Mass transfer by Diffusional Effects 71
3.2 An Expansion on the Basic Principles 72
3.2.1 A Solution of Fick's Second Law 72
3.2.2 The Derivation of the Cottrell Equation:
A Functional Form of the Current-Time Response 73
3.2.3 An Alternative Method to the Direct Analysis of the Current Function:
The Convolution Transform With the Function $(\pi t)^{-1/2}$ 77
3.2.4 The Use of the Convolution Integral in Cyclic Voltammetry 79
3.2.5 The Deconvolution of the Current Function $(\pi t)^{-1/2}$ 84
3.2.6 The Analysis of Coupled Electrochemical Reactions 85
3.3 Description of the Apparatus 87
3.4 The Reagents and Preparation of the Electrodes 89
3.5 Experimental Variables 91
3.5.1 Sample Concentration 91
3.5.2 Scan Speed 91
3.5.3 Temperature 91
3.5.4 Oxygen 92
3.5.5 Electrodes and Solvent System 92
References 93

CHAPTER 4 An Investigation of Dioctyldiphenyl Amine 94
4.1 The Measurement of Amine Antioxidants 95
4.2 Analysis by Differential Scanning Calorimetry (DSC) 98
4.2.1 Preliminary Experiments 98
4.2.2 Experimental 101
4.2.3 Kinetic Analysis 105
4.3 Analysis by Cyclic Voltammetry (CV) 113
4.3.1 The Development of the Final Experimental Method 113
4.3.2 Calibration 119
4.3.3 Kinetic Analysis 123

4.4	Analysis of Oxidised Oil Samples	128
	References	133
CHAPTER 5	The Analysis of Topanol 'O'	135
5.1	An Investigation of Phenolic Antioxidants	136
5.2	Analysis by DSC	142
5.2.1	Experimental	142
5.2.2	Kinetic Analysis	145
5.3	The Analysis by CV	147
5.3.1	Preliminary Experiments	147
5.3.2	Calibration	154
5.3.3	Kinetic Analysis	156
5.4	The Analysis of Oxidised Oil Samples	156
5.5	The Analysis of Oil Samples Containing an Antioxidant Blend	158
	References	163
CHAPTER 6	An Overall Assessment	165
6.1	A Comparison Between DSC and CV	166
6.2	A Comparison Between the Base Oils	168
6.3	A Comparison of the Antioxidants	171
6.4	The Modelling of the Analytical Curves	174
6.4.1	Cyclic voltammetry	174
6.4.2	Differential Scanning Calorimetry	175
6.5	Future Work	185
	References	188
APPENDIX 1	An Expansion on the Basic Principles of Electrochemistry	189
A 1.1	Introduction	190
A 1.2	The Solution of Fick's Second Law	190
A 1.3	The Convolution with the Function $(\pi t)^{-\frac{1}{2}}$	192
A 1.4	The Analysis of the CEC System	195
	References	199
APPENDIX 2	The Stanton Redcroft DSC-700	200
A 2.1	Introduction	201
A 2.2	Apparatus: Description and Development	201

A 2.3	Electrical Calibration	203
A 2.4	Chemical Calibration	207
A 2.5	The Thermal Analysis of Lubricating Oils	209
	Reference	211
APPENDIX 3	The Development of Standard Test Methods	212
A 3.1	Introduction	213
A 3.2	The Stanton Redcroft STA-781	213
A 3.3	Analysis for the Institute of Petroleum	216
A 3.3.1	The Oxidative Stability of Oils	216
A 3.3.2	Volatility Measurements	217
A 3.3.3	Temperature Calibration of the STA-781	218
A 3.4	Analysis for Other Laboratories	219
	References	221

LIST OF SYMBOLS

This list represents a summary of the symbols commonly used in this thesis.

Symbol	S.I. Units	Meaning
A	s^{-1}	Pre-exponential factor
A	m^2	Electrode area
A	m^2	Peak area
A•	-	Antioxidant radical
AH	-	Antioxidant
AOOR	-	Stable antioxidant-peroxy complex
A/D	-	Analogue to digital
A/H	-	Aromatic/Heterocyclic fraction
ASTM	-	American Society for Testing and Materials
B.Pt	K	Boiling point
ºC	K	Degrees Centigrade
CE	-	Counter electrode
$Cj_{(x,t)}$	mol m^{-3}	Concentration of species j, at a distance x from the electrode surface at a time t
$Cj_{(0,t)}$	mol m^{-3}	Concentration of species j at the electrode
Cj^*	mol m^{-3}	Concentration of species j in the bulk solution
cm	m	Centimetre ($1x10^{-2}$ m)
COC	-	Cleveland Open Cup flash point apparatus
CV	-	Cyclic voltammetry
Dj	m^2s^{-1}	Diffusion coefficient of species j
DMF	-	Dimethyl formamide
DODPA	-	Dioctyldiphenyl amine
DQA-TS	-	Directorate of Quality Assurance
DSC	-	Differential Scanning Calorimetry/Calorimeter
DTA	-	Differential Thermal Analysis/Analyser
DTG	-	Differential Thermal Gravimetry
E	V	Potential of the electrochemical cell
E^θ	V	Standard electrode potential
$E_{1/2}$	V	Polarographic half-wave potential
Ea	J mol^{-1}	Activation energy

E_{app}	V	Potential applied to the electrochemical cell
E_{eq}	V	Equilibrium potential of the electrode
E_{ext}	V	Externally applied potential
$E_{i=0}$	V	Potential at which the cell current is zero
E_i	V	Potential at time t = 0
EDL	-	Electrical double layer
erfc	-	Compliment of the normal error function
ESR	-	Electron Spin Resonance
ET	-	Electron transfer
F	C	The faraday; charge of one mole of electrons
F	C	Faraday's constant
GPR	-	General purpose reagent
h	J s	Planck's constant
H	-	Known convolution transform
$h\nu$	-	Light/photoelectric energy
HOMO	-	Highest occupied molecular orbital
HOO· or HO_2·		Hydro-peroxide radical
HOOH	-	Hydrogen peroxide
HPDSC	-	High pressure differential scanning calorimetry
HPLC	-	High pressure liquid chromatography
i	A	Current flowing through the electrochemical cell
iR_s	V	Ohmic potential drop of the solution
i_a	A	Anodic component of the current passing through the cell
i_c	A	Cathodic component of the current
i_L	A	Limiting value of the current
i_o	A	Exchange current
I_1	A $s^{½}$	Convolution of the current function
I_2 or I_3	A $s^{½}$	Convolution integral for a chemical reaction associated to the electrode process
I_L	A $s^{½}$	Maximum convoluted current
$I_{i=0}$	A $s^{½}$	Convoluted current at potential $E_{i=0}$
IHP	-	Inner Helmholtz plane
IP	-	Institute of Petroleum
J	J	Joule (unit of energy)
$Jj_{(x,t)}$	mol m^{-2} s^{-1}	Flux of species j at location x and at time t
k	variable	Rate constant (forward or reverse)

k'	-	Transmission coefficient
k	J K^{-1}	Boltzmann's constant
k_o	m s^{-1}	Rate of electrode reaction
K	-	Constant
K_E	m s^{-1}	Forward potential dependant rate constant
K^{θ}	m s^{-1}	Standard rate constant for heterogeneous electron transfer process
kPa	Pa	Pressure of a gas ($1x10^3$ Pa)
lbf in^{-2}	Pa	Pounds force per square inch pressure (6490 Pa)
LUMO	-	Lowest unoccupied molecular orbital
m	m	Metre
$MeCl_2$	-	Methylene chloride (Dichloromethane)
mg	kg	Milligram ($1x10^{-6}$ kg)
min	s	Minute (60 s)
MOD	-	Ministry of Defence
M.Pt	K	Melting point
Mw	kg	Molecular weight
n	-	Number of electrons involved in a chemical reaction
N/P	-	Naphthenic/paraffinic fraction
O	-	Oxidised species of the standard system O + ne ⇌ R
o/d	-	Outside diameter
OHP	-	Outer Helmholtz plane
p_j	kg m s^{-1}	Momentum of object j
p(x)	Pa	Partial pressure of a gas x
PAN	-	Phenyl α(1) naphthylamine
pm	m	Picometre ($1x10^{-12}$ m)
PCB	-	Poly-chlorinated biphenol compound
PNA	-	Poly-nuclear aromatic compound
Q.F.	-	Quick fit
R	J K^{-1} mol^{-1}	Gas Constant
R	-	Reduced species of the standard system O + ne ⇌ R
R·	-	Hydrocarbon radical
RE	-	Reference electrode
RH	-	Alkane
RO·	-	Alkoxy radical
ROO·	or (RO_2·)	Peroxy radical

ROOH	-	Hydoperoxide
ROOR	-	Peroxide
R_s	Ω	Resistance of the solution
s	s	Second
SCE	-	Standard calomel electrode
t	s	Time
T	K	Temperature
TA	-	Thermal Analysis/Analyser
TAN	-	Total acid number (mg KOH/ g oil)
TBAP	-	Tetrabutylammonium perchlorate
THF	-	Tetrahydro furan
TG	-	Thermo Gravimetry
TLC	-	Thin Layer Chromatography
Tm	K	Temperature of the peak maximum
TMA	-	Thermal Mechanical Analysis/Analyser
Tr	K	Temperature of the reference material
Ts	K	Temperature of the sample material
v	$V\ s^{-1}$	Sweep rate dE/dt
V	V	Volt
W	W	Watt
WE	-	Working electrode
z	-	Charge of a species in signed units of electronic charge
ZDDP	-	Zinc dialkyl(aryl) dithiophosphate

Greek and Mathematical Symbols

Symbol	S.I. Units	Meaning
α	-	Symmetry factor
β	$K\ s^{-1}$	Heating rate
β	$mol\ m\ C^{-1}\ s^{-½}$	$D^{½}$ /nFA
Γf	-	Gamma function of f
$\delta y/\delta x$	-	Partial differential equation
ΔE	V	Change in electrical potential
ΔG	$J\ mol^{-1}$	Change in Gibb's free energy
$\Delta G^{o}_{1}{}^{\ddagger}$	$J\ mol^{-1}$	Standard electrochemical free energy of state 1 (O^{z+} + n electrons on the metal)

$\Delta G_b^{\ddagger}$	J mol^{-1}	Electrochemical free energy of activation
ΔH_{fus}	J	Enthalpy of fusion
ΔH_m	J mol^{-1}	Molar enthalpy of fusion
ΔT	K	Ts - Tr
$d(\Delta Q/dt)$	-	Heat flux/rate of heat flow
ΔT	-	Differential temperature signal
ΔV_m	m^3 mol^{-1}	Molar volume change on melting
ϵ	W V^{-1}	Calibration constant of a DSC cell
η	V	Overpotential
λ	m	Wavelength
$\mu_j^{\ddagger}$	J mol^{-1}	Electrochemical potential of species j
$\mu_j^{o\alpha}$	J mol^{-1}	Standard electrochemical potential, species j in phase α
ν	varies	Rate of reaction (forward or reverse)
ν_{net}	varies	Overall rate of reaction
ϕ^k	V	Absolute electrostatic potential of phase k
Ψ	-	Laplace transform of the deconvolution of H
ε	V	Reduced potential
$\varkappa$	-	Dimensionless current function
∞	-	Infinity
*	-	Convolution transform operation

Figure Legend

Figure	Page	Description
2.1	34	The Different Thermocouple and Furnace Geometries Employed in DSC and DTA
2.2	36	The Du-Pont DSC Cell
2.3	36	The Electric Circuit Employed by Claudy et al
2.4	46	The High Pressure Apparatus
2.5	49	The Calibration of the Du-Pont DSC
3.1	62	The Electrode-Electrolyte Interface
3.2	65	Morse Function Potential Energy Curves for Reactants and Products of an Electron Transfer Process
3.3	65	Separation of Electrochemical Free Energy into Chemical and Electrical Components
3.4	70	The Current/Potential Characteristic for a System Containing Equal Bulk Concentrations of a Reduced and Oxidised Species
3.5	74	The Concentration Profile of a Reactant Species as a Function of Time and the Associated Current Function in Response to a Potential Step
3.6	76	Current-Time-Potential Relationship
3.7	78	The Representation of Cyclic Voltammetric Data
3.8	78	The Construction Proposed by Nicholson for the Measurement of Peak Current Values
3.9	81	Subdivision of Experimental I(t) Data for the Evaluation of the Convolution Integral I_1
3.10	81	A Representation of Raw and Convoluted Data for a Nernstian System
3.11	83	The Extraction of $E_{1/2}$ from Non-Nernstian Data
3.12	86	The Determination of the First Order Rate Constant for the Decay of the Oxidised Species
3.13	88	Schematic Representation of the Metrohm Vessel
3.14	90	Schematic Representation of the Electrodes
4.1	102	The Determination of the Onset of Oil Oxidation Using Isothermal and Dynamic Experiments
4.2	103	Calibration Curves for DODPA in Base Oils by High Pressure DSC
4.3	110	The Determination of the Peak Maximum and Onset Temperatures for an Investigation Into the Kinetics of Oil Oxidation
4.4	112	Variation of the Induction Time With Temperature for the Base Oils and Blends Containing 1.5% w/w DODPA

4.5	116	The Conductivity of THF/DMF Blends Containing 0.1% w/w TBAP at 296.6 (± 1) K
4.6	120	Calibration Curve for DODPA in Mineral and Oligomer Base Oils Using Deconvoluted Data
4.7	122	The Shapes of the Analytical Curves for a Solution Containing 1.9% w/w DODPA in the Oligomer Oil
4.8	124	The Calibration Curve for DODPA in Mineral Oil by CV
4.9	127	The Variation of the Rate Constant for the Decomposition of Electrochemically Oxidised DODPA With Temperature
4.10	131	Variation of Measured DODPA Concentration With Oxidation Time
5.1	144	Calibration Curves for Topanol 'O' in the Base Oils by High Pressure DSC
5.2	146	Variation of the Induction Time With Temperature for the Base Oils and Blends Containing 1.5% w/w Topanol 'O'
5.3	150	The shapes of the Analytical Curves for a Solution Containing 1.9% w/w Topanol 'O' in the Oligomer Oil
5.4	153	Calibration Curves for Topanol 'O' in the Base Oils by CV
5.5	157	Variation of the Measured Topanol 'O' Concentration With Oxidation Time
5.6	159	The Variation of the Measured Antioxidant Concentration for Oxidised and Re-inhibited Mineral Blends
5.7	161	The Study of the Efficiency of Mixed Inhibitor Blends by DSC. A Comparison of Oxidative Stability of Mineral Oil Blends Containing Topanol 'O' and DODPA to one Containing Exclusively DODPA
6.1	172	A Comparison between the Calibration Curves of DODPA and Topanol 'O' in the Mineral oil
6.2	172	A Comparison of the Response of the Ester Oil to DODPA and Topanol 'O'
6.3	176	A Comparison Between an Experimental and Simulated Cyclic Voltammogram
6.4	181	Variation of the Induction Time with Temperature
6.5	183	Variation of the Induction Time with Inhibitor Concentration
6.6	184	An Illustration of the Concentration-Time Data (with the Simulated DSC Curve Superimposed)
A 2.1	202	Illustration of the DSC-700 Thermocouple/Furnace Assembly in the Water-cooled Pressure Jacket

A 2.2	205	Schematic Representation of the Electrical Heaters
A 2.3	205	The Electrical Circuit Employed for Electrical Calibration of a DSC
A 2.4	208	Dynamic Range of the Stanton Redcroft DSC-700 at Atmospheric Pressure and 380°C
A 2.5	208	The Calibration Curves of the DSC-700
A 2.6	210	An Illustration of the Temperature Control of the DSC-700
A 3.1	215	The Stanton Redcroft STA-781 DTA-TG
A 3.2	220	A Comparison of the Results Obtained Using the Du-Pont DSC-990 and Stanton redcroft DSC-700
A 3.3	220	The Ignition Peak of a Lubricating Oil

Table Legend

Table	Page	Description
1.1	25	Typical Properties of the Basestocks
1.2	25	Typical Properties of the Antioxidants
2.1	47	The Enthalpy and Temperature of Fusion of the Metal Calibrants
4.1	111	The Kinetic Data Obtained From DSC Analysis
4.2	117	Voltage Windows of Commonly Used Solvent Systems
4.3	123	The Equations of the Calibration Curves for DODPA using CV
4.4	126	The Activation Energy for the Decomposition of Oxidised DODPA
4.5	129	The Estimation of DODPA in Oxidised samples by DSC and CV
5.1	145	The Kinetic Data Obtained from DSC Analysis
5.2	155	The Equations of the Calibration Curves for Topanol 'O' Using CV. I_1 Response at 1.75 V vs Ag/AgCl
5.3	155	The Oxidation Potentials and Electrochemical Response at 1.75 V vs Ag/AgCl For the Three Basestocks
6.1	168	The Volatility of the Base Oils by the Dynamic DTA-TG Method
6.2	169	The Volatility of the Base Oils by the Isothermal TG Method
6.3	170	The Oxidative Stability of the Base Oils Using the STA-781
6.4	171	A Comparison of the Base Oils
6.5	173	A Comparison of the Antioxidants
6.6	180	The Kinetic Inserted into the Simulation Program
6.7	180	The Effect of the Reaction Rates on the Simulated DSC Curves

Publications

The following publications are associated with this work

Conference Proceedings

1. Feng Hongtu, P. G. Laye and D. J. Rose, 'Ignition Temperatures by Thermal Analysis', Accepted for presentation at 17th International Pyrotechnics Seminar, 1991, Beijing, China.

Journal Papers

1. P. G. Laye, D. J. Rose and N. Taylor, 'Cyclic Voltammetry and Differential Scanning Calorimetry of Lubricating Oils: Amine Antioxidants', Submitted to Anal. Chem., 1991.
2. P. G. Laye, J. F. Griffiths, D. J. Rose and N. Taylor, 'Cyclic Voltammetry and Differential Scanning Calorimetry of Lubricating Oils: Phenolic Antioxidants', Submitted to Anal. Chem., 1991.

Acknowledgements

The work performed for this thesis was conducted in the Department of Physical Chemistry, now the School of Chemistry between January 1988 and December 1990. It has been supervised by Dr. P. G. Laye and Dr. N. Taylor, supported by a grant from MOD/DQA-TS.

I must thank Professor P. Gray for inviting me to study in the Department of Physical Chemistry; Professor M. Pilling and Professor D. Baulch for allowing me to continue to study in the School of Chemistry. I am indebted to DQA-TS for their interest in this project.

I would like to express my gratitude to Dr. Laye and Dr. Taylor for their continual support and guidance. I would like to thank the other members of my research groups for their invaluable help, especially Hock-Ann, Rong and Derek. A mention must be given to Peter Halford-Maw, Dave Foggarty, Gerry Monaghan and the departmental workshops for their excellent technical support. On a lighter note thanks are due to Peter Chambers, Joe Aspinal, Francis Billinghurst, Dorothy Nelson and Hong-tu Feng for some very enjoyable conversations, especially Hong-tu's English lessons!

A special thank you is due to Dr. T. Boddington for his patience, with regards to my writing and understanding the mathematics associated with this thesis. Cheers Terry.

Finally in this long list of thank you's, I must thank Suzanne, Jean, Dorothy, Vicki, Dave and Dr. J. F. Griffiths for proof reading this thesis.

DJR. Mar 1991

Dedications

This work is dedicated to my family and my fiancée Suzanne, but most of all to my Grandfather George who I still miss terribly.

Chapter 1

Introduction

The purpose of this chapter is to introduce general features of the degradation of lubricating oils, the composition of the basestocks and the relationships to oxidative stability, and how the oil 'quality' may be measured. These topics are supported by an overview of hydrocarbon oxidation mechanisms and how these may be modified by catalysts or inhibitors. The specific materials employed in the present work and the preparation of standard solutions are also included in this chapter.

1.1 The Aim of This Work

Engine oils are required to perform numerous tasks, including limiting metal to metal contact (thus reducing friction and wear), and cooling the moving parts. The engine can be regarded as a hostile environment. Lubricating oils are subject to deterioration due to their exposure to oxygen in the atmosphere. Although this may occur during their manufacture and storage, the majority occurs during use. The problem is that once the oil has been oxidised it may not attain the required performance standards set by the engine manufacturers. The oil has to perform many physical and chemical tasks, any of which if not met, can lead to the failure of the engine. The most important of these tasks by far, is the ability to lubricate moving surfaces, and if the oil is severely oxidised, it will fail to do so. Lubricating oils contain additive packages to aid their performance and extend their useful life. The additives only delay the onset of serious deterioration of the oil and, once consumed, the oxidation of the oil proceeds at an accelerated rate compared to that of the base oil.

It is the aim of this work to investigate the performance of inhibitors to prevent the oxidative degradation of lubricating oils. Two analytical techniques were established, for three different basestocks containing two types of antioxidant. One of the experimental techniques makes use of cyclic voltammetry (CV) and the other high pressure differential scanning calorimetry (DSC). A comparison of the information available from the two methods will be made for the first time.

1.2 The Degradation of Lubricating Oils

Oils are required to lubricate systems as diverse as watches and large diesel engines, which in themselves subject the oil to a wide variety of operating conditions. It has been pointed out by Bush et. al. [1], that the composition of the oil in the upper ring zone of an engine (when at top dead centre) is very different to that in the sump, owing to the extreme differences in the environment.

The environment within automobile engines has been the subject of considerable change over the past half century. The development of higher performance engines has increased the maximum compression ratio of an engine from 7:1 in the 1940s to approximately 10:1 today, although the value peaked in the 1970s. Higher compression ratios lead to a rise in the blow-by of the exhaust gases into the crank case. Between 1950 and 1957 the blow-by of exhaust gases rose by 60% [2]. The rise in exhaust gases present in the crank case increased the load exerted on the oil, because the unburnt fuel and unstable mixtures of nitrogen oxides contribute to the catalysis of the oil oxidation processes [3,4].

Wilson [5] noted that the rate of oil oxidation is affected by:

1 oxygen availability,

2 temperature,

3 the presence of catalysts and

4 the composition of the basestock.

The availability of oxygen for chemical reaction increases as the oil becomes more aerated by circulation through the sump. The oxygen availability is also increased by the air present in the exhaust gases blown past the piston rings into the crankcase.

The oil temperature can vary considerably throughout the engine, from 60 to 80°C in the sump and 110 to 140°C at the bearing surfaces, to in excess of 200°C in the journals. The heat is removed from the hot metal surfaces by the oil. As the temperature of the oil rises its viscosity is reduced, producing a corresponding drop in the minimum oil thickness between the working surfaces. Over the temperature range 60 to 80°C, a 1°C temperature rise causes a reduction in film thickness of 1%, which in turn means that the working surfaces reach a higher temperature and the oil is subjected to larger shear forces [6].

Many materials can act as an oxidation catalyst, the most common being particulate metals, organometallic compounds or free radicals in blow-by gases. The mode of action of these catalysts will be discussed in a later section of this chapter. Metals can have a catalytic effect on the oil oxidation processes, whether they exist in solid particulate form or in solution. It has been stated, however [7], that the efficiency of a metal catalyst is directly dependent on the rate of oxidation and dissolution of the metal surface into the oil. Ali and co-workers [7] studied three metals in ester oil formulations and found that copper was the most effective catalyst, followed by

stainless steel and low carbon steel. Using a thermal analytical technique, Cash [8] studied the effects of sample pan material on the oxidation stability of a mineral oil basestock. The materials were ranked in order of inertness as follows; C > Pt > Al > Steel > Oxidised Steel > Au > Inconel > Cu (carbon being most inert, copper most active catalyst). Cash [8] agreed with Ali et. al. [7] in assessing copper as the most potent catalyst. It is interesting to note that inconel (iron/chrome) alloys are used in engine bearings. Furthermore copper and lead (another effective catalyst) are commonly found in bearing metals and metal oil seals.

In a similar study Zeman [9] recorded the effect of pan material on the oxidation stability of ester oils containing two different antioxidant blends. Subtle differences were noted in his ranking of the catalytic effect of metals on the oil blends. These differences illustrate the complexity of the chemical interactions between the antioxidants and the metal catalysts.

The concentration of the metals in the oil can alter their catalytic effect on the oxidation processes of an oil. Knorre et. al. [10] studied the catalytic effect of copper and manganese stearates on hydrocarbons. They found that increasing the concentrations of the metal salts increased the rate of oxidation, until a critical concentration was reached when the oxidation rate was vastly reduced. The stearates acted as pro-oxidants at low concentrations and antioxidants at higher concentrations.

It may be inferred that the catalytic effect of metals depends not only on the basestock, but on the antioxidant package. For example, zinc (noted by Zeman [9] to possess a high catalytic activity) when present in zinc dialkyl(aryl) dithiophosphate (ZDDP) is a very effective antioxidant and metal deactivator. It is possible that the zinc in ZDDP behaves in a similar manner to the stearates studied by Knorre et. al. [10].

The composition of the basestock is governed mainly by the crude oil source, the method and the degree of refinement. The oxidation stability of the basestock is probably its single most important performance criterion from the point of view of chemical reactivity. The oxidation reactions are influenced by the nature of the saturated and aromatic fractions, including the naturally occurring sulphur compounds. The in-service performance of the oil is affected by the additive package added, which usually constitutes 5 to 10% of the total lubricant. However each component added to improve one property may adversely affect another.

1.3 The Composition of the Basestock

When comparing the oxidation performance of several different oil formulations derived from one basestock, a plot of viscosity index versus oxidation lifetime to a specified total acid number [11] gives a straight line correlation [12]. However when a comparison is made between two or more oils from different basestocks there is no correlation between the viscosity and the acid number whatsoever. The discrepancies arise because mineral oils contain both aromatic and saturated hydrocarbon groups, each consisting of many components. Other pertinent differences in basestock composition arise from the multitude of sulphur, oxygen and nitrogen heterocyclic compounds that may be present in varying quantities.

The influence of the quantity of the aromatic compounds present in an oil on its oxidation performance has been well documented. Optimum concentrations (recorded as weight percentages) of aromatic compounds for different oils have been noted to provide a maximum oxidation stability. Leonardi [13] and Burn and Greig [14] recorded the optimum percentages of aromatic compounds as between 5-10% and 10-20% respectively, depending not only on the original basestock but on the temperature of oxidation, while Vesely [15] noted that the composition of the aromatic components also had an effect on the oxidative stability of the oil.

It has been discovered [13,14] that when an oil is split into fractions containing both the aromatic and heterocyclic compounds (A/H) or the naphthenic and paraffinic compounds (N/P), the component fractions are less stable than the oil from which they were extracted. Vesely [15] found that the maximum oxidation stability of the (N/P) fractions was observed when they were recombined with mostly monoaromatic compounds. When multiple aromatic ring hydrocarbons were added to the (N/P) fractions, there was a decline in the maximum stability of the oil. In each case an optimum concentration of aromatic compounds was observed, whose peak moved to a lower concentration of aromatics with increasing condensation. In addition, with increasing condensation the sharpness of the peak relating to the oil stability increased, implying that the concentration of aromatics becomes more critical with increasing condensation.

Some of the sulphur compounds present in mineral oils, especially aliphatic sulphides, were considered to display antioxidant capabilities by decomposing chain initiating hydroperoxides [14,16]. Further work has shown that it is not these sulphur

compounds themselves, but their oxygenated derivatives formed during oxidation, that act as oxidation inhibitors [17]. When sulphur and aromatic compounds are present in the same oil, the oxidative stability recorded is greater than that expected owing to a synergistic effect. Leonardi [13] suggested that the synergism between sulphur compounds and the aromatic portion of the oil resulted from the conversion of the aromatic hydrocarbons into phenolic inhibitors. He stated that oxidised sulphur compounds catalysed the formation of the radical capturing inhibitors, causing the rapid formation of both peroxide decomposing and radical-capture inhibitors.

Burn and Greig [14] studied four different mineral oil basestocks and discovered that when the concentration of A/H compounds exceeded a certain minimum percentage, there was a rapid increase in oil stability. The value of the A/H content was found to be different for each oil, but in each case the total sulphur content was 0.06 weight percent. It was deduced that a certain minimum sulphur content was required before any synergism occurred between the sulphur and the aromatic fraction. They found that the sulphur content of an oil can be a critical factor when determining its oxidation stability. The authors stated that optimum aromaticity only occurs when sulphur compounds are present, the more sulphur there is, the less sharply defined the optimum value. The optimum aromaticity was considered to be due to an increase, then decrease in the synergism between the sulphides and the aromatic compounds as the aromatic content of an oil rose. The authors believed that the decrease in synergism was due to a reduction in the chain length of the hydrocarbon oxidation reactions with increasing aromatic content. This was thought to be because the rate of initiation rose with increasing aromatic content, implying an overall decrease in the maximum stability of the oil under conditions of complete inhibition. It is slightly surprising however, that the maximum stability of the oil increases with increasing aromatic content in the absence of sulphides, owing to the inhibiting effect of the higher aromatics.

It is well known that each component in an oil can undergo oxidation, the rate and type of end product depending on the composition and structure of each molecule. There may also be kinetic interactions in complex combinations that may vary the oxidation rates and products formed. Murray et al. [12] noted that under oxidising conditions branched alkanes are more susceptible to oxidation than other structural types of alkanes, as the hydrogen from a tertiary carbon is preferentially extracted to form a hydrocarbon radical. Aromatic hydrocarbons display a considerable variation

in their inertness, alkylbenzenes degrading only minimally whilst naphtheno-aromatics decay substantially. This is because the hydrogen attached to a carbon next to the aromatic ring is preferentially abstracted.

Saturated hydrocarbons are very responsive to inhibition by chain stopping inhibitors such as phenols and amines, whose hydrogen atoms are preferentially extracted to form very stable radicals. Aromatic hydrocarbons are, therefore, less responsive to these types of inhibitors. Hydroperoxide decomposing or reducing antioxidants such as ZDDP, phosphites or sulphides perform well with aromatic hydrocarbons, because they prevent aromatic compounds breaking down to form radicals.

Walker and Tsang [18] used a DSC to characterise lubricating oils. Three types of oil were tested, unused (virgin) basestocks, fully formulated oils and re-refined base oils. The re-refined oils were fully formulated blends that had been used until they were exhausted and then recycled to remove exhausted additives and oil breakdown products. The authors stated that in scanning experiments, the temperature of onset of oxidation is lowest for virgin base oils, highest for fully formulated oils and intermediate for re-refined basestocks. They suggested that there was possibly a reactive component present in the virgin basestock, probably a lower molecular weight fraction, that was destroyed with use and was therefore absent in the re-refined base oil. Another explanation, supported by Rebbert [19], was that there is a residual amount of antioxidant present in the re-refined oil. Rebbert analysed several basestocks and discovered that for the re-refined oils there was on average 0.08 moles per litre antioxidant present, compared to an average of 0.03 moles per litre of naturally occurring antioxidant in the virgin base oils. Re-refined base oils have been studied because of the growing incentive to recycle raw materials. The re-use of lubricating oils is becoming more common, especially in the United States of America. Recycled oil contains lighter hydrocarbon fractions than virgin basestocks, produced by the oxidation of the oil. The lighter hydrocarbon fractions can cause dermatitis, whilst other chemicals present in the recycled oil such as PCB's (which burn to form dioxins) and PNA's are genotoxic and carcinogenic [20]. The recycled oils may need further refinement or treatment to reduce the dangers of these chemicals, which may have an adverse effect on their performance. Re-refined base oils may overcome this problem, especially if blended with a virgin basestock.

In addition to the oxidation performance, the composition of an oil affects its low temperature characteristics. If an oil contains too large a concentration of paraffinic compounds, these may crystallise from solution on cooling, a problem encountered more frequently during the winter months. If a lower boiling point fraction is taken, the low temperature performance will be improved at the expense of the oxidation performance. If the waxy components are filtered out, when the blend has been cooled, the high temperature running of the oil does not suffer and the overall performance is improved [21].

Cash [8] examined two different basestocks, one mineral and one a synthetic oligomerised oil, to which the antioxidant dioctyldiphenyl amine (DODPA) was then added. Both oils showed an increase in oxidation stability on addition of the inhibitor to a concentration of 0.5 weight percent. The mineral oil became more resistant than the synthetic oil to oxidation. However when fully formulated the relative stabilities of the oils reverted back to that of the basestocks, owing to the responsive nature of saturated alkanes to chain stopping inhibitors.

1.4 The Mechanisms of Hydrocarbon Oxidation

In this section a brief outline of the fundamentally more important liquid phase hydrocarbon oxidation reactions will be given, as applied to a general hydrocarbon. Detailed accounts of the reaction mechanisms are given in the literature [22-24]. The discussion in this section will not deal with all of the reactions involved in the oxidation of lubricating oils, or provide an in depth account as to why one basestock is inherently more stable than another.

The literature contains many articles concerning the breakdown processes in the gaseous state, but the mechanism in the liquid phase is slightly different. This is because the concentration of the free radicals in the liquid phase is much greater than in the vapour phase. Reactions involving hydroperoxides in particular are therefore more important, owing to reduced termination reactions with the cell wall (caused by reduced diffusion rates).

The oxidation of hydrocarbons, first noted in the middle of the last century, consists of a multitude of different reactions that can be categorised under a few simple headings. The general reaction scheme in the liquid phase is primarily considered to be a free radical process [25]. The separate steps that, as a whole make up hydrocarbon

oxidation reactions, are initiation, propagation, branching and termination. The oxidation processes in the liquid phase can be catalysed by metals or inhibited by several different mechanisms. Each of these steps will be discussed individually.

1.4.1 Initiation

The first step in the overall mechanism is the initiation of free radical species. Several possible reactions exist, and under certain conditions each one can predominate. Firstly simple cleavage of the hydrocarbon molecule to form two radicals can begin the process, when the parent molecule is exposed to light or heat. Thermal energy can cleave a hydrocarbon molecule, but because the activation energy required is so large, it is unlikely to form the main source of free radicals, even if the oil dwelt in the upper ring zone for a sufficient period. The reaction can be expressed as

$$RH \rightarrow \text{Alkyl Radicals}, \qquad 1$$

where RH is an alkane. A more probable source of free radicals is realised when the sump oil in an engine is saturated with oxygen. This occurs as a result of the constant churning/pumping action of the oil cooled components. A parallel is obtained between oil oxidation experiments using the thermal analytical technique (DSC) and the engine environment when the DSC cell is pressurised with oxygen to saturate the sample. Oxygen abstracts a hydrogen atom from the hydrocarbon,

$$RH + O_2 \rightarrow R\cdot + HO_2\cdot, \qquad 2$$

to form a hydroperoxy radical. It has been stated by Benson [26], that reaction 2 proceeds very slowly below 150°C, but at higher temperatures this is likely to be the predominant cause of initiation. The general consensus regarding the magnitude of the average activation energy for the initiation reactions is approximately 200 kJ mol^{-1}. This excludes reaction 1 from playing a major part in the overall process, because the energy required on average to cleave a C-H bond is 426 kJ mol^{-1} and that required to cleave a C-C bond is approximately 356 kJ mol^{-1}. It has been mentioned previously that an internal combustion engine provides a hostile environment for a lubricating oil, owing to the presence of blow-by gases in the sump region. The gases that have been blown past the piston rings possess a high concentration of unburnt fuel and unstable mixtures of nitrogen oxides, which are vigorous oxidants and may contribute to initiation.

1.4.2 Propagation and Degenerate Branching

Propagation reactions involve the consumption and regeneration of a 'chain carrier' that is formed in an initiation process. Degenerate branching reactions comprise the

decomposition of an intermediate molecular species (formed from the parent hydrocarbon) as an additional source of free radicals which give rise to a secondary initiation of reaction chains.

The reaction of free radicals generally have low activation energies relative to molecular decomposition or oxidation. In the case of DSC experiments, degenerate chain branching reactions may cause the autocatalysis of the oxidation process to accelerate to a sufficiently high rate that the sample ignites. The first propagation reactions are those that produce peroxy radicals and the corresponding peroxides, ie.

$$R\cdot + O_2 \rightarrow RO_2\cdot \quad 3$$

$$HO_2\cdot + RH \rightarrow HOOH + R\cdot \quad 4$$

$$RO_2\cdot + RH \rightarrow ROOH + R\cdot. \quad 5$$

Other propagation reactions appropriate to relatively high temperatures (~ 750 K) and therefore characterised in gas phase oxidation studies include,

$$R\cdot + O_2 \rightarrow \text{alkene} + HO_2 \quad 6$$

The approximate energy of activation for the reactions are (3) 4 to 8 kJ mol^{-1} [27], (4) 40 to 60 kJ mol^{-1} [28], (5) 40 to 60 kJ mol^{-1} [29] and (6) 30 kJ mol^{-1} [30]. The most important propagation reactions in an engine environment are probably 3 and 5, which produce the hydroperoxide. At temperatures below 250°C, organic peroxides form the basis of many degenerate chain branching reactions. At the temperatures encountered in the upper ring zone, they may decompose to form aldehydes and alkoxy radicals, which can initiate further chains, leading to a more complicated mixture of stable intermediates and final products.

$$RO_2H \rightarrow RO\cdot + OH\cdot \quad 7$$

A major difference between the mineral and synthetic oils on the one hand and the ester oil on the other, is that the peroxide of the ester oil reacts to form a low molecular weight acid [7]. These acids are the major precursors to the production of high molecular weight sludges [7,31]. To demonstrate this, Ingold and Puddington [31] eliminated sludge formation by adding potassium hydroxide to an oil. Ali et. al. [7] discovered that the acids oligomerised in the presence of oxygen to form dimers and trimers (no higher molecular weight material was formed in the absence of oxygen), which then polymerised to form the oil insoluble sludges. They also found that as the molecular weight increased, the number of conjugated bonds increased, these always being conjugated to the carbonyl group. The polymeric products were found to have regular repeating groups, and as the size of the molecule increased so did the number of ketonic groups, these being formed by free radical attack on the C=C bonds. It was

also found that the higher molecular weight alkenes decomposed more rapidly than paraffins with an equal number of carbon atoms. This was because the π bond is a prime target for free radical attack, the activation energy for an addition to the π bond being 1 to 30 kJ mol^{-1} [32].

Bell et. al. [27] proposed a reaction scheme for the oxidation of paraffins, supported by both experimental results and a literature review. The formation of peroxy radicals was taken for granted and the proposed mechanisms all led to the production of alkoxy radicals, such that,

$$ROO\cdot + RH \rightleftharpoons ROOH + R\cdot \quad 5$$

$$ROOH \rightarrow RO\cdot + OH\cdot \quad 7$$

$$2\ ROO\cdot \rightarrow 2\ RO\cdot + O_2 \quad 8$$

$$ROO\cdot + R\cdot \rightarrow ROOR \quad 9$$

$$ROOR \rightarrow 2\ RO\cdot. \quad 10$$

Reaction 9 was only assumed to occur in conditions containing very little oxygen, which prevents the oxidation of alkyl radicals to form alkylperoxy radicals. This can therefore be excluded from the reaction scheme assumed to occur in an engine environment, owing to the excess of oxygen available. Reaction 8 was considered to be part of a larger reaction scheme that demonstrates one route to the vast numbers of products formed in a hydrocarbon oxidation reaction. The molecular product of reaction 5 was assumed to react thus;

$$RO\cdot + ROOH \rightarrow ROH + ROO\cdot \quad 11$$

$$OH\cdot + ROOH \rightarrow H_2O + ROO\cdot \quad 12$$

The peroxy radicals of reactions 11 and 12 combine as given in reaction 8. Reaction 7 is considered to be degenerate chain branching reactions because it acts as a secondary source of initiating reactions. Bell and co-workers [27] considered the reactions of the alkoxy radicals which form alcohols, esters, ketones, aldehydes and ethers. A primary alkoxy radical could undergo the following reactions

$$RCH_2O\cdot \rightarrow R\cdot + CH_2O \quad 13$$

$$RCH_2O\cdot + RH \rightarrow RCH_2OH + R\cdot \quad 14$$

$$RCH_2O\cdot + R\cdot \rightarrow RCHO + RH \text{ or } RCH_2OR \quad 15$$

or

$$RCH_2O\cdot + RO\cdot \rightarrow RCHO + ROH. \quad 16$$

A secondary alkoxy radical could give rise to

$$R_2CHO\cdot \rightarrow R\cdot + RCHO \quad 17$$

$$R_2CHO\cdot + RH \rightarrow R_2CHOH + R\cdot \quad 18$$

$$R_2CHO\cdot + R\cdot \rightarrow R_2CO + RH \quad 19$$

and $$R_2CHO\cdot + RO\cdot \rightarrow R_2CO + ROH. \quad 20$$

Finally for tertiary alkoxy radicals the reactions could be

$$R_3CO\cdot \rightarrow R_2CO\cdot + R\cdot \quad 21$$

or $$R_3CO\cdot + RH \rightarrow R_3COH + R\cdot. \quad 22$$

These reactions further demonstrate the ease with which a myriad of compounds can be produced in an oxidative environment. Many of these reactions will proceed very easily, because the dimerization of radicals (and combination reactions in general) do not require an energy of activation [26,33].

1.4.3 Termination

These reactions involve the destruction of the free radical chain, by the recombination of two free radicals to form a non-chain-carrying product, or by the reaction of a free radical with the surface of the reaction vessel (in this case the engine). There are many termination reactions and the best representation of the quadratic termination is;

$$2\ R\cdot \rightarrow \text{Stable Products.} \quad 23$$

The rate constants of radical recombination (termination) reactions were given by Walker [28] to be 10^8 to 10^9 $dm^3\ mol^{-1}\ s^{-1}$. The termination reactions compete with the propagation and branching reactions for free radicals. If the termination reactions were ineffective the oil would degrade very quickly. The rate of oil degradation can be slowed further by the addition of antioxidants.

1.4.4 Inhibition

The classes and mechanism of antioxidants will be discussed in greater detail during a later section of this thesis. Many hydrocarbon basestocks exhibit a limited degree of inhibition but their antioxidant qualities are not as effective as those of the specific additives added to the formulation to retard the oxidation processes. Phenolic inhibitors are a natural class of antioxidant that function by breaking the peroxide chain, ie.

$$RO_2\cdot + IH \rightarrow RO_2H + I\cdot \text{ (Stable intermediate)} \quad 24$$

and $$RO_2\cdot + I\cdot \rightarrow \text{Stable Product.} \quad 25$$

Further inhibition reactions might involve the reduction of the hydroperoxide, by a sacrificial mechanism, such that

$$RO_2H + X \rightarrow ROH + XO. \quad 26$$

1.4.5 Catalysis

The engine environment is a prime source of contaminants that can catalyse oil oxidation. Most of the catalysts are likely to be free radicals from the blow-by gases or metal/metal complexes that can originate from the wear of moving components. The most common metal catalysts in an engine are iron and copper, which in solid or solution can decompose peroxides, thus initiating the multitude of chain reactions.

$$M + RO_2H \rightarrow M^+ + OH^- + RO\cdot \qquad 27$$

and

$$M^+ + RO_2H \rightarrow M + H^+ + RO_2\cdot. \qquad 28$$

The metal is regenerated in to its initial oxidation state and the H^+ and OH^- ions can undergo further reaction with the substrate (or any stable species) in a series of molecular (not free radical) reactions. The efficiency of a copper catalyst was noticeably reduced by the addition of sodium hydroxide to an oil [31]. The alkali may have increased the oxidative stability of the oil by neutralising acidic oxidation products that would have otherwise attacked the basic antioxidant molecules. Ali et. al. [7] in their study of ester oils found that catalysts accelerated the rate of oil degradation and increased the rate of polymerization to form sludges. On the addition of antioxidant, the rate of oxidation was diminished until the additive was depleted. The relative efficiencies of the metals as catalysts was proposed to be dependent on the concentrations of the metals in the liquid phase. It is interesting to note that the catalysts were deemed to have a greater effect on the polymerization processes than on the initial degradation reactions. The low carbon steel catalyst was thought to aid condensation reactions, which although slower than addition reactions form higher molecular weight products.

1.5 Additives: Their Mode of Action and Effect

There are a whole range of additives that can be blended with lubricating oils to improve their overall performance characteristics, to enable the highest levels of product quality to be attained at an economical production cost [3,34,35]. Each additive can have a synergistic or antagonistic effect on the performance characteristic of another component in the oil blend, but without these additives modern engines would cease to perform satisfactorily. For example the sulphuric acid produced in diesel engines reacts with the lubricating oil in an oxidative manner to form oil insoluble products that adhere to metal surfaces. When the engine is cooled below the dew point of water, the acid may also attack metal surfaces. The acidic products present in oils may be controlled by the addition of basic additives such as antioxidants, dispersants or metal deactivators.

It is not in the scope of this thesis to discuss each oil additive in detail, but a brief outline of the main groups will be made for the sake of completeness.

A. Detergents and Dispersants

These additives are used in the crankcase to keep particulate matter dispersed in the oil and maintain engine cleanliness. To do this, the polar end groups attach themselves to the soot particles, while the non-polar ends remain in solution in the oil. Coagulation of small dirt particles is prevented by steric hindrance, which therefore reduces the levels of sludge found in the sump caused by low temperature running. Although both detergents and dispersants perform the same function, dispersants are more effective during operation at low temperatures, while detergents are associated with high temperature running. They both help with acid neutralisation owing to their basic nature.

B. Viscosity Index Improvers and Pour Point Depressants

Both of these additives work by purely physical means. The viscosity index improvers are generally organic polymers that exist in a random coil or ball form, which are swollen by the lubricating oil. They function by impeding the oil flow in their neighbourhood. The viscosity of the oil decreases with increasing temperature, and to counteract this the ball unravels thus increasing the viscosity. Pour point depressants probably work by absorption on to the faces of young growing crystals. This prevents them interlocking effectively and results in their precipitation from solution at lower temperatures.

C. Corrosion Inhibitors

This group of additives are usually high molecular weight carboxylic, sulphonic or phosphoric acids and their salts, which are formed by neutralization with organic bases. When dissolved in hydrocarbons, corrosion inhibitors adsorb on to metal surfaces to form a hydrophobic film, preventing water and air reaching the metal surface.

D. Copper Deactivators

These are diamines added to deactivate traces of copper present in the oil after the copper sweetening process (a technique employed to improve oil quality). The diamines form a stable copper chelate. The inclusion of this additive into the oil blend reduces the levels of antioxidant required.

E. Antifoams

This group of additive is required whenever there is a violent churning or agitation of the oil, to inhibit the formation of a stable foam that would prevent the adequate supply of oil to the bearing surfaces. They work by reducing the surface tension of the oil at the air interface, but if too much is added, the antifoam acts as a profoamant.

F. Load Bearing Additives

Under ideal conditions, no two metal surfaces in an engine are allowed to come into contact owing to a thick film of lubricant being present between them. Under boundary lubricating conditions intermetallic contact takes place and the type and extent of damage that then occurs is determined by the chemical properties of the oil. Surface films are formed by physical adsorption, chemisorption and chemical reaction of the load carrying additives with the surface. These additives can be split into two groups, antiwear types and extreme pressure types, the latter being effective when the load between the two surfaces is increased. Load carrying additives usually contain organic sulphides which are adsorbed and then react with the metal surface to form sulphide or disulphide films which have a low shear strength owing to the weak sulphide (C-S) and disulphide (S-S) linkages. The radicals produced by the scission of the C-S or S-S bonds are resonance stabilized [35], which facilitates the cleavage of the molecule at these points. Extreme pressure additives generally contain phosphates or dithiophosphates, a group of additives that also act as antioxidants. The mode of chemical action of this group of additive is the subject of debate, the protective layer being considered to be either a phosphide, phosphate, or a low melting eutectic of the two. Chlorine containing extreme pressure additives are becoming less popular, because they form acidic salts that are in general antagonistic toward oil performance.

G. Antioxidants

This is singularly the most important group of additive present in an oil formulation. This group of additive can be further subdivided into two classes.

1. Peroxide decomposers.

This class consists of phosphites, sulphides and most frequently encountered, zinc dialkyl(aryl) dithiophosphates (ZDDP). This last group is a multifunctional additive, being a metal passivator, an extreme pressure additive and a peroxide decomposing antioxidant. Kawamura [36] noted that the chemical reactivity of ZDDP corresponded with the antiwear properties imparted by the additive. The wear scar damage recorded, increased with increasing reactivity for primary ZDDP antioxidants, but decreased for

secondary ZDDP antioxidants which behave as non-sacrificial extreme pressure additives.

The molecular structure of ZDDP does not account for its high antioxidant activity [2]. The antioxidant activity can probably be attributed to the decomposition products, the more easily decomposed the antioxidant the better it performs. The ease of decomposition of the ZDDP correlates to the structure of the alkyl side chains, with additives derived from secondary alcohols being more effective than those from primary alcohols. The length of the side chain length only affects the antioxidant solubility, whilst the degree of branching has little overall effect. Larson [2] found that ZDDP's retard bearing corrosion by two mechanisms, peroxide decomposition and the formation of a protective film. Secondary alkyl ZDDP's were found to be more effective corrosion inhibitors than primary alkyl ZDDP's because they were more easily decomposed. The protective film formed on the bearing surface is known to be a decomposition product, because on examination, proportionally more zinc was found than phosphorus and sulphur. The surface film helps to reduce oil oxidation, by preventing the formation of organo-metallic compounds that act as catalysts for the oil degradation processes. Burn, Cecile and Young [37] studied the action of ZDDP on the decomposition of cumene hydroperoxide, in the presence and absence of radical traps. They found that the catalytic activity of ZDDP meant that it could decompose 10^4 to 10^5 its own molar equivalent of the hydroperoxide. The addition of radical traps increased the induction period before oxidation occurred. Brazier and Elliot [38] performed a literature review on previous work studying the decomposition of ZDDP and concluded that there was little agreement amongst the literature as to the mechanism and end products of the degradation. They found that there were two distinct stages of breakdown, the mechanism being dependent on the molecular structure, but in general the order of product formation was 1-alkene, 2-mercaptan, and 3-H_2S. Brazier and Elliot [38] showed that the decomposition was autocatalytic, in agreement with Burn, Cecile and Young [37] and that the H_2S evolution and sulphide formation was caused by the breakdown of the mercaptan.

The use of ZDDP as an antioxidant was studied by Johnson, Korcek and Zinbo [39], who discovered that the addition of ZDDP to a model hydrocarbon oxidation system did not alter the overall extent of oxidation. They found that the inhibition process existed in three distinct stages, the first being the decomposition of the hydroperoxide. This resulted in the complete consumption of the ZDDP, forming a

disulphide and unidentified products. The second stage was the inhibition period, where peroxy radicals were trapped by decomposition products. This was followed by a second hydroperoxide decomposition stage, where the concentrations of the disulphide and 'unknown' were depleted to form radicals that initiated further oil oxidation, at an accelerated rate. The addition of a hindered phenol was found to extend the inhibition period and completely suppressed oxidation until consumption of the phenol was complete.

The oxidation mechanism of ZDDP has been investigated by Paddy and Co-workers, employing a variety of techniques [40,41]. The antioxidant was oxidised at 30°C or below by cumene hydroperoxide and aliquots withdrawn from the reaction mixture at specified intervals for analysis. The main oxidation products formed were a 'basic-ZDDP' and a disulphide, represented in the reaction scheme

$$4[(RO)_2PS_2]_2Zn + R'O_2H \rightarrow [(RO)_2PS_2]_6Zn_4O + [(RO)_2PS_2]_2 + R'OH,$$

where R is an alkyl grouping. The reaction scheme was followed using ^{31}P NMR and Raman spectroscopy [40], both of which illustrated that the disulphide was stable with respect to oxidation. The 'basic-ZDDP' was shown to slowly oxidise to form more disulphide by oxidative attack at the zinc atoms, causing Zn-S bonds to be broken [40]. The 'basic-ZDDP' was considered by the authors to consist of a tetrahedron of zinc atoms surrounding a central oxygen, with $(RO)_2PS_2$ ligands linked along the edges of the tetrahedron. The oxidation products of cumene hydroxide were studied using HPLC separation followed by ^{31}P NMR and mass spectrometry [41]. The retention times of the oxidation products were compared to those of reference materials, and the uncharacterised fractions were then collected for analysis by ^{31}P NMR and Mass spectrometry. Standard solutions of the non-reference compounds characterised by these methods were employed to calibrate the HPLC peak integrations to permit a kinetic study of the oxidation process. Over the duration of the analysis the 'basic-ZDDP' was shown to decompose half the cumyl peroxide to form mostly cumyl alcohol, with some 2 phenylpropylene and dicumyl peroxide [41]. A reaction scheme was proposed for the formation of the products, in which the 'basic-ZDDP' acted as a radical scavenger to form the 2 phenylpropylene, contrary to the generally assumed acid catalysed reaction. The authors used experimental evidence to support their mechanism and stated (in agreement with Burn et. al. [37]) that ZDDP acted as a pro-oxidant as well as a radical scavenger and a hydroperoxide decomposer.

Hsu and Lin [42] studied the interactions of ZDDP, a succinimide dispersant and a calcium sulphonate detergent in three oil basestocks. There was a significant synergism between additives for two component systems containing ZDDP. Maximum oxidative stabilities were recorded, because the oxidative stability of the oils increased and then decreased as the additive concentrations were altered. With the three component system, an antagonism was noted between the succinimide and the sulphonate, with the sulphonate proving to be a pro-oxidant. They concluded that new additive combinations need to be studied with care, to determine the optimum concentrations of the components.

2. Radical Traps/Propagation Suppressors.

This class of additives contains the two antioxidants studied in this thesis, the hindered phenols and the diphenyl amines.

In one of the earliest investigations of phenolic antioxidants, Reiff [43] described the preparation and the structure of alkylated hydroxy aromatic hydrocarbons. In this comprehensive study, he noted that slight changes in the molecular structure could alter the properties of the additive drastically. Wax substituted hydroxy-aromatic hydrocarbons (formed by reaction of a paraffin with phenol in a Friedel-Crafts reaction [41]) were found to be effective pour point depressants, which upon esterification (by reaction with a polybasic acid), enhanced the thermal stability of the oil. In a similar manner alkylated phenolic acids displayed pour point depressant, antioxidant and viscosity index improvement characteristics. He noted that the corresponding metal salts were more effective additives in every respect.

The radical trapping antioxidants react with peroxy radicals by the loss of a hydrogen atom, to form the corresponding inhibitor radical. The inhibitor radicals do not undergo reaction with the oil because they are resonance stabilized, which breaks the reaction chain [35,44-47].

Rosenwald et al. [48] in a practically orientated presentation compared the potency of alkylated phenols substituted with methyl and butyl alkyl groupings in the 2, 4, and 6 positions of the aromatic ring. When the effect of the number of phenolic substituent groups on the antioxidant efficiency were studied, the potency of the antioxidant increased by increments that were more than additive on addition of further groups. For mono substituted phenols, a change from a methyl to a normal, secondary or

tertiary butyl substituent had little effect on the potency (when the molar mass increase was taken into account for). It was not surprising that ortho substituted alkyl phenols were found to be more effective antioxidants than para substituted alkyl phenols, because the ortho substituent groups can sterically hinder undesirable side reactions. Furthermore ortho substituents ease the abstraction of the hydrogen atom from the phenolic group by electron donation. The role of the para group is less certain, but it is believed to result in the formation of a bisphenol, another potent inhibitor [35]. An increase in the branching of the butyl group was found to increase the potency of the ortho substituted alkyl phenol, but have little effect on para substituted alkyl phenols. For the disubstituted phenols Rosenwald et al. [48] discovered that the configuration of the butyl group had little effect on the potency for 2, methyl 6, butyl; and 2, methyl 4, butyl phenols, whereas the potency was reintroduced for 2, butyl 4, methyl phenol. It is surprising that the effect of the butyl grouping configuration on the potency was not observed for the 2, methyl 6, butyl phenol where the t-butyl group could exert a hindrance effect similar to that in 2, butyl 4, methyl phenol. The workers compared the efficiency of the di and trisubstituted phenols, by varying the positions and configurations of the groupings, but made no effort to explain the results. It is interesting to note that the only additive tested to have a pro-oxidative effect was 2, 4, 6, tri butyl phenol. The lack of antioxidant behaviour was explained by Bailey [49] who stated that the bulky ortho groupings prevent chain transfer reactions. The balance of the transfer reactions with antioxidant efficiency gives a true measure of the effectiveness of the molecule. The author stated that 2, 4, 6, tri methyl phenol inhibited propagation reactions ten times faster than 2, 6, di t-butyl 4, methyl phenol (Topanol 'O'), but readily undergoes undesirable side reactions that transfer the free radical chain. Topanol 'O', because of the bulky ortho groupings does not readily undergo chain transfer reactions, therefore Topanol 'O' is a more effective antioxidant overall. For 2,4,6, tri t-butyl phenol, the author commented that it would not readily undergo transfer reactions, but the rate of reaction with peroxy radicals would be incredibly slow.

A year later than the work of Rosenwald and his co-workers, Bickoff [50] reported a comprehensive study which compared the efficiency of over 100 phenolic antioxidants on the storage lifetime of carotene suspended in an inert mineral oil matrix. Phenol was found to be an ineffective inhibitor, and the introduction of nitro, carboxyl, primary alcohol, or ketonic groups into the ring produced poor antioxidants with little or no increase in efficiency over phenol. Alkylation of the phenolic group had little effect on

the antioxidant activity, but a greater effect was found if alkyl groups or phenolic radicals were substituted into the ring, especially in the ortho and/or para positions. The effectiveness of bisphenols were enhanced when alkyl groups were substituted into the ring. Bickoff [50] found that the addition of a second hydroxyl group to the phenol in the ortho position to form catechol greatly improved its antioxidant properties. The addition of an alkyl group to the catechol nucleus enhanced the antioxidant properties of the molecule in the same manner as for phenol. The substitution of phenol into the catechol molecule was found to have little effect, but linking two catechol molecules dramatically improved the properties of the compound. The addition of a second hydroxyl group to phenol, in the meta position, had less effect than with the ortho substitution, while addition of a second hydroxyl group in the para position, to form hydroquinone, was slightly more effective than in the meta position. The substitution of other groups into the nuclei of these molecules reduced their antioxidant capabilities by varying degrees, depending on the group used.

When trihydroxybenzene derivatives were studied, Bickoff [50] found that the position of the hydroxyl groups was very important, 1, 3, 5, trihydroxybenzene was ineffective, whilst its 1, 2, 3, isomer (pyrogallol) was a very potent antioxidant. Methylation of the hydroxyl groups either reduced or destroyed the antioxidant ability of the molecule, depending on the number of groups substituted. The introduction of carboxylic groups into the molecule virtually removed the antioxidant capability of the molecule, but esterification of the acid produced antioxidants as effective as pyrogallol. Naphthol and amino phenols were also studied by Bickoff [50], who found that α naphthols were more effective than β naphthols, and for dihydroxy naphthalene the positions of the hydroxyl groups greatly influenced the oxidation stability conferred.

It has been demonstrated that the performance of phenolic inhibitors is affected by steric hindrance and resonance stabilization. Similarly, the degree of steric hindrance in an amine antioxidant affects its efficiency, because non-hindered amines are less effective inhibitors due to their participation in side reactions [46]. Much less is known about the aromatic amine radical formed than the phenolic radical. This is a further reflection of the relative amounts of work performed on each antioxidant family. Ford [35] commented that, for amine antioxidants, nitroxy radicals have been formed as intermediates in the oxidation process.

$$>NH + RO_2\cdot \rightarrow >N\cdot + ROOH$$

$$>N\cdot + RO_2\cdot \rightarrow >NO\cdot + RO\cdot$$

The mechanism of the reactions involved in the consumption of the nitroxy radicals were not proposed. As is the case with phenolic inhibitors, amines with electron releasing substituent groups are more effective antioxidants than those without, because the abstraction of the labile amino hydrogen is facilitated [47]. Another similarity between amine and phenolic antioxidants is that the rate determining step in chain termination reactions is not the abstraction of hydrogen atoms from the inhibitor molecule [47]. It was inferred that the peroxy radical abstracted an electron from the amino group to form a complex that then reacted with a second peroxy radical to form a stable compound. This theory is supported by the fact that amines with no labile hydrogen on the amine group act as antioxidants. These amines are not as efficient at terminating chains as amines with a labile hydrogen [47]. It is generally assumed that the reaction mechanism of amine and phenolic antioxidants is essentially the same.

1.6 The Need for Standard Tests

The Institute of Petroleum (IP) and the American Society for Testing and Materials (ASTM), are two governing bodies concerned with the formulation of standard test procedures for the analysis of materials relevant to the oil industry. The standardisation of the test procedures is to enable the meaningful inter-laboratory analysis of samples to be performed.

The aim of the IP and the ASTM is to combine experimental procedures, such that the methods recommended by these governing bodies will be identical. This means that the results obtained by any one laboratory may be reproduced by any other laboratory. The experimental results can then be compared to a standard, to provide valuable information on the performance criterion of the tested material. Clearly this is an important goal, as it will enable basestocks, or blends to be ranked with regards to any one performance characteristic, and this ranking will be recognised worldwide.

The IP and the ASTM publish annual books containing their recommended standards, the reference for the ASTM book of standards being given at the end of this chapter [11].

1.7 The Measurement of Oil Quality

The procedures used to determine the quality of an oil are very much dependent

on the parameter of oil performance of interest. The large number of standard screening test methods developed over the years, reflect the different performance criteria considered to be of importance. One or more of these standard tests have to be passed before an oil is allowed to be used in service.

The figures given in the parentheses after a test method indicate the test procedures recommended by the standard testing bodies. Some of the more facile tests, for example the colour (ASTM D-1500, IP-196) and water content (ASTM D-4377, IP-356), may only take seconds to perform, whilst other tests like the foam test (ASTM D-892) and the oxidation stability (ASTM D-2893, IP-943) take considerably longer.

The low temperature performance characteristics of the oil can be determined from its cloud point (ASTM D-2500, IP-219) or pour point (ASTM D-97, IP-15) and conversely its high temperature performance can be determined by its evaporation loss (ASTM D-972) and volatility measurements. The volatility of an oil can be measured using thermal analytical techniques (see Appendix 3), a highly volatile oil being obviously undesirable. The volatility of a sample is related to its flash point, because this is a measure of the temperature at which the volatilised components can support combustion. There are two standard test methods used to determine the flash point of a sample (ASTM D-92 and D-93, IP-36 and 34), which involve heating the sample in air and passing a flame over its surface until the vapour supports combustion. The change in viscosity of the oil with temperature, viscosity index (ASTM D-2270, IP-226), is a measure of its lubricating ability and like the volatility, is of prime importance to the manufacturers and users alike. There are many other tests frequently performed on oil blends to ascertain their physical and chemical properties, some of which are wear scar, shear test, total acid (or base) number and oxidation stability measurements. The wear scar measurements (ASTM D-4172) assess the quality of the oil under boundary lubricating conditions, while the shear test (ASTM D-2882) monitors the break down of the oil under load. This is done by measuring the viscosity of the oil before and after passing it through a vane pump for a period of 100 hours. The total acid number (ASTM D-974, IP-139) is a measure of the basicity of the blend and the ability of the formulation to neutralise the acidic products formed during service. It was stated by Pawlak et. al. [51] that the measurement of the acid number of an oil using a pH concept was invalid, because acids, bases or salts do not ionise in an oil environment. They studied the acid/base numbers of engine oils, using conductometric, calorimetric and potentiometric methods. These methods were found

to agree well with the standard potentiometric method (ASTM D-2806, IP 276). Of particular importance, especially to synthetic oils is the presence of water, a possible contaminant from the production process, which can lead to corrosion of engines and pumps and the dissolution of polar additives into the aqueous phase. Each screening test can be used to measure the quality of an oil before it is used, but if a new blend is to pass into service it has to pass a number of screening tests and a full engine test. Several engine test procedures are recommended by the ASTM under one test method, ASTM D-4485. These tests are the only completely reliable way to determining the worthiness of an oil, yet as they are both expensive and time consuming to run, the screening tests are used to weed out poor candidates. Hsu and co-workers developed a test procedure to mimic engine conditions [52]. The authors employed a high pressure differential scanning calorimetric (DSC) technique and correlated the results those of a standard engine test. The novelty of their method was that standardised catalysts were added to the oil sample. A metal catalyst, composed of different metals at the relative quantities found in oil sludge and a fuel catalyst, containing products found in blow-by gases were added in equal concentrations prior to analysis. The authors claimed an 'almost' linear relationship between the results of the DSC and engine tests. The relationship was by no means linear.

A test (ASTM D-893) used to measure the insoluble products in an oil can be employed to measure its breakdown during service [53,54]. The method involves dissolving the oil in pentane, then washing and drying the residue to evaluate the pentane insolubles. The procedure is repeated on the residue using benzene, the difference in the residue being referred to as the resin content of the oil. The main performance criterion of an oil is its oxidation stability, which is closely linked to the antioxidant concentration. The remaining service lifetime of an oil can be predicted using a prior knowledge of the physical or chemical properties of the virgin and an exhausted oil. To ascertain the remaining service lifetime of an oil electrochemical, thermal analytical and IR spectrometric techniques can be used [55-59]. Furthermore changes in the total acid number and oil viscosity are commonly used to determine the remaining lifetime of an oil [54,60,61]. Each of these methods monitor the variation of an individual parameter with the duration of service. This monitoring of oil quality whilst it remains in service, is of prime importance, because the maximum lifetime of an oil can be obtained. As a consequence, unnecessary engine shutdowns can be avoided and oil that has not been exhausted, not wasted. The end of the useful life of an oil is defined as the time at which rapid changes in the measurable quantity occur,

or when the antioxidant concentration has been depleted. When an oil is exhausted its viscosity, total acid number and carbonyl content rise dramatically.

The determination of the remaining useful lifetime of an oil must be done with care if the quantitative determination of an element is used (ASTM D-4628). Additives often contain characteristic elements (usually metals). Lubricating oils degrade by two main mechanisms, additive depletion and contamination. During the service lifetime of an oil, the additives are gradually consumed, and they also undergo a slight chemical change. This means that the presence of an additive metal, at a concentration equal to that of the unused oil, does not guarantee that the used oil will display similar properties. Elemental analysis can be used to monitor the presence of contaminants from corrosion, contamination, and engine wear, such as lead from bearings and blow-by products.

A method used to assess the quality of an oil, that has virtually been replaced by more facile modern techniques, is the measurement of its oxygen absorption characteristics. The oil could be titrated against peroxy radicals or merely heated in the presence oxygen, to obtain the induction time, prior to the maximum rate of oxygen absorption being attained [62,63]. This method was used to compare new and used oil formulations to compare the response of the oils to various additives. As a measure of oil quality, oxygen absorption techniques are slow and cumbersome, which has led to their replacement by other techniques. Lamparczyk and Weslowski [64] measured the quality of oils using standard test procedures (flash point, viscosity, foreign solids and oxide ash content), and compared the data obtained from these procedures to the data from thermal analytical techniques. The results were recorded in matrix form to allow a comparison to be performed. In a poorly written article, the procedure appeared to be unnecessarily complicated, and provided a rather laborious route to the characterization of oil quality. The technique used by the authors as a means to measure product quality is becoming increasingly popular. The authors cited some literature to allow the reader to have a better understanding of oil quality measurement using this method [64].

1.8 Materials

Three lubricating oil basestocks, supplied by MOD/DQA-TS, have been used for this work. The mineral oil (BSM-150N) is a low sulphur, North Sea distillate blended with a Middle East cut to enhance its properties [8]. The synthetic basestock (RTS-

9745) was made by oligomerisation of dec-1-ene, followed by hydrogenation of the product to produce an oil with a highly branched molecule [8]. LPE-504 is a pentaerythritol ester based, aviation grade basestock manufactured by Castrol [65]. The properties of these basestocks are given in table 1.1.

Table 1.1
Typical Properties of the Basestocks

Property	BSM-150N	RTS-9745	LPE-504
Density /g cm^{-3}	0.868 at 15°C	0.817 at 20°C	0.998 at 20°C
Pour Point /°C	0.1	-68	-57 to -70
Cloud Point /°C	-	-79	-
Flash Point /°C	201 (COC)	-	255 (COC)
Viscosity /cSt			
at -40°C	-	2900	8000
at 40°C	30.1	18.2	26.5
at 100°C	5.2	4.0	5.0
Viscosity Index	101	118	135
Average Mw	-	423	564

The antioxidants used for the work contained in this thesis were also supplied by MOD/DQA-TS. The amine is dioctyldiphenyl amine (DODPA) and the phenolic inhibitor 2,6, di-t-butyl 4, methyl phenol (Topanol 'O'). The properties of the antioxidants are given in table 1.2.

Table 1.2
Typical Properties of the Antioxidants

Property	DODPA	Topanol 'O'
Formula	$C_{28}H_{48}N$	$C_{15}H_{14}O$
Mw	398	220
M.Pt. /°C	98	70
B.Pt. /°C	-	265
Density /g cm^3	-	0.894 at 20°C

The standardised oil blends used for this work were made by dissolving 1.9% w/w

of the antioxidant in a basestock at room temperature. These blends were prepared in conical flasks which were then stoppered and wrapped in aluminium foil to exclude the light. The flasks were then shaken mechanically for at least one hour after the antioxidant had completely dissolved in the oil. Analytical solutions of lesser concentration consisted of solutions containing 0.05, 0.1, 0.2, 0.3, 0.4, 0.6, 0.8, 1.2 and 1.5% w/w antioxidant in the base oil. These standards were prepared by dilution of the primary standards with the base oils in glass sample tubes. The tubes were sealed with plastic screw lids containing a card seal. The sample tubes were wrapped in aluminium foil and shaken mechanically for at least one hour to homogenise the solutions. After preparation, the oil samples were stored in glass sample tubes in the dark at room temperature.

References

1. G. P. Bush, M. F. Fox, D. J. Picken and L. F. Butcher, *Institute of Petroleum Quarterly J. of Tech. Papers,* Jul-Sept 1988, p 49.
2. R. Larson, *Sci. Lubr.*, 10, 1958, p 12.
3. G. P. Wood, *J. I. P.*, 55, 1969, p 194.
4. L. R. Mahoney, K. Otto, S. Korcek and M. D. Johnson, *Ind. Eng. Chem. Prod. Res. Dev.*, 19, 1980, p 11.
5. A. C. M. Wilson, *J. I. P.*, 50, 1964, p 47.
6. B. D. Campbell, R. Gojon, Y. Serre and J. F. Warner, "Developments in Engine Bearing Design Techniques", *AE Group Technical Symposium,* 1986, Paper No 11.
7. A. Ali, F. Lockwood, E. E. Klaus, J. L. Duda and E. J. Tewksbury, *ASLE,* 22, 1979, p 267.
8. A. A. J. Cash, *Ph.D Thesis,* Dept. of Phys. Chem., Leeds Univ., 1988.
9. A. Zeman, *J. Synth. Lubr.*, 5, 1988, p 133.
10. D. G. Knorre, L. G. Chuchukina and N. M. Emanuel, In N. M. Emanuel, "The Oxidation Of Hydrocarbons In The Liquid Phase", Pergamon Press, London, 1965.
11. The American Society for Testing and Materials, Annual Book Of Standards, 1988. ISBN 0-8031-1163-0 (set).
12. D. W. Murray, J. M. MacDonald, A. M. White and P. G. Wright, *Pet. Rev.*, Feb 1982, p 36.
13. S. J. Leonardi, E. A. Oberright, B. A. Orkin and R. V. White, *A. C. S. Meeting, Div. Petroleum Chemistry, General Papers, Miami,* April 1957, p 35.
14. A. J. Burn and G. Greig, *J. I. P.*, 58, 1972, p 346.
15. V. Vesely, *Rhopa Uhlie,* 11, 1969, p 297.
16. G. H. Denison and P. C. Condit, *Ind. Eng. Chem.*, 37, 1945, p 1102.
17. D. Barnard, L. Bateman, M. E. Cain, T. Colclough and J. I. Cunneen, *J. Chem. Soc.*, 1961, p 5339.
18. J. A. Walker and W. Tsang, *NBS Spec. Publ. 584,* Proc. Joint Conf. On Measurements And Stds. For Recycled Oil/Systems Performance and Durability Held at NBS, Gaithersburg, MD, Oct 23-26, 1979 (issued 1980), p 271.
19. R. E. Rebbert, *NBS Spec. Publ. 584,* Proc. Joint Conf. On Measurements And Stds. For Recycled Oil/Systems Performance and Durability Held at NBS,

Gaithersburg, MD, Oct 23-26, 1979 (issued 1980), p 237.

20. R. K. Hewstone, *Institute of Petroleum Quarterly Journal Of Technical Reports,* Jan-Mar 1988, p 49.
21. R. L. Blaine, *NLGI spokesman,* June 1976.
22. J. L. Bolland, *Quarterly Reviews,* 3, 1949, p 1.
23. L. Bateman, *Quarterly Reviews,* 8, 1954, p 147.
24. L. Reich and S. S. Stivala, "Autoxidation of hydrocarbons and Polyolefins. Kinetics and mechanisms", Dekker, New York, 1969.
25. D. M. Brown and A. Fish, *Proc. Roy. Soc.,* A 308, 1969, p 547.
26. S. W. Benson, "Thermochemical Kinetics", Wiley, New York, 1968.
27. E. R. Bell, J. H. Raley, F. F. Rust, F. H. Seubold and W. E. Vaughan, *Faraday Soc. Disc.-10, Hydrocarbons,* 1951, p 242.
28. R. W. Walker, *Chem. Soc. (Spec. Period. Rep.),* 1, 1975, p 297.
29. M. P. Halstead, L. J. Kirsch, A. Prothero, C. P. Quinn, *Proc. Roy. Soc.,* A 346, 1975, p 515.
30. R. A. Cox and J. A. Cole, *Combust. and Flame,* 60, 1985, p 109.
31. K. U. Ingold and I. E. Puddington, *J. I. P.,* 44, 1958, p 168.
32. L. Mandlecorn and E. W. R. Steacie, *Can. J. Chem.,* 32, 1954, p 474.
33. M. Szwarc, *Faraday Soc. Disc.-10, Hydrocarbons,* 1951, p 143.
34. J. R. Lodwick, *J. I. P.,* 50, 1964, p 297.
35. J. F. Ford, *J. I. P.,* 54, 1968, p 198.
36. M. Kawamura, *Wear,* 77, 1982, p 287.
37. A. J. Burn, R. Cecile and V. O. Young, *J. I. P.,* 57, 1971, p 319.
38. A. D. Brazier and J. S. Elliot, *J. I. P.,* 53, 1967, 63.
39. M. D. Johnson, S. Korcek and M. Zinbo, *SAE Spec. Publ. 558,* 1983, p 71.
40. J. L. Paddy, C. J. Lee, D. N. Waters and W. Trott, *STLE Trib. Trans.,* 33, 1990, p 15.
41. J. L. Paddy, P. S. Brook and D. N. Waters, *J. Chem. Soc. Perkin Trans. II,* 1989, p 1703.
42. S. M. Hsu and R. S. Lin, *SAE Spec. Publ. 558,* 1983, p 61.
43. O. M. Reiff, *Ind. Eng. Chem.,* 33, 1941, p 351.
44. J. L. Bolland and P. ten Have, *Disc. Far. Soc.,* 2, 1947, p 252.
45. A. F. Bickel and C. E. Kooyman, *J. Chem. Soc.,* 2, 1956, p 215.
46. J. H. Gilks, *J. I. P.,* 50, 1964, p 309.
47. C. J. Pederson, *Ind. Eng. Chem.,* 48, 1976, p 1881.
48. R. H. Rosenwald, J. R. Hoatson and J. A. Chenicek, *Ind. Eng. Chem.,* 42,

1950, p 162.

49. H. C. Bailey, *Ind. Chem.*, May 1962, p 215.

50. E. M. Bickoff, *J. Am. Oil Chem. Soc.*, Feb 1951, p 65.

51. Z. Pawlak, E. Giersz, G. Urbanczyk, R. M. Izatt and J. L. Oscarson, *Thermochim. Acta,* 154, 1989, p 187.

52. S. M. Hsu, A. L. Cummings and D. B. Clark, *SAE Technical Paper No. 821252,* 1982.

53. P. A. Asseff, *SAE Technical Paper No. 770642,* 1977.

54. H. H. Abou El Naga and A. E. M. Salem, *Wear,* 96, 1984, p 267.

55. R. E. Kaufmann, U. S. Patent, Patent No. 4,744,870, May 17, 1988.

56. R. E. Kaufmann and W. E. Rhine, *Lubr. Eng.*, 44, 1988, p 154.

57. K. F. Abas, I. Sadek, *Thermochim. Acta,* 126, 1988, p 181.

58. A. Zeman and P. Bartl, *Fresenius Z. Anal. Chem.*, 316, 1983, p 43.

59. J. R. Barcelo and C. Otero, *J. I. P.*, 50, 1964, p 15.

60. R. Cecile, *J. I. P.*, 59, 1973, p 201.

61. S. Korcek, L. R. Mahoney, M. D. Johnson and S. Hoffman, *SAE Technical Paper No. 780955,* 1978.

62. J. H. T. Brook, *J. I. P.*, 48, 1967, p 7.

63. S. Korcek, L. R. Mahoney, M. D. Johnson and K. Otto, *NBS Spec. Publ. 584,* Proc. Joint Conf. On Measurements and Stds. For Recycled Oil/Systems Performance and Durability Held at NBS, Gaithersburg, MD, Oct 23-26 (issued 1980) p 227.

64. H. Lamparczyk and Weslowski, *Thermochim. Acta,* 159, 1990, p 235.

65. S. R. Wallis, Castrol Research Laboratories, Pangbourne, Essex, Private Communication, 1990.

Chapter 2

Thermal Analysis

2.1 Introduction

The IUPAC accepted definition of thermal analysis is 'a group of techniques in which a physical property of a substance and/or its reaction products is measured as a function of temperature whilst the substance is subjected to a controlled temperature programme'. The naming of the thermal analytical technique depends on the physical property being measured [1].

The thermal analytical work described in this thesis has been performed using a Du-Pont heat flux differential scanning calorimeter (DSC) model 990. Some measurements have been performed using a Stanton Redcroft simultaneous differential thermal analyzer/thermal gravimetric analyzer (DTA/TG) model STA-781. The STA-781 will be described in appendix 3. Unless specifically stated, all the underlying theory contained in the text will apply to the Du-Pont DSC.

Thermal analytical techniques either singly or in combination with other analytical methods have been regularly applied to quality control measurements. Thermal analysis has found application in many different areas of science and technology. These techniques are widely employed in the polymer and pharmaceutical industries owing to the high repeatability* and short duration of the experiments. The various techniques have been used in the textile, ceramic, nuclear, petroleum, pyrotechnic, paint, and metallurgical industries, because of their versatility. The properties that can be measured include the glass transition, melting, boiling, sublimation, or solid phase transitions, the specific heat capacity, latent heat of fusion, the hardness or the thermal expansion. The extent of a chemical reaction can be followed by monitoring any one physical property.

The history of thermal analysis was reviewed by MacKenzie in a special edition of Thermochimica Acta in 1984 [2]. The following text is a brief summary of the development of the techniques employed in this research.

** The terms repeatability and reproducibility are of considerable importance to the IP in establishing standard test procedures. Repeatability is defined in terms of results obtained by the same operator working on the same equipment on the same day. Reproducibility is defined in terms of results obtained by different operators, working on different equipment in different laboratories.*

The earliest thermo-analytical experiments concerned the study of cooling curves. In the 19th century Le Chatelier showed that thermocouples could be used for accurate temperature measurements [1]. Heating curves were first described by Le Chatelier in 1887 [3] for the analysis of minerals. The analysis of heating curves involved measuring the temperature of the sample, whilst it was subjected to a temperature programme. The technique described by Le Chatelier was improved upon by Roberts-Austin [4], who increased the sensitivity by using a differential temperature signal, ΔT, thus creating the DTA technique. Initially the use of DTA was sporadic and it was not until 1948 that the first commercial DTA apparatus appeared on the market. Prior to the introduction of commercial instruments, all DTA measurements were performed using purpose built equipment. DTA is the oldest thermal analytical technique, but it is rarely used in its original form. The experimental method at the time was based on the temperature sensors being located within the sample and reference materials themselves. The magnitude of the differential signal was dependent on the thermal resistances within the sample and the reference materials, which rendered the conversion of the measured signal into energy units unreliable. The experimental method was improved further by Boersma [5] in 1951, who located the thermocouples under the sample and reference holders. Boersma DTA is much less dependent on the variable thermal resistances of the sample and reference, which means that the differential signal can be converted into energy units. Boersma DTA is still regarded as a qualitative technique, because the calibration coefficient of the cell relating the differential signal to thermal energy is temperature dependent. A calibration of the apparatus using reliable standards must be performed over its working temperature range to obtain reliable calorimetric measurements.

DSC is a more recent technique than DTA. It was described by Watson et al. [6] in 1964. The first commercial instrument was manufactured by Perkin Elmer. The instrument maintains the sample and the reference materials at the same temperature by applying an electrical signal to individual heaters underneath the sample and reference platforms. The technique has become known as power compensation DSC. In power compensated DSC the measured quantity is proportional to the difference in electrical power required to maintain the sample and reference at the programmed temperature. The signal output is proportional to the differential thermal power ($d\Delta Q/dt$) between the sample and reference. The term heat flux DSC was used by manufacturers of Boersma DTA equipment (such as Du-Pont) to protect their market interests, because the technique known as DSC was proclaimed by Perkin Elmer to be

the only route to quantitative results. In most heat flux DSC apparatus, the instrument signal is derived from a temperature difference established between the sample and the reference. The difference between Boersma DTA and heat flux DSC is very small, the DSC apparatus containing electronic circuitry to linearise the energy calibration curve. In DTA experiments the differential temperature signal is measured, but in heat flux DSC, in which the assembly is very similar, the signal output is the rate of heat flow ($d\Delta Q/dt$) derived from the ΔT signal. The different thermocouple and furnace geometries for DTA and DSC apparatus are illustrated in figure 2.1.

It may be seen that both power compensated and heat flux DSC provide an output signal proportional to the differential thermal power ($d\Delta Q/dt$). The difference between the two types of DSC is the origin of the signal. The output signal when recorded as a function of temperature or time leads to the evaluation of the energy change. The advantage of power compensated DSC over heat flux DSC is that higher heating rates can be employed, whilst heat flux DSC may be used at higher temperatures. Modern commercial DSC equipment is operated by dedicated computer systems and may be linked to a wide range of analytical equipment for evolved gas analysis. The computerised equipment have the capability for fine atmosphere control with the facility to switch or use mixed gases. The heating rates available extend up to 200°C min^{-1}, while the temperature ranges are from -100 to +2000°C. In some instruments, the sample may be irradiated by UV light in situ during the temperature programme.

In both classical (created by Roberts-Austin) and Boersma DTA, the calorimetric sensitivity of the apparatus is dependent on the temperature, heating rate, sample mass, the thermal resistance of the system and sample characteristics (thermal conductivity and heat capacity) [7]. This is not the case for power compensated DSC. Van Humbeek and Bijvoet [7] noted that the Du-Pont DSC proved to be a very sensitive piece of equipment with an instrument sensitivity independent of the furnace temperature, but claimed that it would be more appropriate to name the system a "calorimetric DTA". The authors studied the effects of sample mass, heating rate and temperature on the sensitivity of a Du-Pont DSC coupled to a '910 cell base' and a '990 thermal analyzer'. The authors discovered that the instrument possessed a calibration coefficient dependent on the heating rate, sample mass and heat exchange, but (similar to a Perkin Elmer DSC) independent of the temperature.

The experimental methods are so sensitive that, to ensure the repeatability of the

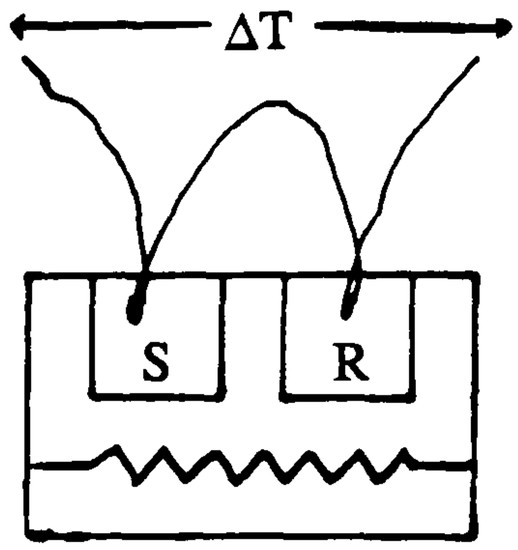

Single Heat Source

Classical DTA

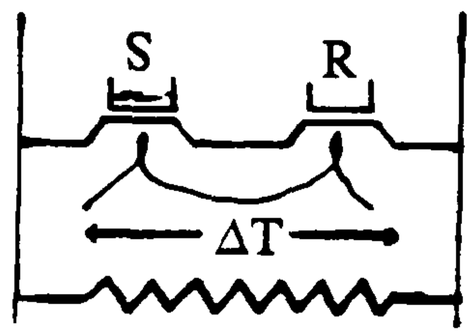

Single Heat Source

Boersma DTA

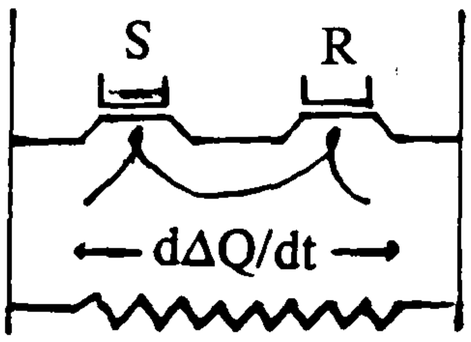

Single Heat Source

Heat Flux DSC

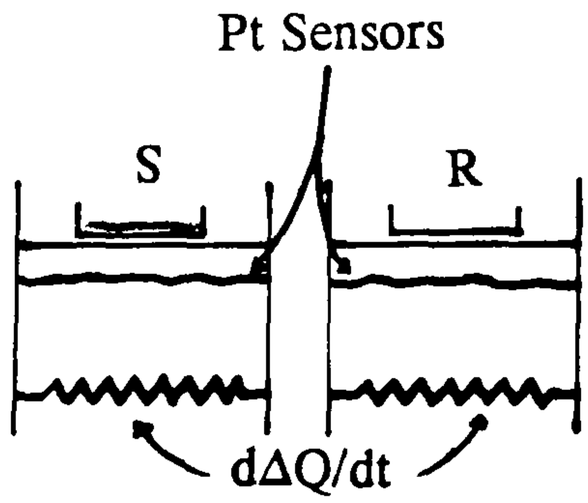

Individual Heaters

Power Compensated DSC

Figure 2.1

The Different Thermocouple and Furnace Geometries Employed in DSC and DTA

results, the positioning of the sample pans, the choice and flow rate of the purge gas must remain constant. The many variables that can affect the reproducibility and repeatability of an experiment will be discussed in further detail in a later section of this thesis.

2.2 Description of the Du-Pont Apparatus

The commercial development of heat flux DSC has led to the introduction of a disk type cell in which the thermocouples form part of a platform. Probably the best known disk type DSC is the Du-Pont system used in the present work. The disk provides the thermal leakage between the sample and reference which leads to the output signal. Different designs of the disk type DSC are used by other manufacturers such as Mettler. These are based on the same operating principles as the Du-Pont apparatus. The Du-Pont design of the DSC cell has been particularly successful and has therefore remained unchanged for many years. The Du-Pont DSC produces an output signal that is very reproducible and noise free. A high sensitivity is obtained via an amplification of 30,000 times and a temperature independent calibration is achieved by linearising the signal.

The Du-Pont DSC-990 consists of three separate component systems, the 990 programmer-controller, the 910 cell base and interchangeable cells. The interchangeable cells accepted by the 990 system allowed DSC, DTA, DTG and TMA analysis. Only the DSC system and cell will be described in the following text. The 990 system, although old and out of date with respect to micro-computer controlled technology was a sensitive, precise and reliable piece of equipment, that employed the same principles as any other controller.

2.2.1 The DSC Cell

The DSC cell (figure 2.2) used a constantan disk to support the sample and reference pans, the sample on the front platform and the reference on the rear. The sample pan location could be aided by the use of a special tool, designed by Yuen and Yosel [8] to improve the reproducibility of each experiment. The temperature of the sample and reference materials were measured by type K (chromel/alumel) thermocouples welded to the underside of the disk. The difference in these signals was amplified in the cell base and recorded on the 990 'two pen' (X-Y-Y') chart recorder. The other pen of the chart recorder recorded the temperature signal obtained from a chromel/alumel thermocouple formed by an alumel wire being welded to the underside

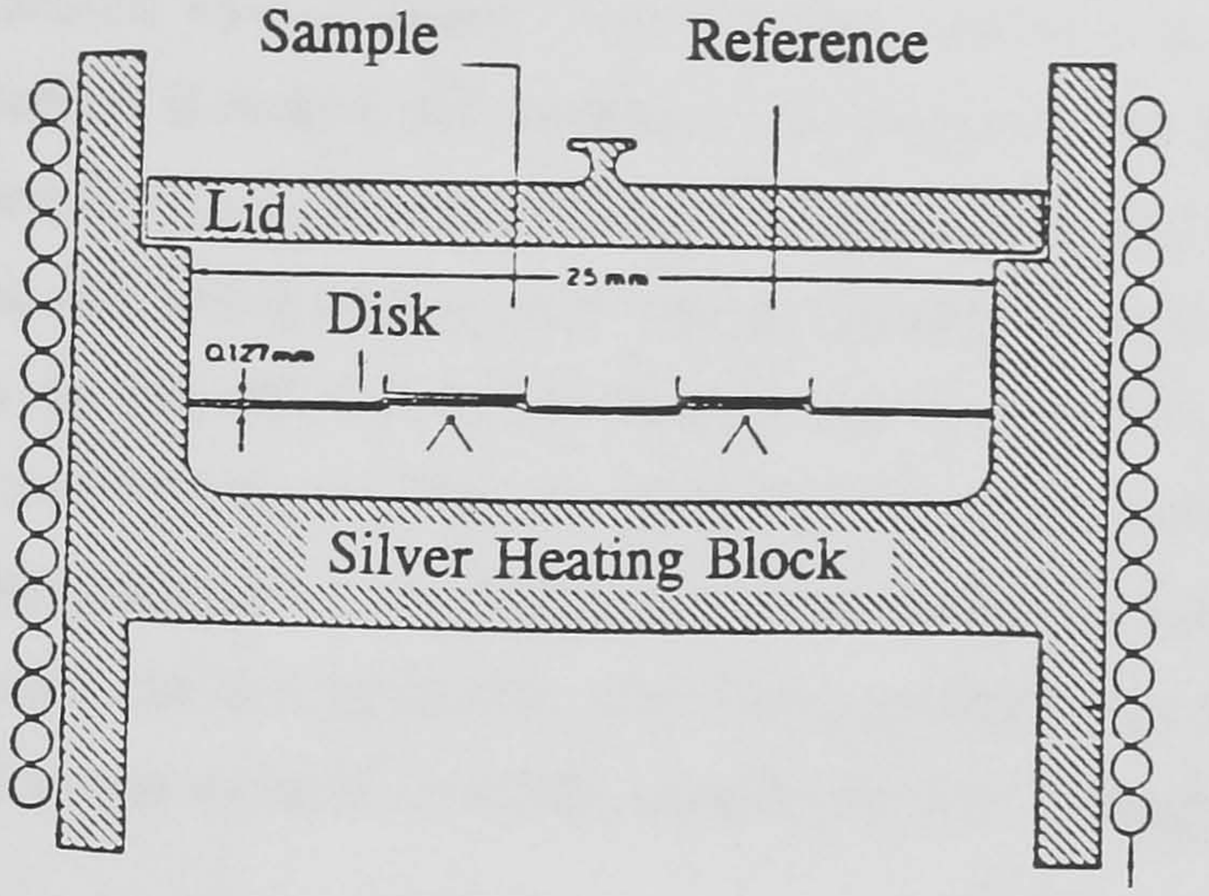

Figure 2.2

The Du-Pont DSC Cell

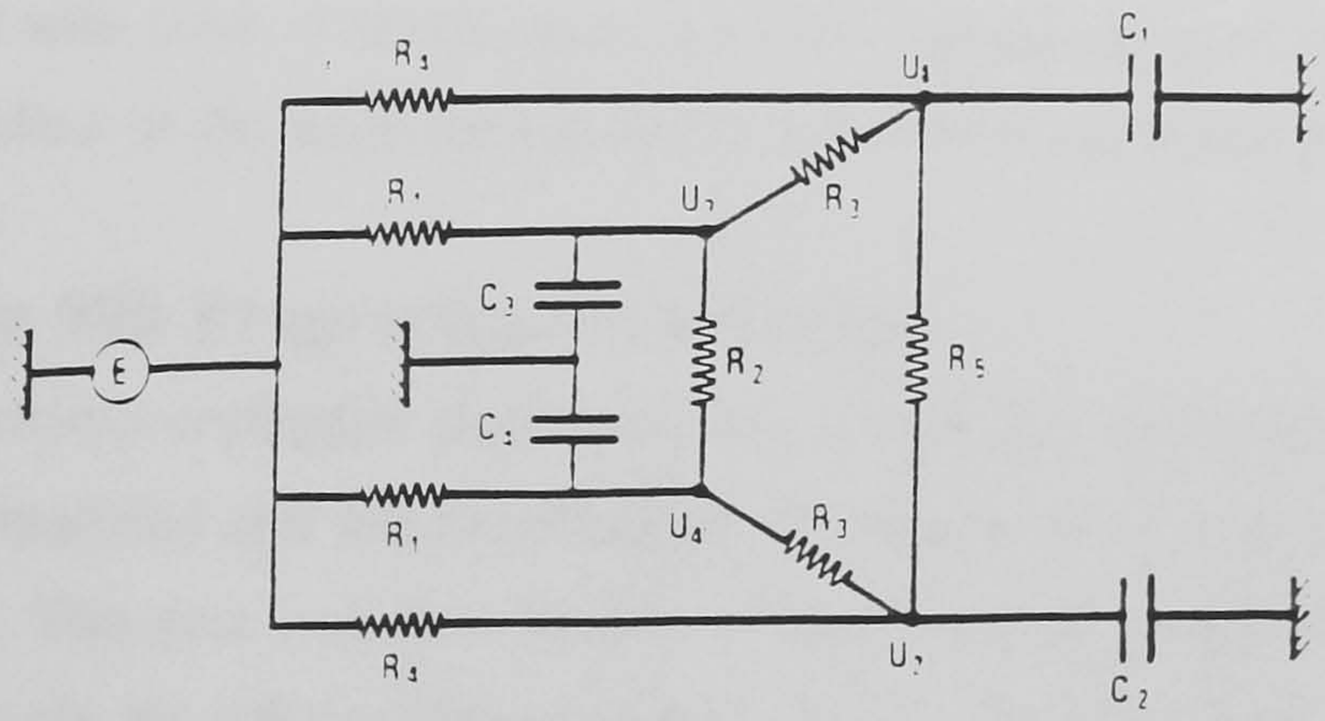

E Furnace temperature; C_1, C_2 thermal capacitors of the sample + crucible and reference + crucible respectively; C_3, C_4 thermal capacitors of the disk; R_1 furnace-crucible thermal resistor (through the disk); R_2 crucible-crucible thermal resistor (through the disk); R_3 disk-crucible thermal resistor; R_4 furnace-crucible thermal resistor (through the gas); R_5 crucible-crucible thermal resistor (through the gas); U_1, U_2, U_3, U_4 temperatures of the sample crucible, reference crucible, disk below the sample crucible and reference respectively

Figure 2.3

The Electrical Circuit Employed by Claudy et al [12]

of the sample platform. To balance the thermal environment of the cell a dummy wire was welded underneath the reference platform.

The cell was heated by a resistive wound heater surrounding the silver heating block in which a platinel II control thermocouple was encased. The majority of the heat from the silver block flowed to the sample and reference platforms radially through the constantan disk, the remaining heat transfer being provided by convection through the gas from the silver lid and cell walls. The furnace had the capacity to heat the sample at a linear rate up to 100°C min^{-1}. The low thermal mass of the furnace allowed a fast rate of cooling. The purge gas entered the sample chamber through a hole in the cell block midway between the two platforms, after being preheated by circulation through the heater block. The gas escaped from the sample chamber through a hole in the cell lid.

The cell design has enabled a high pressure version to be constructed. For some time the Du-Pont high pressure DSC was the only one available commercially. The design and construction of the Leeds University high pressure apparatus is described in a separate section of the text. The pressurisation of the DSC cell has accelerated the distortion of the constantan disk. The disk over a period of several years became concave, consequently both the calibration coefficient and thermal power baseline of the cell altered with time. The deformation of the disk and drift of the cell calibration coefficient resulted in the need for regular calibration experiments to be performed.

2.2.2 The 990 Programmer-Controller

The programmer-controller performed two completely independent functions, the control of the modules and the recording of the results of an analysis on an X-Y-Y' chart recorder. The data was also latterly recorded on an Amstrad PC 1640-HD20 microcomputer via an A/D converter constructed in the School of Chemistry at the university. The program mode was chosen using push button switches, with the initial and final temperature set points being selected by thumb-wheel switches. The analyser operates over a temperature range of -100 to +700°C, although 500°C was never exceeded in the present measurements. The heating rate could be varied between 0 and 100°C min^{-1} at a claimed accuracy of 2% and a reproducibility of 1%. Three of the ramp rates could be selected by the operator. In the isothermal mode, the temperature drift was stated to be no more than 1%. The full specifications of the programmer-controller are given in the manufacturers operating guide [9].

2.2.3 The 910 Cell Base

The 910 cell base was connected to the programmer by a multi-core cable and supported one of the four ancillary cells. The cell base amplified the instrument signal which was fed to the chart recorder (incorporating a switch to increase the sensitivity five fold) by a factor of 30,000 times. This is a very impressive figure which provides an indication of the excellent design and construction of the furnace. The maximum sensitivity of the cell is 0.04 mJ corresponding to a 10 mV full scale deflection on a chart recorder. The cell base also housed an electronic reference junction compensator, thus eliminating the need for an ice junction. The cell base controlled the baseline slope and the retention of a constant calorimetric sensitivity throughout the temperature range of the cell. It is apparent that the increase in thermal conductivity of the purge gas (when combined with the decrease in differential thermocouple sensitivity) with rising temperature leads to a marked decrease in apparatus sensitivity. The retention of a constant calorimetric sensitivity was intended to eliminate the need for energy calibrations at fixed temperatures, but owing to the age of the apparatus, energy calibrations were required.

2.3 An Investigation of a Disk Type DSC Cell

The theory of operation of a disk type DSC cell has been described by Lee and Levy [10], specifically for the Du-Pont apparatus. Claudy et. al. in a series of 3 publications [11-13] studied the heat transfer in a disk type DSC. They constructed a model to represent the data theoretically. The objective was to account for the peak shapes of thermal analysis curves obtained using Du-Pont and predominantly Mettler equipment.

Lee and Levy [10] explained why the sample is analysed with respect to an inert reference. The authors initially described a calorimeter which contained only a sample holder. They said that if the temperature difference across a thermal resistance, ΔT_s, (between the heater and the sample holder) is measured, the power conducted to the sample holder could easily be determined. The heat leakage through the gas was calculated to be approximately 750 times larger than that absorbed by the heat capacity of the sample [10]. Therefore the heat capacity of the sample would have to be deduced from a small change in the temperature difference, ΔT_s. The addition of the reference holder produces a significant improvement in the apparatus sensitivity when the differential temperature is measured between the sample and reference holders (this was initially described by Roberts-Austin [4]). This is ascribed to the heat capacities of the

sample and reference holders cancelling. Furthermore the heat leakages through the gas and the cell tend to cancel (especially at low sample heat capacities or heating rates). The direct thermal link between the sample and reference platform in the Du-Pont cell reduces the sensitivity of the apparatus slightly. A slit in the disk to separate the sample and reference platforms by eliminating the direct thermal link would increase the sensitivity of the apparatus slightly. The Du-Pont DSC does not incorporate a slit in the disk between the two platforms, because sample material falling into the thermocouple region below the disk is highly undesirable [10], although one is present in some instrument designs.

The perfect balance between the leakage fluxes is the major problem encountered when a reference cell is employed [10]. This can be overcome by placing a shield around the holders which follows the temperature of the heat source. The use of the shield reduces the temperature difference between the sample holder and the 'walls' of the apparatus (which would otherwise be a room temperature heat sink).

Lee and Levy [10] employed an analogue electrical circuit diagram to represent the DSC cell, from which they calculated its sensitivity. The authors condensed the sample (and reference) pan and material to points or 'nodes'. This was to simplify the model. They showed that the ΔT signal is related to the differential heat flow from the sample and reference nodes, and that (as previously mentioned) the heat leakage between the two platforms accounted for a slight decrease in sensitivity. The model of Lee and Levy [10] incorporated values for the heat capacities of the sample and reference pans, plus that of the constantan disk. They showed that the ΔT signal is related only to the heat capacity of the sample, not the pans and the regions of the disk surrounding the platforms, which cancel. It was claimed [10] that this characteristic forms the basis of heat capacity measurements by heat flux DSC. The thermal resistance of the constantan disk was calculated using an electrical analogue model, constructed from tin oxide coated in glass, with electrically conducting electrodes 'electrically' cemented to the glass coat [10]. The electrical resistances of the model were transformed to thermal resistances, from which the resistance between the two platforms was calculated to be 200 K W^{-1}. The resistance between the platforms and the furnace were calculated to be 70 K W^{-1}. A computer model was then used to check the results, the latter resistance was revised to 75 K W^{-1}.

Heat transfer between the sample and the constantan disk is dominated by the

thermal conductivity of the gas in the interfacial region between the pan and the disk, not by metal to metal contact. This was illustrated by the drop in interfacial conductance when the cell was evacuated, and the improvement of heat transfer when the sample is tightly packed [10]. Claudy et. al. [11] used both a Du-Pont DSC-990 and a Mettler TA 2000B to show that the thermal resistivity of the purge gas had a large influence on the peak area (therefore the sensitivity of the apparatus). If the purge gas possesses a high thermal resistance the peak area for a given transition would be expected to be small. In practice this is not so, because the thermal loss owing to a purge gas with a low thermal resistance is greater. When the purge gas has a high thermal conductivity, the heat flux from the sample passes through the gas and not to the thermocouple.

For a first order transition, Lee and Levy [10] showed that the leading edge of the peak possessed a constant slope, proportional to the heating rate. The exponential decay of the trailing edge was attributed to heat uptake proportional to the heat capacities of the sample, the pans and the constantan disk as they caught up to their normal temperature lag behind the furnace temperature. A model of the constantan disk, containing a series of concentric segments, each possessing its own heat capacity and thermal resistance in a radial direction, was used to calculate the response time of the apparatus. For a first order transition, the calculated response time was 5.4 s, which compared favourably to the experimentally determined value of 5.1 s.

Lee and Levy [10] concluded that the theory of operation of a 910 DSC is straightforward. The bridging resistance (the link between the sample and reference platforms) was found to exclude sample material from the thermocouple region at the expense of a slight reduction in instrument sensitivity. They showed that for heat capacity and transition energy measurements, the temperature difference between the sample and reference platforms related to the same constant. The constant was derived from the thermal equivalent of Ohm's law to be $(1/R + 1/R_g + 2/R_b)$, where R is the thermal resistance between the sample (or reference) pan and the heater, R_g is the resistance of the gas and R_b is the bridging resistance.

In a series of publications Claudy and co-workers [11-13] compared experimental results to those from a model to validate the model. The model was used to illustrate the direction and magnitudes of the heat fluxes within the DSC cell. The model was eventually used to correct for temperature lag when the instrument was used in the

scanning mode. They showed [11] that the peak shape depended markedly on the nature of the reference material. In their study, the authors compared the fusion peaks of indium measured against an inert reference to those obtained using an indium reference or one with a melting point lower than that of the sample. In the subsequent publication of the series, the authors represented their results on a theoretical model [12]. The model was based on a Mettler TA 2000B, but it applies equally well to the Du-Pont DSC cell, and included four assumptions.

1 the thermal resistors and capacitors were localised,

2 the apparatus can be represented by a symmetrical model,

3 the gas surrounding the disk was conducting, and

4 the crucibles and samples were represented to points.

A comparison was made between the results obtained using reference materials in which the temperature was allowed to fluctuate with those where no temperature change occurred. The electrical model used by Claudy et. al. [12] was slightly more complicated than that used by Lee and Levy [10], as it allowed for the conduction of heat between the sample and the reference pans by the purge gas (figure 2.3). Claudy et al. [12] used their model to demonstrate that "the heat flow exchanged between the crucibles through the disk does not depend on the temperature of the furnace". The authors also showed that the heat flow between the sample and reference materials was independent of the furnace temperature.

Claudy and co-workers [12] calculated iteratively the values of each resistance in the cell by using their electrical analogue model. The response of the cell to the melting of indium against an inert reference was calculated by employing the thermal resistances previously calculated. The calculated response matched that of the experimental results very closely, thus proving that the chosen values for the resistances, heat capacities, temperature gradients and thermocouple sensitivity within the DSC model matched those of the real apparatus. The model was tested further, for a system in which indium was melted with reference to another indium sample of greater mass. Once more the calculated results matched those of the experiment almost perfectly. The authors [12] then concluded that the model correctly represented the calorimeter, despite the assumption made that the thermal resistance between the sample and the reference crucible is constant. They showed experimentally that the resistance varied during an analysis, causing a slight change in the calorimetric signal. A more complex electrical analogue model, one that considers the variable resistance, may provide a better fit to the experimental data, but the determination of every

resistor or capacitor in the model would prove difficult [12].

The third publication in the series by Claudy et. al. [13] considered the 'theoretical and experimental correction of the calorimeter signal in the scanning mode'. The investigation was to enable a correct interpretation of the thermal effect of a transition. They stated that in a purity determination experiment, the purity found depended heavily on the apparatus used. The authors used a Mettler TA 2000B DSC, and showed that for an accurate calibration or purity determination experiment, the sample had to be a piece of foil that covered the bottom of the pan, rather than a piece of wire. They made no mention of a finely powdered sample spread evenly over the pan base, which would be more convenient to handle and introduce into the sample pan. The thermal gradient within the sample pan was investigated by placing two pieces of pure indium in a pan, one as close to the furnace as possible and the other as close to the centre of the pan as possible. Two peaks were obtained that represented the melting of each piece of indium. The thermal gradient across the pan was deduced as 0.1 K at a heating rate of 1 K min^{-1}.

The model used by Claudy and co-workers [13] was based on the electrical representation used in the second part of their study [12]. Estimates of the thermal effects within the cell were used in a simple deconvolution model, to predict the sample purity. The assumption made in the model was that if a short sampling period was used, the thermal effects occurring within the sample were constant (or at least their values could be interpolated linearly), therefore only a very small error would be introduced into the final result. The model was tested as follows. A purity determination experiment was conducted whereby the resistance between the sample and the pan was increased (by placing aluminium foil on the pan base). The peak shape obtained was drastically altered, the leading edge of the peak was not so steep and the melting temperature was 0.2 K higher than a sample measured without the increased resistance. The mathematical model was used to correct the signal (allow for the increased thermal resistance), and the correct melting temperature was deduced. The purity of the sample was deemed to be slightly lower than that of the pure sample without the aluminium foil present on the pan base. The model was also used to discriminate between samples of differing purity. The high and low purity samples were identified and their levels of impurity accurately determined.

The text in this section has discussed the work of Lee and Levy [10] and Claudy

et al. [11-13]. The authors have shown that the modelling of a disk type DSC is possible and from the models an understanding of the performance of the apparatus is possible. The relationships of the heat fluxes to temperature, heat capacities and the thermal resistances within the cell may be investigated using models. The model constructed by Claudy et al [12,13] was shown experimentally to provide a close representation of a disk type cell, but no kinetic information about a sample may be obtained from such a model.

2.4 The Need for High Pressures

It has already been mentioned that Du-Pont were for many years the only manufacturers to provide a commercial high pressure DSC cell. As a consequence Du-Pont captured the market where such measurements were important, e.g. the study of hydrocarbon oxidation. The increased flexibility obtained from using an elevated pressure has persuaded other manufacturers to include a high pressure cell in their product range. Although the use of elevated pressures may facilitate the analysis of many different types of compounds, the discussion contained in this section will be restricted to the analysis of oil samples.

The operation of an experiment under high pressure reduces the volatility of the sample and helps to saturate the sample with the carrier gas. The use of an elevated pressure may help to increase the definition of the thermal analysis curve by eliminating the slow process of the diffusion of the carrier gas into the sample. It has been stated by Brown et al [14] that in oil oxidation experiments the time taken for an oxygen molecule to diffuse to the centre of a typical sample was approximately 0.5 seconds. The analysis of oils using a dynamic test at atmospheric pressure has always been less discriminating (largely owing to sample volatility) than isothermal tests conducted at elevated pressures. An atmosphere of air at 500 lbf in^{-2} (3,500 kPa) is employed in the latest dynamic test to be investigated by the Institute of Petroleum thermal analysis panel STG-9. The repeatability and reproducibility of the dynamic method has already noticeably improved.

At this point it should be noted that the STG-9 panel, on consultation with a Health and Safety Executive publication [15] have recently decided to "recommend the use of air for appropriate high pressure methods, except for instances where oxygen is necessary. The use of oxygen is considered necessary only where air gives unserviceable results. In using oxygen the operator is considered to be aware of the

dangers arising from the use of oxygen under pressure" [16].

The use of air or oxygen under pressure for the study of the oxidation characteristics of hydrocarbons has two major practical advantages over the use of atmospheric pressures.

1. Under dynamic conditions the peak maximum temperature is reduced, despite the peak onset temperature rising slightly. This results in sharper and more clearly defined peak shapes. This facilitates both qualitative and kinetic analysis.

2. Under isothermal conditions the induction time that elapses before the sample oxidation takes place is reduced [17]. The sample oxidises at a greater rate which causes the peak height to increase. The onset of oxidation is more clearly defined which assists sample analysis. It is however very evident that the use of oxygen or air under pressure reduces the temperature at which sample analysis is performed, thus restricting the sample volatility.

The study of the spontaneous ignition temperature of oils using DSC has only been possible practically through the use of high pressures. High pressures are used to simulate the conditions encountered in turbines and compressors [18,19]. One difference from non-ignition experiments was that the onset temperature was found to decrease with increasing oxygen pressure.

A final suggestion regarding the need for high pressures, is that DSC experiments are designed to act as a screening test before the final engine testing of a new oil blend. A requirement of screening tests is that they offer a quick and simple method of qualitative analysis. Small samples of oil are used, to allow the droplet to spread out evenly over the pan base and present a thin film of oil to the carrier gas. It has been stated that the use of elevated pressures increases the partial pressure of oxygen in the system and therefore saturates the sample with oxygen. This means that the differences in induction time or onset temperature between samples can only be due to variations in their oxidative stability.

2.5 The High Pressure Apparatus

The apparatus used for the initial oxidation experiments employed the high pressure vessel described previously by Cash [20], who designed the unit. The cell, capable of withstanding pressures of 2,200 lbf in^{-2} (14,000 kPa), was free-standing and connected to the 910 cell base by a length of 9 core electrical cable.

The DSC cell was mounted in a pressure vessel similar to that described by Levy [21]. The pressure vessel was constructed from a non magnetic stainless steel tube, 18 cm high with an internal diameter of 7.5 cm, and an external diameter of 9 cm. Three long bolts passed from under the base outside the pressure jacket and screwed into the lid at the top. The base plate was 20 cm square and the lid was 13 cm in diameter, each were made of steel, 3 cm thick. A pressure seal was obtained by two viton 'O' rings between the top and bottom internal surfaces of the cylinder and the base and lid respectively. The furnace and radiation shields were mounted on the base plate, which also contained an inlet and outlet port for the purge gas and a 9 way electrical lead through, for the electrical connections. The gas supply was controlled by a medium fine valve (Whitey, type BO-RS2) and passed through a pipe to the base of the furnace beneath the plate thermocouples. A fine control valve (Whitey, type SS21-RS2) was used to release the gas from the pressure vessel. Between the inlet valve and the baseplate was a safety valve (Nupro, type R3A) set to open at 1,200 lbf in^{-2} (8,330 kPa). The pressure at the inlet port was measured by a calibrated Matheson test gauge (part No. 63-5613), which had a resolution of 2 lbf in^{-2}.

When experiments were performed over the course of a day under elevated pressures, the vessel became hot to touch. This caused the set temperature of the apparatus to fluctuate and the reproducibility of the experiments to suffer. To overcome this, a water-cooled pressure vessel was constructed. The water-cooled vessel was designed to fit on the base of the initial high pressure assembly. The vessel had an inside diameter of 7.6 cm, was 21.5 cm high, with a wall thickness of 0.6 cm and a lid 3 cm thick. The vessel was bolted to the base and the lid held in position by three bolts. The new jacket (figure 2.4) reduced the convection of heat from the pressure jacket walls and eliminated the slow set temperature drift noted during the course of the day. This arrangement was used for the remainder of the thermal analysis work.

2.6 Chemical Calibration

The apparatus was calibrated using the fusion peaks of the usual chemical standards, indium, tin, lead and zinc. The calibration constant of the cell, ϵ (W V^{-1}) was defined as

$$\epsilon = A \times \Delta H_{fus} / \text{peak area},$$

where ΔH_{fus} was the enthalpy of fusion (J), and A the amplification of the signal. The peak area was measured in units of V s. The temperature and enthalpy of fusion of the metals are given in table 2.1. The temperature of fusion of the metals under excess

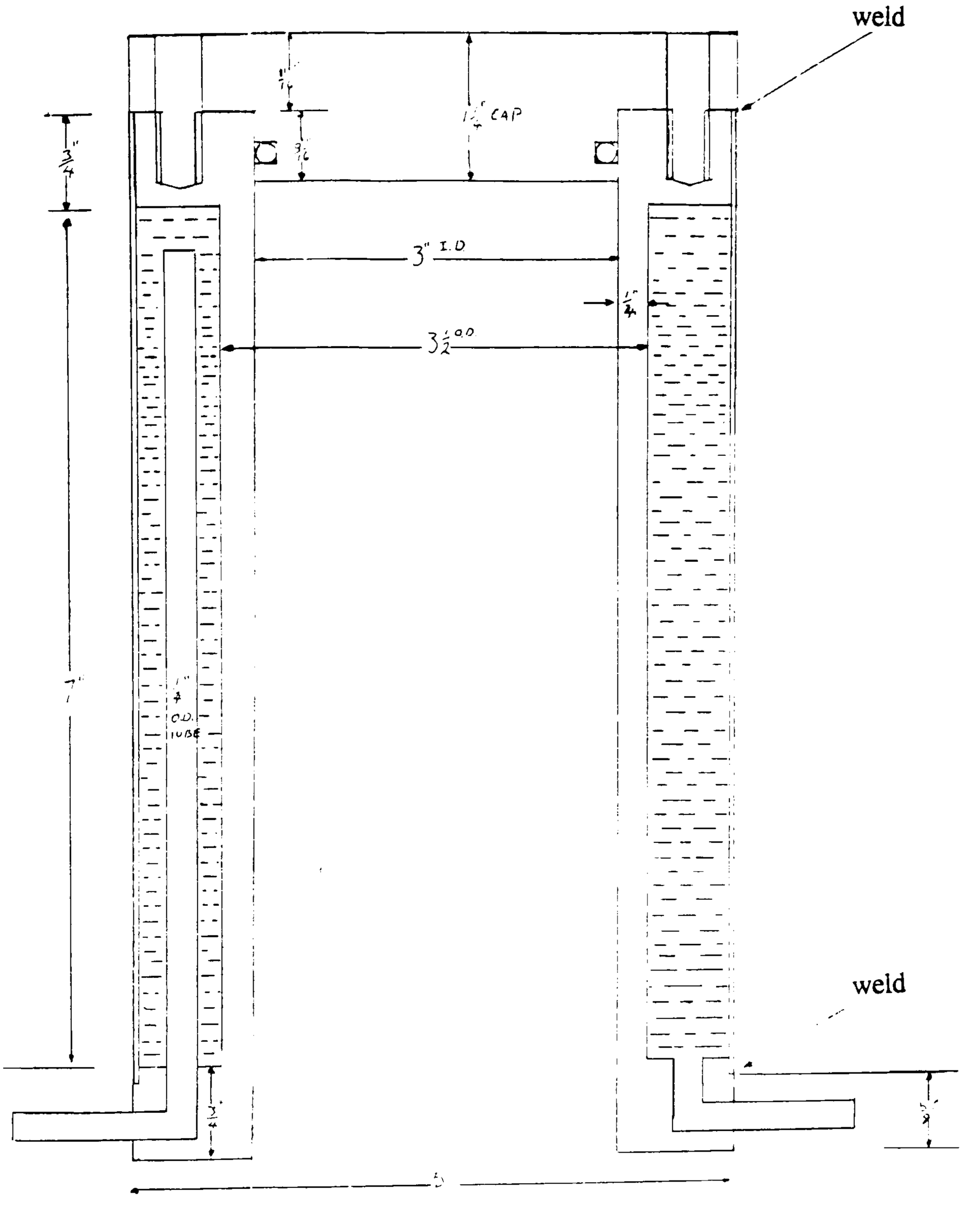

Figure 2.4

The High Pressure Apparatus

pressure was calculated from the Clapeyron equation

$$dp/dT = \Delta H_m / T_f \Delta V_m$$

thus

$$T = T^* e\{(p-p^*)\Delta V_m / \Delta H_m\}$$

In the equation ΔH_m is the molar enthalpy of fusion (J mol^{-1}), ΔV_m, the molar volume change on melting (m^3 mol^{-1}) and T_f, the temperature of melting (K). p is the ambient pressure (Pa) and T is the temperature (K).

Table 2.1

The Enthalpy and Temperature of Fusion of the Metal Calibrants

Metal	ΔH_{fus} /J g^{-1}	14.6 lbf in^{-2}	500 lbf in^{-2}	1,000 lbf in^{-2}
Indium	28.41	156.6	156.8	157.1
Tin	59.78	231.9	232.1	232.3
Lead	23.22	327.4	327.9	328.4
Zinc	111.35	419.0	419.2	419.5

Experiments were carried out using approximately 10 mg samples of the metal powder placed in aluminium pans, whose bases had been previously flattened between two metal presses. The pans were then sealed with a lid and placed on the sample thermocouple. A similar pan containing an equal mass of alumina was placed on the reference thermocouple. Initially the cell was calibrated at atmospheric and elevated pressures, but as work consisted solely of oxidation experiments at 500 lbf in^{-2} (3,500 kPa), calibrations were eventually only performed at this pressure. To calibrate the apparatus at this pressure, the cell was purged with nitrogen at a flow rate of 50 cm^{-3} min^{-1} for 5 minutes. The exhaust valve was then closed and the cell slowly pressurised to 500 lbf in^{-2}. The sample was then heated at 10°C min^{-1} through its melting temperature and the endotherm of fusion recorded. The peak of the first fusion was ignored if it had a poor shape and melting temperature. Generally, only the second and third melts of a calibrant were used for calibration purposes. The subsequent experiments were disregarded to eliminate errors in the temperature and enthalpy of fusion recorded, arising from the formation of inter-metallic compounds. This was caused by the reaction of the pan metal with the calibrant. Pressurised experiments were conducted under a static atmosphere of nitrogen, with the pressure being slowly vented to maintain a stable pressure, but at atmospheric pressure a flow rate of 50 cm^3 min^{-1} was employed. At the end of a pressurised experiment, the pressure vessel was slowly vented to atmospheric pressure and the lid cautiously removed.

The energy calibration of the apparatus varied only marginally during the period over which the apparatus was in use. The alteration of the energy calibration was of little consequence, because of the large exothermicities associated with the oil oxidation reactions. The energy calibration of the apparatus is given in figure 2.5. The temperature calibration of the equipment displayed a dependence on the temperature of the sample. The data were represented using a straight line, plotting the measured temperature of melting against the true temperature (figure 2.5). The straight line plot enabled the true sample temperature to be calculated from that measured. The correlation of the data points to the line was found to be consistently good, with a correlation coefficient of 0.999.

2.7 Experimental Variables

2.7.1 Introduction

Differential scanning calorimetry is a very sensitive analytical technique and to obtain reproducible results, great care must be taken to ensure that the numerous operational variables remain constant.

The effect of some variables on the peak shape, onset temperature, or induction time are more obvious than others. The following text summarises the variables of greatest significance in the work described in this thesis. A concise description of the factors affecting peak shapes obtained in DSC/DTA experiments is given by Wendlandt [22]. In a manner similar to that employed in his book, the variables will be categorised into instrumental and sample variables.

2.7.2 Instrumental Variables

When a comparison is made between the results obtained from different instruments, it is immediately apparent that for the same sample, different peak shapes are obtained. The thermal event may even be recorded at a different temperature. Many of the instrumental variables are fixed to the design of the apparatus and are not accessible to the analyst. Among the instrumental variables are

1 the furnace geometry,

2 the wire and bead size of the thermocouple junction,

3 the speed and response of the recording instrument,

4 the thermocouple location,

5 the sample holder material,

a) Energy Calibration

T /°C	ϵ /mW V^{-1}
81.4	76.3 ± 0.9
124.1	75.5 ± 0.2
156.6	74.4 ± 1.0
232.1	72.4 ± 0.3
327.9	86.2 ± 0.7
419.2	97.2 ± 0.3

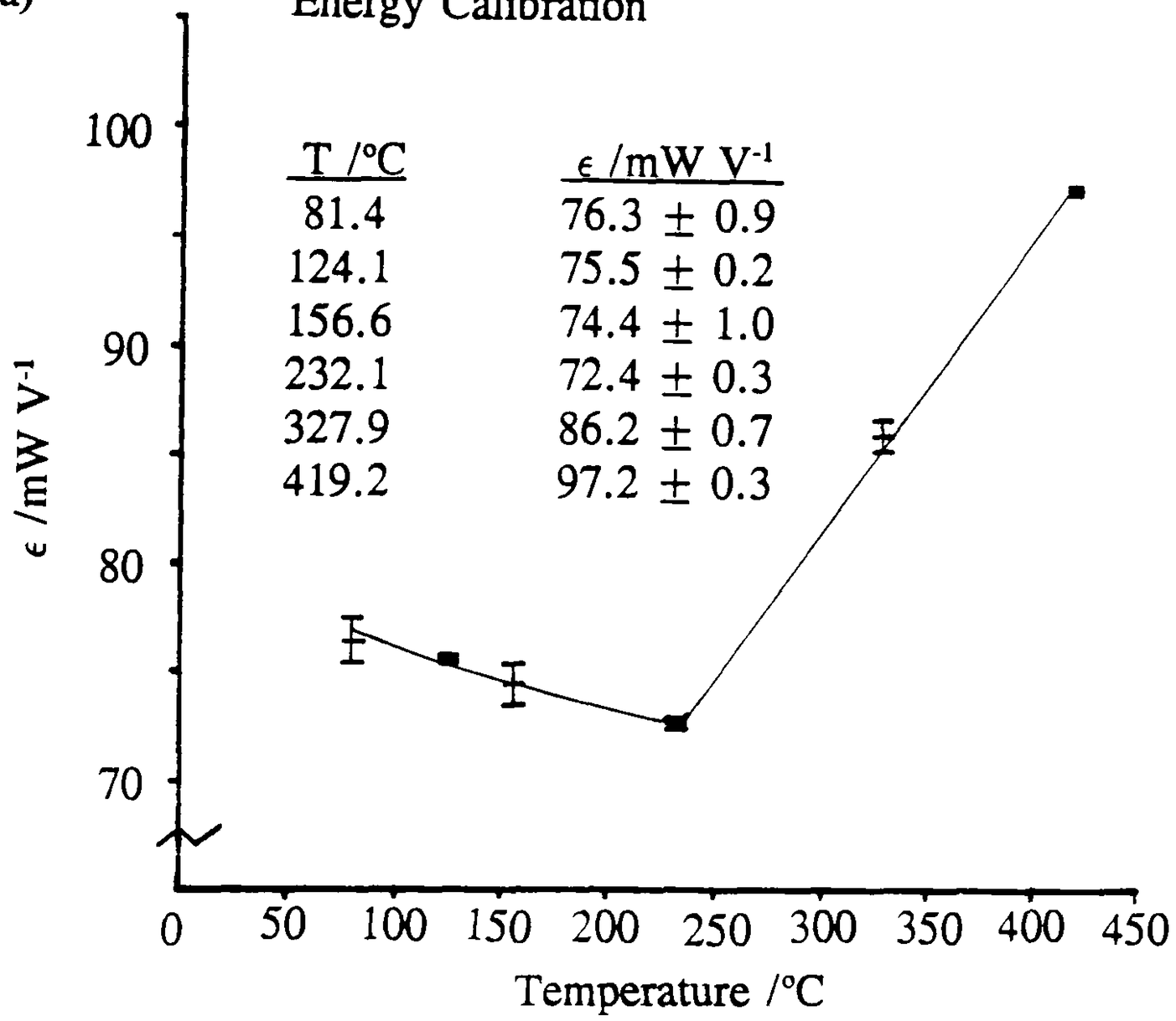

b) Temperature Calibration

$$T/°C = \frac{T_m\ (/°C) - 2.60}{0.993}$$

Corr = 0.999

T /°C	T_m /°C
81.4	80.2 ± 0.6
124.1	126.9 ± 0.0
156.6	160.8 ± 1.0
232.1	232.4 ± 0.3
327.9	329.7 ± 1.6
419.2	417.0 ± 0.2

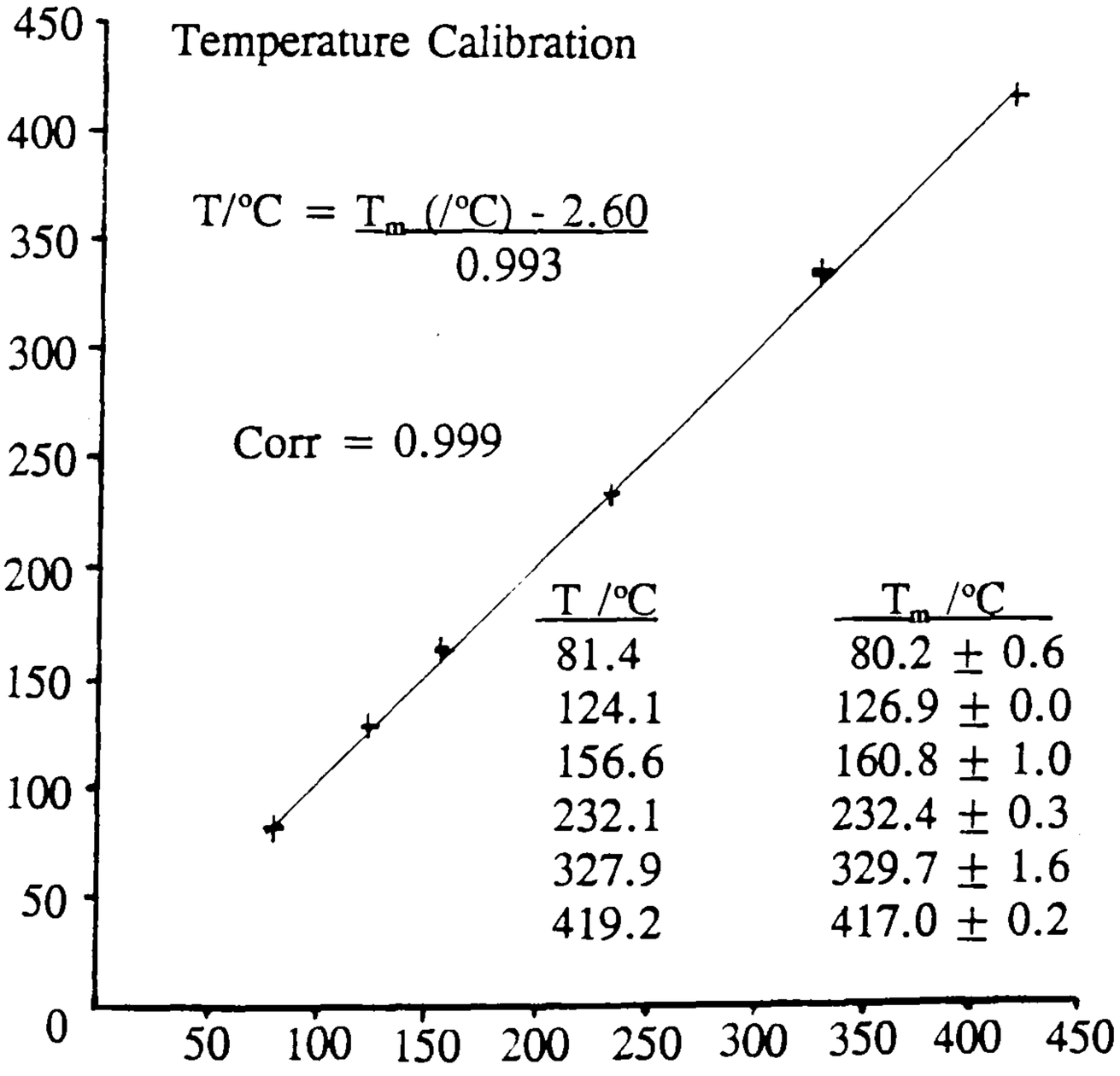

Figure 2.5

The Calibration of the Du-Pont DSC

6 the sample holder geometry,
7 the furnace atmosphere, and
8 the heating rate.
In the following text we will restrict the discussion to variables 5 to 8.

The shape of the recorded peak is dependent on the heat flow from the sample to the thermocouple. In any one experiment heat may be generated or absorbed and the transfer of this energy to the thermocouple is dependent on the sample holder or pan. To ensure that the thermal contact between the pan and the point of measurement is as efficient as possible, the base of the pan has to be flat. During the course of the work for this thesis, the bases of the aluminium pans were flattened between two metal surfaces before a sample was introduced. If the total heat capacity of the sample holder is as small as possible, the instrument will have a higher resolution and be more accurate with regard to instantaneous thermal events. Wendlandt [22] reported the work of several authors, who each agreed that for endothermic reactions, the use of materials with a low thermal conductivity for the sample pans enables better resolution than high thermal conductivity pans. Conversely, for exothermic reactions a pan made from a highly conducting material is preferred.

The effect of the pan material on the catalysis of oil oxidation has been studied by Cash [20] and Zeman [19,23,24]. For his work, Cash [20] studied a mineral oil basestock using the dynamic test and found that carbon pans were the most inert (followed by platinum). He also found that unoxidised copper displayed only a slight catalytic effect on oil oxidation, whereas oxidised copper was by far the most reactive of all materials studied. In his papers Zeman [23,24] studied the effects on ester oils containing two different additive packages using an isothermal method. The ranking of the catalytic activities of the metals was dependent on the inhibitor package present, but although the differences in the hostility toward the oil were slight, an indication of the importance of matching the oil additives to the alloys present in an engine was obtained. Similar care must be taken in the choice of pan material to prevent the catalysis of undesirable reactions. Aluminium pans (whether anodised or not) are usually used for DSC analysis, owing to their inertness, ease of fabrication and the low cost of the material.

Various pan materials were employed by Zeman [19] to help simulate the operating conditions encountered by aviation turbine oils. The spontaneous ignition temperatures

of aviation turbine oils were studied utilising a dynamic method. The different pan materials were used to determine the metals with the highest catalytic activity. His findings were not in total agreement with those found by Cash [20], but he studied fully formulated ester oils under ignition conditions, whereas Cash examined a mineral basestock under non-ignition conditions.

The condition of the pan surface is an equally important variable as its composition. When the pans are pressed, small pieces of ferrous metal can be imbedded in their surface, a rare occurrence, but one that may have a disastrous effect on experimental reproducibility and repeatability. A more common problem is the presence of grease and general dirt on the pan surface after pressing. For this reason, all pans must be thoroughly cleaned and dried before use.

In parallel to the effect of the position of the thermocouples in the instrument, the placement of the pans on the thermocouple platform in a reproducible manner is necessary to ensure consistent results. The Stanton Redcroft DSC-700 and the STA-871 have a positive means of sample location to ensure this, but the Du-Pont DSC-990 requires the use of a special tool described by Yuen and Yosel [8]. If the pan is placed off centre on the thermocouple platform, the peak shape can be distorted as a result of the alteration in the path of the heat flow.

When a larger diameter pan is employed for a DSC experiment, the oil is allowed to spread out over a larger area, thus exposing a greater surface area to the carrier gas. The effect of the size of the sample pan on the onset temperature of an oil oxidation reaction was described by Cash [20]. He discovered that as the pan size increased, the onset and peak maxima temperature decreased. The effect of the surface area of the sample exposed to the carrier gas is explained in greater detail in the sub-section headed sample variables.

The use of different atmospheric conditions enables different results to be obtained from experiments that otherwise employ identical operating conditions. For example, an experiment using nitrogen as the carrier gas will enable volatility or thermal stability measurements to be made, whilst the use of oxygen ensures that the experimental parameter measured is oxidative stability. Furthermore in isothermal experiments, an oil with a low oxidative stability may will begin to oxidise before the set temperature is attained. In this case no induction time (prior to the onset of rapid oxidation) can be

measured, and so no such categorization of the oil can be made. In order to characterize oils of low oxidative stability the apparatus could be heated up to the set temperature under an atmosphere of nitrogen and then when the baseline had settled, the purge gas could be changed to oxygen thus enabling an induction time to be measured from the moment the gases were changed [17].

The effect of the partial pressure of oxygen on the onset temperature of oxidation for a mineral basestock was described by Cash [20]. The total pressure of the purge gas was 2,000 kPa, nitrogen being used as a diluent. At a partial pressure ratio of $p(O_2)/p(N_2) > 0.67$ the results were independent of the partial pressure of oxygen. In consequence he expressed some doubt that air constituted a good oxidising medium for studies of this kind. Nevertheless, air will obviously provide a more realistic representation of engine operating conditions than the mixture described by Cash.

The isothermal experiments used for oil analysis utilise high pressures, while the dynamic experiments usually (but not always) employ atmospheric pressure. The use of a static atmosphere in a DSC cell ensures that any volatile components evolved from a sample are not swept away from the oil/gas interface. This means that the volatile components can react with the sample present in the liquid phase, or in extreme instances ignite, resulting in the complete combustion of the sample. The use of low pressures in dynamic experiments means that the sample is more able to release volatile components into the atmosphere. The use of a flowing atmosphere in these experiments sweeps the volatile fractions away from the sample pan, thus reducing the likelihood of ignition. Cash [20] studied the effect of the flow rate of the purge gas on the peak shape obtained from dynamic experiments using the Du-Pont DSC-990. Analysing a sample of an amine antioxidant in a synthetic oil, he found that there was no dependence of the flow rate between 10 and 150 $cm^3\ min^{-1}$ on the extrapolated onset or the peak maximum temperature. When a static atmosphere was employed, broad and poorly defined peaks were obtained. The high pressures used in isothermal experiments reduces the volatility of the sample [25], meaning that a flowing atmosphere is not required.

Blaine and Levy et al. [26,21] investigated the effect of pressure on the onset temperature of oils in a limited way. The work was expanded in some detail by Komamiya and Toshima [18] and Zeman and Binder [19], who studied the ignition temperatures of oils under pressure. Walker and Tsang [17] studied the effect of

oxygen pressure on the induction time of a lubricating oil using the isothermal technique, demonstrating a reduction in the induction time with increasing pressure. Cash [20] expanded on this work to higher pressures, noting that between 4,000 and 6,000 kPa the samples ignited, reducing the induction time of the experiment by 2 to 3 minutes from approximately 7 minutes. At low pressures he commented that the peaks were broad, and that an increase in pressure did not alter the induction time significantly. Ignition of the sample occurred at 4,000 kPa. The contradiction of the results obtained by Walker and Tsang [17], could be due to the fact that Walker and Tsang used a flowing atmosphere which could flush the oxidation products away from the oil surface, thus increasing the oxygen concentration at the surface.

The effect of the heating rate on the experimental result is probably one of the most widely documented variables. This is discussed in further detail in Chapter 4 of this thesis. The increase in heating rate of an experiment has two conflicting effects on the quality of the results obtained. The increase in peak amplitude with heating rate enables the detection of very small transitional peaks that would otherwise pass unnoticed in an experiment employing a slower heating rate. For experiments using higher heating rates, there is a loss in resolution between two closely associated thermal events, which can only be separated by employing lower heating rates. An increase in the heating rate of an experiment leads to an increase in the peak maximum temperature. The shifting of the thermal events to a higher temperature with an increase in the heating rate is caused by a greater thermal lag between the sample and the point at which the temperature is measured. A further complication is that if the heating rate becomes too great (the value depending on the sample) the sample will ignite. This phenomena is not related to the thermal lag, but is caused by self heating of the sample. Increasing the heating rate leads to an increase in the temperature at which the sample ignites.

2.7.3 Sample Variables

In his book [22] Wendlandt describes the sample variables, most of which are relevant only to solid samples. The sample variables include

1 particle size,

2 packing density,

3 swelling or shrinkage of the sample,

4 effect of diluent,

5 degree of crystallinity,

6 thermal conductivity,

7 heat capacity, and

8 the amount of sample.

Of the variables listed above, only the sample size has any great effect on the analysis of the oxidative stability of oils. The change in the heat capacity of an oil sample is used to determine the glass transition temperature [26], which is considerably below room temperature and therefore not within the scope of this thesis. The high exothermicities associated with the oxidation reactions and the small sample masses used ensure that the thermal conductivity of the sample is of little importance. In the following text the effect of sample size, the position of the sample in the pan and the method of introducing the sample into the pan on oil analysis, will be discussed.

The effect of sample mass on the cooling of crude oils was studied by Claudy and co-workers [27]. The authors noted that the wax crystallisation temperature increased with sample mass. Similarly, for the oxidation of a mineral oil basestock using dynamic experiments, Cash [20] found that an increase in sample mass from 2 to 12 mg caused a steady increase in the peak maximum temperature. A somewhat expected result was that the extrapolated onset temperature did not alter over this mass range. The author discovered that the critical mass of the oil sample was 2 mg, above which the peak onset temperature was independent of the sample mass (work conducted in this research employing a synthetic basestock under ignition conditions gave rise to the same results). There was a decrease in the definition of the peak shape with an increase in the sample mass [20]. This was probably caused by a reduction in the surface area to volume ratio. For isothermal experiments Cash [20] found that an increase in sample mass led to an increase in the induction time and the sharpness of the curve, until a critical mass was attained when the sample ignited. A significant reduction in the induction time was associated with the ignition of the sample.

The effect of the sample surface area on the DSC peak is, in essence, related to the size of the pan used for the experiment. If a large diameter pan is employed, the oil droplet can spread over a larger area, and as a consequence expose a greater surface area to the carrier gas. In a study concerning the effect of pan size on the oxidation peak, Cash [20] discovered that both the extrapolated onset and peak maximum temperature decreased as the diameter of the pan increased. This phenomenon was valid until the diameter of the pan exceeded the size of the oil droplet. With the larger pans, a greater surface area was exposed to the oxidising gas, which facilitated the

diffusional processes of oil degradation. When samples of oil were placed on a bed of alumina inside the pan to increase the surface area further, the sample ignited at a temperature above which it normally oxidised. This is probably due to the high porosity of alumina, which contains a high number of both macro and micro pores in which oil molecules and degradation products can be trapped. The experiments conducted with the alumina diluent displayed poor repeatability. The repeatability of the experiments would possibly have improved if a low surface area powder was used.

The positioning of the sample in the pan is an important factor, especially when working with liquids. If the sample is placed in the centre of the pan, it will spread out evenly over the base, but if placed on the edge of the pan base or at the junction of the base and the side wall it will not do so. An unrepeatable sample surface area will be obtained if the sample is not placed in the centre of the pan base. Consequently the DSC peak shape will be poorly defined and have an unrepeatable shape.

The manner in which the sample is introduced into the pan is very important on the experimental result and so is the implement with which it is introduced. If a steel syringe needle is chosen there is evidence of reaction, albeit only over a period of use of several months. Even when cleaned, a reaction between the oil and the metal will be evident by a brown stain appearing on the needle surface. This is obviously undesirable, therefore some analysts use disposable syringe needles for each sample, while the majority employ a glass 'dropper' for preparing samples. The surface of the glass is inert to the oils and is easily cleaned between samples, thus eliminating any undesirable reactions or contamination.

This section has illustrated the vast number of variables that can affect an experimental result. It may be interesting to realise that the operator only has control over the furnace atmosphere, the heating rate, sample mass, position of the sample in the pan and the pan material.

Repeatable and reproducible results require care and attention to the finest detail. Cleanliness is also the key to success. Contamination of a sample by dirt and dust will not only alter the sample mass considerably (because only milligram samples are studied), but in the case of an oil sample will alter the surface area and possibly catalyse an undesirable reaction. A further variable not mentioned earlier as it is specific to the analysis hydrocarbons, is that the sample platform and thermocouple

assembly require regular cleaning. Condensates of volatilised oil oxidation products collect on the surfaces of the calorimeter and can affect the results of an experiment by oxidising themselves. The furnace assembly can be cleaned by heating it to approximately 500°C under an atmosphere of oxygen at 500 lbf in^{-2} and remaining at that temperature until all the condensates have burned off. This can be seen by increasing the sensitivity of the apparatus to observe the reaction of the condensates, the oven being clean when the recorder pen settles to constant position at its maximum sensitivity.

References

1. P. G. Laye and R. C. MacKenzie, *Chem. Br.*, 22, 1986, p 1005.
2. R. C. MacKenzie, *Thermochim. Acta,* 73, 1984, p 251.
3. H. Le Chatelier, *Bull. Soc. Fr. Mineral Chrystallog.*, 10, 1887, p 204.
4. W. C. Roberts-Austin, *Proc. Inst. Mech. Eng.*, 1891, p 543.
5. S. L. Boersma, *J. Am. Chem. Soc.*, 34, 1951, p 221.
6. E. S. Watson, M. J. O'Neill, J. Justin and N. Brenner, *Anal. Chem.*, 36, 1964, p 1233.
7. J. Van Humbeek and M. Bijvoet, *Thermochim. Acta,* 120, 1987, p 55.
8. H. K. Yuen and C. J. Yosel, *Thermochim. Acta,* 33, 1979, p 281.
9. Du-Pont 990 Instrument Manual.
10. J. D. Levy and P. F. Levy, *NATAS,* Proc. 11th Conf., 1981, p 215.
11. P. Claudy, J. C. Commercon and J. M. Letoffe, *Thermochim. Acta,* 65, 1983, p 245.
12. P. Claudy, J. C. Commercon and J. M. Letoffe, *Thermochim. Acta,* 68, 1983, p 305.
13. P. Claudy, J. C. Commercon and J. M. Letoffe, *Thermochim. Acta,* 68, 1983, p 317.
14. R. L. Brown, J. A. Walker and W. Tsang, *NATAS,* Proc. 11th Conf., 1981, p 507 .
15 D. W. G. Dicker and R. K. Wharton, "Flammability and Sensitivity of Materials in Oxygen Enriched Atmospheres", Vol. 3, ASTM STP 986, Ed. D. W. Schroll, ASTM Philadelphia, 1988, p 318.
16. Minutes of the 29th Meeting of the Thermal Analysis Panel STG-9, at the Institute of Petroleum, London, 15th Oct. 1990.
17. J. A. Walker and W. Tsang, *NBS Spec. Publ. 584,* Proc. Joint Conf. On Measurements And Stds. For Recycled Oils/Systems Performance And Durability held at NBS, MD, Oct 23-26, 1979 (issued 1980), p 271.
18. K. Komamiya and K. Toshima, *Proc. 5th Int. Conf. Therm. Anal.*, Ed. H. Chihara, 1977, p 387.
19. A. Zeman and P. Binder, *Thermochim. Acta,* 98, 1986, p 159.
20. A. A. J. Cash, *Ph.D Thesis,* Dept. of Phys. Chem., Leeds Univ., 1988.
21. P. F. Levy, G. Niewoboer and L. C. Semanski, *Thermochim. Acta,* 1, 1970, p 429.

22. W. W. Wendlandt, "Thermal Analysis", 3rd Ed., John Wiley and Sons, Chichester, 1986.

23. A. Zeman, R. Stuwe and K. Koch, *Thermochim. Acta,* 80, 1984, p 1.

24. A. Zeman, *J. Synth. Lubr.*, 5, 1988, p 133.

25. P. W. Atkins, "Physical Chemistry", Oxford Univ. Press, 1978.

26. R. L. Blaine, *American Lab.*, 1974.

27. P. Claudy, J. M. Letoffe, B. Chague and J. Orrit, *Fuel,* 67, 1988, p 55.

Chapter 3

Cyclic Voltammetry

The text contained in sections 1 and 2 of this chapter is designed to provide a somewhat lengthy, but thorough account of the theories and developments relevant to the electrochemical work performed in this thesis. The ideas in the text are not original, but it is necessary to include them to enable the electrochemical work to be understood.

3.1 The Basic Principles

3.1.1 The Electrochemical Cell

Electrochemistry is the study of charge transport across an interface between chemical phases. In one phase, the electrode, the charge is carried by electronic movement whilst in the other, the electrolyte, charge is carried by the movement of ions. In the majority of cases the electrode is a metal and the electrolyte a liquid. The simplest electrochemical cells consist of two electrodes in the electrolyte solution. The electrode where the reaction of interest occurs is called the working electrode (WE). The second electrode, against which it is measured is called the reference electrode (RE), and therefore must consist of phases with a known and constant composition. When the resistance of the electrolyte is small the two electrode system can be used to measure the i-E curve for that cell, but when the resistance is high the potential of the RE is affected and the potential measured is inaccurate, ie.

$$E_{app} = E + iR_s = E_{eq} + \eta + iR_s. \qquad 1.1$$

E_{app} is the potential applied with an external power source; E is the potential of the cell; i the current flowing through the cell; R_s the resistance of the solution; E_{eq} the equilibrium potential of the electrode and η the overpotential. The ohmic potential drop of the solution, iR_s is part of the measured potential and therefore becomes significant when the current or solution resistance is large. It may be regarded as a form of overpotential, an assumption that introduces inaccuracies, because the iR_s term is a characteristic of the bulk solution and not the electrode reaction. To overcome this problem a three electrode cell is normally used. In these arrangements the current passes between the WE and the third electrode (counter electrode, CE) which may be constructed from any material (provided that its electrochemical properties do not affect the electrode of interest). The potential of the WE is measured relative to the RE through a volt meter. This is of a high impedance to prevent any measurable current

passing through the RE circuit. If only a negligible current flows through the circuit, the RE potential remains constant and equal to the open circuit value. Furthermore by arranging the cell so that the RE and the WE are as close together as possible the iR_s contribution to the measured cell potential is kept to a minimum.

3.1.2 Energy Levels at the Electrode Electrolyte Interface

The ability to alter the potential across the electrode electrolyte interface means that the direction of movement of the charge carriers can be controlled. It is this control and the monitoring of the resultant current that forms the basis of electrochemistry.

A change in the potential difference across the cell represents a change in the energy of the electrons in the WE. Through changing the potential in the negative direction the energy of the electrons are increased until they can transfer from the electrode and enter the lowest unoccupied molecular orbital (LUMO) of the electrolyte, the overall process being a reduction. Conversely in an oxidation process an oxidative current flows if the energy of the electrons are reduced by imposing a more positive potential. At this instant the energy of the electrons fall below the energy level of the highest occupied molecular orbital (HOMO) of the electrolyte allowing an electron to pass from the electrolyte to the electrode. The observed current flow can be termed as Faradaic, since from Faraday's law the extent of chemical reaction caused is directly proportional to the amount of charge passed, however both Faradaic and non-Faradaic currents can be observed at the same instant. The non-Faradaic currents arise from processes such as adsorption or desorption of ions from the electrode. These processes alter the electrode-solution interface and themselves can be caused by alterations in the solution composition or potential. The interface is commonly known as the electrical double layer (EDL) and generally it behaves in a similar manner to a capacitor, with a capacitance of 20-40 μF cm^{-2} [1]. At any given potential there will be a charge on the metal surface with an equal and opposite charge in the solution, the magnitude of which depends on the potential across the interface. The charge on the metal electrode occupies a very thin layer on its surface (<10 pm), while the charge in the solution consists of an excess of either anions or cations very close to the electrode surface. Although other ions may be present, the double layer is thought to consist of mainly specifically adsorbed solvent molecules (figure 3.1), the locus of their electrical centres being called the inner Helmholtz plane (IHP). The locus of the electrical centres of the solvated ions closest to the electrode is called the outer Helmholtz plane (OHP). These ions are unable to approach as close to the electrode as the solvent molecules, owing

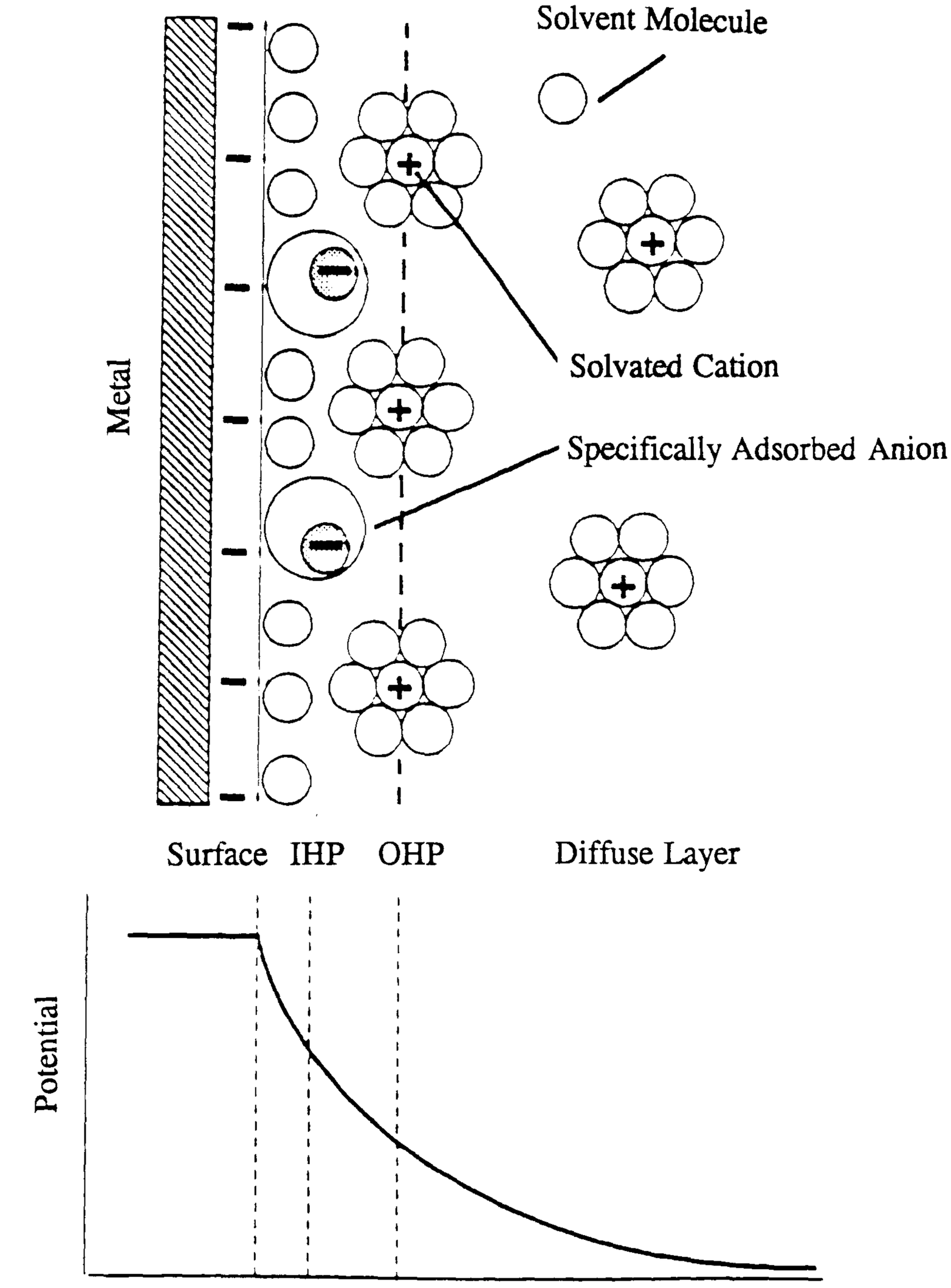

Figure 3.1

The Electrode-Electrolyte Interface

to their size, and therefore can only interact with the electrode via long range electrostatic forces. These non-specifically adsorbed ions are distributed in a three dimensional region called the diffuse layer, which extends from the OHP to the bulk of the solution by thermal agitation (figure 3.1). The thickness of the layer depends on the concentration of the bulk solution, for example, when the solution has a concentration greater than $1x10^{-2}$ mol dm^{-3} the thickness is less than 30 nm.

The double layer structure is described in detail with respect to capillary action, surface excess and Gibb's adsorption isotherms by Bard and Faulkner [1]. Theories of the structure of the double layer have been described concurrently by Helmholtz, Gouy and Chapman and then Stern. The weakness of the theory proposed by Helmholtz was that it assumed that the capacitance of the double layer is constant, which is widely known not to be the case. The Gouy-Chapman theory made improvements on that proposed by Helmholtz, but the weakness of their approach was that they assumed that charges were 'pin points'. This implies that the charges could approach an electrode until the effective separation was zero. Stern then extended the work to form the Gouy-Chapman-Stern theory which accounted for the finite size of the ions and the specifically adsorbed IHP. This was done by combining the Helmholtz theory for the ions closest to the electrode and the Gouy-Chapman model outside the OHP.

If the transition between reactants and products proceeds according to the activated complex theory, the rate of passage of charge across the potential energy barrier is governed by the Boltzmann energy distribution. If this is the case most electron transfer reactions would be very slow. For a barrier of 1 eV in magnitude it has been estimated that the probability of an electron tunnelling through the barrier is approximately 2.8 x 10^7 that of the classical probability of crossing [2]. The phenomena of electron tunnelling is a direct result of the wave properties of the particles whose wavelength is given by de Broglie's equation

$$\lambda = h/p, \qquad 1.2$$

where λ is the wavelength, h is Planck's constant and p the momentum of the particle. From this it may be concluded that the wavelength of an ion is much less than that of an electron. This in turn means that the probability of their tunnelling through a barrier is similarly reduced. With the exception of protons, charge cannot be effectively transferred by ions.

The phenomena of tunnelling is only possible because of the probability distribution

of a particle. There are restrictions on the process, namely that radiation can neither be emitted or absorbed. An electron can therefore only tunnel to a state of equivalent energy to the one it has just left. It can only do so if that state is no more than singularly occupied, as stipulated by the Pauli exclusion principle.

The process of heterogeneous charge transfer across the EDL can be depicted in a Morse diagram. This describes the potential energy change for the reactants and the products in terms of their interatomic positions. The change in the electrical potential, ΔE, can be related to the Gibb's free energy ΔG, by the equation

$$\Delta G = -nF\Delta E,$$

where n is the number of electrons involved in the reaction and F is Faraday's constant. Applying an external potential to the electrode, the energy of the electrons within the electrode can be altered by

$$\Delta G = -nF(E_{ext}-E_{eqm}), \qquad 1.3$$

where E_{ext} is the externally applied potential and E_{eqm} is the potential independent (chemical) term. If the Morse functions (figure 3.2) are assumed to be linear in the region of the intersection then the actual change in the potential energy barrier owing to the externally applied potential is

$$\Delta G_f = -\alpha nF(E_{ext}-E_{eqm}) \qquad 1.4$$

and for the reverse process

$$\Delta G_b = -(1-\alpha)nF(E_{ext}-E_{eqm}), \qquad 1.5$$

which when summed gives equation 1.3. The term α is called the 'symmetry factor' and it is used to describe the degree of symmetry of the two Morse curves.

Assuming the activated complex theory to be valid, for a reaction to take place from A→B the energy barrier ΔG_f has to be surmounted to reach the complex (and ΔG_b for the reverse reaction). When the system is in thermal equilibrium the concentration of the complex can be calculated from the free energies of activation.

$$[\text{Complex}]/[A] = \exp -\Delta G_f/RT \qquad 1.6$$

and

$$[\text{Complex}]/[B] = \exp -\Delta G_b/RT, \qquad 1.7$$

where T is the temperature (K). The complex decays into either products or reactants (A or B) with a combined rate constant k which can be divided into four fractions; (a) A→Comp→A f_{aa}, (b) A→Comp→B f_{ab}, (c) B→Comp→A f_{ba} and (d) B→Comp→B f_{bb}. When the system is at equilibrium f_{ab} and f_{ba} must be equal to k'/2, where k', the transmission coefficient, has a value from zero to unity.

Thus

$$k_f = kk'/2 \exp -\Delta G_f/RT \qquad 1.8$$

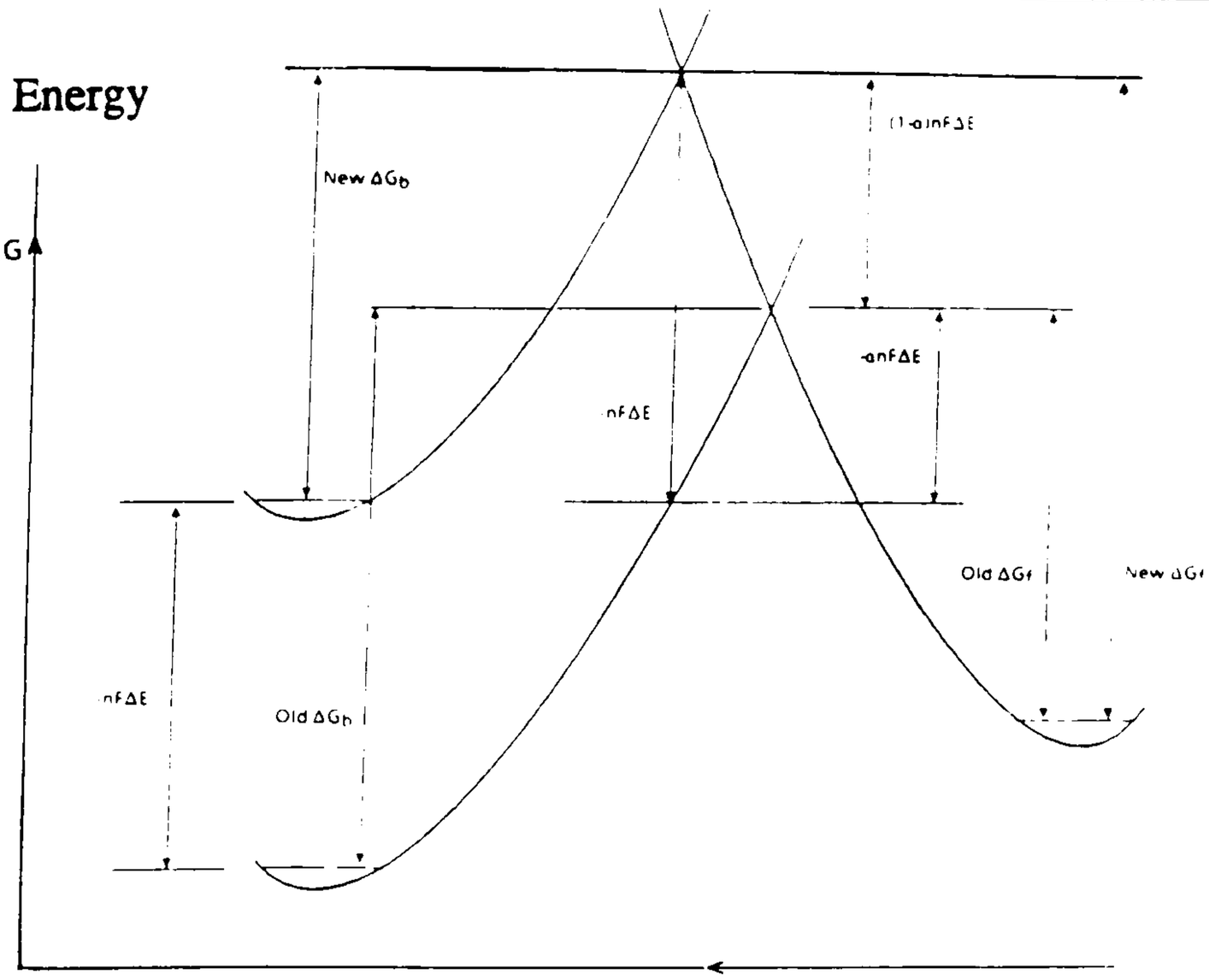

Figure 3.2

Morse Function Potential Energy Curves for Reactants and Products of an Electron Transfer Reaction

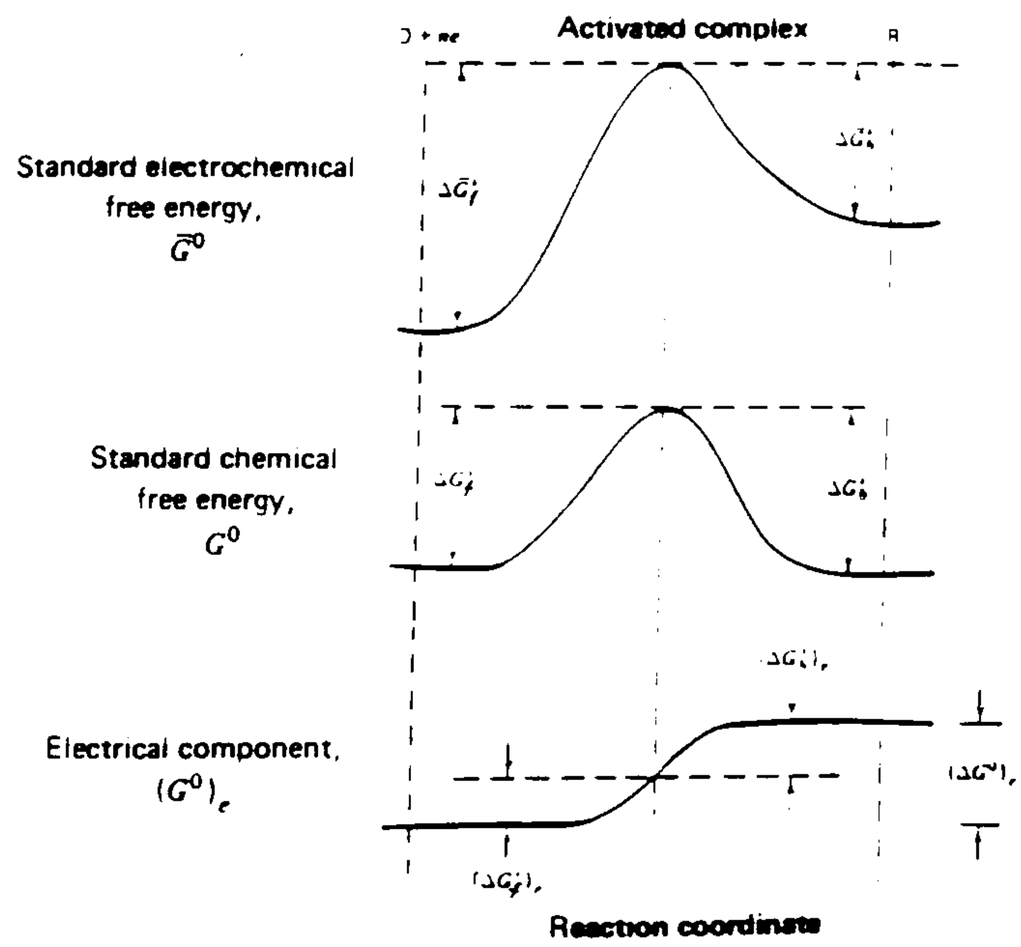

Figure 3.3

Separation of the Electrochemical Free Energy (upper curve) into Chemical and Electrical Components (lower two curves) [1]

and $$k_b = kk'/2 \exp -\Delta G_b/RT. \quad 1.9$$

In the simplest cases $k=2kT/h$ where k is Boltzmann's constant. The above expressions apply to a system at equilibrium and are independent of both reactant and product concentrations.

Combining equations 1.4 and 1.5 with 1.8 and 1.9 the latter equations can be split into chemical and electrical effects:

$$k_f = \frac{kk'}{2} \exp\left(\frac{-\Delta G_f(eqm)}{RT}\right) \exp\left(\frac{-\alpha nF\Delta E}{RT}\right), \quad 1.10$$

$$k_b = \frac{kk'}{2} \exp\left(\frac{-\Delta G_b(eqm)}{RT}\right) \exp\left(\frac{(1-\alpha)nF\Delta E}{RT}\right), \quad 1.11$$

where ΔE is given by $E_{ext}-E_{eqm}$. Grouping all the potential independent terms into an experimental constant, K_f^θ or K_b^θ, gives

$$k_f = K_f^\theta \exp -\alpha nF\Delta E/RT \quad 1.12$$

and $$k_b = K_b^\theta \exp (1-\alpha)nF\Delta E/RT. \quad 1.13$$

The rate constants k_f and k_b are therefore potential dependent. At the potential that reduces the ΔE term to zero the forward and reverse rates become equal. This introduces the idea of a standard electrode potential (E^θ) at which equation 1.14 would be valid.

$$K^\theta = K_f^\theta \exp\left(\frac{-\alpha nF(E-E^\theta)}{RT}\right) = K_b^\theta \exp\left(\frac{(1-\alpha)nF(E-E^\theta)}{RT}\right) \quad 1.14$$

K^θ is the standard rate constant for the heterogeneous electron transfer process. Using the standard electrode potential the rate of charge transfer across the EDL is

$$k_f = K^\theta \exp [-\alpha nF(E-E^\theta)/RT], \quad 1.15$$

$$k_b = K^\theta \exp [(1-\alpha)nF(E-E^\theta)/RT]. \quad 1.16$$

Electrode reactions at equilibrium are characterised by the Nernst equation which links the electrode potential to the bulk concentration of the participating species:

$$E = E^\theta + RT/nF \ln [A]/[B]. \quad 1.17$$

The current passing through a cell is often related to the overpotential by a relationship, discovered by Tafel in 1905, which is given by

$$\eta = a + b \log i, \quad 1.18$$

where i is the current and a and b are constants.

For the reaction

$$O + ne^- \rightleftharpoons R \quad 1.19$$

the forward component must proceed at a rate ν_f proportional to the surface

concentration of O, which at a distance x from the surface of the electrode at a time, t, is $Co_{(x,t)}$. It follows that the surface concentration is $Co_{(0,t)}$. The rate constant k_f links the surface concentration and the reaction rate ν_f by the equation

$$\nu_f = k_f.Co_{(0,t)} = i_c/nFA, \qquad 1.20$$

where A is the area of the electrode. The current i_c, which is proportional to the reaction rate is cathodic because the forward reaction is a reduction. Similarly for the backward reaction

$$\nu_b = k_b.Cr_{(0,t)} = i_a/nFA, \qquad 1.21$$

where i_a is the anodic component of the total current. The net rate is

$$\nu_{net} = \nu_f - \nu_b = k_f.Co_{(0,t)} - k_b.Cr_{(0,t)} = i/nFA. \qquad 1.22$$

It follows that

$$i = i_c - i_a = nFA[k_f.Co_{(0,t)} - k_b.Cr_{(0,t)}]. \qquad 1.23$$

For heterogeneous systems, reaction velocities refer to the unit of interfacial area, and have the dimensions of mol s^{-1} cm^{-2}, because the concentration is expressed in the units of mol cm^{-3} whilst the rate constant has the units of cm s^{-1}. The interface only reacts with its immediate surroundings which means that the concentrations referred to in the rate expressions are concentrations at the surface. These may differ from that of the bulk solution. It will be shown that the participating species have a kinetic behaviour that is strongly influenced by the potential difference. For electrode reactions two different approaches lead to the same result for the prediction of the response of k_f and k_b to the applied potential.

3.1.3 A Kinetic Model Based on Electrochemical Potentials

The electrochemical free energy of activation $\Delta G_f^{\ddagger}$ or $\Delta G_b^{\ddagger}$ can be separated into chemical and electrical components. It is assumed that the chemical free energy of activation does not vary with the applied potential, which means that the effect of potential is entirely due to the electrical component. A further assumption is made, in that the electrical components of the activation energy are fixed fractions of the overall electrical free energy change, as illustrated in figure 3.3.

That is

$$(\Delta G_f)_e = \alpha(\Delta G^o)_e \qquad 1.24$$

and

$$(\Delta G_b)_e = -(1-\alpha)(\Delta G^o)_e. \qquad 1.25$$

The standard electrochemical free energy of the state corresponding to the species O^{z+} + n electrons on the metal M (state 1), $G^o{}_1^{\ddagger}$ is given by

$$G^o{}_1^{\ddagger} = \mu_o^{\ddagger} + n\mu_e^{\ddagger} = \mu_o^{os} + n\mu_e^{om} - nF\phi^m - zF\phi^s. \qquad 1.26$$

The equivalent free energy (state 2) for the species $R^{z'}$ is

$$G^{o}_{2}{}^{\ddagger} = \mu_r^{\ddagger} = \mu_r^{os} + z'F\phi^s, \qquad 1.27$$

where $\mu_j^{\ddagger}$ is the electrochemical potential of species j, $\mu_j^{o\alpha}$ is the standard electrochemical potential of species j in phase α and ϕ^k is the absolute electrostatic potential of phase k. The component $(\Delta G^o)_e$ is the difference between the electrical terms, ie.

$$(\Delta G^o)_e = (z'-z)F\phi^s + nF\phi^m = nF(\phi^m-\phi^s). \qquad 1.28$$

The electrode potential E is related to the interfacial potential difference $(\phi^m - \phi^s)$ by a constant K

$$E = (\phi^m - \phi^s) + K, \qquad 1.29$$

so $$(\Delta G_f)_e = \alpha nF(E-K) \qquad 1.30$$

and $$(\Delta G_b)_e = -(1-\alpha)nF(E-K), \qquad 1.31$$

Substituting 1.30 and 1.31 into

$$\Delta G_f^{\ddagger} = \Delta G_f + (\Delta G_f)_e \qquad 1.32$$

and $$\Delta G_b^{\ddagger} = \Delta G_b + (\Delta G_b)_e \qquad 1.33$$

we have $$\Delta G_f^{\ddagger} = \Delta G_f + \alpha nF(E-K) \qquad 1.34$$

and $$\Delta G_b^{\ddagger} = \Delta G_b - (1-\alpha)nF(E-K). \qquad 1.35$$

These when substituted in turn into

$$k_f = kT/h \exp [-\Delta G_f^{\ddagger}/RT] \qquad 1.36$$

and $$k_b = kT/h \exp [-\Delta G_b^{\ddagger}/RT] \qquad 1.37$$

give $$k_f = kT/h \exp -\Delta G_f/RT \exp -\alpha nFE/RT \exp \alpha nFK/RT, \qquad 1.38$$

$$k_b = kT/h \exp -\Delta G_b/RT \exp -(1-\alpha)nFK/RT \exp (1-\alpha)nFE/RT. \qquad 1.39$$

The potential independent factors can be collected into constants K_f^{θ} and K_b^{θ} to give

$$k_f = K_f^{\theta} \exp [-\alpha nFE/RT] \qquad 1.40$$

and $$k_b = K_b^{\theta} \exp [(1-\alpha)nFE/RT] \qquad 1.41$$

This treatment assumes that ΔG_f and ΔG_b are independent of the applied potential and that $(\Delta G_f)_e$ and $(\Delta G_b)_e$ are constant fractions of $(\Delta G^o)_e$. These assumptions hold true if the position of the activated complex does not alter with the applied potential.

3.1.4 The Current Potential Relationship

At equilibrium, the net current flowing across the EDL is zero and the electrode adopts a potential given by the Nernst equation. At zero current from the equation

$$i/nFA = k_f.Co_{(0,t)}$$

we obtain the expression

$$nFAK^{\theta}.Co_{(0,t)} \exp\left(\frac{-\alpha nF(E_{eq}-E^{\theta})}{RT}\right) = nFAK^{\theta}.Cr_{(0,t)} \exp\left(\frac{(1-\alpha)nF(E_{eq}-E^{\theta})}{RT}\right). \qquad 1.42$$

The bulk concentrations (Co^* and Cr^*) are found at the electrode surface because the system is at equilibrium. Thus

$$\exp nF(E_{eq}-E^{\theta})/RT = Co^*/Cr^*, \qquad 1.43$$

which is an exponential form of the Nernst equation. Although the net current is zero at equilibrium, the balanced Faradaic activity is expressed by the exchange current, i_o, which is equal in magnitude to both i_c and i_a:

$$i_o = nFAK^{\theta}Co^* \exp -\alpha nF(E_{eq}-E^{\theta})/RT. \qquad 1.44$$

If equation 1.43 is raised to the power of $-\alpha$ we obtain

$$\exp -\alpha nF(E_{eq}-E^{\theta})/RT = (Co^*/Cr^*)^{-\alpha}, \qquad 1.45$$

which when combined with equation 1.44 gives

$$i_o = nFAK^{\theta}(Co^*)^{(1-\alpha)}(Cr^*)^{\alpha}. \qquad 1.46$$

It can be seen that i_o is proportional to K^{θ}.

The current can be described in terms of the overpotential η, and by working with i_o instead of K^{θ}, using the equation derived earlier we now have

$$i = nFAK^{\theta}\left[Co_{(0,t)} \exp\left(\frac{-\alpha nF(E-E^{\theta})}{RT} \right) - Cr_{(0,t)} \exp\left(\frac{(1-\alpha)nF(E-E^{\theta})}{RT} \right)\right], \qquad 1.47$$

which when divided by equation 1.46 gives

$$i/i_o = \frac{Co_{(0,t)} \exp(-\alpha nF(E-E^{\theta})/RT)}{(Co^*)^{(1-\alpha)}(Cr^*)^{\alpha}} - \frac{Cr_{(0,t)} \exp(1-\alpha)nF(E-E^{\theta})/RT}{(Co^*)^{(1-\alpha)}(Cr^*)^{\alpha}}, \qquad 1.48$$

or

$$\frac{i}{i_o} = \left(\frac{Co_{(0,t)}}{Co^*} \exp \frac{-\alpha nF(E-E^{\theta})}{RT} \right)\left(\frac{Co^*}{Cr^*} \right)^{\alpha} - \left(\frac{Cr_{(0,t)}}{Cr^*} \exp \frac{(1-\alpha)nF(E-E^{\theta})}{RT} \right)\left(\frac{Co^*}{Cr^*} \right)^{-(1-\alpha)}. \qquad 1.49$$

The ratios $(Co^*/Cr^*)^{\alpha}$ and $(Co^*/Cr^*)^{-(1-\alpha)}$ can be evaluated by equations 1.43 and 1.45, from which the following relation can be derived.

$$i = i_o \left(\frac{Co_{(0,t)}}{Co^*} \exp \frac{-\alpha nF\eta}{RT} - \frac{Cr_{(0,t)}}{Cr^*} \exp \frac{(1-\alpha)nF\eta}{RT} \right). \qquad 1.50$$

The equation above predicts the current overpotential curve by the summation of two terms. For large overpotentials the current levels off to a limiting value, i_L due to restricted mass transfer of the reactant instead of the undergoing rapid rise predicted by the exponential factors, figure 3.4.

The Butler-Volmer equation applies if the diffusion and convection processes of mass transfer are reduced to insignificant levels by stirring, which causes the surface concentration and the bulk concentrations to be equal. The Butler-Volmer equation

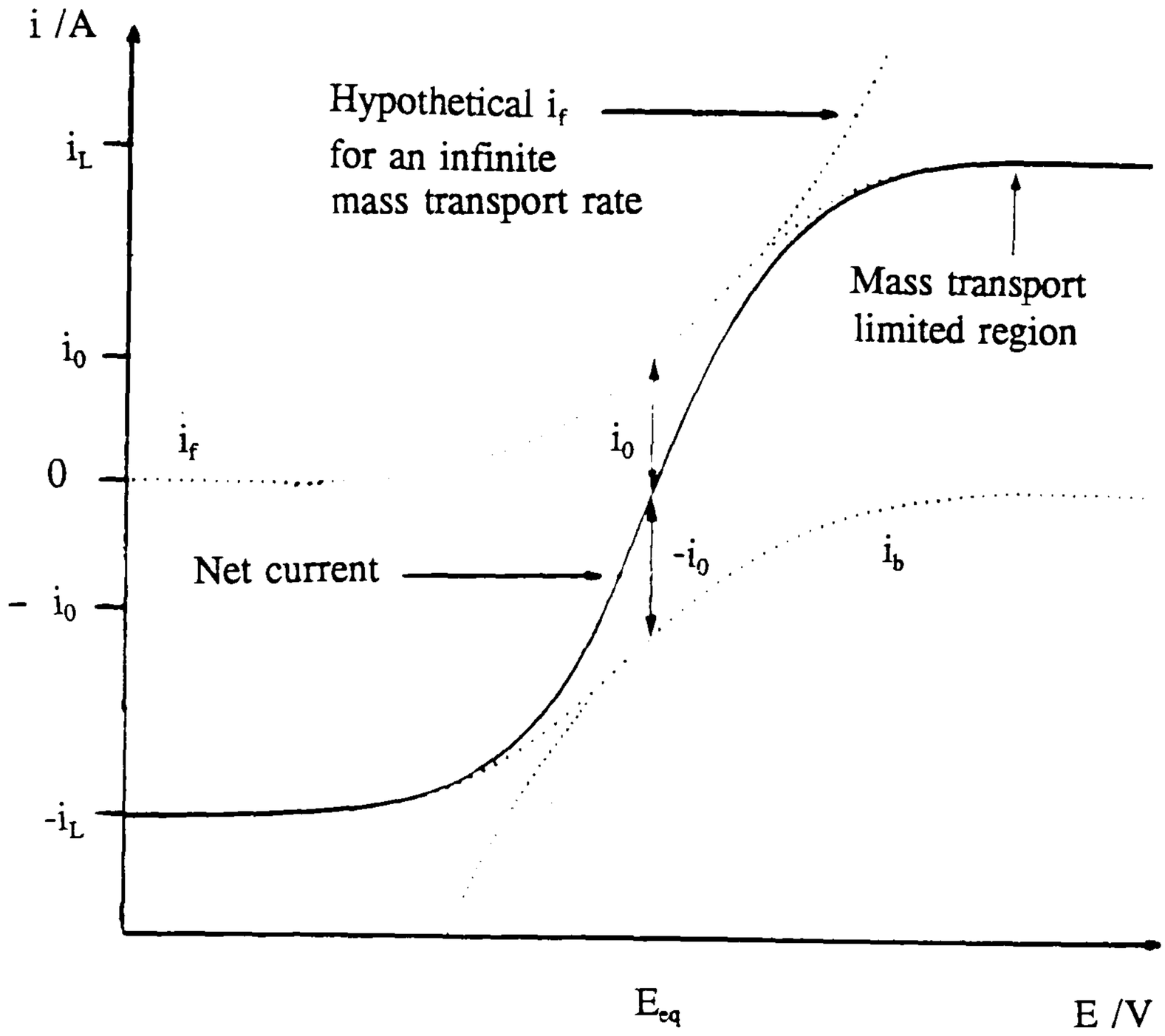

Figure 3.4

The Current/Potential Characteristic for a System

Containing Equal Bulk Concentrations of

a Reduced and Oxidised Species

(1.51), which is a simplification of equation 1.50 applies when the current flowing through the cell is small.

$$i = i_o[(\exp -\alpha nF\eta/RT) - (\exp(1-\alpha)nF\eta/RT)]. \qquad 1.51$$

3.1.5 Mass Transfer by Diffusional Effects

Mass transfer in the solution of an electrochemical cell is brought about by a gradient in the concentration or electrochemical potential, $\mu^{\ddagger}$, (diffusion and migration) or by convection. In an unstirred cell the convection processes can be reduced to a minimum by ensuring that the cell is free from temperature gradients and has settled down after degassing. The individual components of the Faradaic current flowing through the external circuit (due to the migrational and diffusional effects) may oppose each other depending on the direction of the electric field and the charge of the electroactive species. The mathematical treatment of electrochemical studies can be simplified by reducing the migration component until it becomes insignificant. This can be effected by the addition of a large molar excess of a supporting electrolyte that is electroinactive in the potential region of interest. The supporting electrolyte reduces the resistance of the electrolyte, ensuring that the electroactive species reaches the electrode by diffusional processes (except for approximately 0.5% of the total flux which is due to migration). The mathematics can be simplified further by assuming that the diffusion field is normal to the electrode surface.

Quantitative relationships

Consider a small section of the solution where there are two points Y and Z that are separated infinitesimally. At these two points there exists an imbalance in the electrochemical potential owing to a concentration gradient or an electric field. At a time t, the number of molecules of O at point Y are $No_{(x)}$ and at point Z $No_{(x+\Delta x)}$. After a passage of time Δt, the random movement of molecules means that half the molecules move by Δx in either direction. The difference in the number of molecules moving in either direction is the net flux through an area A. The situation above is given by the expression

$$J_{o(x,t)} = 1/A[\tfrac{1}{2}No_{(x)} - \tfrac{1}{2}No_{(x+\Delta x)}]/\Delta t, \qquad 1.52$$

where $J_{o(x,t)}$ is the net flux. Multiplying by $\Delta x^2/\Delta x^2$ (((YES))) and noting that the concentration of species O is given by $Co = No/A\Delta x$, we obtain

$$- J_{o(x,t)} = \frac{\Delta x^2}{2\Delta t} \cdot \frac{Co_{(x+\Delta x)} - Co_{(x)}}{\Delta x} \qquad 1.53$$

When we factorize the first term into a constant, called the diffusion coefficient, Do,

and allow Δx and Δt to tend to zero we obtain equation 1.54. This equation is Fick's first law of diffusion which states that the flux is proportional to the concentration gradient, ($\delta Co/\delta x$):

$$-J_{o(x,t)} = Do.\frac{\delta}{\delta x}Co_{(x,t)}. \qquad 1.54$$

The term '$\delta y/\delta x$' is used to represent a partial differential equation. Equation 1.54 provides the flux of material at an instant in time but in reality the variation of concentration is required. The change in concentration at any given location is determined by the incoming and outgoing flux from a volume of width dx:

$$\frac{\delta Co_{(x,t)}}{\delta t} = \frac{J_{(x,t)} - J_{(x+dx,t)}}{dx} \qquad 1.55$$

The flux at (x + dx) can be written as

$$J_{(x+dx,t)} = J_{(x,t)} + [\delta J_{(x,t)}/\delta x].dx, \qquad 1.56$$

which, when combined with Fick's first law, gives

$$\frac{-\delta J_{(x,t)}}{\delta x} = \frac{\delta}{\delta x}\left[Do.\frac{\delta Co_{(x,t)}}{\delta x} \right]. \qquad 1.57$$

A combination of equations 1.55 and 1.57 gives

$$\frac{\delta Co_{(x,t)}}{\delta t} = \frac{\delta}{\delta x}\left[Do.\frac{\delta Co_{(x,t)}}{\delta x} \right]. \qquad 1.58$$

If we take Do to be independent of position, we finally find a form of Fick's second law

$$\frac{\delta Co_{(x,t)}}{\delta t} = Do.\frac{\delta^2 Co_{(x,t)}}{\delta x^2}, \qquad 1.59$$

which when solved enables concentration profiles to be obtained. This in turn leads to the experimentally observed current.

3.2 An Expansion on the Basic Principles

3.2.1 A Solution of Fick's Second Law

The most common method used in solving the second law is that employing Laplace transformations. These are described in the literature [1,3-5]. The transformations enable a problematical equation to be converted into a domain where a simpler manipulation is possible, their most common use is for the solution of linear

differential equations. Partial differential equations can be transformed into ordinary differential equations that can be solved by conventional means or transformed again to yield a solution. The inverse transformation is then used to obtain the final answer.

The solution of Fick's second law by use of Laplace transformations is given in appendix 1. In order to solve the partial differential equation 1.59 we require one initial and two boundary conditions. The initial condition is that at the beginning of the experiment (t=0) the concentration of the species O is equal to that of the bulk solution, Co^*. We can write

$$Co_{(x,t)} = Co^*.$$

The first of the two boundary conditions is that at a sufficiently extreme potential, the surface concentration of species O is driven to zero, which means that the problem is purely diffusion controlled. Thus

$$Co_{(0,t)} = 0, \text{ for } t > 0.$$

The second boundary condition stipulates that at distances far enough away from the electrode, the events at the electrode surface will pass unnoticed, therefore

$$Co_{(x,t)} = Co^*, \text{ for } x \rightarrow \infty.$$

The analysis is given in terms of a component species O, the final result being:

$$Co_{(x,t)} = Co^* - Co^* \operatorname{erfc}(x/2[Do.t]^{1/2}) \qquad 2.1$$

The term erfc is the compliment of the normal error function. This is defined by the equation

$$\operatorname{erf} = 2/\pi \int \exp - x^2 \, . \, dx,$$

between the limits x and infinity. Equation 2.1 provides us with the concentration profile in terms of space and time. As time progresses the result of the electron transfer reaction is the depletion of species O from the electrode surface and a reduction of the concentration profile gradient, as the depletion of O spreads into the bulk solution (figure 3.5). Recalling Fick's first law it can be noted that the current response gradually decays with time after a potential step has been made (figure 3.5).

3.2.2 The Derivation of the Cottrell Equation: A Functional Form of the Current-Time Response

Fick's second law (equation 2.2) relates the current and the concentration gradient at the electrode such that

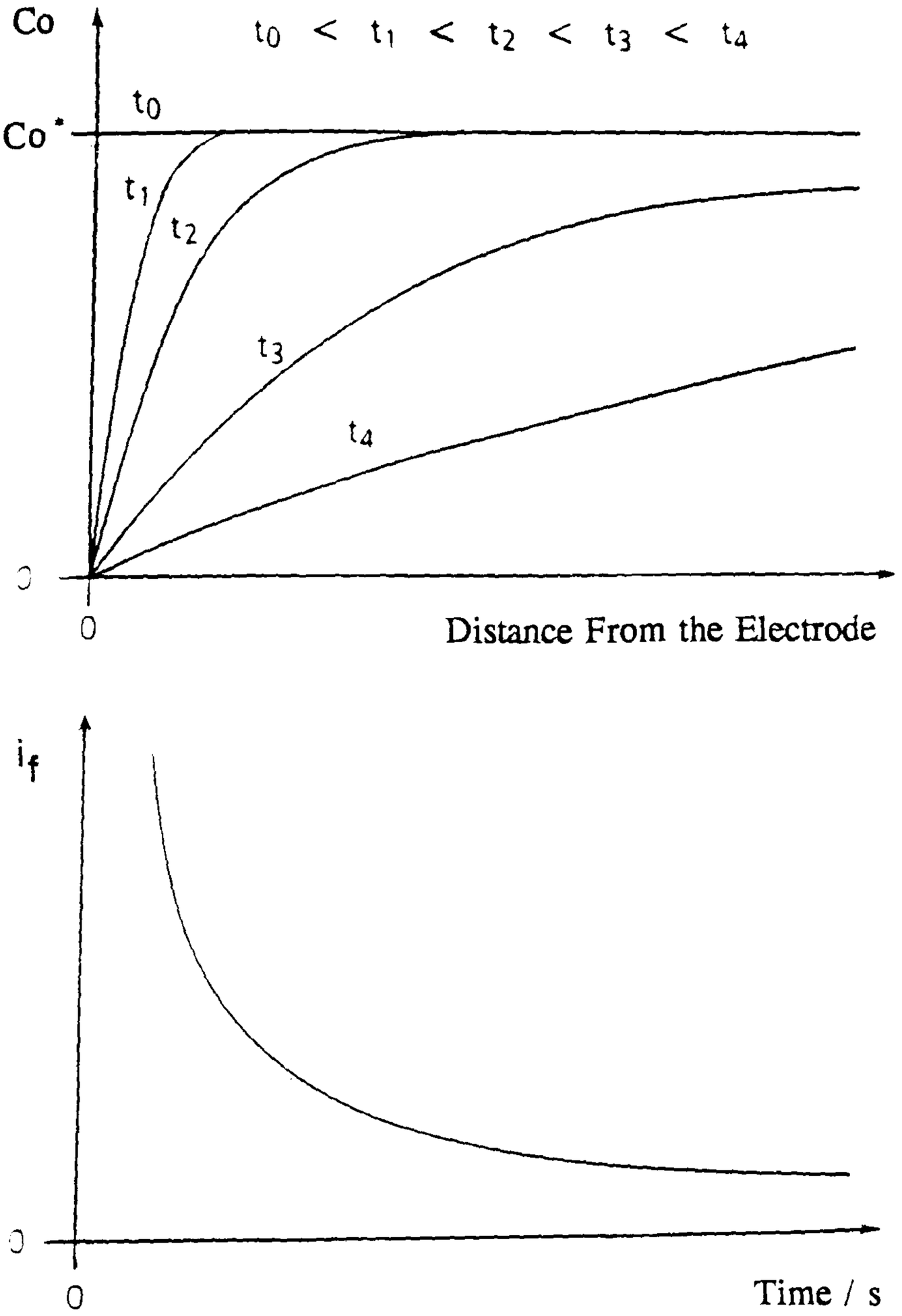

Figure 3.5

The Concentration Profile of a Reactant Species

as a Function of Time and the Associated

Current Function in Response to a Potential Step

$$\frac{\delta}{\delta t} Co_{(x,t)} = Do.\frac{\delta^2}{\delta^2 x} Co_{(x,t)}. \qquad 2.2$$

Equation 2.2 can be solved, to provide a solution with respect to a current function, by using Laplace transformations. This solution (which is subject to the initial and boundary conditions, described in the previous section, being obeyed) yields the Cottrell equation, which is given by

$$i = nFA.Do^{½}Co^{*}/(\pi t)^{½}. \qquad 2.3$$

The Cottrell equation predicts the current-time response for systems under purely diffusional control to be inversely proportional to the square root of time. Equation 2.3 has been derived for a system whereby the rate of electron transfer is limited by diffusion control, therefore it should be noted that the term $1/(\pi t)^{½}$ is a generalisation of the influence of diffusion on the electrochemical current-time response.

The current, time, potential relationship can be represented in a three dimensional diagram, by combining the current-potential characteristic (the sections orthogonal to the time axis) and the general current-time behaviour (giving the sections parallel to the time axis). Figure 3.6 represents this combination of characteristics, in an example where the forward electron exchange kinetics are fast (so that the concentration of species O at the electrode surface at $t>0$ is always zero) and the rate for the reverse direction is zero. From the diagram we can see the type of current response for a potential variation of the form

$$E = E_i + vt, \qquad 2.4$$

where v is the sweep rate dE/dt (expressed in the SI units of V s^{-1}). The potential at a time $t=0$ is E_i. On the t, E plane an excursion is made at an angle dependent on the sweep rate, and the intersection of this line with the surface provides us with the current profile for this particular electrode reaction scheme. The diagram shows that if a scan is performed at a fast sweep rate a larger peak current will be observed.

Cyclic voltammetric experiments offer the opportunity to obtain more data from an experiment. In these, the direction of the potential scan is reversed at some fixed potential. Scanning in the forward direction the electron transfer process is typically driven progressively faster up to the diffusion limit to produce products. As the scan returns to its original value the forward electron transfer reaction rate decreases and the reverse electron transfer process begins to dominate. Cyclic voltammetry is the most frequently employed technique for the investigation of electrode reaction

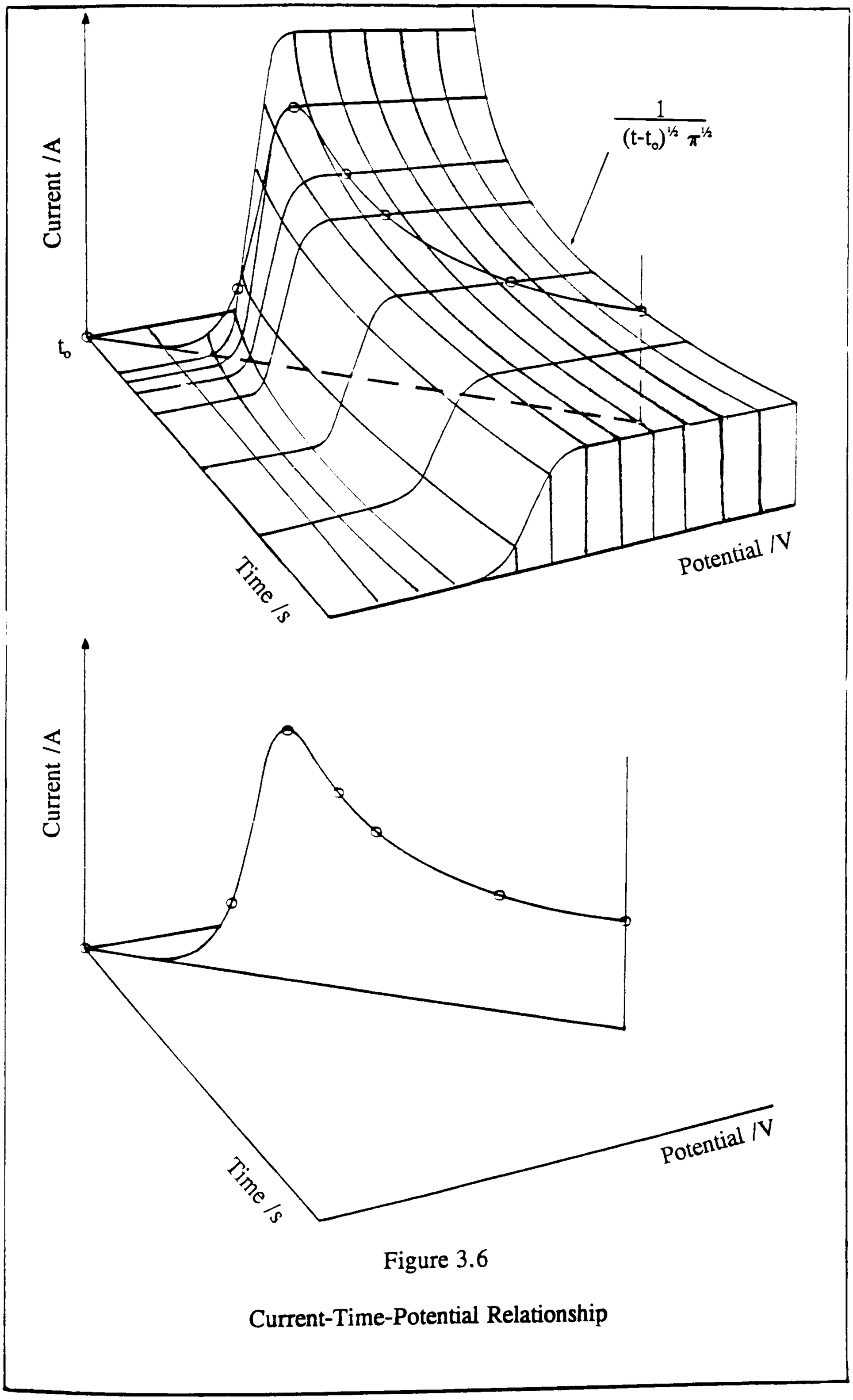

Figure 3.6

Current-Time-Potential Relationship

mechanisms because it is possible to discriminate between several reaction schemes by following the behaviour of specific characteristic points of the current function as the sweep rate is varied. The data are normally expressed in terms of current against potential, rather than time, which means that the parameters are seen as in figure 3.7.

3.2.3 An Alternative Method to the Direct Analysis of the Current Function: The Convolution Transform With the Function $(\pi t)^{-1/2}$

Cyclic voltammetry employs a triangular ramp on the applied potential, the apex being referred to as the switching or reversal potential. Up to the reversal potential the potential is a simply defined function of time, which for a reduction process is given as

$$E_{(t)} = E_i - vt. \qquad 2.5$$

In the case of an electron transfer system in which the rate of transfer is fast, the electrode surface concentrations are effectively determined by the Nernst equation. In this case the condition imposed at the electrode boundary is time-dependent. Thus for the reaction

$$O + ne^- \rightleftharpoons R \qquad 2.6$$

The boundary condition at the electrode is

$$Co_{(0,t)}/Cr_{(0,t)} = \exp nF(E-E^{\theta})/RT. \qquad 2.7$$

Substituting the potential in from equation 2.5 we obtain

$$Co_{(0,t)}/Cr_{(0,t)} = \exp nF(E_i-vt-E^{\theta})/RT. \qquad 2.8$$

It is impossible to solve the above equation to obtain the current function by the use of Laplace transformations, although Nicholson and Shain probably gave the most comprehensive treatment [6]. Their work is summarised in appendix 1. The resulting equation is an integral which can be solved numerically to give the current as a function of the potential.

$$\int_0^t \frac{i(u)}{nFA} \cdot \frac{1}{(t-u)^{1/2}} .du = \frac{Co^*.(\pi.Do)^{1/2}}{1+(Do/Dr)^{1/2} \exp nF(E_i-vt-E^{\theta})/RT} \qquad 2.9$$

Nicholson and Shain [6] give the solution to the equation in terms of a dimensionless current function $\varkappa$.

$$i = nFACo^*(\pi.Do.nFv/RT)^{1/2}\varkappa \qquad 2.10$$

where
$$\varkappa = [\sum (-1)^{J+1}J^{1/2} \exp[-JnF(E-E^{\theta})/RT]]/\pi^{1/2} \qquad 2.11$$

The range of the summation is from J=1 to infinity. The term E^{θ} in equation 2.11 can be replaced by $E_{1/2}$ which represents the polarographic half-wave potential. In this example $E_{1/2}$ is the potential at which the oxidised and reduced species are present at

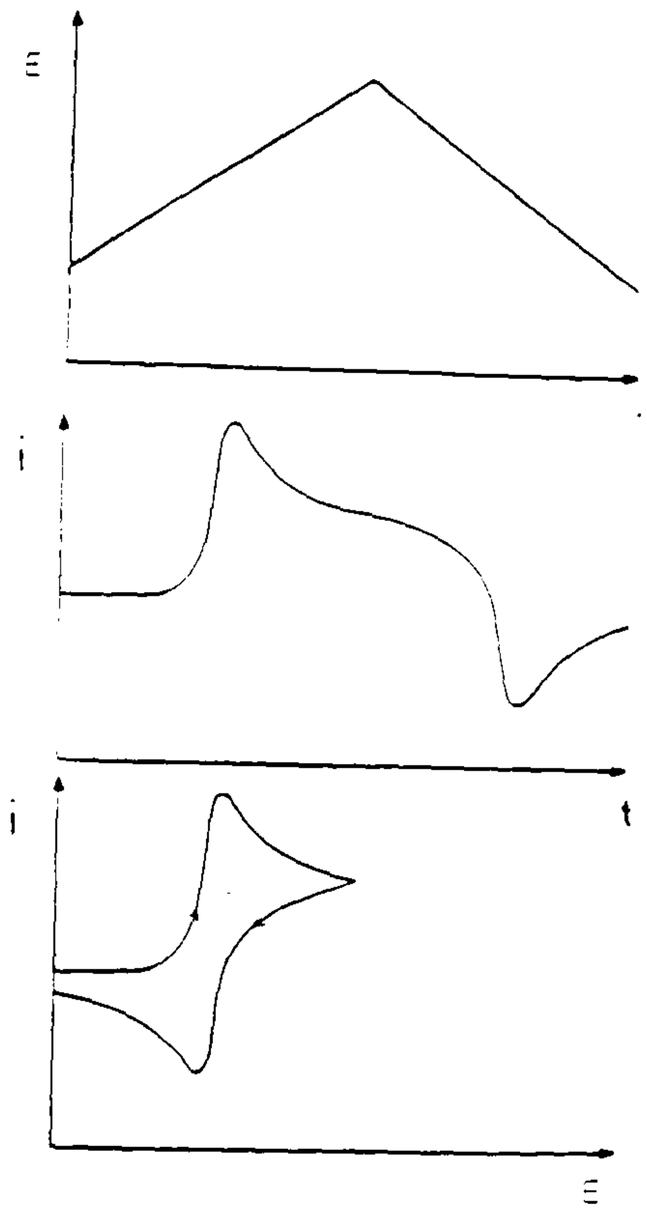

Figure 3.7

The Representation of Cyclic Voltammetric Data

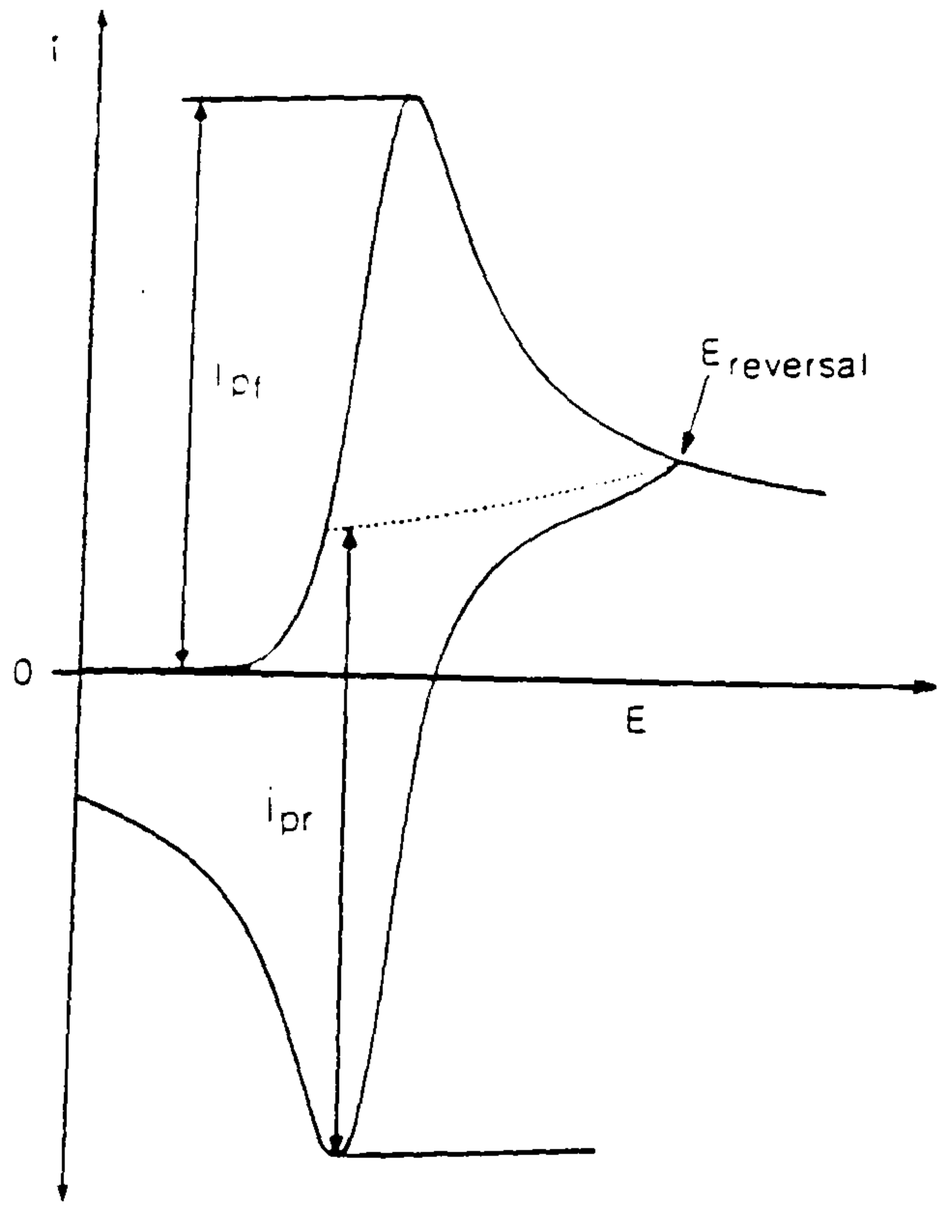

Figure 3.8

The Construction Proposed by Nicholson [6]
for the Measurement of Peak Current Values

the electrode surface in equal concentrations. The half-wave potential and the standard electrode potential, E^{θ}, are related by the expression

$$E_{1/2} = E^{\theta} - (RT/nF) \ln (Do/Dr). \qquad 2.12$$

$E_{1/2}$ is equal to E^{θ} when the diffusion coefficients of the oxidised and reduced species are the same. From equation 2.10 it can be seen that the size of the peak current is proportional to $v^{1/2}$ and to the bulk concentration of the starting species. In a similar manner equation 2.11 shows that the potential of the maximum current is independent of the sweep rate and the starting concentration.

There are shortcomings associated with the testing of experimental data to fit a mechanistic or kinetic model. Firstly they normally only use the peak current and its associated potential. This is compounded by the fact that the magnitude of the reverse peak has to be determined from the interpolated current value for the falling baseline of the forward sweep, a method prone to introducing errors (figure 3.8). Furthermore before analysis of a current- potential response can be made, the mechanistic model must have already been assumed. This restricts the scope for investigation. In the above example it has been assumed that the electron transfer is fast, so that the Nernst equation is obeyed. It could have equally well been assumed that the electrode boundary condition was given by the Butler-Volmer model. Another drawback is that the response functions are exceedingly complex in nature, the solution of even simple system requiring very complicated mathematics.

Cyclic voltammetry is a very popular analytical technique, despite the limitations involved in directly examining the current function. To overcome these problems, an alternative approach based on the convolution integral can be used. This is described below.

3.2.4 The Use of the Convolution Integral in Cyclic Voltammetry

Using equation 2.13 (derived in appendix 1)

$$Co_{(0,t)} = Co^{*} - \frac{1}{(\pi.Do)^{1/2}} \int_0^t \frac{i(u)}{nFA} \cdot \frac{1}{(t-u)^{1/2}} \cdot du \qquad 2.13$$

and rearranging the constant terms, the concentration of the species O under semi-infinite linear-diffusion conditions can be obtained. It has the form

$$Co_{(0,t)} = Co^{*} - \left(\frac{1}{nFA.Do^{1/2}}\right)\left[\frac{1}{\pi^{1/2}} \int_0^t \frac{i(u)}{(t-u)^{1/2}} \cdot du\right]. \qquad 2.14$$

The term in square brackets can be rewritten in terms of a convolution transform I(t) of the experimental data, i(t).

$$I(t) = \frac{1}{\pi^{1/2}} \int \frac{i(u)}{(t-u)^{1/2}} \cdot du. \qquad 2.15$$

These equations have been derived without assuming any kinetic model for electron transfer. They allow reaction concentrations to be obtained in a function of the potential, rather than depending on rates. In order to do this the convolution integral has to be evaluated to obtain a transformed function that is related to the surface concentrations of the reactant and product, as a function of the potential. This method of approach has been followed independently by both Saveant [7,8] and Oldham [9,10]. Substitution of 2.15 into 2.14 and rearrangement gives

$$I(t) = nFA.Do^{1/2}(Co^{*} - Co_{(0,t)}) \qquad 2.16$$

and for the reduced species

$$I(t) = nFA.Dr^{1/2}.Cr_{(0,t)}. \qquad 2.17$$

From equation 2.16 it can be seen that I(t) takes on a limiting value when $Co_{(0,t)} = 0$; thus the maximum convoluted current obtainable under diffusion controlled conditions is

$$I_L = nFA.Do^{1/2}.Co^{*}. \qquad 2.18$$

This equation is valid no matter what form of potential variation is used to drive $Co_{(0,t)}$ to zero.

A convenient and fast method of evaluating the convolution integral I(t) is the use of the expansion (over the range J=1 to K)

$$I(t) = \frac{1}{\pi^{1/2}} \sum \frac{\Gamma(K-J+1/2)}{(K-J)!} \Delta t^{1/2} i(J\Delta t). \qquad 2.19$$

Here K is the index for the particular I, being calculated; J is the series counter for the discrete points 0 to K at which the current is sampled; Δt is the time interval between successive data points and Γf is the gamma function of f. The appropriate values of Γf for the semi-integral values of f are given by the series

$\Gamma(1/2) = \pi^{1/2}$

$\Gamma(1\,1/2) = 1/2.\pi^{1/2}$

$\Gamma(2\,1/2) = 1\,1/2.1/2.\pi^{1/2}$

$\Gamma(3\,1/2) = 2\,1/2.1\,1/2.1/2.\pi^{1/2}$ etc.

The significance of the variables t and u is shown in figure 3.9. The evaluation of I_1, using equation 2.19 requires that the data be in numerical form. This is facilitated by the use of computers for data capture. By using equation 2.18 the concentration of the

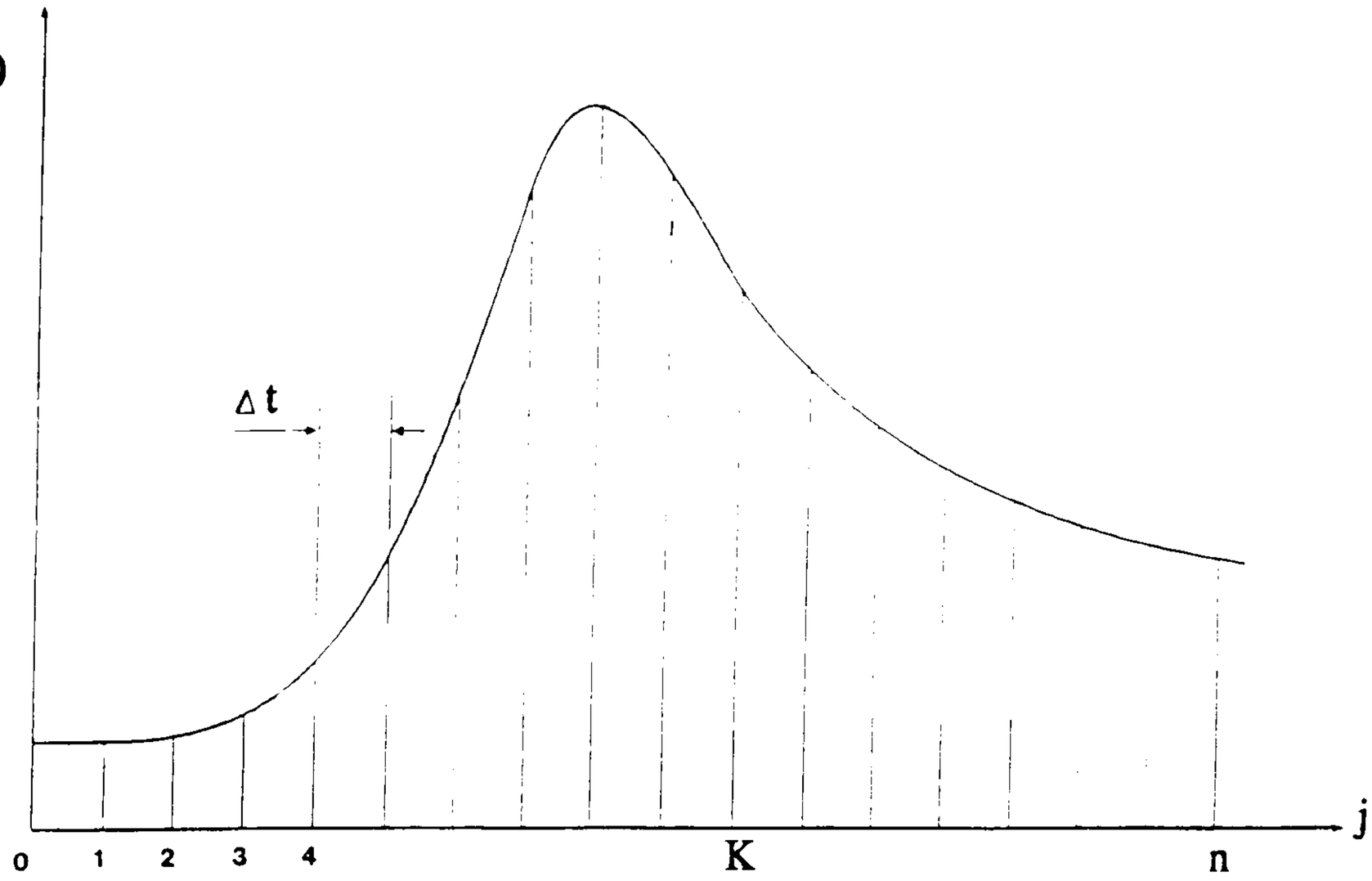

Figure 3.9

Subdivision of Experimental I(t) Data for
the Evaluation of the Convolution Integral I_1

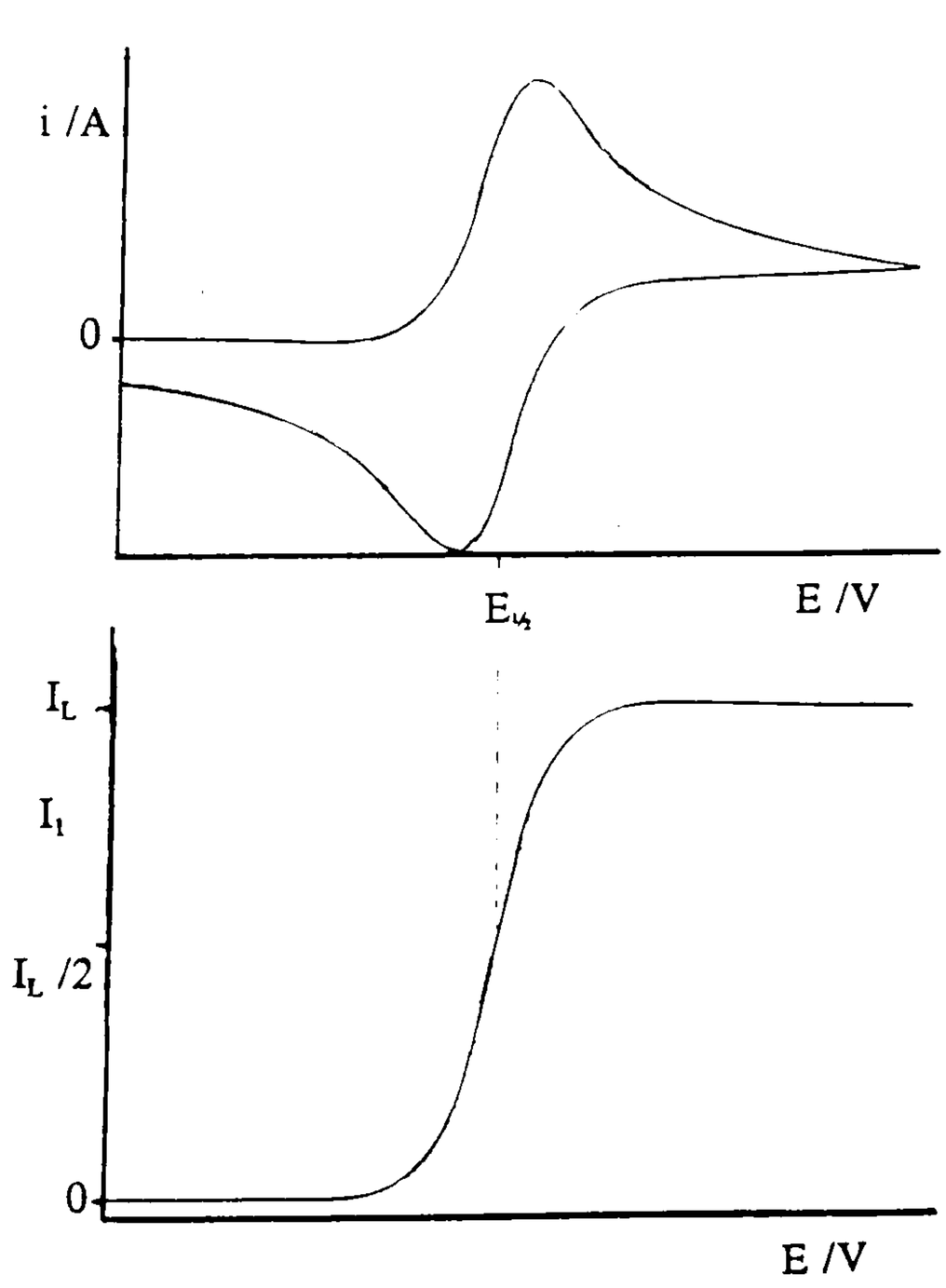

Figure 3.10
A Representation of Raw and Convoluted Data for a Nernstian System

bulk solution at t=0 can be related to a limiting convoluted current. The following equation is derived in this manner.

$$Co_{(0,t)} = [I_L - I_1]/nFA.Do^{½}. \qquad 2.20$$

The Nernst equation, given in terms of equation 2.17 and 2.20 is now

$$E = E^{\theta} + \frac{RT}{nF} \ln\left(\frac{I_L - I_1}{I_1}\right) + \ln\left(\frac{Do^{½}}{Dr^{½}}\right) \qquad 2.21$$

Assuming that the diffusion coefficients are equal, equation 2.21 simplifies to

$$E = E^{\theta} + \frac{RT}{nF} \ln\left(\frac{I_L - I_1}{I_1}\right), \qquad 2.22$$

yielding the characteristic functional form as shown in figure 3.10. If a set of experimental data follows Nernstian behaviour, a plot of $\ln(I_L-I_1/I_1)$ against E gives a straight line with a slope of RT/nF and an intercept of $E_{½}$. Unlike traditional methods of electrochemical analysis, all the data points are used. A further test of Nernstian behaviour is the coincidence of the forward and reverse sweeps over a wide range of potential scan rates. In the case of an irreversible system, where the rate of electron transfer is finite in the forward direction and zero in the reverse, a plot of $\ln(I_L-I_1/i)$ against E gives a gradient of $RT/\alpha nF$. This provides us with a simple method to obtain the symmetry factor α.

For a non-Nernstian response, the general form of the rate law for electron transfer is applicable:

$$i = nFAK_E[Co_{(0,t)} - Cr_{(0,t)}] \exp nF(E-E^{\theta})/RT, \qquad 2.23$$

where K_E represents the forward, potential dependent, rate constant. The substitution of $Co_{(0,t)}$ and $Cr_{(0,t)}$ respectively into their $(\pi t)^{-½}$ convoluted current expressions allows the potential dependent rate of electron transfer for the forward reaction to be expressed as

$$\ln K_E = \ln Do^{½} - \ln\left[\frac{(I_L-I_1)(1 + \exp nF(E-E_{½})/RT)}{i}\right]. \qquad 2.24$$

The above expression has not been derived by recourse to the Butler-Volmer kinetic model, and has been used to measure the potential dependence of the symmetry factor by observing the deviations from linearity of $\ln K_E$ against E plots [11]. The equation can also be used to determine the half-wave potential $E_{½}$ from both Nernstian and Quasi-reversible systems. Considering the system whose current and convoluted current are shown in figure 3.11, the current passes through zero at a potential given by $E_{i=0}$

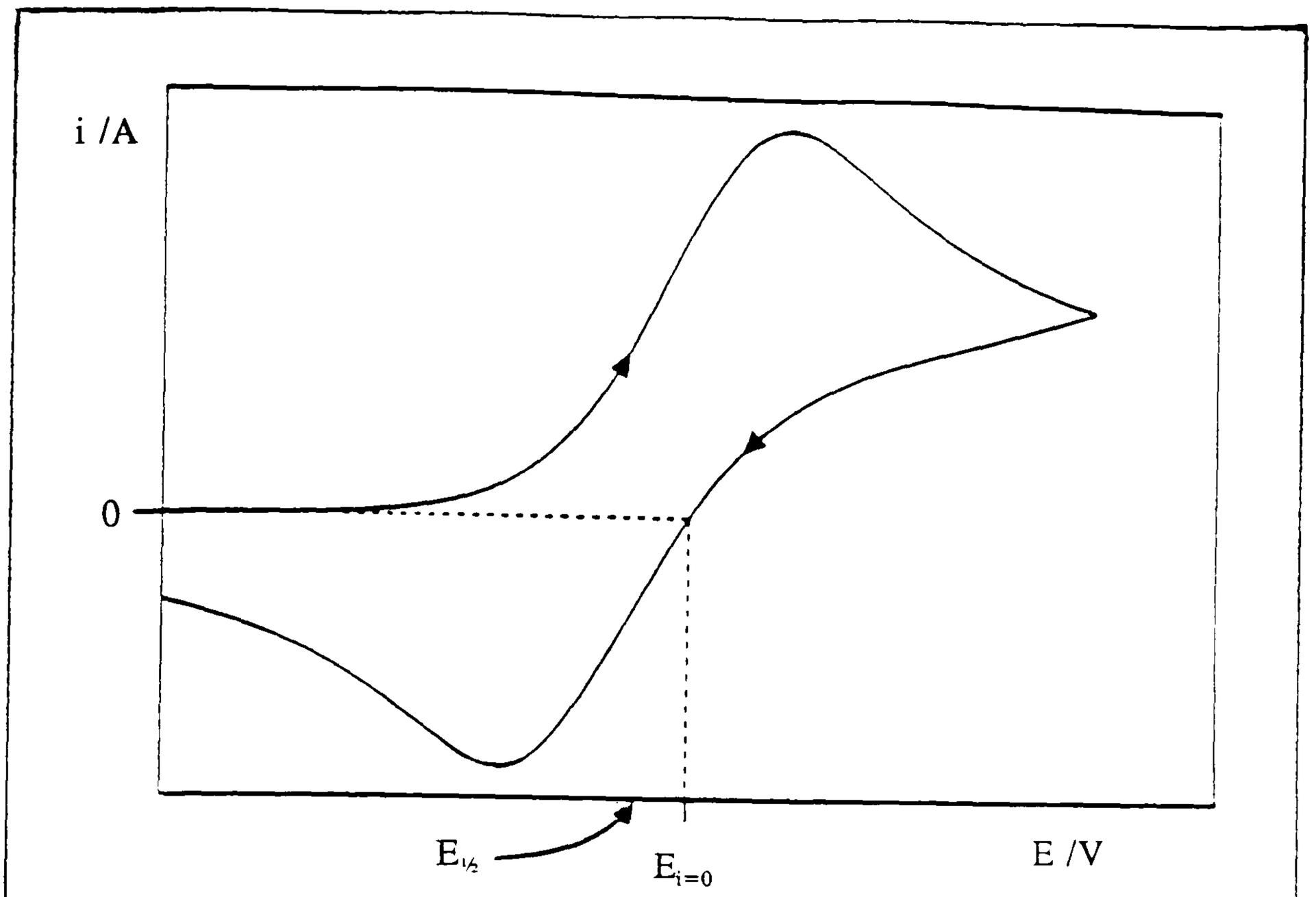

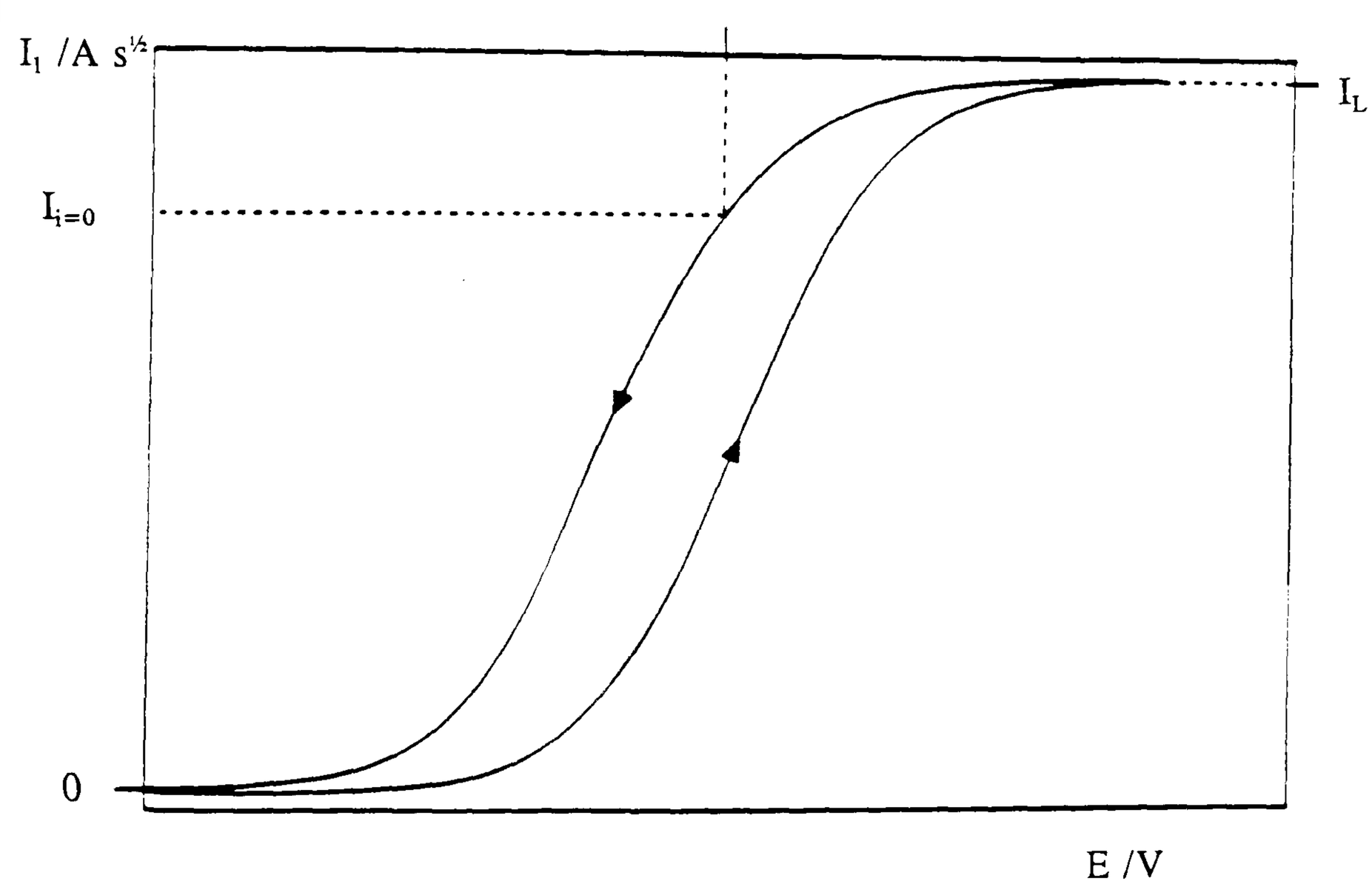

Figure 3.11

The Extraction of $E_{1/2}$ from Non-Nernstian Data

on the reverse sweep. At this potential the convoluted current is given by $I_{i=0}$. The forward rate is finite (realised by inspection of the forward-sweep current response) and in order to satisfy this requirement, the numerator of the second term on the right-hand side of equation 2.24 must be zero (since the denominator by definition is zero). Therefore

$$I_L = I_{i=0} (1 + \exp nF(E_{i=0}-E_{½})/RT) = 0. \qquad 2.25$$

On rearrangement to obtain $E_{½}$ we find

$$E_{½} = E_{i=0} + \frac{RT}{nF} \ln\left(\frac{I_L-I_{i=0}}{I_{i=0}}\right). \qquad 2.26$$

The $(\pi t)^{-½}$ convolution transform can be used to test the adherence of a system to certain kinetic models. Using all the data points for the superimposition of logarithm functions against potential for both the forward and reverse sweeps, plus the independence of these plots to both sweep rate and starting concentrations, the method lends itself to a greater degree of confidence in the adoption of a particular kinetic model.

3.2.5 The Deconvolution of the Current Function $(\pi t)^{-½}$

Let us consider a known convolution transform (H) of an unknown current with an analytically specified function F, of time:

$$H_{(t)} = i*F_{(t)}, \qquad 2.27$$

where * represents the convolution transform operation. If a suitable Laplace transform exists the deconvolution of H gives us the unknown current in the required form

$$i = d(H*\Psi)/dt \qquad 2.28$$

where $\Psi = L^{-1}[S.L(F)]^{-1}$, in which L is the Laplace operator and L^{-1} its inverse. The term S is a dummy variable introduced in a transform and lost on performing the inverse transform. This general example when applied to our specific case gives

$$I_{1(t)} = i*1/(\pi t)^{½}, \qquad 2.29$$

so we have

$$\Psi_t = L^{-1}([S.L(\pi t)^{-½}]^{-1}) \qquad 2.30$$

Since the Laplace transform of $(\pi t)^{-½} = S^{-½}$, equation 2.30 can be rewritten as

$$\Psi_t = L^{-1}[(S.S^{-½})^{-1}] = L^{-1}\, S^{-½}, \qquad 2.31$$

which gives $\Psi_t = (\pi t)^{-½}$, so that the function F and Ψ are identical. Equation 2.28 can now be rewritten as

$$i = d[(\pi t)^{-½}*I_1]/dt. \qquad 2.32$$

The convolution of the I_1 function with $(\pi t)^{-½}$ gives the integral of the current, i.e. the charge passed. Deconvolution of both sides of equation 2.32 illustrates that the deconvolution transform of the current with the function $(\pi t)^{-½}$ is given by the first differential of the convolution transform I_1 with respect to time. The data when

displayed in a deconvoluted format shows an increased resolution in detail over the current potential data. Overlapping electrode processes are more easily identifiable, coupled chemical reactions can be evaluated rapidly and in the case of electrode reactions that undergo fast electron transfer, the half wave potential is obtained from the maxima of symmetrical peaked responses.

3.2.6 The Analysis of Coupled Electrochemical Reactions

The advantage of using the I_1 convolution for the analysis of a simple electrochemical reaction where it is applied in a quantitative manner has already been outlined. In the instances where the electron transfer reaction is complicated by a coupled chemical reaction, its use is limited to a qualitative analysis. If certain kinetic behaviour is assumed [11], the I_1 convolution can still be applied advantageously. In appendix 1, the methods of analysis are described in further detail for each of the various combinations of electrochemical-chemical reaction.

The systems encountered in this thesis have been of the simplest group encountered; the EC scheme. This is where a unidirectional chemical process follows the electrode process. The convolution integral (derived in appendix 1) for the associated chemical process is given by

$$I_3 = \frac{1}{\pi^{1/2}} \int_0^t \frac{i(u) \exp [- k_f'(t-u)]}{(t-u)^{1/2}} .du \qquad 2.33$$

The variable k_f' is the first-order rate constant for the associated chemical reaction that consumes the product of the electrode reaction:

$$A \overset{ET}{\rightleftharpoons} B \overset{k_f'}{\rightarrow} C. \qquad 2.34$$

The value of the rate constant can be evaluated by use of the I_3 transform by an iterative process, which converges on the solution. From expression 2.35 derived in appendix 1 it can be seen that the value of I_3' is directly proportional to the concentration of the oxidised species at the electrode surface, $Cb_{(x=0)}$:

$$Cb_{(x=0)} = \beta.D^{1/2}.I_3'. \qquad 2.35$$

During the course of an experiment the value of I_3' will rise from zero to a finite value and then fall again to a minimum. The transform is tested by inserting values of k_f' until the transform returns to zero at the end of the cyclic experiment (figure 3.12). When a value for k_f' has been determined, the heterogeneous parameters can be obtained by using the equation

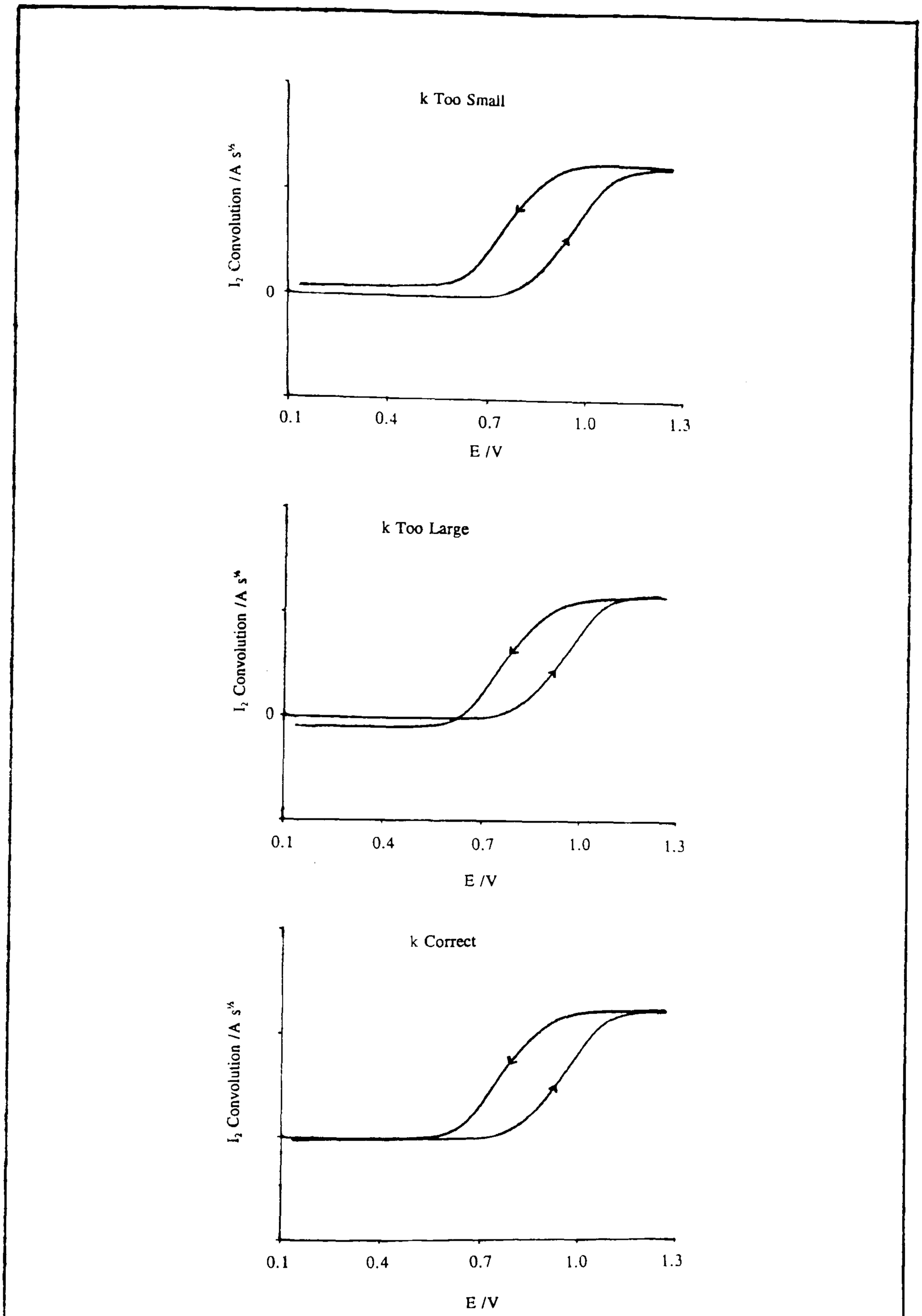

Figure 3.12

The Determination of the First Order Rate Constant

for the Decay of the Oxidised Species

$$-\varepsilon = \ln \frac{I_L - I_1}{\left(\frac{i}{i_0}\left[I_L \exp\left(1-\alpha\right)\varepsilon\right] + I_3'\right)} \qquad 2.36$$

where the reduced potential, $\varepsilon = (E-E_{1/2})F/RT$.

The determination of the chemical rate constant in this manner means that no prior knowledge of the heterogeneous kinetics is required and that no restrictions on the electron transfer kinetics are made. The method used by Saveant [12] depends on the peak current variations and requires that the process is Nernstian in behaviour. The method proposed by Woodward requires α, $E_{1/2}$ and k^{θ} to be determined by experiments with timescales such that no appreciable chemical reaction can occur [13]. In the method used in this work all data points are used to obtain the results, instead of just single points on the i-E curve.

3.3 Description of the Apparatus

The electrochemical cell was a 50 cm^3 capacity Metrohm cell. It was surrounded by a water-cooled jacket that maintained the temperature at 18 to 20°C. The analytical cell was closed by a plastic lid, with an 'O' ring, that had 5 Q.F. 14/23 female joints providing ports for the electrodes, the thermometer and a water-cooled condenser. The condenser itself provided the port for the nitrogen gas purge tube (figure 3.13). The nitrogen gas stream was dried by passing it through a column of activated silica gel and the flow rate metered after drying.

The reference electrode was silver / silver chloride / saturated lithium chloride solution; the working electrode was glassy carbon embedded in an epoxy resin coating; the counter electrode was a 1 cm square of platinum foil 0.25 mm thick. A 30×10^{-9} farad capacitor was fitted between the reference and counter electrodes to smooth the voltage ramp supplied by the programmer.

The Model 363 Potentiostat/Galvanostat and the Model 175 Universal Programmer are manufactured by Princeton Applied Research Corporation. The programmer allowed a series of complicated programs to be specified, with one or multiple sweeps and sweep rates of 1 mV s^{-1} to 1000 V s^{-1} permitted. The Galvanostat, which had a current range of 1 μ A to 1 A was triggered by the programmer to give a triangular wave form thus enabling experimental data to be obtained. The signal output from the cell was captured using an Amstrad PC 1640-HD20 computer via an analogue to digital

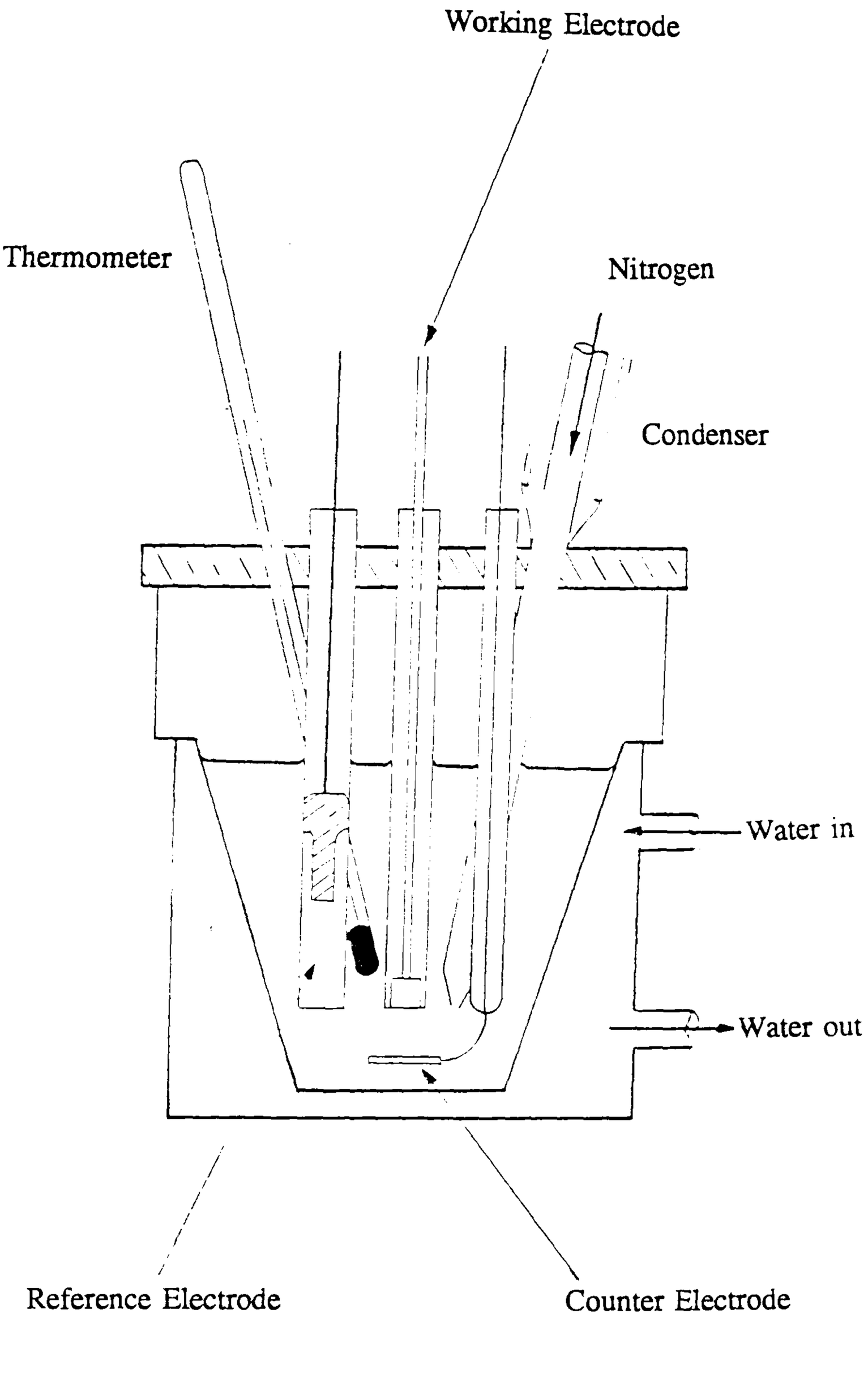

Figure 3.13

Schematic Representation of the Metrohm Vessel

converter designed and constructed in the School of Chemistry workshops. The conversion time of the A/D converter being 50 μs. Data capture/convolutive software was provided by the commercially available CONDECON package developed in the Department of Physical Chemistry, University of Leeds. The software allowed a minimum acquisition time of 100 μs per point. Each experiment consisted of 2000 data points, equally spaced in time. The software package also allowed the current response to be convoluted as a function of time and displayed in a number of forms relevant to kinetic diagnosis. The final output of the data was obtained on a NEC P2200 printer or a Graphtec XY MP4300 plotter.

3.4 The Reagents and Preparation of the Electrodes

The solvent used was HPLC grade dichloromethane ($MeCl_2$) supplied by May and Baker. This was dried by passing it through a column of activated silica gel (Fisons, 60-120 mesh). The electrolyte, >98% pure tetrabutylammonium perchlorate (TBAP) was obtained from Fluka and the lithium chloride (GPR) from Fisons.

The base oils, Mobil RTS-9745, Castrol LPE 504 and BSM 150 were supplied by the Ministry of Defence, Directorate of Quality Assurance (DQA-TS). The antioxidants, dioctyldiphenyl amine and Topanol 'O' were also supplied by DQA-TS.

The vycor plugs used for the reference electrode were supplied by EG&G along with the glassy-carbon working electrode and the silica grinding paste. The counter electrode was constructed out of a 1x1 cm^2 piece of platinum foil, 0.25 mm thick, spot-welded to a 0.3 mm diameter platinum wire, 5 cm in length. The wire was inserted into a 6 mm diameter, 20 cm long soda-glass tube with the lower end subsequently fused to it to prevent seepage of the electrolyte into the electrode. Electrical contact was made between the platinum wire and the counter electrode lead from the potentiostat/galvanostat by means of a mercury pool figure 3.14. The reference electrode was made from a QF straight air/stream inlet tube with a 14/23 cone (cat. MF 15/1) modified by fitting a vycor plug at the end. Electrical contact was made by inserting a 1 mm diameter silver wire into the electrode solution, figure 3.14. The working electrode was made of a epoxy resin sleeve containing a 5 mm diameter glassy-carbon block in electrical contact with a stainless-steel rod held in place by a PTFE collar, figure 3.14.

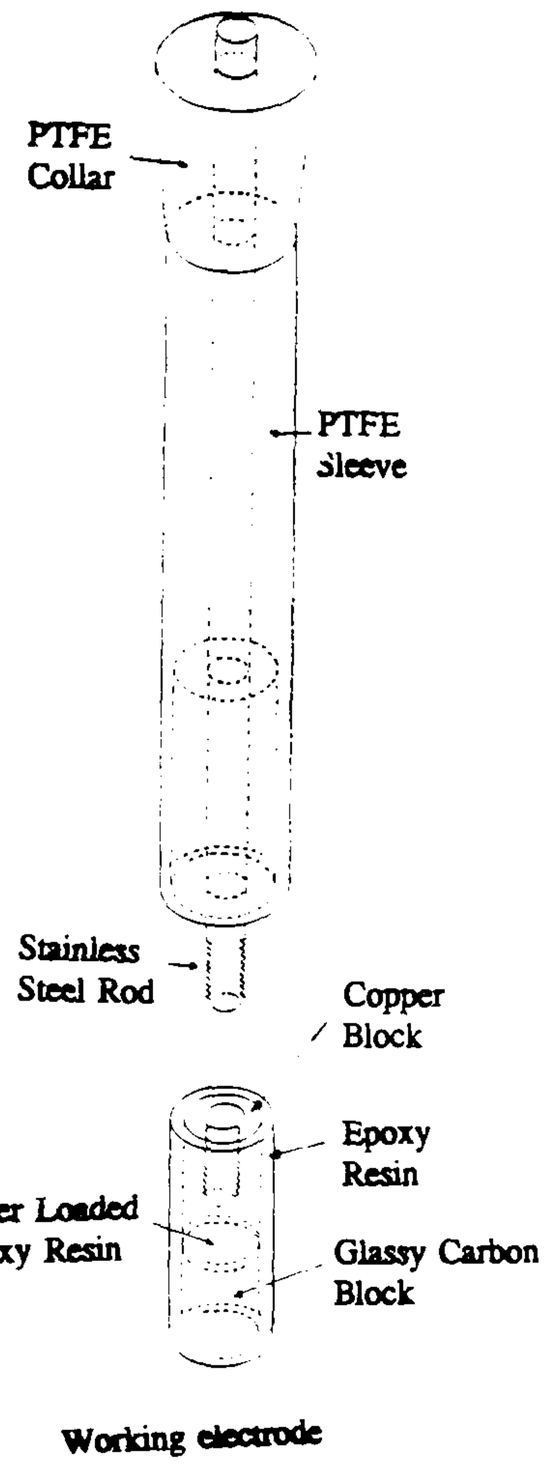

Working electrode

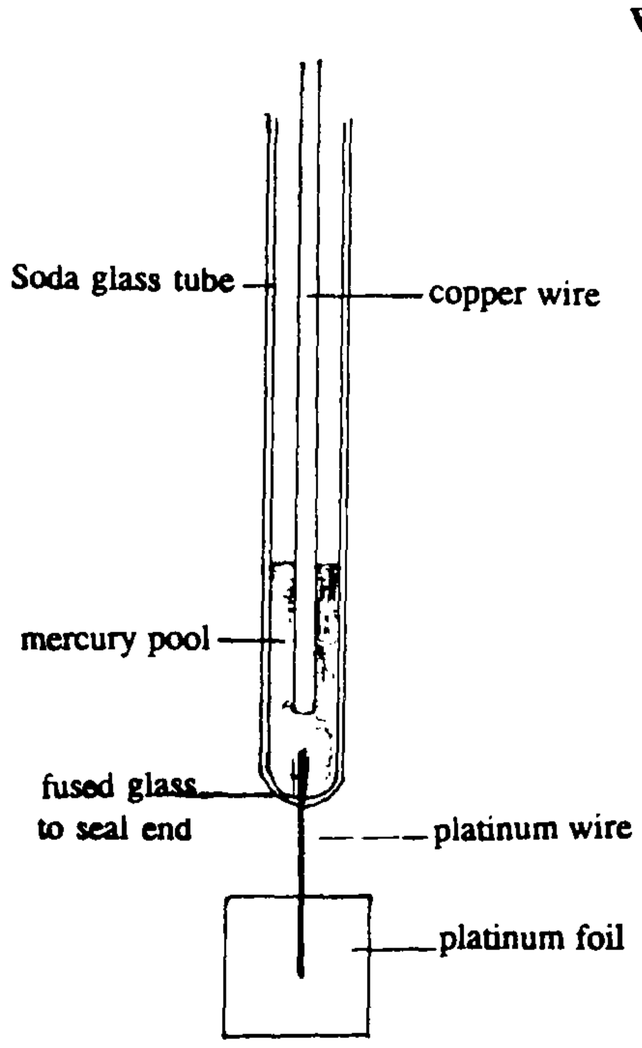

Counter Electrode

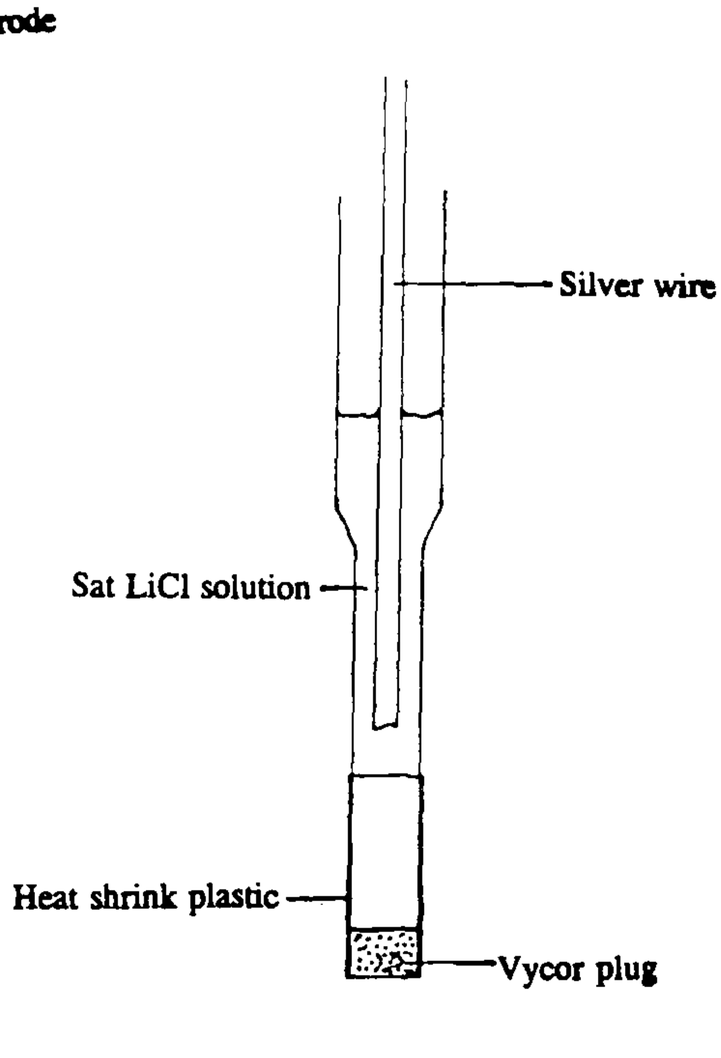

Reference electrode

Figure 3.14

Schematic Representation of the Electrodes

3.5 Experimental Variables

3.5.1 Sample Concentration

The effect of sample concentration is one encountered by most analytical chemists. If the sample concentration is too low the errors associated with the analysis become proportionally larger. In the case of the amine antioxidant, the lower limit of detection was approximately $1x10^{-3}$% w/w in the analytical solution. The amine could be detected at a lower concentration than this, but without any degree of confidence in the precision of the result. The magnitude of the error associated with an experimental result was $\pm$ 2%.

The concentration of the oil in the test solution was chosen as 3% w/w, to provide a large concentration of antioxidant in the analytical solution without needing too large a sample of oil. If a 1% solution was chosen, oils with antioxidant levels below 0.1 to 0.2% would be impossible to analyse. The analytical solution was able to dissolve in excess of 10% w/w of oil, which gave very clearly defined peaks but would mean that large samples of oil are required to enable duplicate analyses to be performed. This is only a minor problem, because the usual analytical techniques require large samples to be taken.

3.5.2 Scan Speed

The effect of the scan speed has been discussed previously in this chapter. The experimental perturbation is larger when a larger scan speed is employed, but at the cost of a reduction in the resolution of an electrochemical event. This is illustrated by the use of the I_1 convolution to analyse the experimental results. When the scan speed is slow, below 1 V s^{-1}, the convolution levels off to a plateau at the end of the electrochemical reaction. Conversely when the scan speed is above 2 V s^{-1} the convolution does not attain a steady value, but continues to rise slowly as more reactant reaches the electrode surface. If the scan speed is too slow, below 0.005 V s^{-1}, then the duration of the experiment becomes such that diffusion of the reactant or product away from the electrode becomes significant. This effect can lead to noisy analytical signals. Furthermore these effects can complicate mechanistic analysis if they are ignored.

3.5.3 Temperature

The effect of temperature on the experimental result enables a mechanistic analysis to be performed. The rate of the coupled chemical reaction increases with temperature.

The quantitative analysis of the antioxidants was found not to alter noticeably with temperature, but during the summer months evaporation of the solvent caused stirring by convection effects and an increase in the concentration of the solution. These effects were overcome by the use of a cell with an integral water jacket that maintained the analysis temperature at approximately 20°C.

During the kinetic analysis of the amine antioxidant, when the analytical solution temperature was decreased sufficiently, the solvent system froze. The points of crystal nucleation were the electrode surfaces. This effect, like the evaporation of the solvent lead to misshapen analytical curves, rendering the experiment useless.

3.5.4 Oxygen

The presence of oxygen in the analytical solution lead to a peak in the reduction sweep of the voltammogram at -0.8 V vs the Ag/AgCl reference. This was due to the reduction of the molecular oxygen. The peak was found when analysing a solution of an oxidised oil. It was initially thought to be the reduction curve of oxidised antioxidant. This illustrates the need for thorough degassing. Although the presence of oxygen in the solution did not affect the analysis of the unoxidised amine antioxidant it may facilitate the contamination of the electrode surfaces.

3.5.5 Electrodes and Solvent System

The effect of the choice of the main experimental parameters on the final result is illustrated in the experimental chapters. It should be noted that the voltammogram can be complicated by adsorption of the solvent, electrolyte or oil system onto the electrode surface. These effects can be reduced or eliminated by the correct choice of electrode.

The choice of solvent is usually determined by the solubility of the oil, the voltage window and the conductivity of the solvent system. If the solvent has a low conductivity the iR term becomes significant and has to be compensated for in the analysis. A high solution resistance tends to cause the peaks to spread apart hindering analysis. A factor not often considered is the volatility and toxicity of the solvent. When a volatile solvent is used a sealed cell has to be used to prevent evaporation loss and when solvents such as acetonitrile are used (both volatile and toxic) the analysis must be performed taking the necessary precautions.

References

1. A. J. Bard and L. R. Faulkner, "Electrochemical Methods, Fundamentals and Applications", John Wiley and Sons, New York, 1980.
2. W. J. Moore, "Physical Chemistry", 5th Edition, Longman, London, 1972.
3. G. Doetsch, "Introduction to The Theory and Application of The Laplace Transformation", Translated by W. Nader, Springer-Verlag Berlin Heidelberg, New York, 1974.
4. G. Stephenson, "Mathematical Methods For Science Students", 2nd Edition Longman, London, 1986.
5. "Handbook of Mathematical Functions, With Formulas, Graphs and Mathematical Tables", Edited by M. Abramowitz and I. A. Stegun, Dover, New York, 1965.
6. R. S. Nicholson and I. Shain, *Anal. Chem.*, 36, 1964, p 706.
7. C. P. Andrieux, L. Nadjo and J. M. Saveant, *J. Electroanal. Chem. and Interfac. Electrochem.*, 26, 1970, p 147.*
8. J. C. Imbeaux and J. M. Saveant, *J. Electroanal. Chem. and Interfac. Electrochem.*, 44, 1973, p 169.
9. K. B. Oldham, *Anal. Chem.*, 44, 1972, p 196.
10. M. Grenness and K. B. Oldham, *Anal. Chem.*, 44, 1972, p 1121.
11. J. M. Saveant and D. Tessier, *J. Electroanal. Chem. and Interfac. Electrochem.*, 65, 1975, p 57.
12. L. Nadjo and J. M. Saveant, *J. Electroanal. Chem. and Interfac. Electrochem.*, 48, 1973, p 113.
13. F. E. Woodward, Monsanto Report MSL 3320, 1983.
14. N. K. Blackwell, *Ph.D Thesis*, Dept. of Phys. Chem., Leeds Univ., 1988.

* Formerly *J. Electroanal. Chem.*

Chapter 4

An Investigation of Dioctyldiphenyl Amine

4.1 The Measurement of Amine Antioxidants

Amine antioxidants have been incorporated in lubricating oils as a primary additive for some time. The determination of the oxidative resistance of the base oils and fully formulated blends has until recently been mainly confined to the use of oxidation bomb tests or oxygen absorption experiments. These methods are not specific to the determination of amine antioxidants because the quantity that is measured is the overall oxidative resistance of the oil blend. This non-specificity (with respect to the antioxidant) is also a characteristic of DSC, unlike electrochemical techniques such as CV. The determination of the oxidative resistance of an oil by DSC is a more realistic simulation of engine conditions than either the bomb or oxygen absorption experiments. The added realism may be due the thin film of oil used in DSC measurements providing a closer representation of bearing conditions.

An oxidation bomb was used by Gilks [1] to produce calibration curves relating the antioxidant concentration in an oil to the induction period. The experimental procedure is described in the test methods IP 40 and ASTM D-525. The antioxidant systems studied were various groups of substituted diphenyl amines. He found that the variation in the structure of the substituted group had a greater effect on the antioxidant activity than the change in molar mass of the active species. This result is hardly surprising, considering the fact that secondary alkyl substituents will lose a hydrogen atom with greater ease than a primary alkyl substituent and therefore impart a greater antioxidant efficiency. Using the same method Pederson [2] compared the behaviour of various aromatic amines in gasoline to a standard blend. He concluded that the rate determining step in chain termination, was not the abstraction of hydrogen from the nitrogen group. This infers that the chain carrying capacity of the peroxy radical was not destroyed by being converted to the hydroperoxide. These reactions have also been described in chapter 1. Pederson proposed that the peroxy radical abstracted an electron from the amino group, to form a complex which then reacted with another peroxy radical. His results agreed with those of Gilks, in that the antioxidant capability was not only affected by the basicity of the molecule, but by steric hindrance. He found that non-hindered compounds were less efficient as antioxidants, because they participated more readily in undesirable molecular side reactions. Steric hindrance has little effect on the free radical reactions that occur in hydrocarbon oils.

Ivanov and Vilyanskaya [3] used both an oxygen absorption technique, and the measurement of the acid number of the oil, to classify 21 different antioxidants into 3

groups. The compounds tested contained amino, phenolic and sulphide groups. The categorisation depended on their effectiveness in retarding hydrocarbon oxidation at different stages in the oxidation process. It was discovered that the presence of metal catalysts had no effect on the action of the inhibitors. In the absence of metal catalysts the main end products were alcohols, but when catalysts were added the final products tended to be organic acids. The mode of action of every antioxidant was independent of its initial concentration. All compounds tested were found to retard the formation of hydroperoxide molecules. The first category contained additives that had no effect on the rate of decomposition of the hydroperoxides, while those in the second group accelerated it. The additives in the third category, whose behaviour was intermediate between that of the first two, accelerated the thermal decomposition but only to a limited extent. The antioxidants in the first group were discovered to retard the rate of oxidation only if added before oxidation had begun. Compounds belonging to the second group slowed the rate of oxidation whenever added to the blend. Additives in the third category were found to retard the oxidation process only if added before the transition from the auto-catalytic to the steady rate stage. The authors found that the structure of the functional group did not itself completely determine the category to which it belonged, although it was found to have an influence. It was realised that the position of the functional group in the inhibitor molecule was the primary factor in determining the manner in which the inhibitor influenced the rate of oxidation. If a hindered phenol possessed a substituent group in the active ortho or para positions, it would belong to the second category. If the hindered phenol was substituted in the meta position it would belong to group 3. When an antioxidant of the second group lost its primary character as a result of introducing a phenyl radical it would then belong to the first category.

Mahoney et. al. [4,5] measured the rate of oxygen absorption of various hydrocarbon-antioxidant blends. The rate of oxygen absorption for an uninhibited oil was measured, and then the time for that rate to be attained for blends containing increasing concentrations of antioxidant. Using these methods they found that the stoichiometry for the reaction between DODPA and the cyclohexenylperoxyl radical used as an initiator was 1:4. The number of peroxy radicals destroyed per antioxidant molecule is a direct measure of its efficiency. Kennerly and Patterson jr. [6] used the oxygen absorbtion technique to study the synergism between inhibitors and peroxide decomposers while Massey and Wilson used a static absorption test to measure the useful life of various oil blends [7]. The useful life was defined as the time taken for

100 g of oil to absorb 300 ml of oxygen. A further development was the determination of the post-useful life of the same oil. This was the time taken to absorb an extra 700 ml of oxygen, over and above the initial 300 ml. They presented calibration curves for both the useful and post-useful life verses antioxidant concentration and then studied the effect of adding extra antioxidant to oxidised oil samples. For the amine antioxidants, the effect was to impart a resistance to oxidation that surpassed even that of the fully formulated unoxidised oil. They concluded that even when exhausted there must be a certain amount of inactive antioxidant remaining in solution which became active on introduction of extra antioxidant. A more probable explanation is that polymerisation of the oil and amine, together with the evaporation of light fractions impart oxidative resistance. The more stable high molecular weight fractions and the polymeric residues being less susceptible to thermal degradation than the low molecular weight fractions.

Several authors have studied amine antioxidants using DSC. Tong [8] and Cash [9] studied DODPA in both synthetic and mineral base oils using dynamic and isothermal techniques. Zeman [10-12] compared DODPA, phenothiazine and N-phenyl 1,naphthyl amine (PAN) in ester oils and showed that the catalytic effect of metals towards oil degradation varied with the antioxidant blends present. In each instance iron had the greatest catalytic effect on degradation and molybdenum the lowest. Al-Sammerrai and Salih [13] showed that the results obtained by DSC analysis ranked the oxidative stability of oil blends in the same order as the results obtained by acidity change (ASTM D-974) and viscosity change (ASTM D-445) measurements. The work consisted of oxidising oil samples containing an amine antioxidant and comparing the measurements both prior to, and after oxidation. The DSC experiments provided the authors with a less time-consuming method for the determination of oil stability than the standard tests normally used. The acidity and viscosity changes are measured over a 120 hr period.

Very few authors have studied amine antioxidants using electrochemical techniques. The systems studied have been in the aqueous phase, rendering the methods useless for the analysis of oil blends. Despite the popularity of disubstituted amine antioxidants, no work has been performed to investigate their electrode reactions. Adams and Parker [14] performed a quantitative study of phenylene diamines electrochemically using a potential scanning method, whereby the limiting current was measured in an aqueous solution. Determinations were found to be too difficult and at best semi-quantitative,

but later experiments using chrono-potentiometry proved to be more successful [15]. The antioxidants were dissolved in aqueous solutions and the time taken to reach a measured potential at a constant current was plotted against the antioxidant concentration. A straight line plot up to a concentration of 6 x 10^{-3} mol dm^{-3} was obtained. The authors claimed that at higher concentrations, fouling of the electrode surface during electrolysis by an invisible electro-inactive coat caused the line to tail off. At sufficiently high antioxidant concentrations the electrochemical response decreased. This limited the technique to the analysis of solutions with a low antioxidant concentration. Above the critical concentration at which the calibration curve tailed off, an increase in concentration gave a smaller response rendering the technique useless. The presence of the electro-inactive coating, that only manifests itself at high concentrations, must raise questions of the reliability of any results obtained.

The analysis of DODPA by HPLC and UV spectroscopy [16] suggests that under oxidation conditions it polymerises to long chains of similar properties to the parent antioxidant molecule. The analysis of oxidised oil samples by HPLC provided several single peaks obtained at different retention times, which when analysed by UV spectroscopy showed products of a similar nature to DODPA [16]. This conclusion is further supported by the DSC results obtained for this work. The analysis of oxidised oil samples by DSC shows that the oxidative resistance of the oil remains equal to that of the fresh oil for several hours before the resistance begins to decay. The polymeric products appear to have antioxidant characteristics.

4.2 Analysis by Differential Scanning Calorimetry (DSC)

4.2.1 Preliminary Experiments

The comparison of the oxidative stabilities of lubricating oils using DSC has been the subject of considerable work over the last few decades [17-19]. Noel [17] modified a Perkin Elmer DSC to run under elevated pressures and used this apparatus to produce curves relating antioxidant concentration to the temperature of the onset of oxidation. Noel also discovered a correlation between the temperature of oxidation and the results from the rotating bomb test (ASTM D-2272), while El Naga and Salem [18] related the results from DSC to those of the standard oxidation test, IP 306. The relationship between the peak onset temperature and the measured total oxidation products (IP 306) gave a straight line with a correlation coefficient of 0.924 at a confidence level of greater than 99.9%. El Naga and Salem determined the optimum experimental

conditions for the isothermal and dynamic methods before any comparison of the results could be made. When the results of the IP test were compared to those of the DSC experiments, it was found that the dynamic method gave a far better correlation than the isothermal technique. In their paper [19] Walker and Tsang used HPDSC to characterize the oxidative stability of formulated and virgin/recycled basestocks. They observed that the re-refined basestocks had an oxidative stability intermediate between the formulated and virgin oils. The explanation proposed for this, was that either a reactive component present in the virgin basestock had been destroyed or that some antioxidant was carried over into the recycled oil from the refining process. The authors claimed that the shape of a thermal analysis curve provided a "fingerprint" of the material similar to, and as unique as, an IR spectra or a boiling point determination. Furthermore the repeatability of the data was claimed to be 0.5 to 1.2% for a dynamic experiment and 4.5% for an isothermal experiment. The claim that the shape of a thermal analysis curve is unique is a dubious one, for if it were true, then the use of peak shape analysis to determine oil composition would be commonplace. The repeatability of the dynamic experiment obtained is quite remarkable, three times better than that obtained by most authors. Some recent work has been published concerning base oils from different fractions, both commercial oils and ester oil blends [20-22]. The two methods of analysis being reviewed by the I.P. for the study of lubricating oils are the dynamic and isothermal methods. In the dynamic method the temperature of the sample is increased linearly with time. The atmosphere normally used is flowing air or oxygen at atmospheric pressure. It has been stated [22] that this method suffers from the problem that the temperature at which a thermal event is detected will always lag behind the true temperature at which it commenced. As reactions accelerate at the higher temperatures attained, the dynamic method may discriminate between thermal events less satisfactorily than the isothermal method. A more likely reason for this method being less popular than the isothermal method is that it can provide a poor resolution between samples. It also suffers from problems of sample volatility, incurred by the use of a low pressure atmosphere and higher temperatures. The ASTM test method to measure the thermal stability of chemicals (ASTM E-537) recommends the dynamic experiment. The magnitude of the heating rate, sample mass, purge gas and pressure are only recommendations and are not fixed. This would appear to be a somewhat vague standard test method and more of an in-house procedure in practice. In the isothermal method the sample temperature is raised as fast as possible ($\geq 100°C\ min^{-1}$) to the required temperature and then held constant. In this method the atmosphere is static, at a pressure of 500 lb f in^{-2}. This value was

chosen because it is above the region at which the atmospheric pressure may affect the results obtained and because it is commonly used by other authors. The induction period obtained in an isothermal experiment is a measure of the time taken to consume the antioxidant in the oil.

The isothermal method was chosen for the comparison of oil blends in this thesis because it is a more reproducible and discriminating technique than the dynamic experiment. The majority of the preliminary work concerned with studying lubricating oils by thermal analysis was performed by Cash [9]. He was concerned with the establishment of standard test methods by observing the effects of the different operational parameters on the experimental result.

Before use, the Du-Pont DSC-990 was stripped, cleaned and then serviced for the following [23]:

1 ΔT gain check,

2 5X gain check,

3 ΔT zero adjustment,

4 baseline slope check,

5 noise check,

6 calibration of E-compensator, and

7 optimisation of the proportional band and rate mode for isothermal analysis.

The area below the furnace was lagged, and screened cables were used to connect the high pressure unit to the 910 cell base to improve signal quality. The cell was then conditioned by cycling the temperature programme between room temperature and 500°C under an atmosphere of nitrogen. The DSC cell has over the years been subjected to a considerable amount of use, which has caused the constantan disk to buckle slightly and become concave. Obviously this has a detrimental effect on the signal quality and as a result, the sensitivity of the apparatus has been reduced. The loss of sensitivity is of little consequence because the oil oxidation reaction is extremely exothermic. Even so it was found invariably that the first measurement in any day gave a poor peak shape with an induction time that was judged to be unreliable.

The temperature and energy calibration of the apparatus was performed before the analysis of an oil was made. The method of instrument calibration is described in chapter 2.

4.2.2 Experimental

Calibration curves to relate the antioxidant concentration in an oil to the induction time before the onset of oxidation were produced using the following experimental procedure. The sample pans were made from aluminium, 0.125 mm thick with a 7 mm o/d and 2 mm side walls. The pans were not coated with an oxide film (anodized). The treatment of the pans produces a surface that has a different catalytic effect on the oil and therefore obviously leads to different results than those obtained when untreated pans are employed. Before use the pans were cleaned in dichloromethane, followed by acetone and then oven dried. The base of the pans were flattened to ensure good thermal contact between the pan and the thermocouple platform. A 2.00 $\pm$ 0.05 mg sample of the oil was placed in the centre of a pan using a clean glass rod. An empty pan was used for the reference in each experiment. The sample pan was positioned centrally on the front thermocouple platform, the furnace lid and radiation shielding were assembled and the pressure vessel lid secured by the three locating bolts. The cell was purged for five minutes with oxygen at a flow rate of approximately 50 cm^3 min^{-1} before being pressurised to 500 lb f in^{-2} (3495 kPa). The sample was then heated to the required temperature at a rate of 100°C min^{-1} and held isothermally until the oil oxidation was complete. The atmosphere in the cell was static and only vented during the heating period to maintain a constant pressure. The temperature chosen for each set of calibration experiments was one where an easily measurable induction time for the base oil could be attained, without an inordinately long time for a fully formulated oil. The induction time was measured from the beginning of the isothermal period to the onset of oil oxidation. The onset of oxidation was taken from the intersect of the leading edge of the curve with the baseline (figure 4.1). After each experiment the cell was slowly depressurised and the pressure vessel cautiously dismantled.

The temperature chosen for the analysis of each oil blend was different, reflecting the different stabilities of each base oil and fully formulated blend. Barnes and Bell [22] chose the isothermal temperature for oil analysis as 40 to 50°C below that at which the oil oxidised during a dynamic experiment at a heating rate of 20°C min^{-1}. It was found, during consultancy work that when this method was employed, some oil samples had a tendency to ignite during the isothermal experiment. In the present work temperatures were selected to avoid ignition of the sample. The reason for omitting ignition experiments is although the induction times are very reproducible the oil is involved in a different kinetic regime to that of slow auto-oxidation. The calibration curves are illustrated in figure 4.2. Each experiment was repeated in triplicate or more.

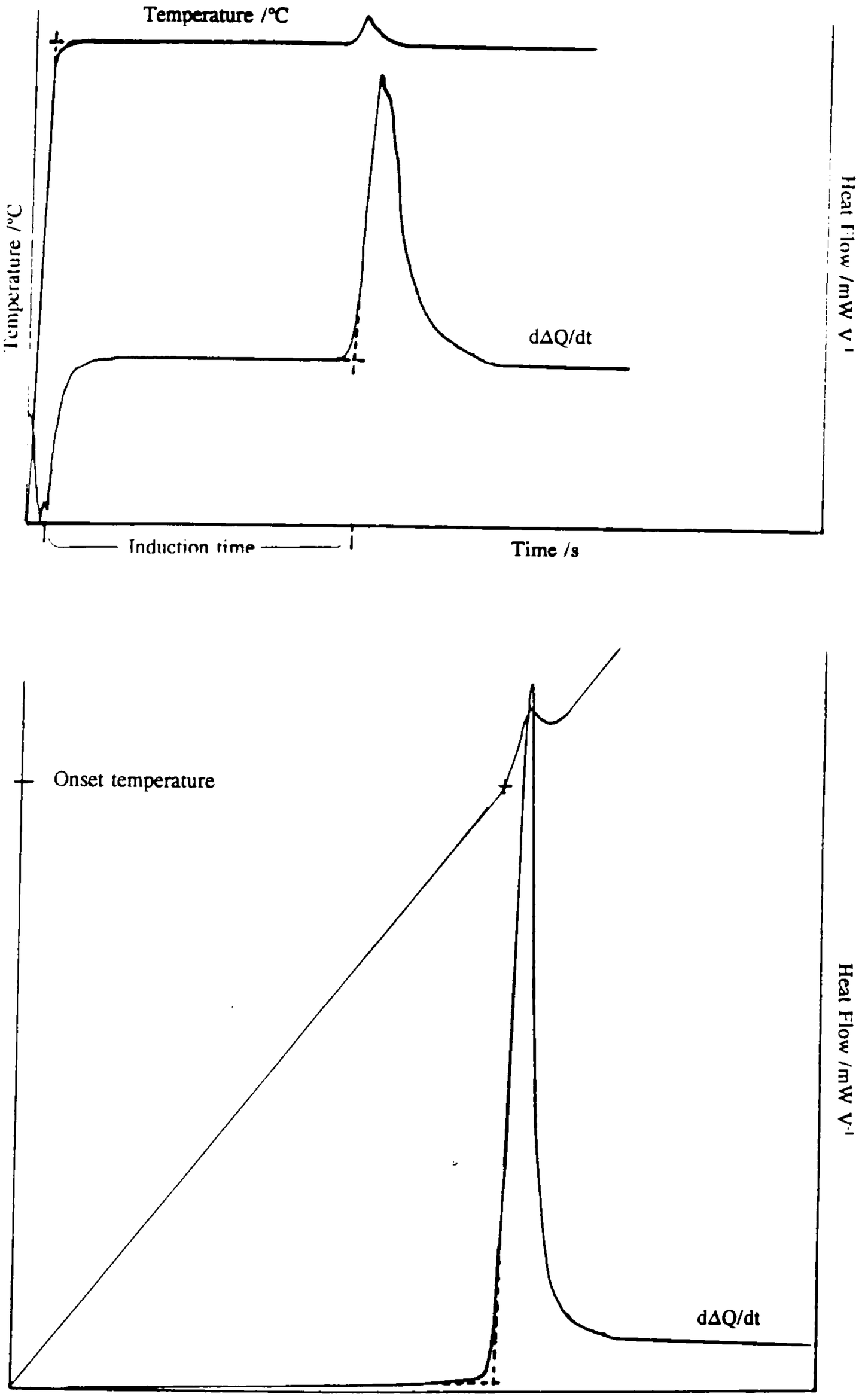

Figure 4.1

The Determination of the Onset of Oil Oxidation
Using Isothermal and Dynamic Experiments

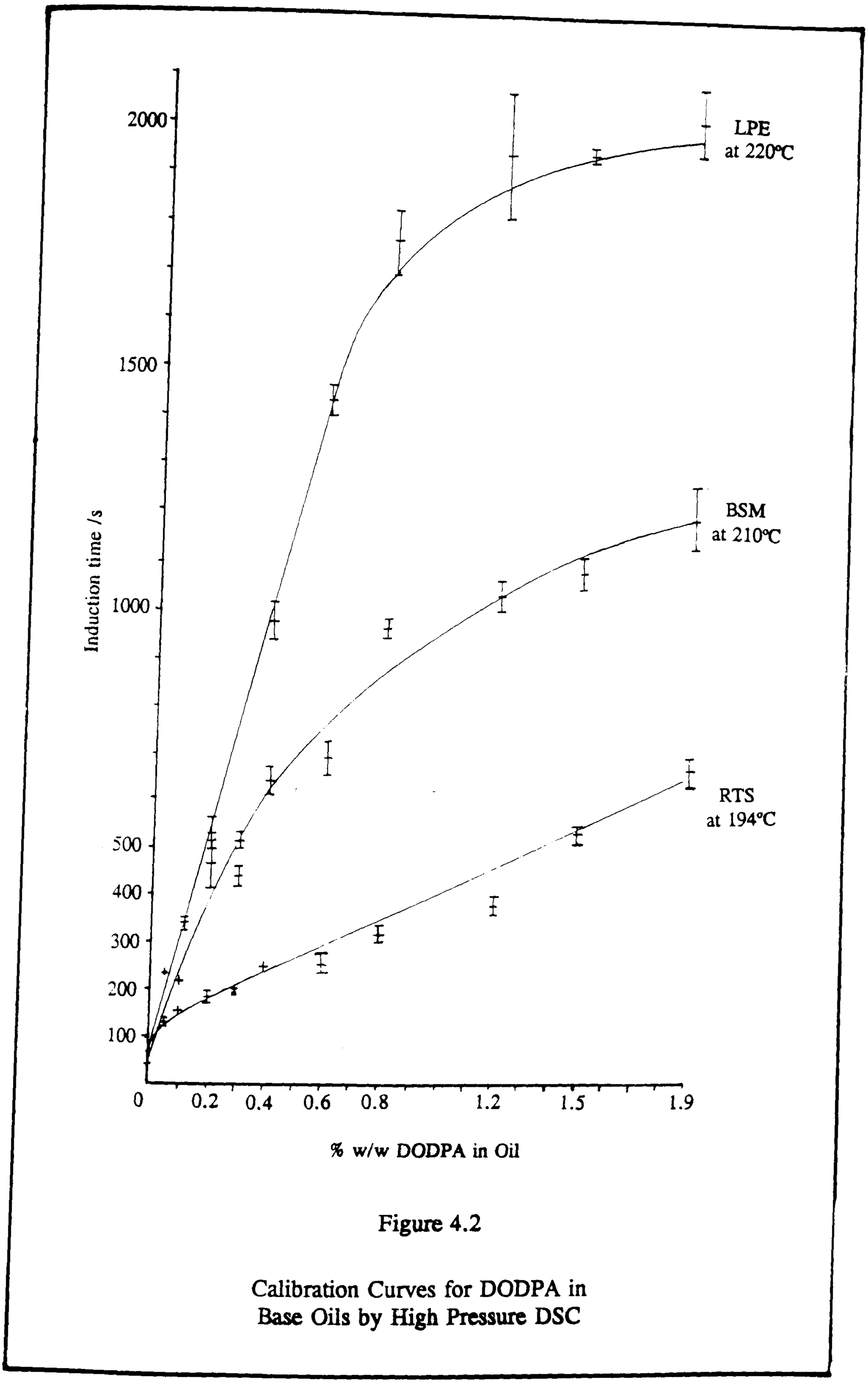

Figure 4.2

Calibration Curves for DODPA in
Base Oils by High Pressure DSC

The induction times are given for the intersection of the leading edge of the main oxidation peak with the baseline. The analysis of the mineral oil containing the amine antioxidant was hampered by the presence of pre-peaks and shoulders on the main oxidation peak. The thermal analysis curves of the basestock and of blends containing up to 0.3% w/w antioxidant usually possessed a shoulder on the leading edge of the main peak. Above 0.2% w/w DODPA a pre-peak was sometimes present on the curve. As the inhibitor concentration increased, the probability of the pre-peak being present rose. The presence of the pre-peaks and shoulders on the mineral oil curves was investigated as a means of calibration. The position and presence of the pre-peaks and shoulders was found to be unreliable for calibration purposes. The use of the main oxidation peak was the only reliable route to relate the antioxidant concentration to the induction time obtained. Pre-peaks and shoulders were absent from the thermal analysis curves of oligomer and ester oil blends. The presence of shoulders and pre-peaks may be a reflection of the composition of the mineral oil. The oil contains aromatic, paraffinic and olefinic fractions from the blending of oils from two different sources. The absence of the pre-peaks at low additive concentrations may be due to the fact that the bulk of the sample undergoes rapid oxidation. When larger concentrations of inhibitor are present, a fraction of the oil with a low oxidative stability may oxidise preferentially, prior to the main body of the blend. The presence of fractions with different oxidative stabilities within the mineral oil is also suggested by the results of analysis under dynamic conditions.

The average error associated with the measurement of any induction time was 3.5%. In many instances the error bars are less than 1% in size, but for a few oil blends the errors were about 5%. This is a further example of the complexity of the nature of oil blends. It should be noted that the calibration curve for DODPA in the synthetic oil RTS-9745 was completed before the water cooled pressure jacket was constructed. The errors associated with the measurement and attainment of the set temperature are larger than those for the other antioxidant systems where the water cooled pressure jacket was employed. This places an increased uncertainty in the results obtained for this system, especially those where the induction period is longer. This is because the pressure vessel attained higher temperatures during the course of the day, leading to increased thermal conduction and convection.

The variation in the extent of sample self-heating with antioxidant concentration was investigated. No relationship was found between the oil composition and the

temperature rise of the sample during 'isothermal' experiments. This applied equally to ignition and non-ignition experiments. However the range of self-heating for non-ignition experiments was 4 to 30 K, while that of ignition experiments was found to be 35 to 91 K.

An attempt was made to relate the peak shape to the composition of an oil blend. No correlation was found between the peak area and the antioxidant concentration, or for oxidised samples, the duration of oxidation. As the concentration of the antioxidant rose, the width of the oxidation peak increased and the height of the peak ($d\Delta Q/dt$) decreased. In general, the onset of the peaks became sharper and more clearly defined, with a very slow tail off after the peak maximum. The widths of the peaks were dependent on the base oil as well as the antioxidant concentration. The base of the curves were 20 minutes wide for the ester base oil, 10 minutes wide for the mineral oil and 1 minute wide for the oligomer oil. The figures just given were recorded at the temperatures used for the calibration of the oil blends. The relative rates of heat evolution (peak height) also varied between the base oils. The induction times of the mineral and ester oils were difficult to measure as the oxidation processes were so slow that the rate of heat evolution was low. The end of the peak for mineral oil samples was also difficult to measure, because the curve did not return to the same baseline as that used before the peak began. No relationship was found between the peak shape of a thermal analysis curve and the composition of the oil sample. The peak width, height, area, sample mass loss and the gradient of the leading edge of the peak were compared to the oil composition individually and in a variety of combinations. It is our belief that the peak shape is related to oil composition, but the parameters investigated could not be measured precisely enough for any discriminating analysis.

4.2.3 Kinetic Analysis

Interpretation of results to give more fundamental physico-chemical information is fraught with difficulty because of the complex nature of the oil. A kinetic parameter cannot be assigned to one process with any degree of certainty, because it is highly likely that many reactions occur simultaneously. Each reaction can have an effect on the measured parameter, so that care must be taken in any assumption or assignment made.

The use of isothermal experiments at different temperatures facilitates the investigation of physico-chemical parameters. This is because the sample temperature

is assumed to be held constant and the extent of oxidation is the only variable. This is not strictly true because the sample undergoes self-heating. Many authors have chosen to consider the oxidation of oils to be a first order process [10-12,24,25]. Again this is probably an oversimplification, but owing to the complexity of the underlying processes this is often overlooked. In DSC, the value of $d\Delta Q/dt$ obtained from an experiment is the net sum of the concurrent reactions. In an isothermal experiment the large oxygen pressure employed and the high temperature encountered ensures that the oxidation reactions have a short chain length and that the exotherm probably arises from peroxide decomposition [24]. Noel and Cranton [24] used the isothermal method for measuring the activation energy of oil oxidation processes. They assumed that the reaction rate was first order and that the thermal analysis curves were symmetrical in shape. They measured the time interval from the onset of oxidation to the peak maximum, assuming the peak maximum to represent the time at which half the reaction had occurred. They plotted the results in an Arrhenius fashion (ln k vs 1/T) for both inhibited and uninhibited oils. Both oils gave the same slope, with a change in gradient at 190°C suggesting that there were two different kinetic regimes. The authors showed that the rates of reaction of the two oils were equal. It was considered that the presence of an inhibitor did not affect the overall oxidation rate because the antioxidant had been completely consumed. This assumption may indeed be valid, but the peak shape of an isothermal DSC curve is by no means symmetrical, which casts doubt on the method of interpretation to the behaviour of the base oils. From the experimental results obtained for this work, the isothermal DSC curves tail off very slowly after the peak maximum.

The Arrhenius relationship between reaction rate and temperature is commonly used for obtaining kinetic data [22, 26], the reaction rate being interpreted as the reciprocal of the time to the peak onset. However, if the reaction mechanism changes within the temperature range being studied, the resulting plot will be curved and the application of these data to this technique is then invalidated. It may also be tempting to extrapolate the line beyond the temperature range being studied, but this is valid only if the reaction mechanism remains unaltered. The gradient of ln k vs 1/T is generally interpreted to be proportional to the activation energy of the reactions governing the auto-oxidation of the oil. For systems as complex as oils, it is probably best to regard the gradient as a useful illustration of the empirical relationship between the temperature and the induction time before auto-oxidation. A distinct difference between the base oil and a formulated oil is revealed on analysis. Following other

authors we have adopted the term activation energy, but with the reservations already mentioned. Zeman [10-12] used the Arrhenius relationship to illustrate the effect of the ageing of oils on the oxidative resistance of oil blends. He also used the plots to determine the induction time for an oil when the time was too large or small to be measured.

Cash employed two isothermal techniques to obtain kinetic data. The first method was the isothermal technique described above and the second was the iso-q-line method [27]. In the latter method the rate of heat evolution is measured at an equal extent of reaction and the measurement of this property at various temperatures enables the activation energy to be obtained from an Arrhenius relationship. The procedure was found to be very laborious and because Cash obtained the same results from both methods, the Arrhenius relationship between the induction time and temperature was used in the present work.

The peak area of the isothermal thermal analysis curve was found to increase with temperature for both mineral and ester oil samples, but this trend was qualitative rather than quantitative and therefore could not be applied to any specific analysis. It was found that the peak width reduced and the maximum peak height increased with a rise in the analysis temperature. The onset of oil oxidation became more clearly defined as the peaks became sharper. If the temperature was increased too high, the sample ignited.

Very little work has been done to obtain kinetic data from oil systems by use of dynamic experiments. This could be due to the simplicity of the isothermal method and the difficulty in interpreting results obtained from the dynamic experiments. The disagreement between authors regarding the validity of different techniques has possibly further reduced the number of people using dynamic experiments. Both Brown and Wendlandt [28,29] describe the most popular methods for calculating kinetic parameters from dynamic DSC results, giving an indication of the advantages and limitations of each technique. In their books they describe the assumptions made and the mathematics associated with each method. One of the most commonly used techniques is that developed by Borchardt and Daniels [30], but this method of analysis was excluded from use for oil systems by Cash [9], because it requires that the baseline is accurately defined. In the present work it was often difficult to define the end of the oxidation peak. As a consequence the interpretation of the baseline at the end of an

experiment may have been difficult. The kinetics of oil shale pyrolysis was studied by Skala et al. [26] using a standard test method ASTM E-698 derived from that of Ozawa [30]. In this method the natural logarithm of the reciprocal of the heating rate (ln $1/\beta$) is plotted against the reciprocal of the peak temperature (Tm). The original method by Ozawa plotted ln β instead of ln $1/\beta$ against 1/Tm. For both methods the activation energy of the reaction is derived from the slope of the curve. In their work Skala et al. [26] assumed that the reaction rate was first order, but stated that the approach was only applicable as a method for the preliminary characterisation of the overall process. The authors stated that the kinetics were only appropriate to the stage of the pyrolysis in which thermal decomposition of the organic matter occurred to form non-volatile products.

The Kissinger method [31,32] is probably one of the most widely used (and misused) methods for gaining kinetic parameters from dynamic experiments, although there is little difference between the Kissinger method and that of Ozawa. The method was originally proposed for DTA, but the Du-Pont DSC is similar in configuration. Experiments are carried out under non-ignition conditions and it is assumed that the maximum rate of reaction coincides with the maximum of the DSC curve. In the first publication [31] it was also assumed that the relationship developed was independent of reaction rate, but it was found to hold true only if the reaction was first order. The second publication included a modification to the theory to make the method applicable to reactions of any order. The method was criticised by several parties who stated that the peak maximum did not coincide with the maximum rate of reaction, but the criticism is less valid when using DSC equipment [9]. Cash questioned the use of the Kissinger method for the complex regime of lubricating oils based on the results he obtained using the iso-q-line method. He noted that as the reaction proceeded the mechanism changed, a phenomenon reflected by a change in activation energy. The change in activation energy was of the order of 8% over the extent of reaction from 50% to 70%. Since only a small change in activation energy was noted and the complexity of the systems under investigation the plot used by the Kissinger method (ln (β/Tm^2) verses 1/Tm) is probably as valid as many others. The standard test method used by Skala et al [25] includes the method described by Kissinger. The results obtained from the plot of ln (β/Tm^2) verses 1/Tm are in good agreement with those obtained using other methods (eg ln $1/\beta$ vs 1/Tm), indicating that its application was suitable. However, the Kissinger method itself is not valid for the study of oil oxidation, because it does not cater for systems where different reactions proceed

simultaneously.

For the dynamic experiments a mass of 0.5 or 1.00 ± 0.05 mg of oil was heated at various rates under a static oxygen atmosphere at 500 lb f in^{-2} and the peak temperature recorded (figure 4.3). The system was vented as necessary during the heating process to maintain a constant pressure in the cell. The effect of the heating rate on the peak temperature was studied, using both of the ASTM E-698 methods to obtain the activation energy for the decay of the system. The sample mass used for these experiments was lowered to avoid ignition of the samples under high heating rates. For the non-ignition dynamic experiments the peak onset and peak maximum temperatures were found to increase with heating rate (as expected). The width of the base of the peaks decreased with an increase in the heating rate. The maximum rate of heat evolution of the sample also increased as the heating rate rose (the peaks became sharper) until the heating rate was so great that the sample ignited.

A difference between the base oils was realised using the non-ignition dynamic experiments, because the oxidation of the mineral oil occurred at a slower rate than that of the oligomer and ester oils. The thermal analysis of the mineral oil yielded a lower peak height which was also wider than those of the other base oils. It has already been mentioned that the oxidation peaks of the mineral oil contained several closely linked thermal events. At slower heating rates these thermal events displayed signs of separation, but as the heating rate rose the resolution between them decreased.

In another set of experiments the sample mass was left at 2.00 mg and the oils studied under ignition conditions. The ignition onset temperature (figure 4.3) was plotted against the heating rate to study an empirical theory proposed by Boddington et al. [33], which gave information of the activation energy, the pre-exponential factor and the response time of the DSC cell itself. The DSC peaks obtained in dynamic ignition experiments gave rise to a second peak after the main ignition peak. The second thermal event was not an ignition and may have been due to the oxidation of the ignition products. A similarity with the non-ignition experiments is that the peak width decreased with an increase in the heating rate. At lower heating rates an endotherm was noticed after the oxidation peak. The mineral oil again displayed differences in the shape of the DSC curves. At lower heating rates the base oil gave rise to a shoulder on the leading edge of the ignition peak. For a sample of the mineral oil containing DODPA a pre-peak was always visible, approximately 20°C prior to the

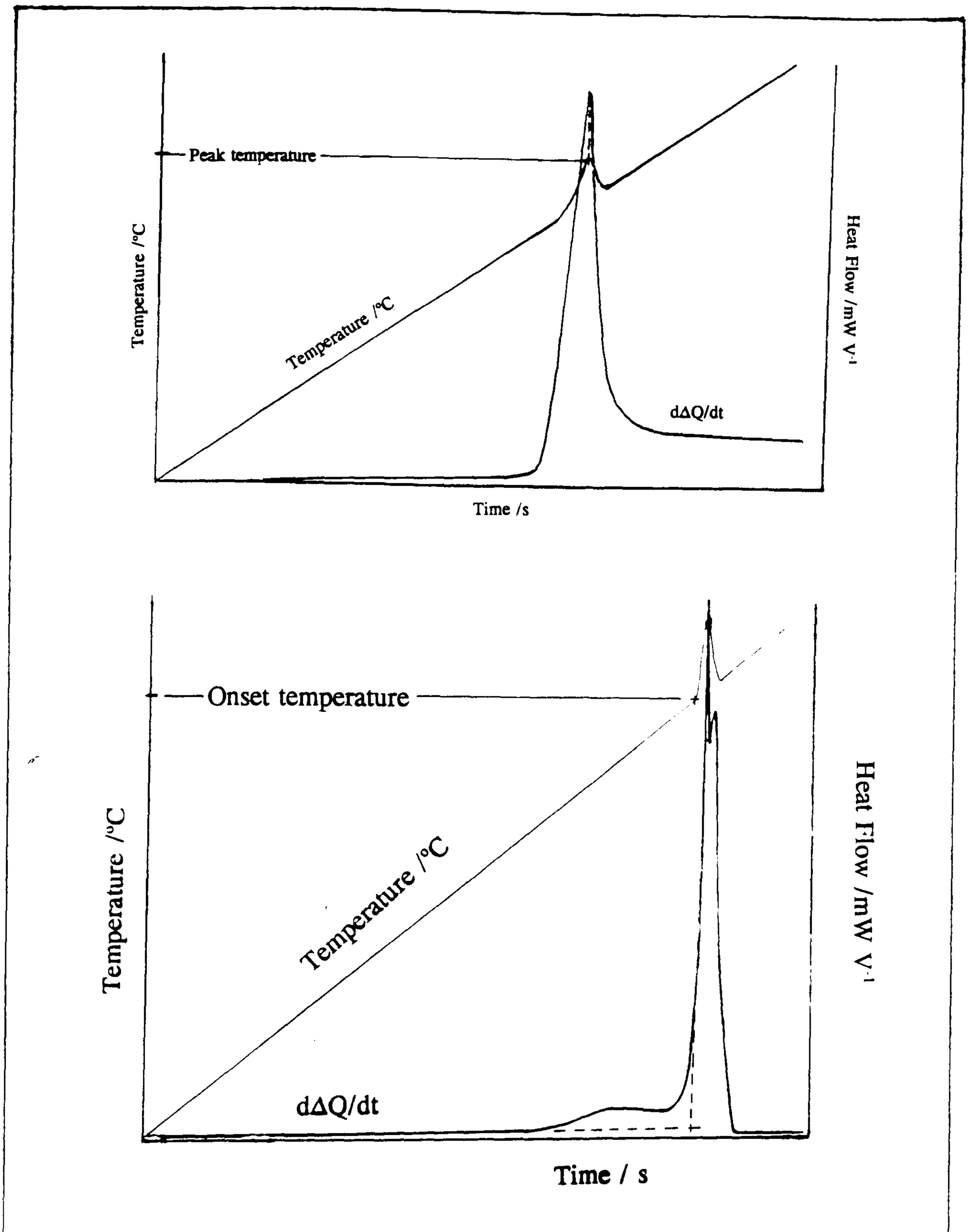

Figure 4.3

The Determination of the Peak Maximum and Onset Temperatures for an Investigation Into the Kinetics of Oil Oxidation

onset of the main ignition peak. The separation of the pre-peak from the main peak was more clearly defined at slower heating rates.

The activation energy derived by the method proposed by Boddington et al [33] for the oxidation of the oligomer oil containing DODPA was 266 kJ mol^{-1}. The response time of the Du-Pont obtained using this method was found to be 14 s, compared to the measured value of 5 s [34].

The kinetic data obtained using the isothermal and dynamic methods are given in table 4.1 and the isothermal results illustrated in figure 4.4, the values being given with the reservations expressed earlier.

Table 4.1
The Kinetic Data Obtained From DSC Analysis

% w/w DODPA in Sample	Method of Analysis	Activation Energy / kJ mol^{-1} Mineral Oil	Oligomer Oil	Ester Oil
None (Base Oil)	Isothermal	171 ± 12	70 ± 10	103 ± 11
	Dynamic			
	ln (β/Tm^2) vs 1/Tm	136 ± 2	-	155 ± 18
	ln (1/β) vs 1/Tm	128 ± 5	-	139 ± 17
1.5	Isothermal	131 ± 11	134 ± 10	108 ± 16
	Dynamic			
	ln (β/Tm^2) vs 1/Tm	141 ± 11	98 ± 4	Sample Ignited
	ln (1/β) vs 1/Tm	149 ± 11	104 ± 4	Sample Ignited
1.2 (Sample Oxidised)	Isothermal	-	111 ± 10	-
1.2 (Sample Oxidised Then Re-inhibited)	Isothermal	-	148 ± 3	-

The isothermal method produced a straight line plot of ln k vs 1/T over the temperature range 436 to 511 K. The dynamic methods yielded straight lines of ln (β/Tm^2) vs 1/Tm and ln (1/β) vs 1/Tm over the heating rates 2 to 100 K min^{-1}. The

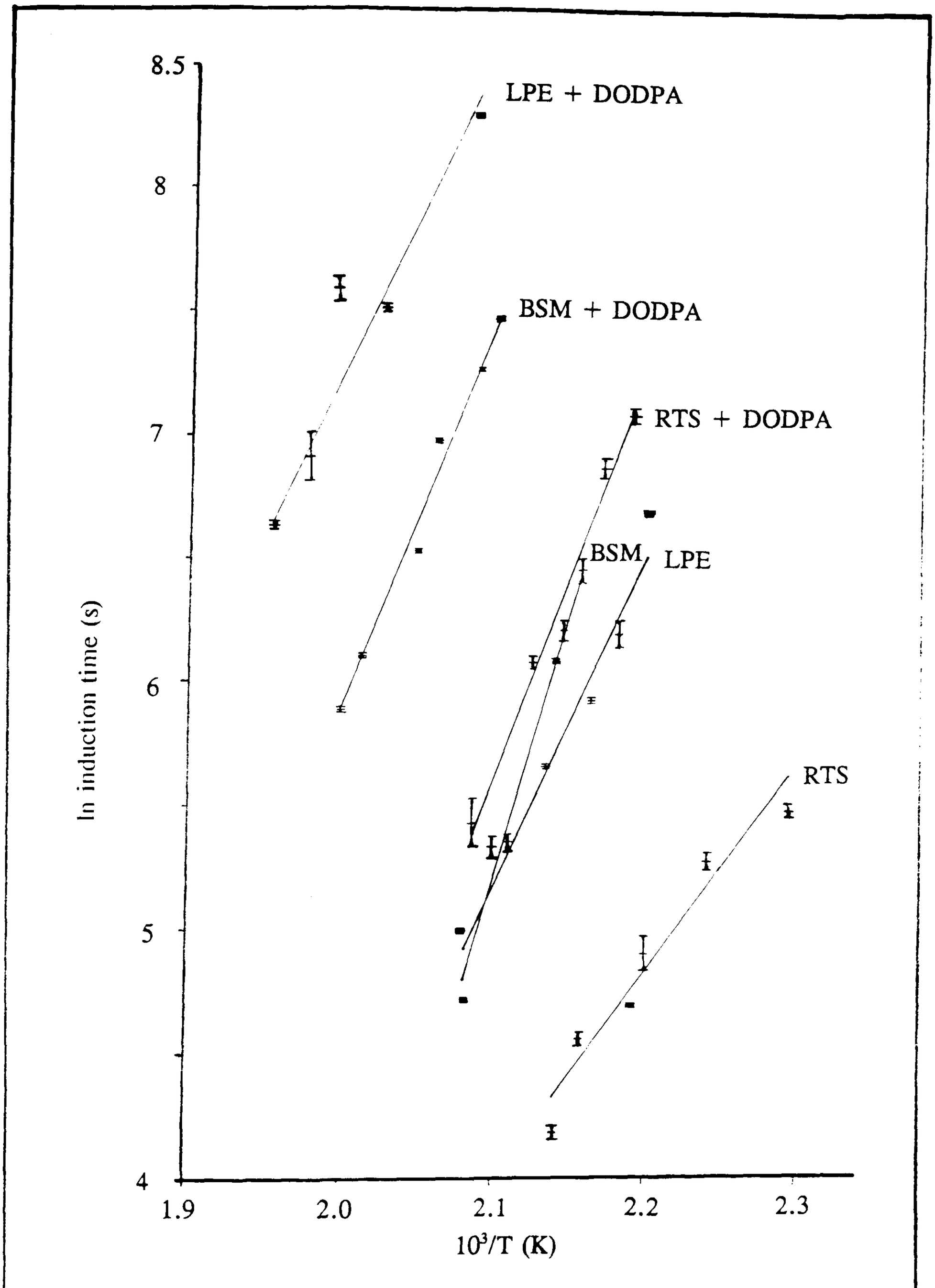

Figure 4.4

Variation of the Induction Time with Temperature for the Base Oils and Blends Containing 1.5% w/w DODPA

straight line plots obtained using the dynamic and isothermal methods imply that the mechanism of consumption of the antioxidant is constant over the temperature ranges of the study. If the plots were extrapolated to higher and lower temperatures and heating rates, this would assume that no change in reaction mechanism would occur. It can be seen that the addition of an antioxidant to an oil can either decrease or increase the activation energy of the processes leading up to the auto-catalytic oxidation of the oil itself. This is a reflection of the complexity of the oil systems and illustrates the different interactions obtained between the antioxidant and basestocks.

The different 'activation energies' obtained by the use of dynamic and isothermal experiments may be explained by the different operating conditions. The dynamic experiments subject the samples to higher temperatures than the isothermal method and as a consequence the extent of sample consumption is greater in a given time. The mass loss during an isothermal experiment accounts for 25 to 65% of the original sample. The residue obtained from an isothermal experiment was a dark brown oil or tar. No relationship was found between the mass loss and the temperature of analysis, the antioxidant concentration or the duration with which the sample had been oxidised in an oil bath. For non-ignition dynamic experiments the mass loss varied between 85 to 99% w/w. The high percentage mass loss explained the appearance of the residue, which was a brown or black lacquer. Below 10°C min^{-1}, an increase in the heating rate resulted in a greater mass loss over a given temperature range. This may be explained by the higher sample temperatures attained before and during the oxidation processes. When the sample ignited in either dynamic or isothermal experiments, the residue resembled a cobweb of soot on the base of the pan. The weight loss that occurred during the experiment exceeded 99%.

4.3 The Analysis by Cyclic Voltammetry (CV)

4.3.1 The Development of the Final Experimental Method

In this section the developments and decisions made to establish a standard test method are written in chronological order. The initial experimental procedure used a sample of oil dissolved in an electrolyte system consisting of 0.1 mol dm^{-3} tetra butyl ammonium perchlorate (TBAP) in dimethyl formamide (DMF). Before analysis the solution was degassed with nitrogen. The final arrangement of the electrochemical cell was described in chapter 3. Initially the electrodes were 1 cm^2 quasi planar platinum counter and working electrodes (CE and WE respectively) with a reference electrode

(RE) of silver wire immersed in a solution of 0.01 mol dm^{-3} silver nitrate in the electrolyte system. The voltage was ramped linearly with time at a rate of 0.5 V s^{-1} over the range -0.4 V to +0.5 V, then to -2.4 V and back to the starting potential. The early experiments were concerned with a comparison between fresh and oxidised oil samples supplied by DQA. There were several large peaks present in the unoxidised oil solutions that were assumed to be due to the oil degrading electrochemically. The early work was aimed at reducing the size of the peaks by the addition of an antioxidant. Under conditions of use the antioxidant is consumed preferentially to the base oil, therefore it was hoped that the presence of an antioxidant would prevent the oil degrading. The variation of the peak potential with inhibitor concentration was also considered. All comparisons were made using the deconvoluted data plotted against potential.

The use of the experimental arrangement discussed above proved to be unreliable. The potential that corresponded to the peak maxima varied randomly, albeit only very slightly. The study of peak heights was hampered by the irreproducibility of the system. It was found at a very early stage that cleanliness of the sample cell, the electrodes and the glassware used was critical. Contamination of any component would invalidate an experiment. The purity of the electrolyte (TBAP) did not seem to be of great importance, since the recrystallisation of TBAP from methanol had little or no effect on the voltammograms. The presence of water in the solvent made analysis unreliable, making it imperative to dry the solvent before use. The solvent was dried by passing it through a column of activated silica gel. The working and counter electrodes required cleaning after each experiment by heating in the flame of a Bunsen burner until red hot to remove any adsorbed contaminants.

It was decided that the platinum WE was the cause of some of the problems of irreproducibility, and it was replaced with one of glassy carbon. The literature reviewed [35-38] indicated that antioxidant systems could be studied using a glassy carbon WE. The references gave no indication as to whether any other electrode arrangements were tested, the experimental procedures merely listed that glassy carbon or graphite electrodes were used. Franzke et al.[38] stated that antioxidant systems were normally investigated using platinum or graphite electrodes, because mercury has a lower oxidation potential than the phenols under scrutiny. In this work the signal quality obtained was improved significantly by using a glassy carbon WE. This enabled the relationship between peak height and antioxidant concentration to be established.

The electrochemical peak observed was owing to the oxidation of the antioxidant and not the oil.

It was found that not all of the oil systems studied could be dissolved in DMF, so alternative solvents were examined. The solvents tested were acetone, benzene, cyclohexane, hexane, pentane and tetrahydrofuran (THF). The solvents tested varied in their capacity to dissolve the oils. THF was chosen because, not only did it dissolve the oils with ease, but it is a well known electrolytic solvent with a large voltage window before electrochemical degradation. Paradoxically THF was found to be poor at conducting electricity, which meant that the iR term (explained in chapter 3) became significant, causing the oxidation and reduction peaks owing to the presence of DODPA to shift apart. The most probable explanation for the common application of THF as a solvent is that it is employed in micro-electrode systems where the electrodes are separated by only minute distances, reducing the potential drop measured between the electrodes. For this reason solvent mixes of 75:25, 50:50 and 25:75 % by volume THF:DMF were tested to determine whether the resistance of the solution could be overcome. Two solutions of 0.1 mol dm^{-3} TBAP in DMF and THF were prepared and blended together and the conductivity of the solutions measured (figure 4.5). The conductivity measurements indicated that the mix 25:75 THF:DMF containing TBAP would have the least resistance, but it did not dissolve the oil blends. The mixed solvent 75:25 THF:DMF (with the electrolyte TBAP) was chosen due to the high solubility of the oils in THF despite the high resistance of the blend.

The next step was to determine the optimum concentration of oil in the electrolyte solution. The concentration of oils tested in the electrolyte ranged from 0.5 to 10% by weight. The higher the concentration of oil in solution, the larger and more clearly defined were the peaks. An upper limit of 10% oil in the electrolyte solution was chosen to reduce the sample size required for analysis. To determine whether any peaks in the voltammogram were due to the oil oxidising or adsorbing onto the electrode surface, the 0.5% by weight concentration oil solution was used as the background for a 10% oil solution instead of the electrolyte only. No difference was noticed between the shape of the two voltammograms. Thus no peaks were present owing to interactions of the oil with the electrode over the potential range investigated.

It had been stated in the literature [37,39] that the addition of either pyridine or glacial acetic acid would improve the peak shape and facilitate analysis accordingly.

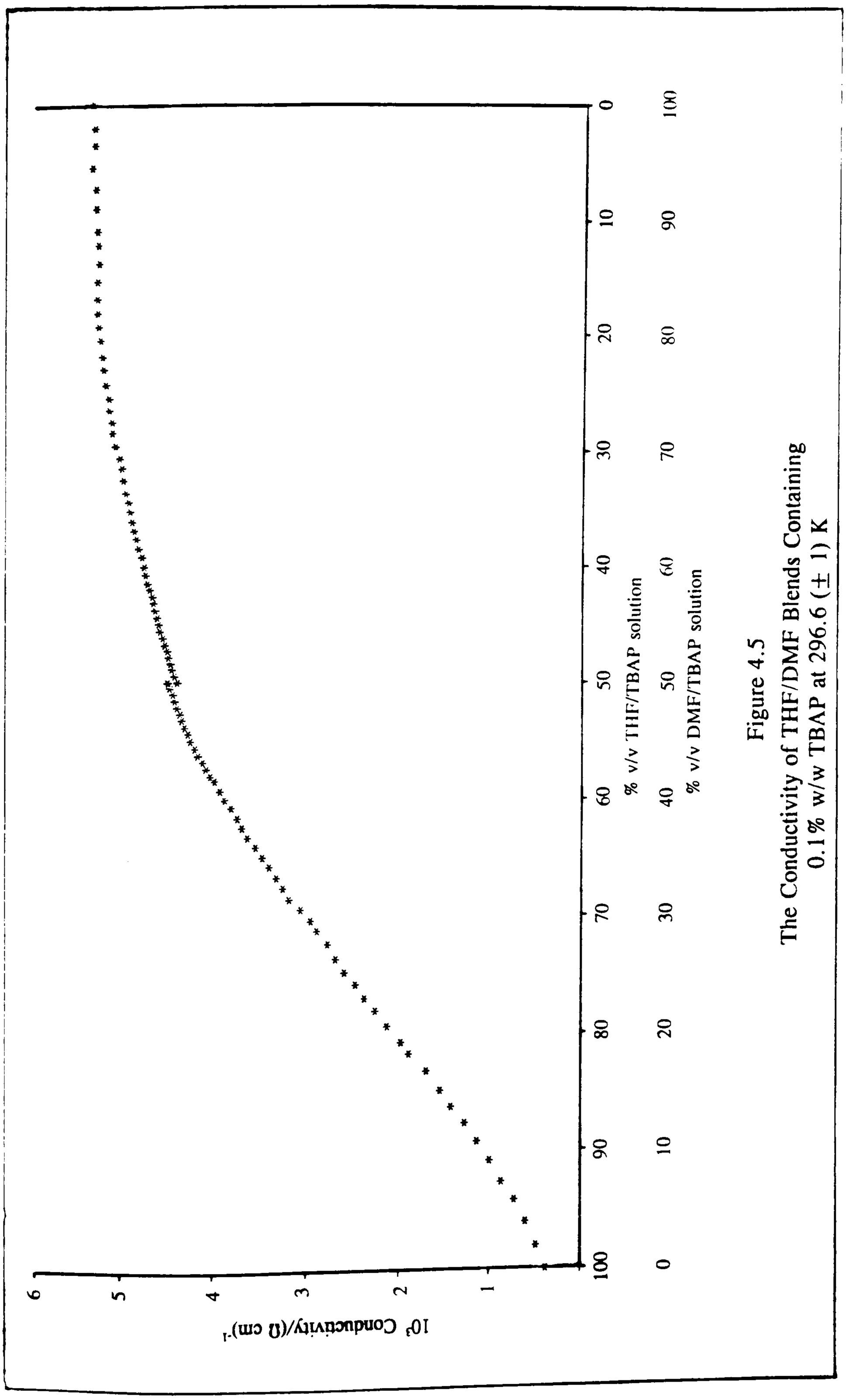

Figure 4.5

The Conductivity of THF/DMF Blends Containing 0.1% w/w TBAP at 296.6 (± 1) K

Kauffman [37] used the reduction peaks of a voltammogram to evaluate the remaining useful life of a lubricant. In his patent, the relation of the reduction peak to the remaining useful life was 'formula dependent'. The formula dependence was eliminated by the addition of an organic base, such a pyridine. Kuznetsov and Fedurenko [39] studied zinc dialkyl dithiophosphates using a polarographic technique, and found that the addition of acetic acid enlarged the size of the response obtained. The increase in the size of the polarographic wave was due to the activation of the basic salts of zinc. The basic salts of zinc were electro-inactive and the addition of acid enabled the ratio of the zinc bonded to the anion to that bonded to basic salts to be determined. The presence of either the acid or the base merely complicated the experimental procedure. The interpretation of the peak shape was not aided by either the acid or the base and so this approach was discontinued.

Owing to the low conductivity of the 75:25 THF:DMF mixed solvent, the kinetic analysis of the electrochemically oxidised species of the amine antioxidant would prove to be virtually impossible. Furthermore the solvent resistance led to questions about the quality of the deconvoluted signal. When this was combined with the necessity of blending the solvent, methylene chloride ($MeCl_2$) was tested as an alternative. $MeCl_2$ is another commonly used electrochemical solvent and $MeCl_2$ containing TBAP has a more positive voltage window before degradation occurs than either THF or DMF. The potential ranges over which the solvents are electrically inactive are illustrated in table 4.2. Each of these may reasonably be employed in an electrochemical experiment over the potential ranges given.

Table 4.2
Voltage Windows of Commonly Used Solvent Systems

Solvent + 0.1 mol dm^{-3} TBAP	Voltage Window (vs. SCE*) /V
Methylene Chloride	-1.8 to +1.8
Dimethyl formamide	-2.9 to +1.5
Tetrahydrofuran	-3.1 to +1.3

* SCE is the standard calomel electrode, a universal standard against which solvent ranges can be measured.

For solutions of DODPA in the $MeCl_2$ electrolyte solution, the peak heights of the

deconvoluted data at +0.8 V verses the Ag/Ag^+ electrode were proportional to the antioxidant concentration. No peaks were present with solutions of the base oil only. The reference electrode solution used in both the THF and DMF solutions (and blends thereof) was silver nitrate. Silver nitrate was found to be insoluble in $MeCl_2$ so a saturated solution of lithium chloride was used as an alternative. When using THF:DMF solvent mixtures, different concentrations of silver nitrate were used in the reference electrode and found to give similar results. It was inferred that the concentration of the reference electrode solution had no effect on the voltammogram, provided that the silver wire was coated with a salt (chloride or nitrate).

The effect of the magnitude of the sweep rate on peak shape and the resolution between electrochemical events was then investigated. The faster the sweep rate the larger the peak became, but the resolution of the electrochemical event was reduced. The best compromise between a large curve and one that was well defined, was found to be given by a sweep rate of 0.5 V s^{-1}.

In a test of the longevity of the analytical solutions, a sample of 1.9% DODPA in synthetic oil was left in the electrochemical cell for 4 days after analysis. The electrolyte evaporated only slightly and was then 'topped up' to the predetermined level. The electrodes were cleaned, the solution degassed and then analysed. The antioxidant concentration had been found to decrease by approximately 36% over this time period. Furthermore when a solution was analysed on concurrent days, the measured antioxidant concentration was lower on the second day than on the first. Therefore solutions must be prepared and analysed as soon as possible to avoid sample degradation. If this stipulation was adhered to the analysis of different solutions of antioxidant, on different days (in the presence or absence of oil), fell on the same calibration line.

There was no means of controlling the temperature of the electrochemical cell used to develop the analytical technique. During the summer months the ambient temperature could rise by up to 14°C above that obtained during winter. If the temperature of the cell rose above 25°C, evaporation of the solvent became noticeable and undesirable convection owing to thermal gradients became prominent. The cell was changed for one equipped with an integral water jacket and the lid fitted with a water cooled condenser to reduce evaporation losses.

The calibration of DODPA in the presence of the synthetic and mineral oils gave very reproducible results that fitted on to the same graph (figure 4.6). With the ester oil, the results appeared to be scattered an in almost a random manner. The analysis of DODPA in the ester oil using the deconvoluted experimental data was unreliable. This was due to the fact that the peak height of the deconvolution is solvent dependent. The peak shape from solutions containing the ester oil varied considerably, from small and broad to large and narrow.

The deconvoluted data were initially chosen for analysis because the electrochemical events are more clearly defined than for the primary current-potential data. The convolution of the primary data is the integral of the deconvolution and therefore proportional to the area under the deconvoluted curve. The limiting value of the convolution, I_L, is independent of the solvent system and a more reliable method for quantitative analysis. The convolution of the primary data is, like the deconvoluted data, solvent dependent. The disadvantage in using the convolution is that the onset and finish of an electrochemical event can be difficult to determine. Ideally the convolution reaches a plateau, the value of which is proportional to the concentration of the electroactive species. The oxidation of DODPA was followed by a chemical reaction that masked the plateau region very slightly, but using the convolution of the experimental data a single calibration plot could be determined for all three base oils containing the antioxidant.

4.3.2 Calibration

The electrolyte was prepared using dichloromethane that had been dried by passing it through a column of activated silica gel. The electrolyte was a 0.1 mol dm^{-3} solution of TBAP in $MeCl_2$ and the reference electrode solution was a saturated solution of lithium chloride in the electrolyte.

The oil samples were prepared for analysis by weighing 1.1 to 1.3 g of oil into a conical flask (50 cm^3) and adding electrolyte to give a total mass of 35 to 40 g. The flasks were stoppered and shaken by hand to ensure that the oil was entirely dissolved in the electrolyte. The flasks were then stored in the dark before analysis, to ensure that no degradation of the sample occurred.

The electrochemical cell and electrodes were washed with electrolyte before each determination. The reference electrode was replenished with fresh saturated lithium

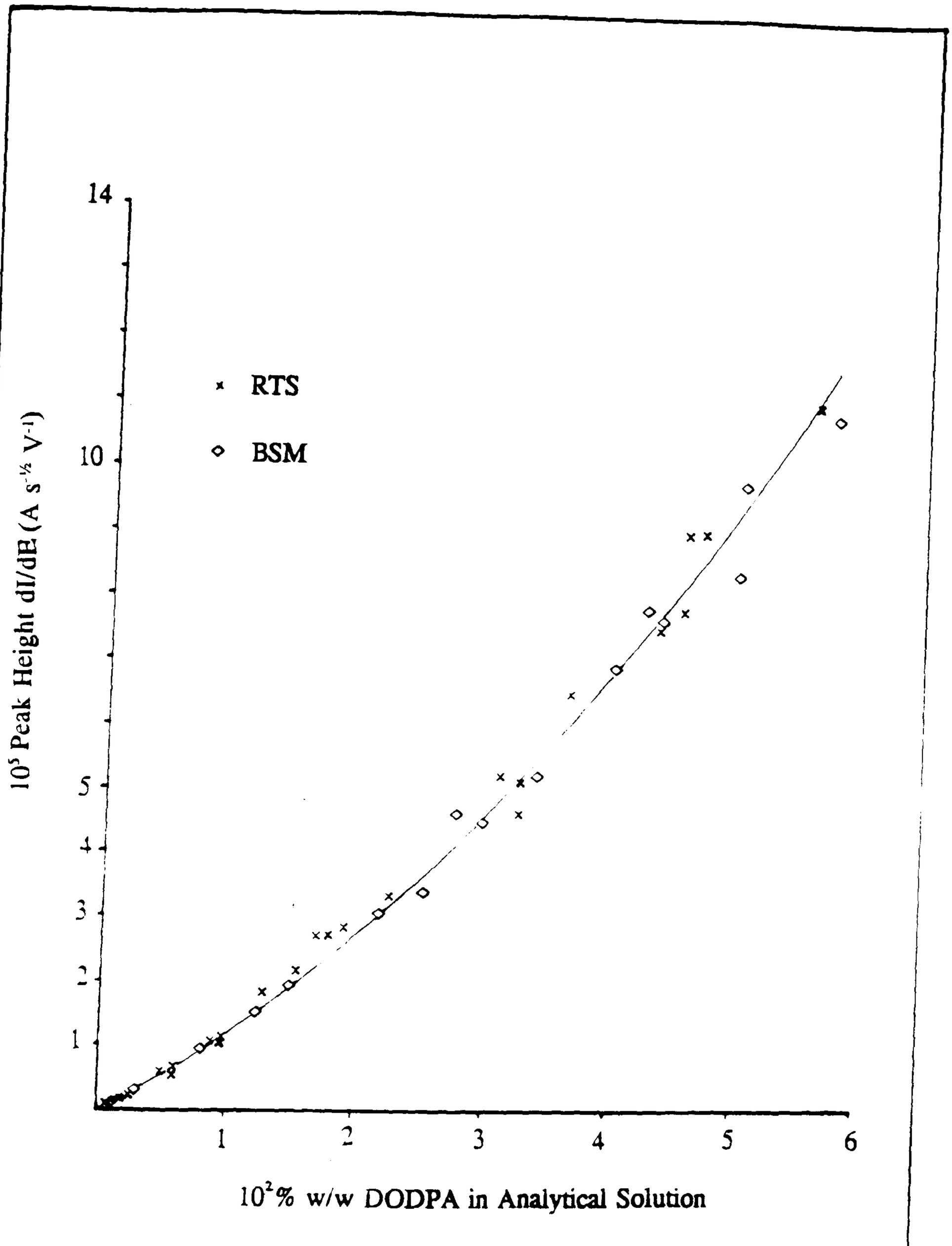

Figure 4.6

Calibration Curve for DODPA in Mineral and Oligomer Base Oils Using Deconvoluted Data

chloride solution. The working electrode was cleaned by grinding the glassy carbon with a silica paste and the counter electrode heated until red hot in a Bunsen flame to remove any adsorbed impurities. It was important to use a flame that would not deposit impurities on the platinum. The cell was assembled and washed with fresh electrolyte. The performance of the routine described above was essential to the success of the experiment.

The first measurement was the background solution (blank), which consisted of electrolyte only. The electrolyte was degassed in the cell for ten minutes with oxygen-free nitrogen at a flow rate of 15 cm^3 min^{-1}. The potential at which no current passed through the counter electrode circuit was measured. This value was approximately +0.1 V for the TBAP/$MeCl_2$ system. In the subsequent experiments the voltage was cycled once at a linear sweep rate of 0.5 Vs^{-1} between this value and +1.3 V. The first experiment to record the voltammogram of the background was followed by measurements on oil samples. Two or three oil samples were analysed for every blank experiment conducted. All measurements were conducted over the temperature range 18 to 20°C.

A typical experimental curve is shown in figure 4.7, together with the corresponding convoluted and deconvoluted curves. The convoluted and deconvoluted curves show the effect of subtracting the blank. For calibration purposes, the limiting value of the convoluted data was recorded as a function of the inhibitor concentration.

There was a six month period over which data were collected for the construction of the calibration curves. This an illustration of the reproducibility of the results obtained from the technique. The equations of the calibration curves for the relevant oil-antioxidant blends are given in table 4.3. It can be seen that the curves pass through the origin, as expected, and from this it is assumed that the errors are only in the measurement of the gradient. The form of the calibration curves is,

$$Y\ (A\ s^{1/2}) = m \times \text{Antioxidant Concentration (\% w/w DODPA)} + C\ (A\ s^{1/2}).$$

In the equation above, m is the gradient of the curve and C is the intercept with the Y axis (limiting value of the I_1 convolution). The calibration curves are valid over the antioxidant concentration 0 to 6.5 x 10^{-2} % w/w in the analytical solution.

It should be noted that the calibration curve for DODPA in the absence of an oil has a larger gradient than when in the presence of an oil. This is due to a reduction in

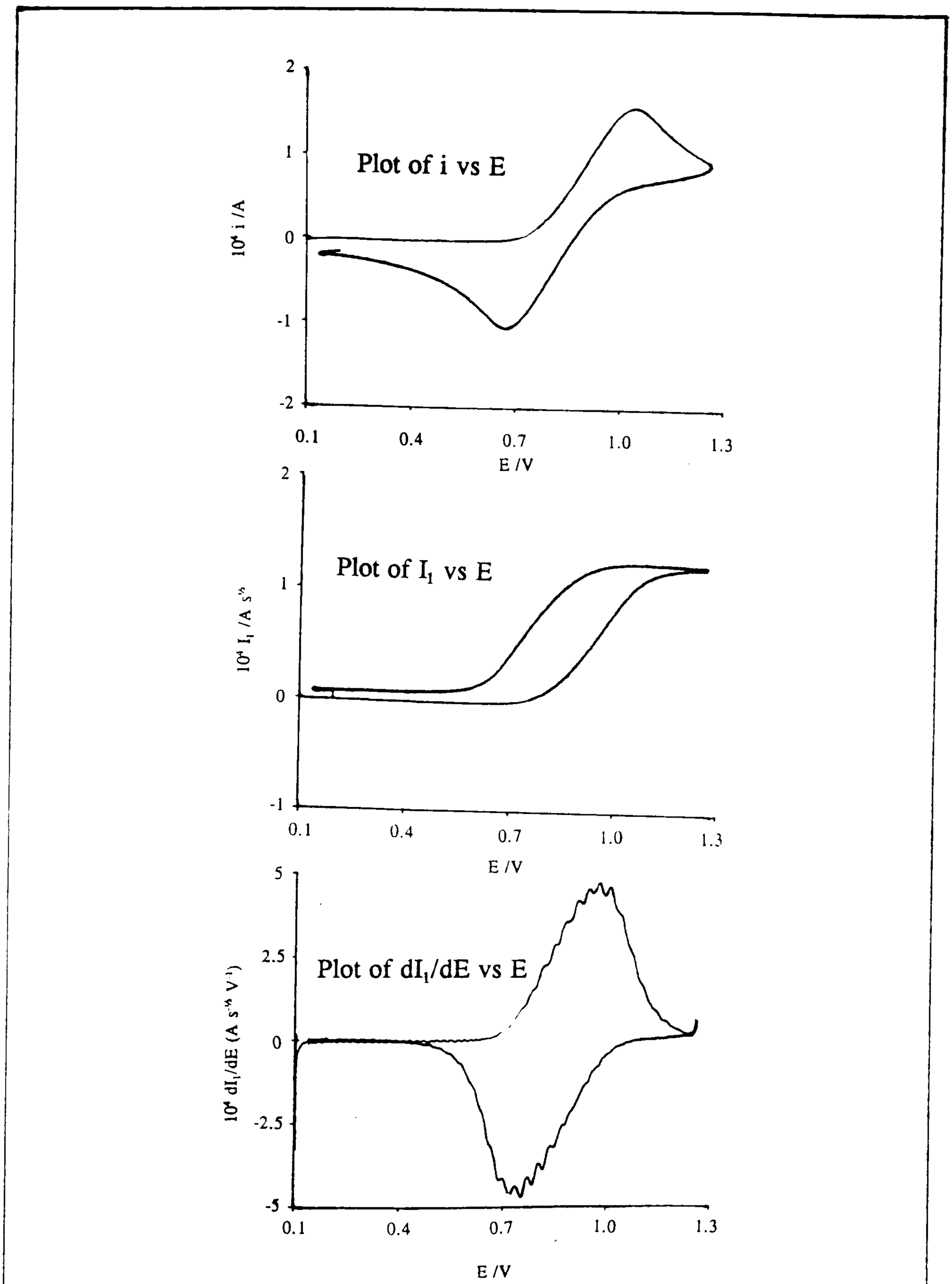

Figure 4.7

The Shapes of the Analytical Curves for a Solution Containing 1.9% w/w DODPA in the Oligomer oil

the diffusion coefficient of the antioxidant caused by the oils. The signal response of the convolution is proportional to the diffusion coefficient of the amine in the electrolyte system. An example of the calibration curves obtained is illustrated in figure 4.8.

Table 4.3
The Equations of the Calibration Curves for DODPA Using CV

System	Gradient / A $s^{½}$ % $DODPA^{-1}$	Intercept / A $s^{½}$
DODPA in Ester Oil	1.95 ($\pm$ 0.08) x 10^{-3}	+ 2.7 ($\pm$ 3.2) x 10^{-6}
DODPA in Mineral Oil	2.07 ($\pm$ 0.03) x 10^{-3}	+ 2.6 ($\pm$ 1.2) x 10^{-6}
DODPA in Oligomer Oil	2.14 ($\pm$ 0.02) x 10^{-3}	- 0.7 ($\pm$ 3.9) x 10^{-6}
DODPA in Oil	2.05 ($\pm$ 0.02) x 10^{-3}	+ 1.2 ($\pm$ 4.7) x 10^{-6}
DODPA Only (No Oil)	2.32 ($\pm$ 0.06) x 10^{-3}	- 2.7 ($\pm$ 1.8) x 10^{-6}
DODPA All Data Points	2.12 ($\pm$ 0.03) x 10^{-3}	- 0.3 ($\pm$ 1.1) x 10^{-6}

4.3.3 Kinetic Analysis

The study of the convoluted and deconvoluted curves of an electrochemical experiment gives an indication of the kinetics of the electrode processes. Amines when oxidised electrochemically tend to lose an electron from the nitrogen [40]. In the case of aromatic amines the charge is delocalised over the whole molecule. It was expected that the molecule DODPA would be very stable in the oxidised form due to resonance stabilisation. The analysis of the deconvoluted data showed that the electron transfer reaction is fast. This conclusion was reached because the oxidation and reduction peaks occurred at the same potential and were not displaced by an amount dependent on the sweep rate. For systems that exhibit purely Nernstian behaviour the peak width at half height should be (90/n) mV, where n is the number of electrons involved in the electrode process. The peak widths of the analytical solutions varied from 105 to 112 mV (with the exception of ester oil solutions where the peak widths varied from 200 to 240 mV) indicating that complicating chemical processes were occurring in parallel to the electrochemical event. For oxidised oil samples the peak width at half height varied from 135 to 150 mV an indication of the increased concentration of reactive contaminants.

The electrochemical response of octyl aniline, a molecule with a similar structure to DODPA was studied in an attempt to determine the electrode reactions of DODPA.

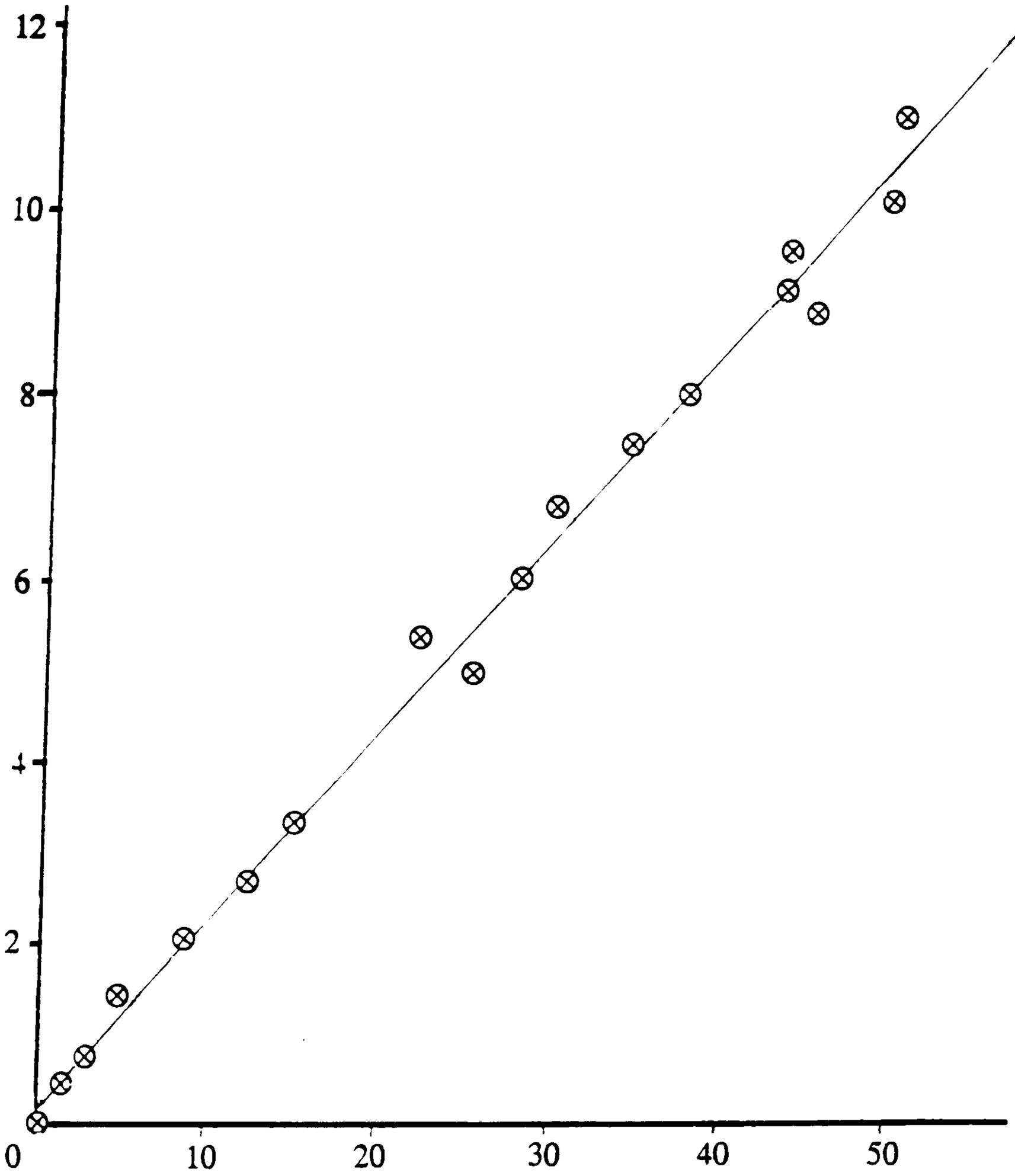

Figure 4.8

The Calibration Curve for DODPA in Mineral Oil by CV

A similar concentration of octyl aniline, as a weight percentage, gave a response nearly two orders in magnitude larger than that of an equal concentration of DODPA. The peak width at half the height of the deconvoluted curve was found to be 322 mV. The electrode reaction of octyl aniline was therefore also a single electron transfer process. This implies that there was nearly twice the abundance of electroactive sites in a solution of octyl aniline. The molar mass of DODPA is 1.94 times that of octyl aniline, accounting for the difference in the size of the signal response. An equal weight percentage of octyl aniline would contain 1.94 times the number of molecules and therefore nitrogen atoms as would DODPA.

The experimental technique described in section 4.3.2 was varied only minimally to enable the electrochemical reactions to be studied. On these occasions the temperature was altered from that used for analysis (291 to 293 K), to the range 240 to 305 K. Below 240 K the analytical solution began to freeze, depositing crystals on the electrodes and above 305 K evaporation of the solvent became significant. The sweep rate was varied between 0.5 V s^{-1} and 0.002 V s^{-1}. If a higher sweep rate was employed no degradation of the oxidised species occurred. If the duration of the experiment was too long the oxidised species diffused away from the electrode surface.

In the initial work an attempt was made to measure the magnitude of the oxidation and reduction peaks at different scan speeds. From the size of the respective peaks, the depletion of the oxidised species was calculated. At each temperature, the half life of the oxidised species could be estimated by extrapolation of the concentration-time plots. The assumption was being made that the reaction was first order and that no errors were introduced upon extrapolation of the data. The determination of the rate constant for the decomposition of the electrochemically oxidised species in this manner was fraught with doubt due to the assumptions made.

An alternative route to the kinetics of the electrochemical reactions involved the use of the I_2 convolution of the current-potential data. The I_2 convolution was used to obtain the rate constant by an iterative process. The value of the rate constant was that which caused the return sweep of the convolution to overlap the outward sweep. A value of the rate constant was estimated and inserted into the convolution (described in appendix 1, section 1.4) and the shape of the convolution studied. If the return sweep did not return to zero, then the rate constant was taken to be too small and a larger value inserted into the expression. If the return sweep passed through zero to a

negative value, then the rate constant was too large and a smaller value taken. The determination of the rate constant in this manner is shown in figure 3.12. The systems studied were DODPA in the absence and presence of the synthetic oil and in an oxidised oil sample.

The order of the reaction for the decomposition of the oxidised species was investigated using the I_2 Convolution. The value of the reaction rate constant was determined at different initial concentrations of antioxidant in the analytical solution and at different sweep rates. The value of the rate constant did not deviate with inhibitor concentration or sweep rate. This implies that the reaction was first order, but it is more likely that the reaction was pseudo first order.

An Arrhenius plot of the natural logarithm of the rate constant versus the reciprocal of the temperature of analysis gives a line with a gradient proportional to the activation energy of the degradation reaction (figure 4.9). The values of the activation energies (E_a) obtained are given in table 4.4.

Table 4.4

The Activation Energy for the Decomposition of Oxidised DODPA

System	E_a /kJ mol^{-1}
DODPA only	11.2 ± 0.1
DODPA in oil	11.7 ± 0.4
DODPA in oil (oxidised)	11.9 ± 0.7

The magnitude of the activation energy suggests that the reaction is one involving free radicals and that the reaction is diffusion controlled. The errors associated with the activation energies are expressed as standard deviations. The reaction rate would be very fast if the oxidised species reacted with the solvent. To determine whether the electrolyte salt participated in the degradation reaction the rate constant was measured for solutions containing different concentrations of TBAP. The value of the rate constant was measured in solutions containing 0.05, 0.1 and 0.2 mol dm^{-3} TBAP. The rate constant remained unaltered, therefore the probable cause of the consumption of the oxidised species is a dimerisation reaction between two oxidised radicals, or one radical and one unoxidised molecule. If the consumption of the oxidised species was caused by the dimerisation of two radicals, the rate of the reduction would be

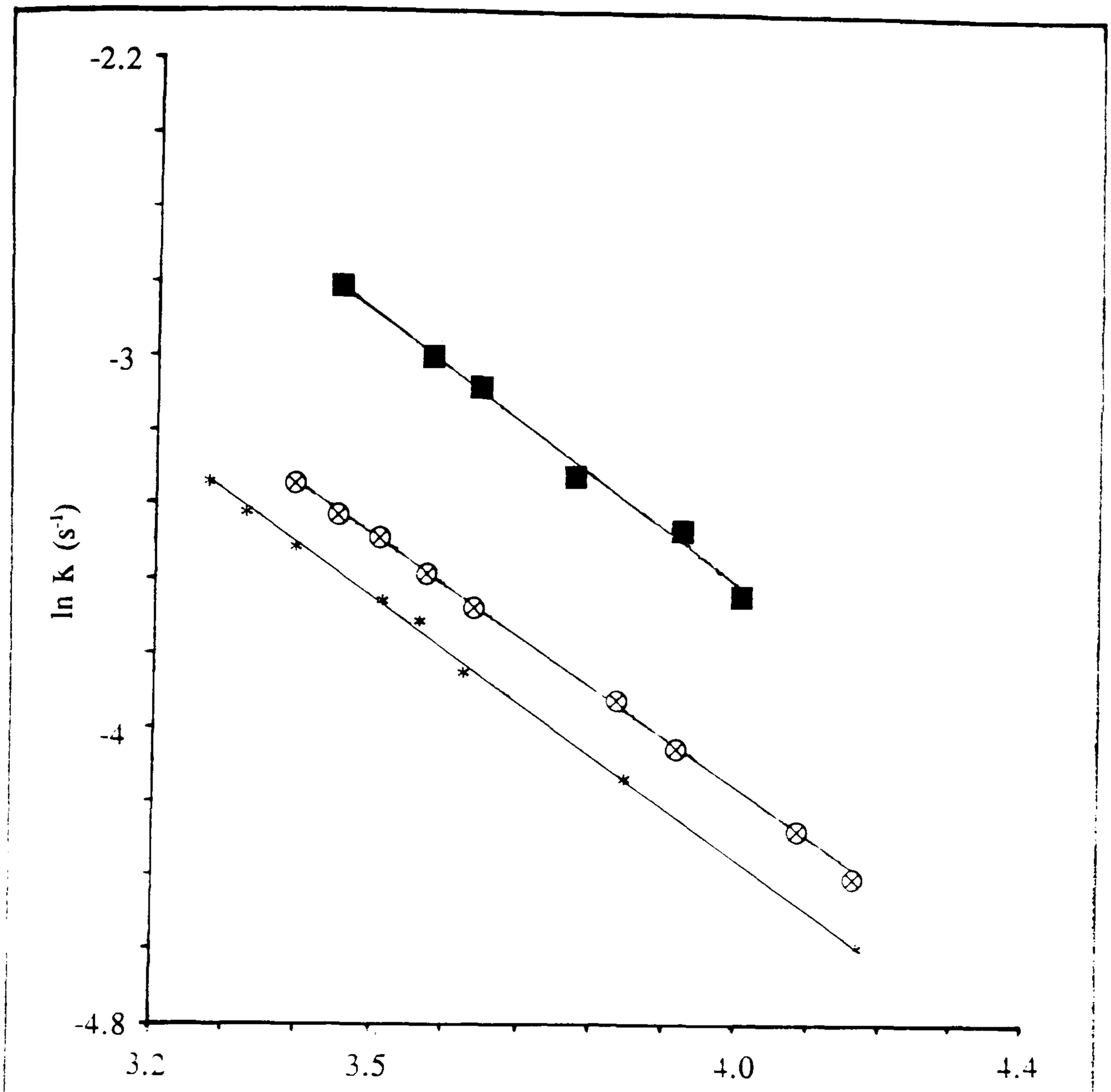

Figure 4.9

The Variation of the Rate Constant for the Decomposition of Electrochemically Oxidised DODPA with Temperature

proportional to the square of the concentration of the free radicals. The solution of the mathematical equations related to this particular set of electrode reactions have not, as yet been solved. The dimerisation reaction of one radical with one unoxidised molecule would be expected to display pseudo first order kinetics when the unoxidised species is present in excess. Since the electrode reactions of substituted diphenyl amines have not been studied, the identity of the product is unknown. The analysis of this compound could be the subject of future work.

The limiting value of the convolution is proportional to the diffusion coefficient of DODPA and for solutions ranging in concentration from 0.2 to 1.9 % DODPA in oil, the diffusion coefficient of DODPA was found to be 1.1 ($\pm$ 0.1) x 10^{-9} m^2 s^{-1} at 290 K. A plot of the natural logarithm of the diffusion coefficient against the reciprocal of the temperature gives an Arrhenius plot with a gradient proportional to the activation energy of the diffusion process. For solutions containing the amine antioxidant only this was found to be 10.5 $\pm$ 0.1 kJ mol^{-1} but in the presence of an oil this rose to 12.1 $\pm$ 2.2 kJ mol^{-1}.

The rate of the electrode reaction can be estimated by employing the simulation program "Condesim" developed at Leeds University by Dr. N. Taylor and Mr. R. Luo. The "Condesim" program is used to simulate the current-potential curve shapes for an electrochemical reaction. The use of the simulation program is described in chapter 6. Values for the experimental parameters were inserted into the program to simulate the current-potential curve shape of experimental data. Different values for the rate constant are tested until the position of both the outward and return peaks match those obtained experimentally. The values obtained were k_o = 5.5 x 10^{-5} m s^{-1} at 295 K and k_o = 3.9 x 10^{-5} m s^{-1} at 245 K. The values of the rate constant imply that the electrode reaction is one of a 'quasi-reversible' regime where the reaction is considered to be neither fast nor slow. In these cases the electron transfer is regarded to be reasonably easy, similar to that observed for many compounds, but slower than that for a polynuclear aromatic compound (k_o = 1 to 100 m s^{-1}) and faster than that for an azo dye (k_o = < 10^{-8} m s^{-1}). The activation energy obtained from these values, 3.94 kJ mol^{-1}, is a combination of all the electrical and chemical terms for the electron transfer reaction.

4.4 The Analysis of Oxidised Oil Samples

Samples of partially oxidised oil were prepared by placing 12.5 cm^3 of fresh oil

into a sample bottle with an internal surface area of 2.5 cm^2. The sample bottle was then placed in a thermostated silicone oil bath at a temperature of 152 $\pm$ 1 °C with the oil sample level below that of the oil in the bath. The oil samples were left open to the atmosphere for gaseous exchange to take place. The oil bath was situated in a fume hood and the samples exposed to both daylight and the fluorescent light of the fume hood while being oxidised. When the samples were removed from the bath the bottle lid was screwed on and they were stored in darkness at room temperature.

The oxidised oil samples were analysed under identical conditions to the calibration standards. The results of some experiments performed on samples oxidised for 36 hours are given in table 4.5. The results show that CV measures antioxidant concentration directly whilst DSC measures oxidation stability.

Table 4.5

The Estimation of DODPA in Oxidised Oil Samples by DSC and CV

Sample	% w/w DODPA by DSC	% w/w DODPA by CV
Base Oil RTS-9745	Induction time too small	0.000 $\pm$ 0.000
0.31% DODPA in RTS	0.08 $\pm$ 0.02	0.055 $\pm$ 0.001
0.61% DODPA in RTS	0.32 $\pm$ 0.05	0.102 $\pm$ 0.002
1.20% DODPA in RTS	1.15 $\pm$ 0.04	0.287 $\pm$ 0.006
1.91% DODPA in RTS	1.88 $\pm$ 0.02	0.76 $\pm$ 0.02
Oil samples oxidised and then inhibited with DODPA		
Base Oil RTS + 0.9% DODPA	1.47 $\pm$ 0.02	0.79 $\pm$ 0.02
1.2% DODPA in RTS + 0.76% DODPA	2.29 $\pm$ 0.01	1.12 $\pm$ 0.02

An interesting result was obtained for the two oxidised samples that were re-inhibited with extra DODPA after testing. Cyclic voltammetry still gave a measure of the antioxidant concentration in the oil but the results obtained by DSC indicated that the samples had an increased oxidation stability over and above that expected. The increase in oxidation stability of the sample appeared to increase by a factor of 50% above that expected for the amount of antioxidant added. For example, the addition of 1% antioxidant conferred a resistance to oxidation equivalent to an addition of 1.5% antioxidant. If oxidation stability were the only consideration governing the lifetime of an oil, then oil changes would be unnecessary and additive 'top ups' would replace

them. Clearly this is unrealistic but the phenomena, also noted by Massey and Wilson using oxygen absorption techniques, is interesting [7]. When an oil is subjected to engine conditions it undergoes several significant changes. These changes can be seen when the colour of the oil and the contents of an oil filter are examineded. The oil turns a dark colour and the filter becomes clogged with oil insoluble materials. The oil loses some light fractions due to volatilisation and both the oil and the additives are subjected to polymerisation. The exhaust gases that blow past the piston rings have a detrimental effect on the oil, especially when its resistance to oxidation is considered. For these reasons alone, the idea of topping up depleted additives is an unrealistic proposition.

Subsequent work has been performed with oil blends containing 1.9% DODPA, that were oxidised in the oil bath for various lengths of time. The results of the analysis are illustrated in figure 4.10. These also show the difference between the measurements made by the two analytical techniques. The electrochemical results show that the concentration of the antioxidant decays almost immediately once the oxidation process has begun, but the thermal analysis shows that the oils only lose oxidation stability after an induction period. This result suggests that the degradation products of the oil blend confer some oxidation resistance in addition to that of the basestock itself (shown by the calibration curves, figure 4.2). The measured concentration of DODPA in the oil blends using the DSC technique was estimated from the calibration curves (figure 4.2). The use of the calibration curves to estimate the concentration of DODPA in an oxidised oil blend assumes that the reduction in oxidative stability of the oil is due to antioxidant consumption. This may not be unreasonable in the early stages of oxidation, because the antioxidant is added to oxidise sacrificially (ie before the oil itself oxidises). At the later stages of oxidation the use of the calibration curves to estimate the antioxidant concentration may not be valid. A normalised plot of the induction time of each blend (with respect to the unoxidised sample) against the oxidation period showed a similar trend to those illustrated in figure 4.10.

For the synthetic oil RTS-9745 the decay of the amine was found to occur exponentially with a half life of 54 hours. The identification of a first order regime for the consumption of DODPA in the oligomer oil may be fortuitous, because the consumption of DODPA in the mineral and ester oils was not found to be either first or second order. The rate and extent of antioxidant depletion for the ester and mineral oil blends was less than that for the oligomer oil. The rates of antioxidant consumption

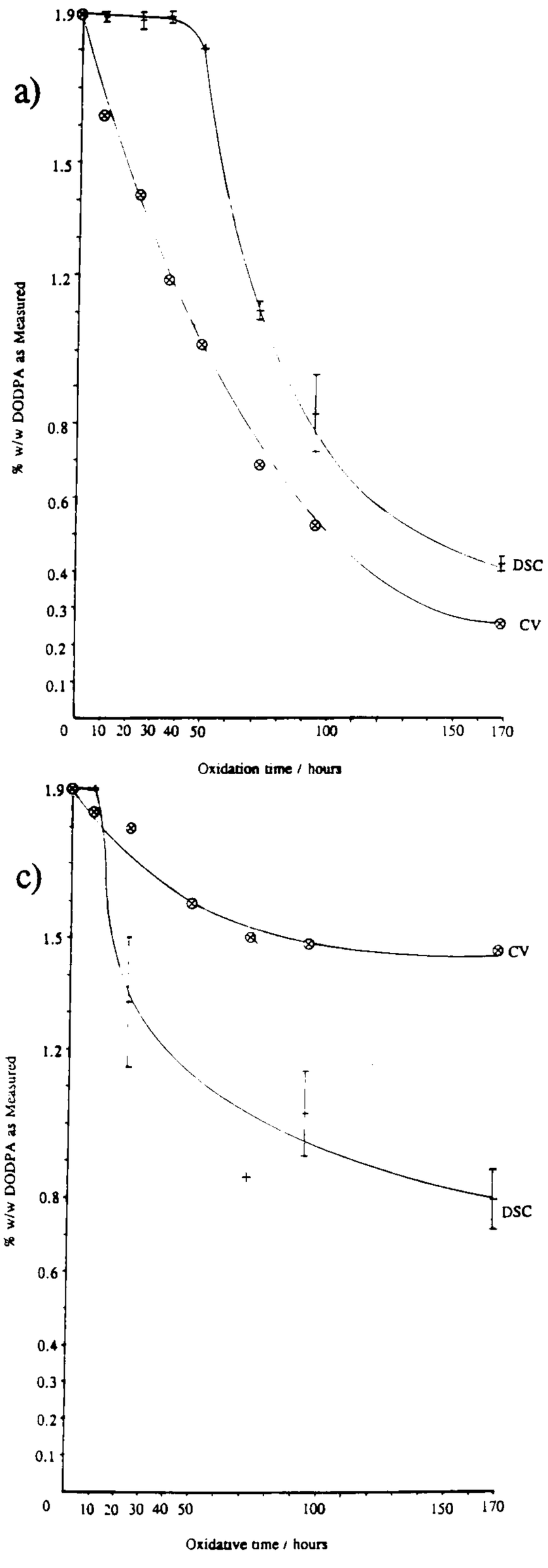

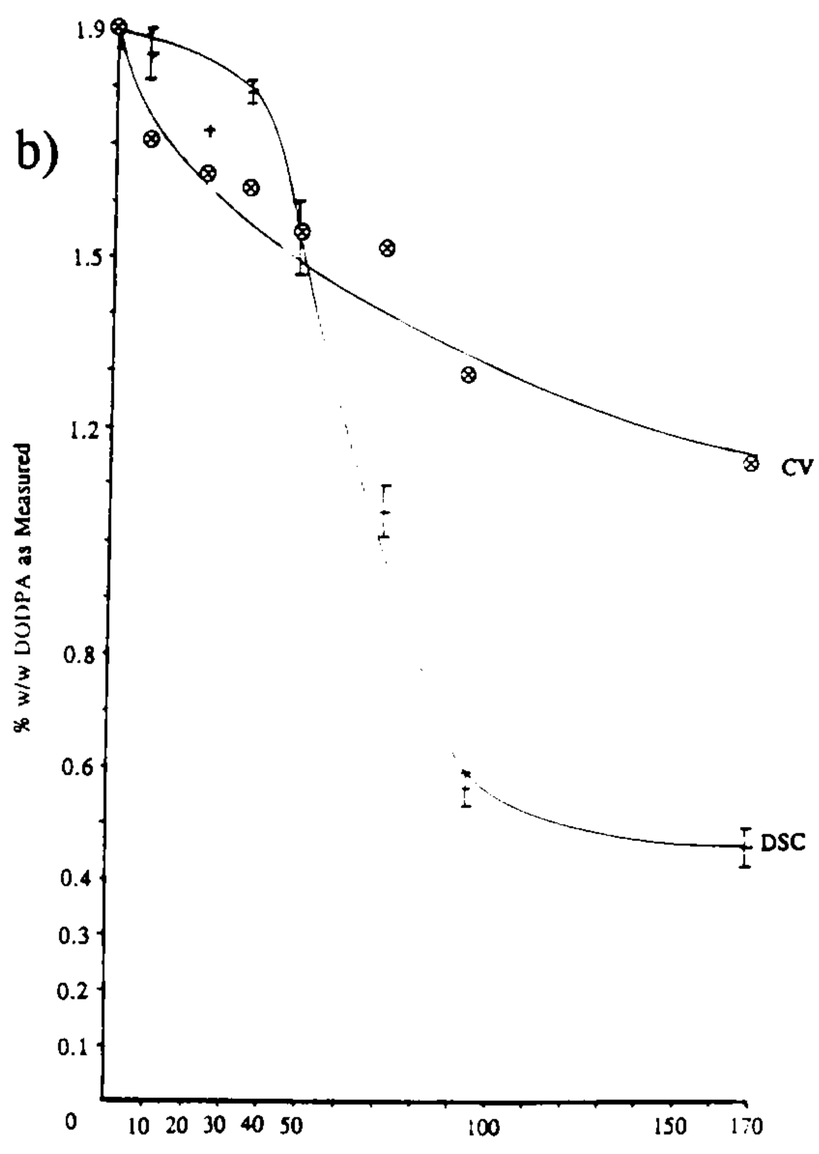

a) RTS-9745 Base Oil

b) BSM-105 Base Oil

c) LPE-504 Base Oil

Figure 4.10

Variation of Measured DODPA
Concentration With Oxidation Time

may reflect the relative oxidative stabilities of the base oils. The thermal stability of the oil after oxidation was lower than that expected for an oil with the corresponding antioxidant concentration for both the mineral and ester oils. These factors reflect the effectiveness of the amine antioxidant in the three base oils and the differences in the oxidation mechanisms. The results illustrated in figure 4.10 may suggest that the ester oil blend containing DODPA possessed the greatest oxidative stability. The oligomer oil blend showed the largest decrease in antioxidant concentration and oxidative stability. These results are also consistent with the trend shown in figure 4.2. The calibration curves show that the ester oil has the greatest oxidative stability and that it has the largest response to DODPA.

An oxidised oil sample supplied by MOD/DQA-TS was analysed using the two experimental techniques. The sample consisted of the ester base stock inhibited by DODPA and phenyl α naphthylamine (PAN). A gas chromatographic study showed the oil to contain 1.18% DODPA and 0.87% PAN on a weight basis. Analysis by high pressure DSC showed the oil to have a superior oxidative stability to the ester oil containing 1.9% DODPA. The electrochemical analysis showed the oil to contain 1.6% DODPA, a combination of the response owing to DODPA and PAN. The two amine antioxidants were not distinguished by the voltammetric method. The electrochemical response is proportional to both the concentration of the active species and its diffusion coefficient. Thus PAN, being a more bulky molecule than DODPA and having a lower diffusion coefficient, therefore 'contributed' less to the electrochemical response. CV can be used for the analysis of mixed inhibitor oil blends, but it is doubtful as to whether it could be used to discriminate between DODPA and PAN.

References

1. J. H. Gilks, *J.I.P.*, 50, 1964, p 309.
2. C. J. Pederson, *Ind. Eng. Chem.*, 48, 1976, p 1881.
3. K. I. Ivanov and Ye. D. Vilyanskaya, In N. M. Emanuel, "The Oxidation Of Hydrocarbons In The Liquid Phase", Translated by K. R. Dobson and B. J. Hazzard, Pergamon Press, London, 1965.
4. L. R. Mahoney, S. Korcek, S. Hoffman and P. A. Willermet, *Ind. Eng. Chem. Prod. Res. Dev.*, 17, 1978, p 250.
5. S. Korcek, L. R. Mahoney, M. D. Johnson and K. Otto, *NBS Spec. Publ. 584,* Proc. Joint Conf. On Measurements and Stds. For Recycled Oils/Systems Performance And Durability, Held At Gaithersburg MD. Oct 23-26 1979 (issued Nov 1980), p 227.
6. G. W. Kennerly and W. L. Patterson jr., *Ind. Eng.Chem.*, 1956, 48, p 1917.
7. L. Massey and A. C. M. Wilson, *J.I.P.*, 44, 1958, p 336.
8. A. Tong, "Determination Of the Oxidation Stability Of Several Antioxidant /Base Oil Mixtures By Pressure DSC", Technical Report, DQA/TS Harefield.
9. A. A. J. Cash, *Ph.D Thesis,* Dept. of Phys. Chem., Leeds Univ., 1988.
10. A. Zeman, *J. Synth. Lubr.*, 5, 1988, p 133.
11. A. Zeman, *Thermochim. Acta,* 80, 1984, p 1.
12. A. Zeman, *Fresenius. Z. Anal. Chem.*, 43, 1983, p 43.
13. D. Al-Sammerrai and Z. S. Salih, *Thermochim. Acta,* 108, 1986, p 91.
14. R. N. Adams and R. E. Parker, *Anal. Chem.*, 1956, 28, p 828.
15. R. N. Adams, J. H. McLure and J. B. Morris, *Anal. Chem.*, 30, 1958, p 471.
16. P. Bromley, DQA Woolwich Arsenal, Private Communication, 1989.
17. F. Noel, *J. I. P.*, 57, 1971, p 355.
18. H. H. Abou El Naga and A. E. M. Salem, *J. Therm. Anal.*, 1987, 32, p 1401.
19. J. A. Walker and W. Tsang, *NBS Spec. Publ. 584,* Proc. Joint Conf. On Measurements and Stds. For Recycled Oil/ Systems Performance And Durability, Held at NBS, Gaithersburg, MD., Oct 23-24, 1979 (Issued Nov 1980), p 271.
20. M. Paczuski and K. Kardasz, *J. Therm. Anal.*, 32, 1987, p 1805.
21. A. K. Aboul-Gheit and A. H. M. Summan, *Thermochim. Acta,* 152, 1989, p 427.
22. J. R. Barnes and J. C. Bell, *Lubr. Eng.*, 45, 1989, p 549.

23. Du-Pont 990 Operations Manual, 1977.

24. F. Noel and G. E. Cranton, *Anal. Calorimetry,* 3, 1974, p 305.

25. D. Skala, H. Kopsch, M. Sokic, H. J. Neumann and J. Jovanovic, *Fuel,* 66, 1987, p 1185.

26. M. E. Brown, C. P. J. Van Vuuren and A. Lithauer, *Thermochim. Acta*, 49, 1981, p 247.

27. A. Tain, *C. R. Acad. Sci. Fr.*, 1924, p 705.

28. M. E. Brown, "Introduction To Thermal Analysis", Chapman and Hall, London, 1988.

29. W. W. Wendlandt, "Thermal Analysis", 3rd Edition, John Wiley and Sons, Chichester, 1986.

30. H. J. Borchardt and F. Daniels, *J. Am. Chem. Soc.*, 79, 1957, p 41.

31. H. E. Kissinger, *J. Res. Nat. Bur. Stand.*, 57, 1956, p 217.

32. H. E. Kissinger, *Anal. Chem.*, 29, 1957, p 1702.

33. T. Boddington, Feng Hong-Tu, P. G. Laye, M. Nawaz, D. C. Nelson, *Thermochim. Acta,* 170, 1990, p 81.

34. J. D. Lee and P. F. Levy, *NATAS,* Proc. 11th Conf., 1981, p 215.

35. H. D. McBride and D. H. Evans, *Anal. Chem.*, 45, 1973, p 446.

36. H. M. J. Ploegmakers and W. J. Van Oort, *J. Autom. Chem.*, 10, 1988, p 135.

37. R. E. Kauffman, U. S. Patent, Patent No. 4,744,870, May 17, 1988.

38. C. L. Franzke, F. Kretschmann, K. Beining, *Fette Seifen Anstrichmittel,* 70, 1968, p 472.

39. U. A. Kuznetsov and L. G. Fedurenko, *Khim. Tekhnol. Topl. Masel.*, 10, 1974, p 56.

40. S. D. Ross, M. Finkelstein, E. J. Rudd, "Anodic Oxidation", Organic Chemistry, A Series Of Monographs, Vol. 32, Academic Press, London, 1975.

Chapter 5

The Analysis of Topanol 'O'

In this chapter the analysis of Topanol 'O' by cyclic voltammetry (CV) and differential scanning calorimetry (DSC) will be discussed. Topanol 'O' is the trade name for the hindered phenol 2, 6, di t-butyl 4, methyl phenol. The analysis of oils containing antioxidant blends will be discussed. The antioxidant blends contain Topanol 'O' and a second antioxidant, either dioctyldiphenyl amine (DODPA) or Topanol 'A'. Topanol 'A' is the trade name for the antioxidant 2, 4, di methyl 6 t-butyl phenol.

5.1 An Investigation of Phenolic Antioxidants

Phenolic antioxidants are probably the most commonly investigated group of additives. This is because they were one of the first groups of antioxidants discovered, there are a great number of different compounds within the category and because they are employed in a variety of diverse applications, such as food stuffs and automobile engines. Topanol antioxidants suppress the propagation reactions of oil degradation, but studies have shown that they are not as effective as some other families of antioxidant. The number of peroxy radicals consumed per Topanol molecule has been calculated as two, in comparison with amine inhibitors, three or four, and bisphenols, four (another group of phenolic antioxidants) [1-3].

The initial work concerning phenolic antioxidants was to investigate the effect of molecular structure on the efficiency with which oxidation reactions were suppressed [4-6]. The authors aimed their work at understanding the reaction mechanisms and ranking the inhibitors in their effectiveness at suppressing oxidation using a variety of techniques. Reiff [4] used an engine test, while Rosenwald et al. employed a bomb test [5]. Bickoff [6] studied the effect of phenolic antioxidants in carotene, and determined the time to degrade 20% of the carotene at 75°C. Although the mechanism of inhibition by phenolic antioxidants is not completely understood the general consensus is

$$AH + ROO\cdot \rightarrow A\cdot + ROOH$$

$$A\cdot + ROO\cdot \rightarrow AOOR.$$

In the equations above AH represents the antioxidant, ROO· the peroxy radical, A· the antioxidant radical and ROOH a hydroperoxide. The term AOOR represents the stable complex formed between the peroxy radical and the antioxidant radical. Bolland and ten Have [7] concluded that if Topanols were not resonance stabilized, their radicals would react with the oil substrate in a propagation reaction. They found that propagation reactions between the oil and inhibitor occur if the phenol is only slightly hindered and that tri-substituted topanols undergo no chain transfer reactions at all. This interpretation was supported nearly a decade later by Bickel and Kooyman [8]

who proposed the above mechanism for the inhibition reaction involving one Topanol molecule and two peroxy radicals.

The early work was of great importance in the development and understanding of phenolic antioxidants. Not all of the work concerning the study of hindered phenols was of use to industry. In one such study Yohe and co-workers [9] oxidised Topanol 'O' in a solution of aqueous sodium hydroxide at approximately 100°C in the presence of oxygen gas to form a compound with a formula of $C_{14}H_{22}O_3$. It may be a while before this investigation finds an application in an industrial process.

Cook et al. [10] questioned whether the phenoxy (inhibitor) radical reacted with a second peroxy radical (after the initial reaction of the inhibitor with a peroxy radical). The authors studied the oxidation of Topanol 'O' and quantitatively analysed the products, which led them to suggest that the phenoxy radical, through resonance stabilization, transformed to the corresponding benzyl radical. The benzyl radical (I) was said to dimerize to form 1, 2 bis (3, 5, di t-butyl 4 hydroxyphenyl) ethane (II), which upon oxidation formed 3, 5, 3', 5', tetra t-butylstilbene 4, 4', quinone, as illustrated below.

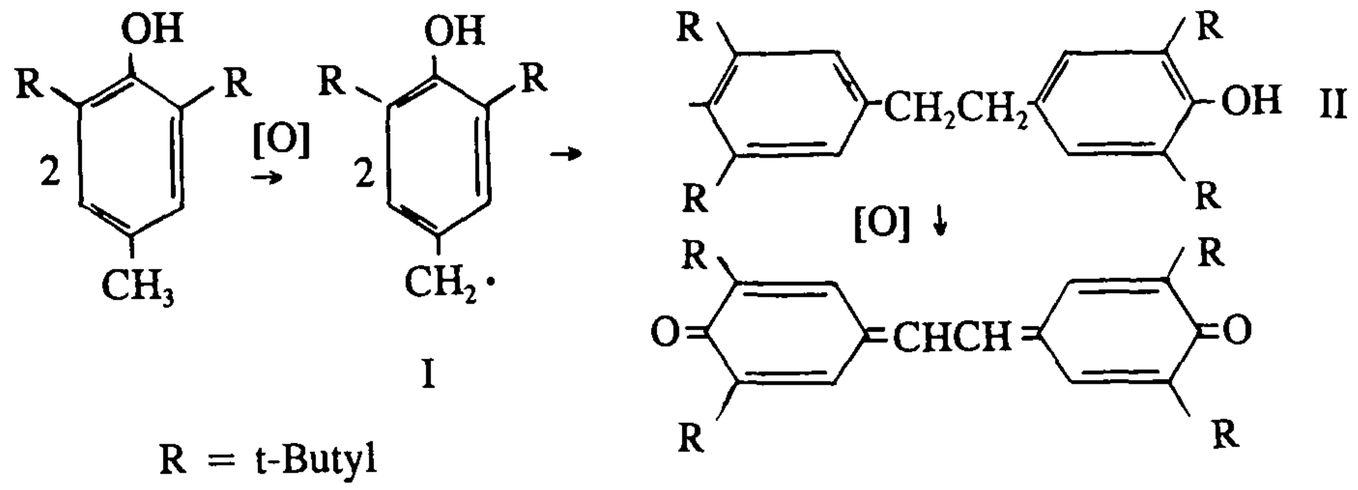

Cook et al [10] stated that there was no record in the literature of a stable mono phenoxy radical other than the 2, 4, 6, tri t-butyl phenoxy radical, which was the subject of a short communication several years later [11] by the same authors. Bennett [12] used ESR studies to support the work of Cook and co-workers, studying the oxidation of 2, 6, di t-butyl 4, alkyl phenols. The author showed that for the methyl and ethyl substituted molecules, the decay was a first order reaction, while for the isopropyl containing molecule the reaction was second order, and the t-butyl derivative was found to be stable. In a further short communication Cook and Norcross [13] studied the solvent effects on the disproportionation reactions of phenoxy radicals using a spectrophotometric technique. They discovered that the rate of disproportionation for 2,6, di t-butyl 4 alkyl phenols was isopropyl > cyclohexenyl > sec butyl, based on the assumption that the spectrophotometric extinction coefficients for the reactants were the

same. The methyl and ethyl containing species disappeared too quickly for the rate to be measured, leading the authors to conclude that the rate of reaction was governed by steric hindrance effects. The phenoxy radicals were reported to form a head-to-tail intermediate before cleaving to form the original phenol and a quinone methide. The rates of disproportionation were found to be independent of the solvent system used.

Cook and Bennett studied the side reactions of alkylated phenols and their results generally contradicted the results reached by many other authors. The two publications by Cook discussed previously have, using the same starting materials (radicals of hindered phenols) described different reactions and end products. Hammond et al. [14] did not consider the formation of a phenoxy radical. They suggested that the rate determining step of the inhibition reactions of alkylated phenols was not the abstraction of a phenolic hydrogen atom, but the formation of a complex that subsequently reacted with another peroxy radical. Ingold [15] studied the inhibition of oil oxidation by 2,6, di t-butyl 4 alkyl phenols. He found that electron releasing substituents increased the efficiency of the inhibitor and that replacement of the phenolic hydrogen by deuterium had no effect on the reaction rate. His conclusion agreed with that of Hammond et al. [14] in that the rate determining step of oil oxidation was an addition reaction (possibly by charge transfer) in which the peroxy radical was conjugated with the aromatic ring of the inhibitor (probably a π electron on the phenolic end of the molecule).

Nixon and co-workers [16] studied the effect of alkyl phenols on the storage and high temperature stabilities of gasoline, drawing the same conclusions as Rosenwald et al. [5] with respect to the antioxidant efficiency in relation to the position of the substituent groups. They then compared the efficiencies of Topanol 'O' and phenylene diamine. The authors discovered that the amine was a more effective antioxidant but the phenol was superior with respect to conferred storage stability and the quantity of deposits formed in an engine manifold [16]. A synergism (an enhancement of the individual performances) was found between the two antioxidants, when added in equal concentrations in certain gasoline blends, which illustrates that the antioxidants may react using different reaction mechanisms. This effect was also discovered by Walters et al. [17] who investigated gum formation in gasoline blends using an accelerated storage test. The synergism reported by Walters et al [17] occurred between a natural and a synthetic antioxidant.

Ivanov and Vilyanskaya [18] studied 21 different antioxidants, using oxygen

absorption and acid number measurements. The action of Topanol 'O' was found to be independent of its concentration in the oil and the absence or presence of a metal catalyst. Antioxidants that behave in a manner similar to Topanol 'O' were found to retard the oxidation process only if added before the steady state region (during the auto-catalytic stage) or before the oxidation processes had begun [18]. An oxygen absorption technique was employed by Massey and Wilson [19] to study the relative efficiencies of antioxidants. Of the antioxidants studied by the authors, amine antioxidants were considered to be more potent than Topanol 'O', which in turn was more effective than Topanol 'A'. This conclusion was reached by studying the oxidation induction times obtained for various concentrations of inhibitor and the variation of the induction time with temperature. They found that when inhibitors were blended, the presence of the 'poor' inhibitor severely impaired the performance of the 'good' antioxidant.

Warne and Vienna [20] studied the high temperature oxidation of lubricating oils, to develop a test method to supplement the existing ASTM D-943 oxidation test. The authors used the new test method to screen inhibitors for use in oil blends. Topanol 'O' was found to be the most effective phenolic antioxidant. The inhibitors with a lower molecular mass were more volatile and therefore less effective. They found that antioxidant mixtures containing Topanol 'O' and another less hindered phenol (name not given) were less effective than Topanol 'O' alone.

In a paper concerned with the analysis of Topanol 'A' in aviation turbine fuel Amos [21] described the development of a procedure using thin layer chromatography. The author employed a densitometer to measure the concentration of the inhibitor in the spots on the plates, claiming an accuracy of $\pm$ 5%. He stated that a better precision could be obtained, if the spots were not allowed to grow so large that their diameter exceeded the slit length of the densitometer. The use of an IR spectrometric technique was employed by Barcelo and Otero [22] to monitor the oxidation of oils. The method followed the growth of the 1710 cm^{-1} carbonyl peak with oxidation time. The method described by Barcelo and Otero [22] was similar to DSC in that it could not be used to discriminate between basestocks or inhibitors.

The investigation of phenolic antioxidants in lubricating oils by thermal analytical techniques has been limited to a small number of publications [23-27]. The results of a HPDSC dynamic experiment for various concentrations of a phenolic antioxidant in

an oil were related to the ASTM D-2272 rotating bomb oxidation test. A straight line was obtained when the increase in induction time (compared to the base oil) was plotted against the onset temperature for various concentrations of antioxidant in an oil [25].

Tong [26] performed a comprehensive study of lubricant-antioxidant mixtures by HPDSC. The mixtures included ester, mineral and oligomer base oils with amine and phenolic antioxidants. When the isothermal method was used, he found that for blends containing up to 1.5% w/w antioxidant, a straight line correlation was found between the additive concentration and the induction time. Concentrations of antioxidant above 1.5% w/w in the oil were not investigated. These results do not agree with those reported in this thesis, where the induction time (and therefore oxidation stability) increased at a decelerating rate with increasing antioxidant concentration. The difference in results may be due to the fact that antioxidant concentrations up to 2% w/w were investigated in this work. Using the dynamic method, Tong [26] found a limiting oxidative stability for the oil blends, in agreement with the isothermal experiments reported in this thesis. Tong stated that the analysis of Topanol 'O' in the mineral oil under investigation was impossible, because the onset of oxidation was insufficiently distinct [26]. The poor definition of the peak onset was due to the presence of pre-peaks or shoulders preceding the main oxidation peak. The presence of pre-peaks has also been noted for mineral oil blends examined in this work. However we found that the analysis of Topanol 'O' in the ester oil LPE-504 proved to be the most difficult. This was because the oil oxidised very slowly, rendering the detection of the peak onset very difficult. If a higher temperature was employed for the study, the induction times for the oil blends decreased accordingly, causing the discrimination between samples to diminish.

Barbooti and Al-Sammerai [27] studied the effect of introducing a ring nitrogen atom on the antioxidant efficiency of 1-naphthol. The experimental procedure compared the onset temperatures of oil blends containing the quinoline compounds to those containing equal concentrations of Topanol 'O'. Whereas the efficiency of Topanol 'O' is dependent on the antioxidant radical being stabilised by steric hindrance, the quinoline radicals were stabilised by the conjugation of double bonds within the aromatic system. The formation of some quinoline radicals were hindered by intra-molecular hydrogen bonding through two adjacent electronegative sites. The addition of a 'hindered' quinoline compound to an oil blend had no effect on the oil stability

whilst the resonance stabilised quinolines were found to be even more effective antioxidants than Topanol 'O' [27].

The electrochemical study of phenolic antioxidants has also been somewhat limited. The majority of investigations have been concerned with multiple ring or phenolic group compounds in the aqueous phase. The electrode reactions of catechol in an acidic solution were studied by Ryan et al. [28]. Catechol was oxidised to form ortho-quinone which coupled with unoxidised catechol to form several unstable products. The unstable products were themselves oxidised at the electrode surface, detected by an increase in the electrochemical response. The anodic oxidation of catechol in an acidic solution was also studied by Papouchado et al [29]. They stated that after oxidation at the electrode surface 1, 2, 4, tri-hydroxy benzene was formed in a subsequent chemical reaction in strong acid solutions. Secondary dimerization occurred at medium pH values, along with the formation of a film over the electrode surface. The authors also studied phenols at a carbon electrode, commenting that the electrode reactions were 'quite complex'. The phenols were oxidised to quinones, then reduced to form hydroxyquinones. The formation of hydroxyquinones was linked to the oxidative coupling to form dimers and polymers [29].

Franzke et al [30] studied phenolic antioxidants in oils and fats using a benzene-methanol solvent to dissolve the oils and the additive. The authors employed a graphite electrode to measure the antioxidants quantitatively, because univalent phenols oxidise at greater potentials than mercury. The solutions contained a buffer to maintain a constant pH and serve as the electrolyte. Qualitative determinations were considered to be of limited use because the half-wave potentials some antioxidants were so similar that differentiation between antioxidants was rendered impossible [30]. It was stated that the analysis of Topanol 'O' was possible only in an alkaline solution, at the expense of a considerable loss in sensitivity. The authors reported that the quantitative determination of Topanol 'O' was impossible [30].

Tonmanee and Archer [31] investigated tertiary butyl hydroxy quinone (TBHQ) using a dropping mercury electrode. The differential pulse polarographic method proved to be successful for the analysis of di-hydroxy-benzene compounds. When phenolic compounds were added to the test solution, no difference in signal response was observed [31]. This was to be expected considering the comment by Franzke et al. [30] which stated that phenolic compounds oxidise at a greater potential than

mercury.

A linear sweep voltammetric method (using a glassy carbon working electrode) was employed by McBride and Evans for the estimation of Tocopherols and antioxidants in fats and oil [32]. The estimation of Topanol 'O' was attempted but it was concluded to be impossible. The oxidation potential of the Topanol was so high that it coincided with the rapid current increase associated with the oxidation of the oil. Topanol 'O' could only be detected when it was present at high concentrations [32].

5.2 Analysis by DSC

5.2.1 Experimental

Much of the preliminary experiments for the analysis of oil samples have been described in chapter 4, along with the experimental method used for oil analysis. The relevant section describes the experimental procedure used to obtain calibration curves, relating the oxidative stability of the oil (in this case the induction time) to the concentration of the antioxidant in the blend.

The shape of the DSC oxidation peaks were studied to ascertain whether there was any dependence of the peak shape on antioxidant concentration. The size and the shape of the isothermal DSC curves did not vary with the concentration of Topanol 'O' in an oil blend. There was a difference in peak shape between the three base oils. For blends made from the mineral base oil the DSC peaks possessed shoulders on the leading edge of the curve and occasionally a pre-peak. The time to the onset of the pre-peak or shoulder proved to be unreliable. The rate of heat release (height of the DSC peak) was highest for the oligomer oil blends and lowest for the ester oil. The rate of heat release for the ester oil blends was considerably lower than for blends made with the other base oils, which rendered the detection of the peak onset difficult. The low rate of heat release reflected the inertness of the ester oil towards oxidation. The peaks obtained for the ester oil blends were considerably wider than those of the oligomer and mineral oils. The mineral oil samples were the narrowest. No change in peak shape was recorded with the extent of oxidation for partially oxidised oil samples containing Topanol 'O'. The magnitude of the peak height and width did not alter with the extent of oxidation, which may suggest that the oxidation products of Topanol 'O' do not confer any oxidative resistance on the oil blend.

For the investigation of oil blends using the isothermal method, the oxidation peaks became sharper as the temperature of analysis increased. The induction time before the oxidation peaks decreased with an increase in temperature, resulting in a reduction of the resolution between oil blends. For mineral oil samples (in the presence or absence of Topanol 'O') the pre-peaks and shoulder on the leading edge of the curve become less distinct with an increase in temperature of analysis.

When oil samples containing Topanol 'O' were analysed using the dynamic method the peaks became sharper with increasing heating rate. For mineral oil samples the resolution between the closely linked thermal events reduced as the heating rate was increased. For samples containing Topanol 'O', the residues after oxidation were similar in appearance to those containing the amine antioxidant. The sample mass loss during an experiment was equivalent to that lost when the sample contained DODPA. No relationship was found between peak shape, size or sample mass loss and the composition of the oil.

The calibration curves obtained from the isothermal analysis of the oil blends are given in figure 5.1. The determination of the induction time before the onset of rapid oxidation is defined in chapter 4. The temperatures used for the analysis of the Topanol 'O' blends were lower than those employed for the analysis of the DODPA blends. The calibration curves given in figure 5.1 relate the induction time to the antioxidant concentration in the oil blend. The average error associated with the measurement of any induction time was 3.5%. The average errors in the measurements obtained for oligomer oil samples were lower than those for samples prepared from the mineral and ester base oils. The wide range in the magnitude of the error bars (taken as the standard deviation of the data) may be a reflection of the intricate nature of lubricating oils. From the diagram it can be seen that Topanol 'O' is not such an effective an inhibitor as DODPA for any of the base oils. The comparison between the efficiencies of DODPA and Topanol 'O' can be made by referring to figures 4.2, 5.1, 6.1 and 6.2. The induction times for the fully formulated oils containing the hindered phenol were less than those containing the amine despite, the lower temperatures used.

The response of the base oils to the additive could clearly be seen. The ester oil responded to the greatest extent to the presence of Topanol 'O' and the oligomer oil the least. When the percentage increase in induction time above that of the base oil is compared, the response of the base oils to the antioxidant is reversed. The ester and

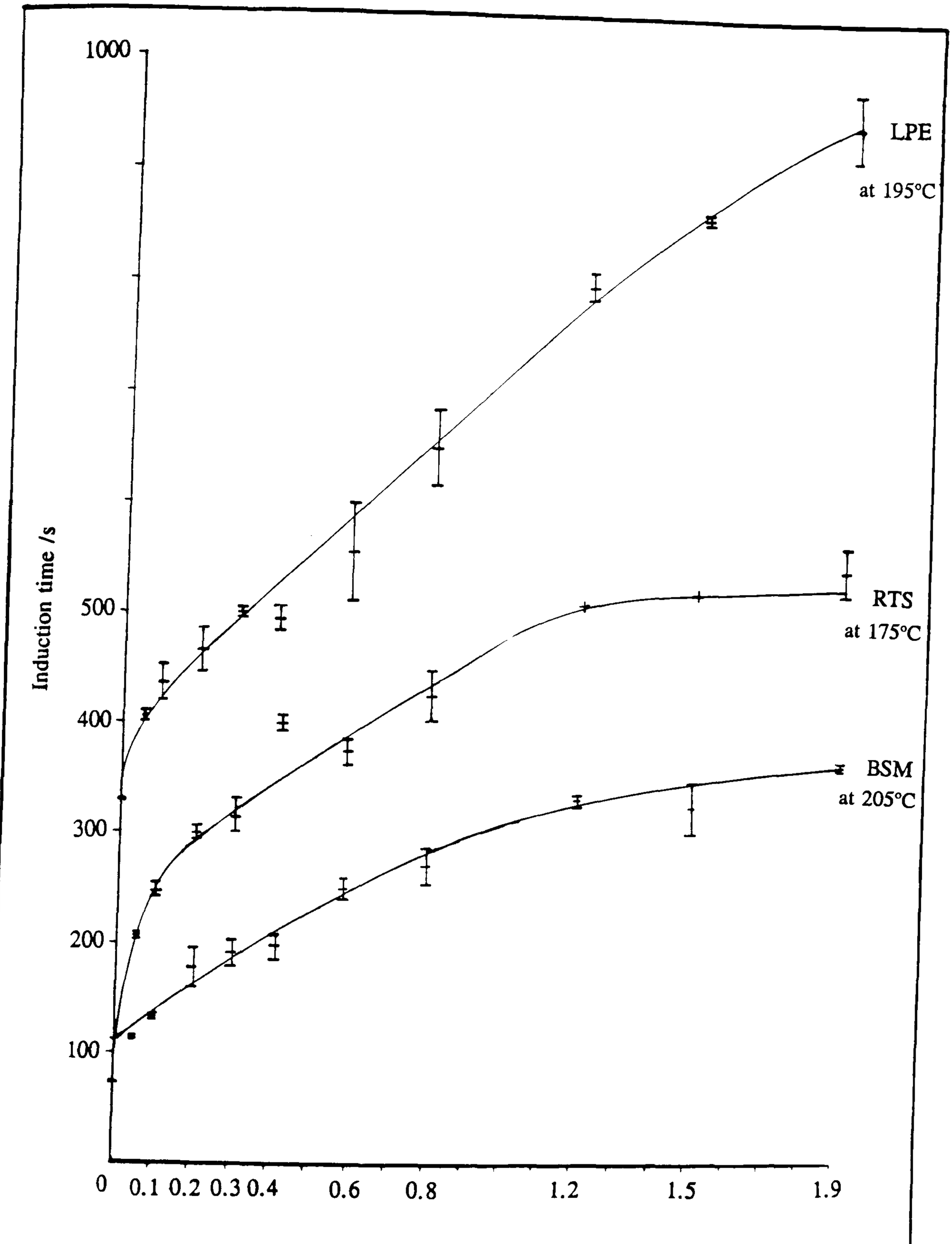

Figure 5.1

Calibration Curves for Topanol 'O' in the Base Oils by High Pressure DSC

oligomer oils are saturated hydrocarbons, which in general are very responsive to chain stopping inhibitors such as amines and hindered phenols. The oligomer base oil, owing its highly branched nature exhibits a lower oxidative stability. A synergism between the sulphur compounds present in the mineral oil and the Topanol 'O' could account for the high oxidative stability of the blend.

5.2.2 Kinetic Analysis

The experimental procedures employed to obtain the kinetic data have been described in the previous chapter. The doubts expressed in chapter 4, regarding the significance of the parameters measured and the use of the term 'activation energy' must be reiterated. The so called 'activation energies' measured encompass the activation energies for the initiation and propagation reactions involved in the oil degradation process. The 'activation energies' measured represent the temperature dependence of the reaction rates studied. To ascribe a specific value to any one process would be very speculative and possibly incorrect.

The kinetic data obtained using the isothermal and dynamic techniques are given in table 5.1 and figure 5.2. The isothermal method provided a straight line plot over a temperature range of 432 to 491 K. The dynamic methods produced straight lines over the heating rates 5 to 100 K min^{-1}.

Table 5.1
The Kinetic Data Obtained from DSC Analysis

% w/w Topanol 'O' in Sample	Method of Analysis	Activation Energy / kJ mol^{-1}		
		Mineral Oil	Oligomer Oil	Ester Oil
None (Base Oil)	Isothermal	171 ± 12	70 ± 10	103 ± 11
	Dynamic			
	ln (β/Tm^2) vs 1/Tm	136 ± 2	-	155 ± 18
	ln (1/β) vs 1/Tm	128 ± 5	-	139 ± 17
1.5	Isothermal	116 ± 5	103 ± 11	148 ± 7
	Dynamic			
	ln (β/Tm^2) vs 1/Tm	91 ± 3	85 ± 8	125 ± 8
	ln (1/β) vs 1/Tm	99 ± 3	89 ± 6	103 ± 8

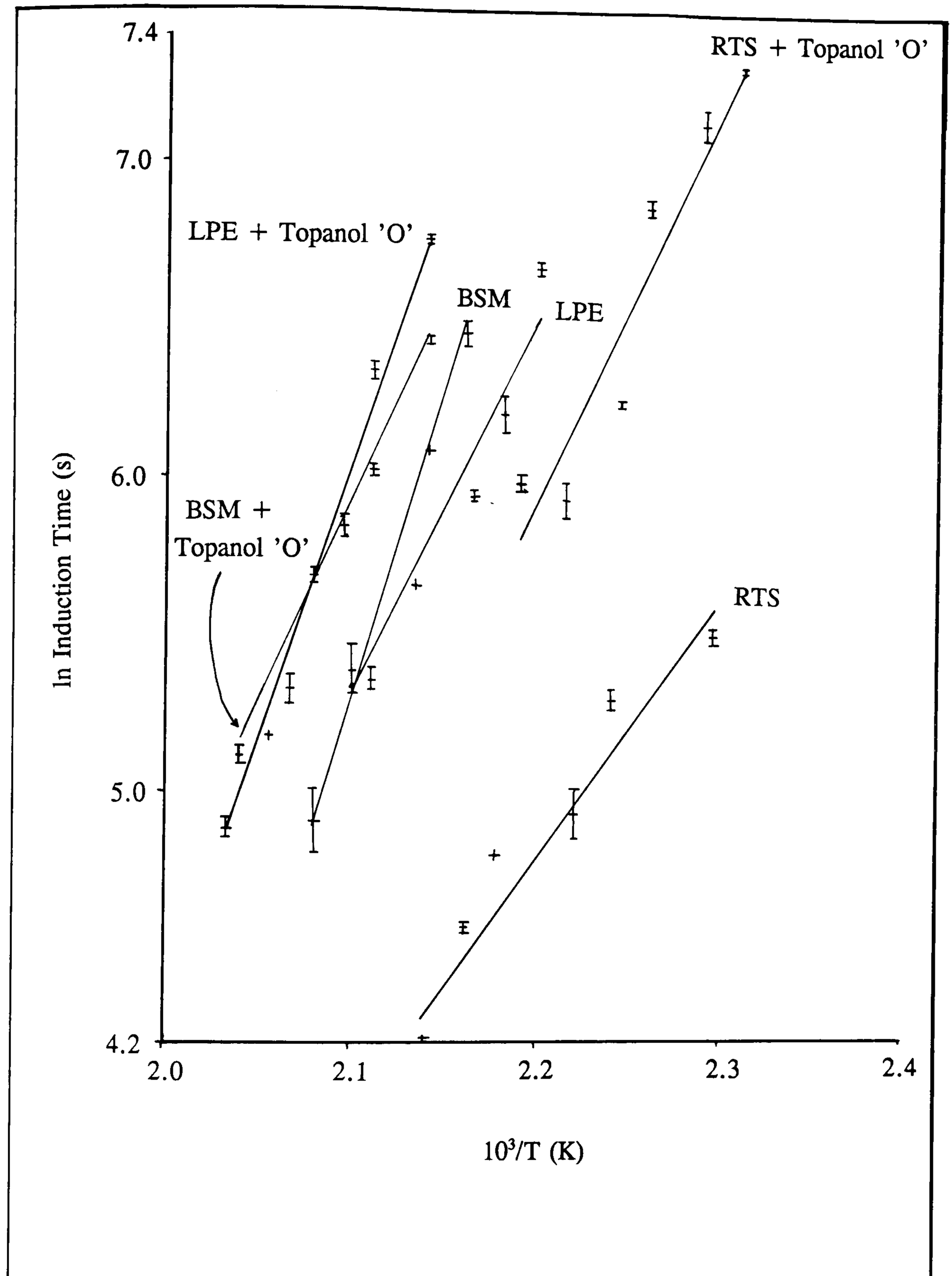

Figure 5.2

Variation of the Induction Time With Temperature for
the Base Oils and Blends Containing 1.5% w/w Topanol 'O'

As mentioned in the previous chapter, this implies a single rate law for the oxidation processes. Extrapolation of the data to higher and lower temperatures, or heating rates would not be valid since it would have to be assumed that no change in reaction mechanism would occur. This is clearly not the case, because at low temperatures the oxidation reactions are governed by hydroperoxide decomposition, while at higher temperatures the decomposition products mainly consist of aldehydes and alkoxy radicals.

As was the case with the 'kinetic' results obtained in chapter 4, no definite conclusions can be drawn about the mechanism of the initiation and propagation reactions. The induction time leading to the rapid oxidation of the oil is measured using the isothermal technique. The 'kinetic measurements' derived from this technique may indicate the magnitude of the activation energies associated with the initiation and inhibition processes. The use of the isothermal technique indicated that the 'activation energy' of the initiation reactions for the synthetic oils increased upon addition of the phenolic antioxidant. This was not the case for the mineral oil where phenolic compounds were already present. The 'kinetic' parameters obtained using the dynamic technique imply that the measured 'activation energy' of the oxidation processes decreased upon addition of the antioxidant. For the antioxidant to be consumed in preference to the base oil, the rate constant associated with its oxidation should be lower than the propagation reactions of oil oxidation. This may have the effect of lowering the 'activation energy' of the overall oxidation process.

5.3 The Analysis by CV

5.3.1 Preliminary Experiments

To study the system successfully a solvent was required that would dissolve the oils and not degrade at the same potential as the antioxidant. A list of the more common electrolyte blends is given by Bard and Faulkner [30] which indicates the potential ranges of the solvent mixtures against a standard calomel electrode. The majority of the experiments concerned with optimising the experimental technique for the analysis of Topanol 'O' had been performed to enable the study of DODPA. It was stated by Franzke et al. [31], that the oxidation potential of phenolic antioxidants was greater than that of mercury, necessitating the use of carbon or platinum electrodes. The prejudice in the literature concerning the use of graphite or carbon electrodes led to the decision to retain the electrode arrangement used for the study of the amine [31,33-35].

The electrochemical cell with an integral water-cooled jacket and a lid fitted with a condenser was used for all experiments. The following is a resumé (written in chronological order) of the work performed to optimise the experimental conditions used for the analysis of the phenolic inhibitor.

The initial experiments were aimed at measuring peak heights of the deconvoluted data and not the limiting value of the I_l convolution. The voltammograms of solutions containing Topanol 'O' in the presence of an oil gave rise to no discernible peaks, although for pure solutions of the inhibitor a peak owing to the antioxidant was evident. Prior to an analysis being made, the two components had to be separated. Separation of the antioxidant from the oil blend was achieved by washing the oil with aqueous sodium hydroxide and then washing with dilute hydrochloric acid. The aqueous phases were collected, neutralised and washed with methylene chloride ($MeCl_2$),which was then collected in weighed conical flasks. The solvent was evaporated over an oil bath to collect the antioxidant which was then redissolved in fresh electrolyte ready for analysis. This method of extraction was very effective. The voltammograms of solvent extracted Topanol solutions compared favourably to those of fresh antioxidant solutions in the absence of an oil, with respect to the peak shape, size and position. The analysis of Topanol 'O' after solvent extraction further complicated the analytical procedure and increased the possible sources of error in any quantitative measurement. For this reason it was decided to investigate the analysis of the antioxidant without extraction from the base oil.

The use of a methanol/potassium hydroxide solvent system was employed to study the electrode reactions of Topanol 'O' [36]. The authors employed a reference electrode (RE) of silver/silver chloride (Ag/AgCl), using a working (WE) electrode of graphite. The antioxidant was studied in a reductive sweep [36]. In our experiments, the electrolyte did not dissolve the oils or, more importantly, silver chloride used for the reference electrode (a milky white precipitate was formed). Solutions containing the oil existed purely as an emulsion, which gave rise to poor voltammograms. On the occasions where an oil droplet settled on the surface of the working electrode, the analytical signal was very noisy, and once removed from the electrode, the voltammogram obtained was indistinguishable from a blank experiment.

The next solvent system tested was TBAP dissolved in DMF. Solutions of the antioxidant were examined using scan speeds varying from 0.2 to 5.0 V s^{-1}, to

determine the optimum sweep rate for the analysis. As the sweep rate increased the noise of the analytical signal rose proportionally and the peaks became less well defined. The convoluted data was studied to establish whether the signal reached a plateau at the end of the electrode reaction. At every scan speed studied the convoluted data failed to attain a limiting value. In comparison to the response obtained for the amine antioxidant, the phenolic system produced peaks that were small and poorly defined. The poor resolution of the results led to the investigation of the voltammogram over the complete electrochemical range of the solvent. A peak of two to three orders of magnitude larger than the one previously studied was found at a potential of approximately +1.6 to +1.7 V vs. the Ag/AgCl RE. The peak was equally evident for solutions that contained the oil as for antioxidant alone. The peak at +1.6 to +1.7 V was at the edge of the electrochemical potential range of DMF.

$MeCl_2$ was then tested, because it possessed a more positive potential window and because it was capable of dissolving the oils. Despite the highly positive voltage window of $MeCl_2$, the study of Topanol 'O' did not produce data that on convolution attained a limiting value (figure 5.3). When the deconvoluted data was studied it could be seen that the peak did not return to the baseline before the degradation of the solvent dominated over the electrode reaction of interest. This meant that the antioxidant had not been completely oxidised before the solvent had started to degrade owing to the applied potential. A study of the raw current-potential data of the blank illustrated that the solvent had began to degrade at the potential range of interest.

Two solvents (propylene carbonate and sulphur dioxide) with a more positive potential window than $MeCl_2$ were excluded from the study because they would not dissolve the oil blends and would prove too difficult to use. Acetonitrile and benzonitrile, each have a potential window more positive than $MeCl_2$, but the oligomer oil could not be dissolved in either of these solvents. Other solvents with the ability to dissolve the oils were considered, as blends with either acetonitrile or benzonitrile. Such a mixture must also be capable of dissolving the antioxidant and the electrolyte salt. The mixture of 60:40 v/v benzonitrile : pentane was chosen, because acetonitrile and pentane were immiscible. The maximum solubility of the oils were 1% w/w in the solvent mix.

The convoluted data from experiments conducted using the benzonitrile : pentane solvent mixture still did not reach a limiting value despite the fact that the

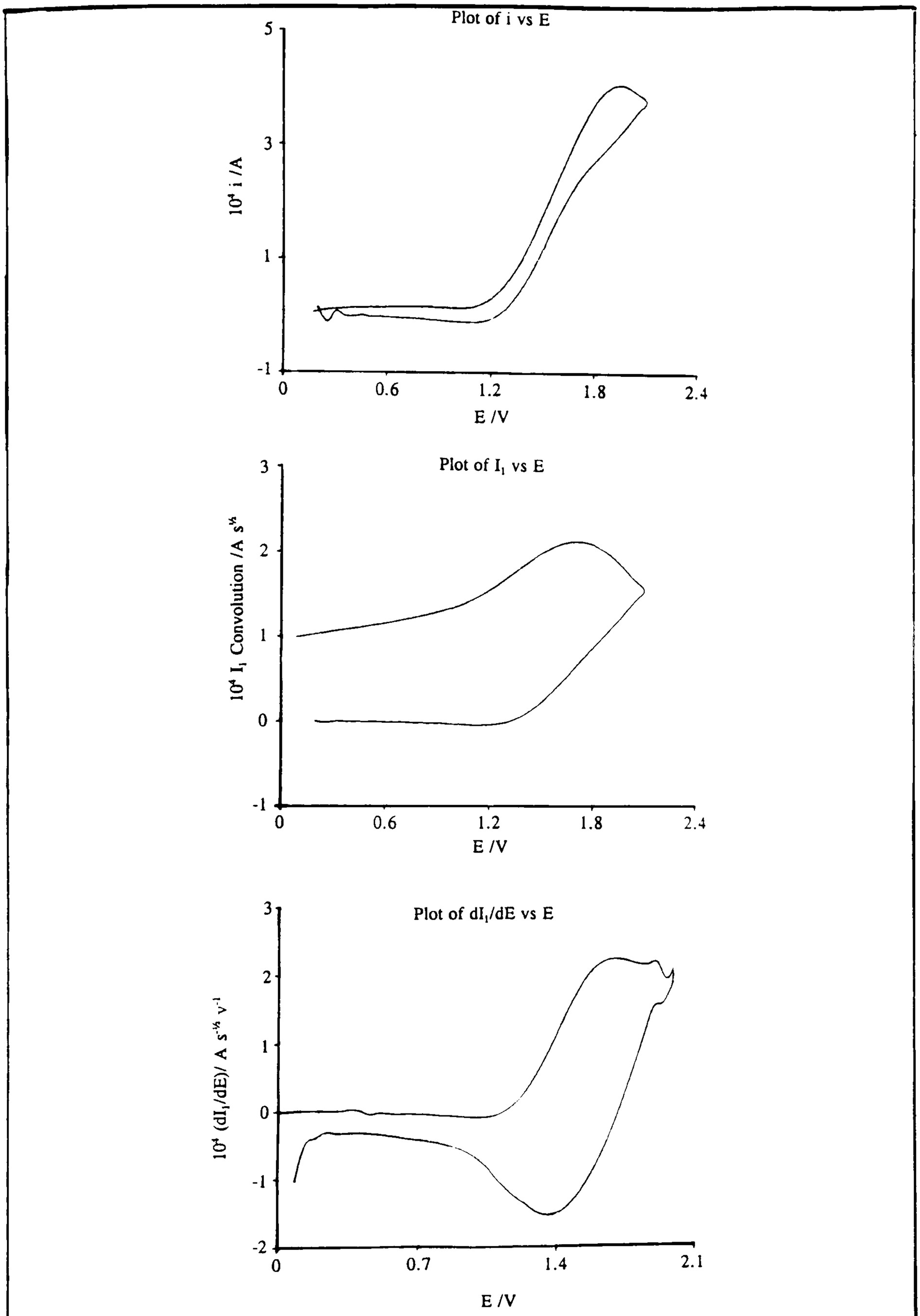

Figure 5.3

The Shapes of the Analytical Curves for a Solution Containing 1.9% w/w Topanol 'O' in the Oligomer Oil

voltammograms were scanned to high positive potentials (up to 2.35 V vs. the Ag/AgCl RE). The high vapour pressure of the solvent was an undesirable feature of the blend. Further solvent mixtures were investigated in an attempt to reduce the volatility of the solvent mixture and allow a more positive potential to be reached before solvent degradation became significant. Benzonitrile was blended with cyclohexane, hexadecane, hexane, benzene, and toluene. All the blends dissolved the oils with ease, except the mixture containing hexadecane, which was immiscible. A literature search of the vapour pressure and the boiling point of potentially suitable solvents was conducted to establish which solvents may have had a sufficiently low volatility. The conductivity of the blends containing the electrolyte salt were then studied before the solvent mix of 50:50 v/v benzonitrile:benzene was finally chosen.

The use of the new solvent mix allowed a more positive potential to be reached before the onset of solvent degradation, but the convoluted data obtained for antioxidant solutions still did not reach a limiting value. This led to the decision to study the raw current-potential data and the convoluted data at set potentials. The object of this study was to ascertain whether any relationship between antioxidant concentration and signal response could be found. Straight line correlations were found between the concentration and the signal response for the raw current-potential data but the error in the gradient ranged from 5 to 14%, depending on the potential used for the study. A further complication was that the calibration plots did not pass through the origin. When the convoluted data was examined in a similar manner, a better correlation was obtained between the signal response and the inhibitor concentration. The potentials studied ranged from 1.65 to 2.05 V in 0.05 V increments, and the errors associated with the gradient of the calibration curves varied from 3 to 9%. The variation of the I_l response with inhibitor concentration was studied at 1.75 V, because the error associated with the gradient was at its smallest value and the plot passed closest to the origin.

The toxic nature of both benzene and benzonitrile necessitated the experiments being conducted in a fume hood, but because one was unavailable, a fume box was constructed around the electrochemical cell. A pump was used to draw air into the box and pump it out of the building, which eliminated the smell of the solvents from the laboratory. The data obtained from each set of experiments lay on straight calibration lines, with a small error in the gradient, but the results from each data set possessed a different gradient. The lack of reproducibility of the technique was initially thought

to be due to the preparation of the solvent mix or the sensitivity of the solution to sunlight. When the cell was shielded from the light, the inconsistency between groups of samples remained. It was then realised that the pump was drawing off the solvent as the sample was being degassed, thus altering sample concentration. When the vacuum pump was not used, the experimental results were more reproducible, but the problem associated with the smell of the solvent (and its toxic nature) returned. No advantage had been gained from using the blended solvent over $MeCl_2$, because the convoluted data did not reach a plateau at the higher potentials attained.

When the problems associated with blending the solvent, the toxicity and the volatility of the components were considered, it was decided to use $MeCl_2$ as the solvent for the study of Topanol 'O'. The data accumulated before the mixed solvent system was investigated, were analysed at potentials ranging from 1.25 to 2.05 V, in 0.05 V increments. This was to find the potential at which the effect of the solvent on the electrode reaction was minimal. At potentials where the solvent interacted with the electrode reaction the electrochemical response to the sample concentration reached a limiting value. The potential chosen for the study of the antioxidant was 1.75 V verses the Ag/AgCl RE. The choice of 1.75 V as the potential of analysis was made because the calibration curve had the smallest error associated with the gradient and because the curve passed close to the origin (see figure 5.4). It is interesting to note that the same potential was chosen for the study of Topanol 'O' in the mixed solvent system.

The peak widths at half height, of deconvoluted data for Topanol 'O' solutions were studied. This was done to determine the number of electrons associated with the electrode reaction. The peak widths were approximately 110 mV (130 mV in the presence of an oil), which indicated a single electron transfer process, complicated by an associated chemical reaction. In an attempt to determine the electrode reaction, phenol was analysed in the same manner as the antioxidant. The electrochemical response obtained from the oxidation of an equal concentration of phenol (on a molar basis), had an identical shape and peak potential and magnitude to that of the Topanol. Furthermore, when phenol was added to an analytical solution containing Topanol 'O' the shape of the analytical curve did not change, but merely grew in size. It was concluded from this that the electrode reaction of Topanol 'O' is the abstraction of an electron from the phenolic grouping of the molecule. This is because the electrochemical oxidation of phenol occurs by the loss of a single electron from the phenolic grouping.

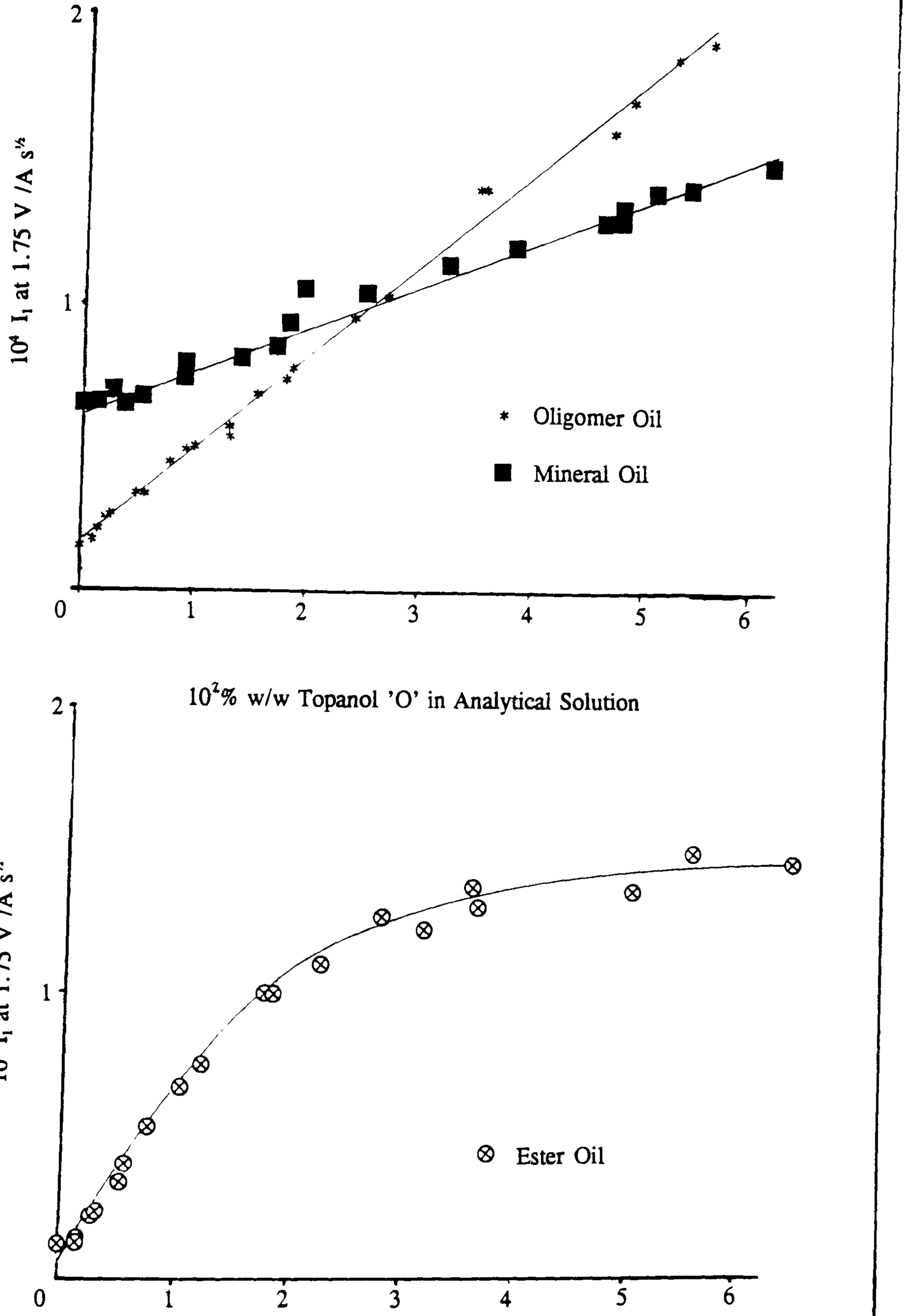

Figure 5.4

Calibration Curves for Topanol 'O'
in the Base Oils by CV

The variation of the scan speed on the I_1 convolution, was examined using scan speeds from 0.1 to 10 V s^{-1}. Little variation in the convolution was found between scan speeds of 0.1 to 0.5 V s^{-1} but above 0.5 V s^{-1} the convolution shape became less well defined with increasing scan speed.

5.3.2 Calibration

The experimental technique employed for the calibration of the electrochemical response to the concentration of Topanol 'O', was the virtually same as that used for DODPA. The exception being that the voltammogram was obtained between +0.1 V and +2.1 V (instead of +0.1 and +1.3 V), and the value of the I_1 convolution of the oxidation sweep was recorded at a potential of +1.75 V.

Data were collected for the construction of a calibration curve over a time period of several months to illustrate the reproducibility of the technique. The relevant calibration curves are illustrated in figure 5.4 and the equations given in table 5.2. The equations show that the lines do not pass through the origin, which means that for oil solutions containing no antioxidant, a signal response is to be expected. The electrochemical oxidation of the three basestocks gave signal responses at +1.75 V very similar to the intercepts given in the equations (table 5.3), validating the use of calibration curves that do not pass through the origin. The calibration curves for Topanol 'O' in the mineral and oligomer oil are of the form

$$Y\ (A\ s^{1/2}) = m \times \text{Antioxidant concentration (\% w/w Topanol 'O')} + c\ (A\ s^{1/2}),$$

where m is the gradient of the curve and c is the intercept with the Y axis. For the analysis of Topanol 'O' in the ester oil the curve was fitted to a third order polynomial of the form

$$Y\ (A\ s^{1/2}) = aX + bX^2 + cX^3 + d\ (A\ s^{1/2})$$

where a, b and c are constants. X is the antioxidant concentration in the analytical solution (% w/w) and d is the intercept with the Y axis. The calibration curves are valid over the concentration ranges shown in figure 5.4. It can be seen that the analysis of the ester oil was complicated by chemical reactions (figure 5.4). When voltammograms of the basestocks were investigated it could be seen that the potential of the oxidation peak of the ester oil coincided with the potential chosen for the

analysis of the inhibitor (table 5.3). When the effect of solvent degradation was combined with that of oil oxidation, a curved calibration plot resulted for the ester oil.

Table 5.2
The Equations of the Calibration Curves for Topanol 'O' Using CV. I_1 Response at 1.75 V vs Ag/AgCl

Base Oil	Gradient	Intercept/ A $s^{½}$
Oligomer	$3.21 (\pm 0.04) \times 10^{-3}$	$1.74 (\pm 0.09) \times 10^{-5}$
Mineral	$1.49 (\pm 0.03) \times 10^{-3}$	$6.1 (\pm 0.1) \times 10^{-5}$
Ester	$a = 6.77 (\pm 0.03) \times 10^{-3}$	$2.33 (\pm 0.02) \times 10^{-6}$
	$b = -1.11 (\pm 0.01) \times 10^{-1}$	
	$c = 6.25 (\pm 0.03) \times 10^{-1}$	

Table 5.3
The Oxidation Potentials and Electrochemical Response at 1.75 V vs Ag/AgCl For the Three Basestocks

Base Oil	Peak Maximum Potential/ V	10^5 I_1 Convolution at 1.75 V/ A $s^{½}$
Oligomer	1.58	1.52
Mineral	2.00	6.54
Ester	1.75	1.23

The analysis of Topanol 'O' in the ester oil was attempted at various other potentials, but on each occasion a curve with a shape similar to that illustrated in figure 5.4 was obtained. Some of the curves obtained at different potentials tended to be more linear than that depicted in figure 5.4, but they possessed a greater degree of uncertainty in the gradient (as illustrated by the standard deviation). Some of the curves obtained were considerably more curved. The analysis of Topanol 'O' in the ester oil at 1.75 V was a compromise between a straighter curve and a greater degree of confidence in the curve.

The difference in the intercept and gradients for the equations of the calibration

curves obtained using mineral and oligomer oils was due to the different oxidation potentials and solvent effects associated with the basestocks themselves.

5.3.3 Kinetic Analysis

The irreproducibility of the I_1 convolution, with respect to its levelling off to a limiting value has meant that a kinetic analysis of the electrode reaction was impossible. The 'plateau' obtained on rare occasions at very slow scan speeds did not level off to a limiting value. It would appear that the antioxidant system continued to oxidise until the reversal potential had been reached and, as the value of the convoluted data continued to rise during the return sweep, it is clear that a kinetic analysis was impossible. A more important factor is that the oxidation of solvent rendered the precise measurement of a reaction rate implausible.

5.4 The Analysis of Oxidised Oil Samples

The procedure used to prepare partially oxidised oil samples was described in chapter 4 (section 4.4). When the oxidised oil samples containing Topanol 'O' were analysed under identical conditions to those used for the calibration experiments, the consumption of the antioxidant was evident. The oxidative stability of the oxidised oil samples depleted immediately. This is in contrast to the system containing DODPA, where the oxidative stability of the oil remained constant before decaying, despite the depletion of the antioxidant. The conclusion that can be drawn from this, is that the oxidation products of the phenolic inhibitor, unlike those of the amine additive, do not confer oxidative stability to the oil blend (figure 5.5).

The electrochemical results show that the antioxidant level decays very rapidly with time to a minimum value. The level to which the antioxidant was reduced was dependent on the basestock. The rate of decay of the Topanol concentration was the slowest for the mineral oil basestock. This may indicate that individual components of the oil degrade by propagation and branching reactions more readily than they react with the antioxidant. The antioxidant level was depleted the most in the ester oil, which is thermally the most stable. This could be due to the antioxidant consuming the peroxy radicals before the radicals can be involved in the branching and propagation reactions associated with oil oxidation.

The results of the thermal analytical investigation of partially oxidized samples

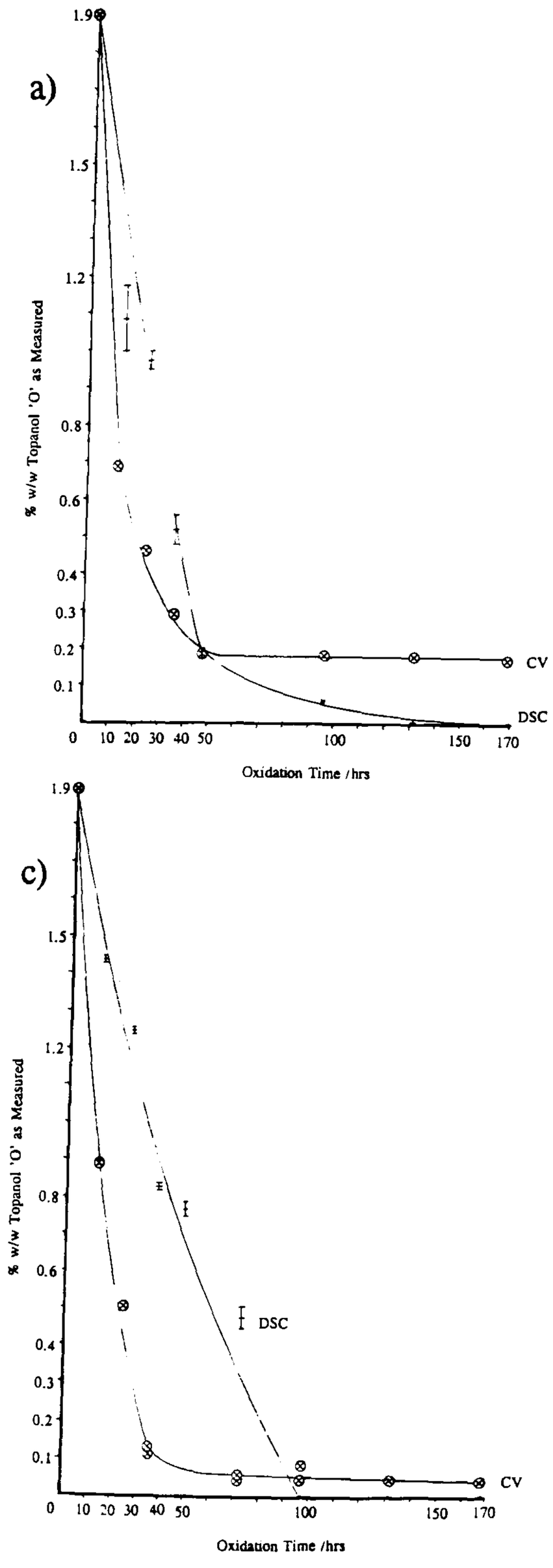

a) RTS-9745 Base Oil

b) BSM-105 Base Oil

c) LPE-504 Base Oil

Figure 5.5

Variation of the Measured Topanol 'O' Concentration With Oxidation Time

show that the oxidative stability of the synthetic and mineral oils decay at a similar rate while the ester oil has a superior resistance towards oxidation. It was noted that oxidative stability of the synthetic and ester oil mixtures were depleted to below that of the fresh base oils. The mineral oil blends retained some resistance towards oxidation. The retention of oxidative stability for the mineral oil blends may be due to the natural inhibitors present in the oil, volatilisation of the light fractions of the oil or polymerization of the degradation products to confer a certain degree of oxidative stability.

When partially oxidised oil samples were re-inhibited and analysed electrochemically the measured concentration of inhibitor increased by a larger increment than that added (figure 5.6). This is in agreement with the finding of Massey and Wilson [19], who reported that the addition of extra antioxidant to an oxidised sample reactivated some of the previously exhausted inhibitor. This seems an unlikely explanation. The reason is also unlikely to be the experimental error of the measurements, because the results are systematic and the precision of the technique is high (the uncertainty is approximately $\pm$ 3% of the value obtained). Another explanation, possibly more plausible, for the discrepancy is that the Topanol reacted with a residue of the consumed antioxidant to form another compound that contained a phenolic grouping. Some support for this may be obtained from the results of the DSC investigation. When the samples were measured using the thermal analytical technique, it was noted that the oxidative stability of the samples were initially reduced before increasing (figure 5.6). The initial reduction of the overall oxidative stability of the blend could be due to the oxidative stability of the antioxidant being lower than that of the oil. It was suggested that in an oil blend, an increase in aromatic hydrocarbon content increased the rate of initiation [37]. If this is the explanation for the decrease in oxidative stability, then the antioxidant behaviour of the Topanol is a balance between this antagonistic effect and the propagation suppressing nature of the molecule. An explanation that is somewhat more likely (it also supports the electrochemical results), is that the Topanol 'O' reacted with a residue of the oxidation process to form a compound with pro-oxidative characteristics. When the consumption of this 'residue' was complete, the oxidative stability of the blend increased.

5.5 The Analysis of Oil Samples Containing an Antioxidant Blend

A sample of the oligomer basestock was inhibited with equal quantities of Topanol 'O' and Topanol 'A', to give a total antioxidant concentration of approximately 1%

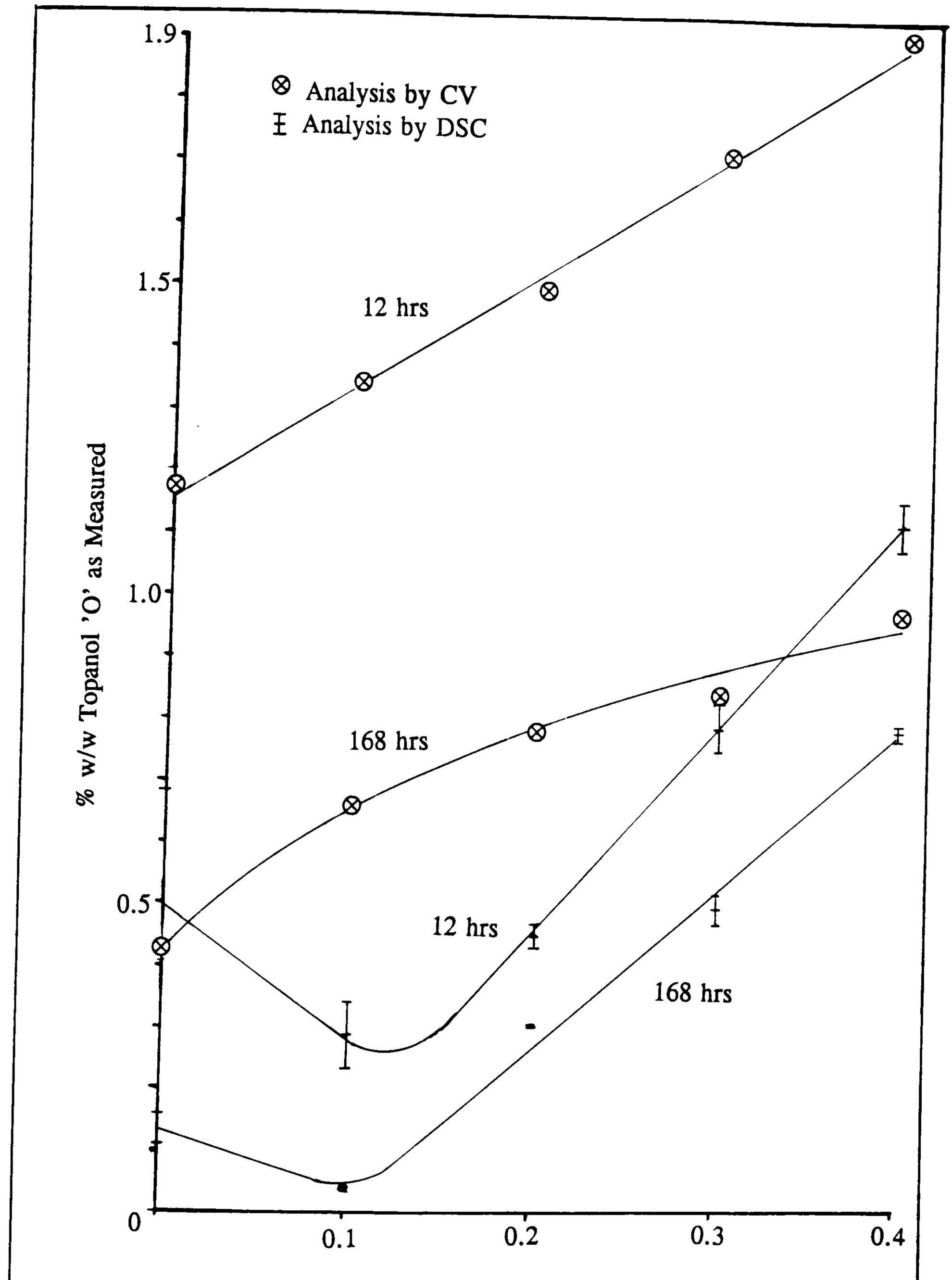

Figure 5.6

The Variation of the Measured Antioxidant Concentration
For Oxidised and Re-inhibited Mineral Blends

w/w. When the sample was analysed using HPDSC it was found to have an oxidative stability equivalent to that of an oil containing 0.17% w/w Topanol 'O'. The Topanol 'A' had a very marked detrimental effect on the oxidative stability of the oil, which could be due to its high vapour pressure. The calibration curve of Topanol 'A' in the oligomer base oil was not calculated so the effect of Topanol 'O' on the performance of Topanol 'A' could not be determined. The poor antioxidant efficiency of Topanol 'A' has already been discussed [19,20,26], Warne and Vienna [20] relating the performance to the high volatility of the antioxidant. The blending of two inhibitors has been noted to impair the efficiency of the more effective additive [19,20]. It has been noted (in a manner similar to that recorded here) that the presence of a second antioxidant can reduce the oxidative stability of the oil to below that of a blend containing just one antioxidant [20]. The electrochemical technique could not be used to distinguish between the two antioxidants, because both inhibitors were oxidised by the loss of one electron from the phenolic group, but from the analysis the concentration of Topanol 'O' in the oil was estimated to be 1.09% w/w. The quantitative result is based on the assumption that the Topanols have the same diffusion coefficient. Topanol 'A' is a slightly less bulky molecule and therefore will have a greater diffusion coefficient than Topanol 'O', which may account for the high value obtained.

To determine whether there would be any synergism between the phenolic and the amine antioxidant several samples containing both antioxidants were prepared in the mineral oil. Each sample was formulated to contain approximately 1% w/w total antioxidant. When the samples were compared to the oxidative stability of an oil containing only Topanol 'O' a small addition of DODPA had a dramatic effect on the oxidative stability of the oil, increasing it to a value over and above that of the fully formulated oil. If however, the same oil formulation was compared to one containing DODPA only, then the addition of Topanol 'O' drastically reduced the oxidative stability of the oil. The loss of oxidative stability of the oil was merely due to the dilution of the more effective amine antioxidant with the hindered phenol, and not due to any antagonistic effects. The greater antioxidant efficiency of the amine, over that of the phenol, has been discussed earlier, and is supported in the experimental results obtained in this thesis. When the concentration of 'DODPA as measured' using isothermal HPDSC for the mixed inhibitor oil blend was plotted against the actual concentration of DODPA in the oil (or the concentration of Topanol 'O'), a straight line graph was obtained (figure 5.7). The data point correlating to 0% DODPA and 1%

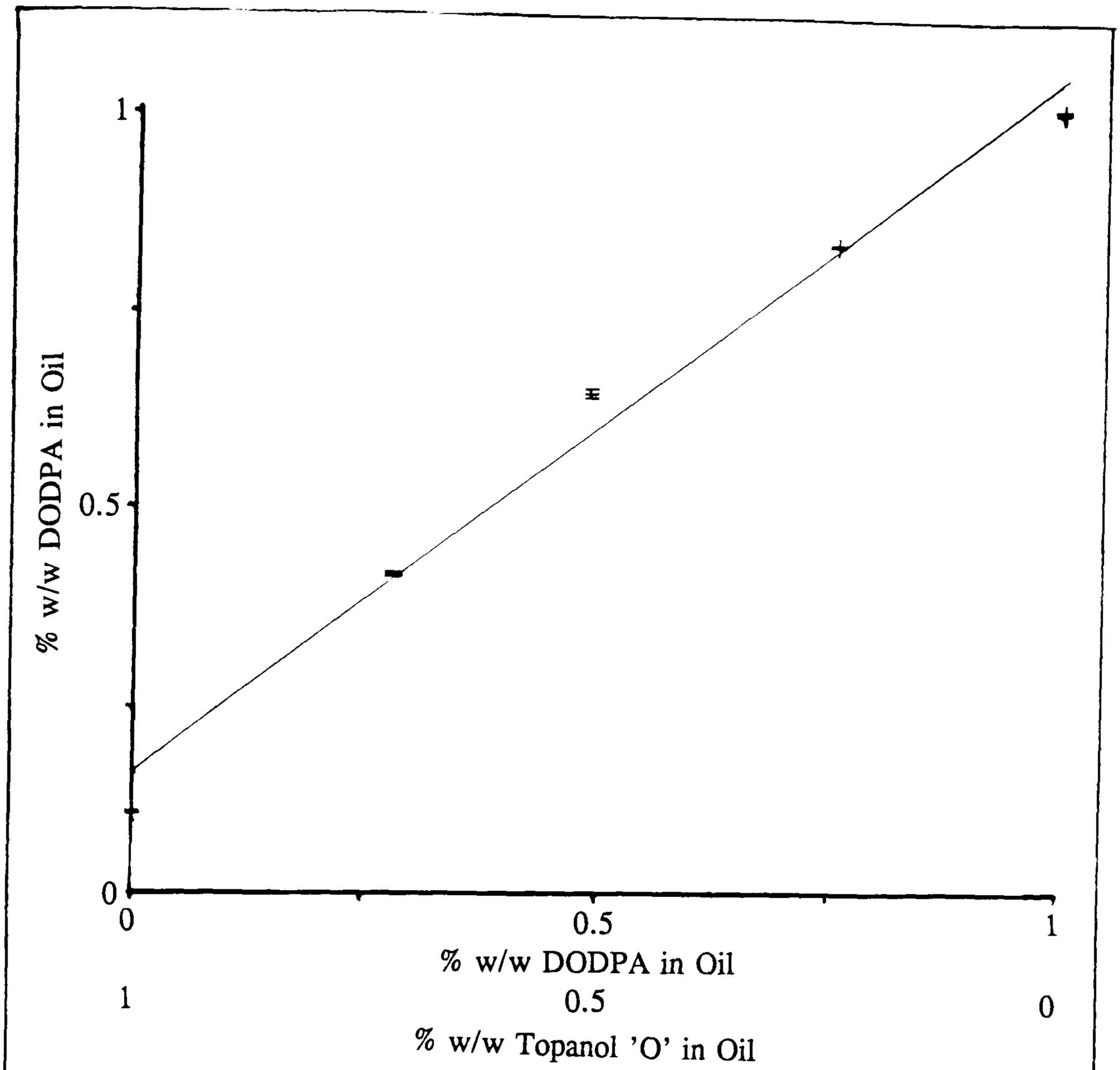

Figure 5.7

The Study of the Efficiency of Mixed Inhibitor Blends by DSC.
A Comparison of the Oxidative Stability of Mineral Oil Blends Containing Topanol 'O' and DODPA to one Containing Exclusively DODPA

Topanol 'O' was estimated using the Arrhenius relationship employed to obtain kinetic data for the formulated oil by HPDSC and the induction time for the oil at a lower temperature.

Antagonism between amine and phenolic inhibitors can be due to the antioxidants reacting with each other. The reaction of the acidic phenol and the basic amine may produce a complex that is ineffective with regards to peroxide trapping. Furthermore the radicals derived from the two inhibitors may undergo a rapid cross termination reaction [38,39]

When one of the mixed oil samples was analysed electrochemically, the deconvoluted data indicated that two separate electrochemical events were occurring, with little or no overlap between the two. The convoluted data, when examined, showed signs of a plateau corresponding to the amine antioxidant, followed by an increase in response due to the phenolic antioxidant. The concentration of the Topanol and the DODPA were measured at 0.92 and 0.22% w/w respectively, when they were actually 0.72 and 0.27% w/w. It is obviously possible to distinguish between the two groups of antioxidant and to calculate their respective concentrations, although for this to be done a new series of calibration curves is required.

References

1. L. R. Mahoney, S. Korcek, S. Hoffman and P. A. Willermet, *Ind. Eng. Chem. Prod. Res. Dev.*, 17, 1978, p 250.
2. S. Korcek, L. R. Mahoney, M. D. Johnson and S. Hoffman, *SAE Technical Paper No. 780966,* 1978.
3. H. C. Bailey, *Ind. Chem.*, May 1962, p 215.
4. O. M. Reiff, *Ind. Eng. Chem.*, 33, 1941, p 351.
5. R. H. Rosenwald, J. R. Hoatson and J. A. Chenicek, *Ind. Eng. Chem.*, 42, 1950, p 162.
6. E. M. Bickoff, *J. Am. Oil Chem. Soc.*, Feb 1951, p 65.
7. J. L. Bolland and P. ten Have, *Disc. Faraday Soc.*, 2, 1947, p 252.
8. A. F. Bickel and C. E. Kooyman, *J, Chem. Soc.*, 2, 1956, p 215.
9. G. R. Yohe, J. E. Dunbar, M. W. Lansford, R. L. Pedrotti, F. M. Scheidt, F. G. H. Lee and E. C. Smith, *J. Org. Chem.*, 24, 1959, p 1251.
10. C. D. Cook, N. G. Nash and H. R. Flanagan, *J. Am. Chem. Soc.*, 77, 1955 p 1783.
11. C. D. Cook and C. B. DePatie, *J. Org Chem.*, 24, 1959, p 1144.
12. J. E. Bennett, *Nature,* 186, April 30, 1960, p 385.
13. C. D. Cook and B. E. Norcross, *J. Am. Chem. Soc.*, 81, 1959, p 1176.
14. G. S. Hammond, C. E. Boozer and J. N. Sen, *J. Am. Chem. Soc.*, 77, 1955, p 238.
15. K. U. Ingold, *J. Phys. Chem.*, 64, 1960, p 1636.
16. A. C. Nixon, H. B. Minor and G. M. Calhoun, *Ind. Eng. Chem.*, 48, 1956, p 1874.
17. E. L. Walters. H. B. Minor and D. L. Yabroff, *Ind. Eng. Chem.*, 41, 1949, p 1723.
18. K. Ivanov and Ye. D. Vilyanskaya, In N. M. Emanuel, "The Oxidation Of Hydrocarbons In The Liquid Phase", Translated by K. R. Dobson and B. J. Hazzard, Pergamon Press, London, 1965.
19. L. Massey and A. C. M. Wilson, *J. I. P.*, 44, 1958, p 336.
20. T. M. Warne and P. C. Vienna, *Lubr. Eng.*, 40, 1984, p 211.
21. R. Amos, *J. I. P.*, 54, 1968, p 9.
22. J. R. Barcelo and C. Otero, *J. I. P.*, 50, 1964, p 15.
23. D. Al Sammerai and Z. S. Salih, *Thermochim. Acta,* 108, 1986, p 91.
24. M. Palzuski and K. Kardasz, *J. Therm. Anal.*, 32, 1987, p 1805.

25. F. Noel, *J. I. P.*, 57, 1971, p 357.

26. A. Tong, "Determination Of The Oxidation Stability Of several Antioxidant/ Base Oil Mixtures By Pressure DSC", Technical Report, DQA/TS, Harefield.

27. M. M. Barbooti and D. A. Al-Sammerai, *Thermochim. Acta,* 76, 1984, p 221.

28. M. D. Ryan, A. Yueh and W. Y. Chen, *J. Electrochem. Soc.*, 127, 1980, p 1489.

29. C. L. Papouchado, G. Petrie and R. N. Adams, *Electroanal. Chem. and Interfac. Electrochem.*, 38, 1972, p 389.

30. A. J. Bard and L. R. Faulkner, "Electrochemical Methods, Fundamentals and Applications", John Wiley and Sons, New York, 1980.

31. C. L. Franzke, F. Kretschmann and K. Beining, *Fette Seifen Anstrichmittel,* 70, 1968, p 472.

32. T. Tonmanee and V. S. Archer, *Talanta,* 29, 1989, p 905.

33. H. D. McBride and D. H. Evans, *Anal. Chem.*, 45, 1973, p 446.

34. R. E. Kaufmann, U. S. Patent, Patent No. 4,744, 870, May 17, 1988.

35. H. M. J. Ploegmakers and W. J. Van Oort, *J. Autom. Chem.*, 10, 1988, p 135.

36. C. R. C. Handbook Series in Organo Electrochem., Vol l-V, Ed. L. Meites and P. Zonan, Date Unknown.

37. A. J. Burn and G. Greig, *J. I. P.*, 58, 1972, p 346.

38. L. Reich and S. S. Stivala, "Autoxidation of Hydrocarbons and Polyolefins. Kinetics and Mechanisms" Marcel Dekker inc., New York, 1969.

39. K. U. Ingold and J. E. Puddington, *Ind. Eng. Chem.*, 51, 1959, p 1319.

Chapter 6

An Overall Assessment

The work in this thesis allows for the first time a comparison between the results from the two analytical techniques (DSC and CV). A comparison between the three base oils and between the two antioxidants will be made, in addition to highlighting the contrast between CV and DSC. The modelling of experimental DSC and CV curves will also be discussed. Future work relating to the further understanding of antioxidant behaviour in lubricating oils will be discussed in the final section of this chapter.

6.1 A Comparison Between DSC and CV

The most striking difference between the two experimental techniques is that cyclic voltammetry is used to measure the concentration of the antioxidant in the oil whereas DSC is used to determine the total oxidative resistance of the oil. From a thermal analytical measurement an estimate of the antioxidant concentration in an oil blend can be made only from the total oxidative resistance. The estimation of the antioxidant concentration in a used oil by DSC may introduce errors, because the oxidative stability of an oxidised oil will be different from that of a fresh sample. When the information obtained from CV and DSC is combined a more in-depth knowledge of the oil blend is available.

Each technique has advantages and disadvantages. DSC is a flexible technique which allows the different physical and chemical properties of a sample to be measured. For example, from one thermal analysis curve, the glass transition and the wax appearance temperatures (along with the wax content) of an oil sample can be measured, together with the pour point, cloud point and sample volatility [1]. These measurements are usually made under an atmosphere of nitrogen. Using an oxygen or air atmosphere, the oxidative stability of an oil sample can be ascertained. The duration of an isothermal DSC experiment may exceed half an hour. To perform a DSC analysis, expensive equipment is required, while an electrochemical technique, in its simplest form needs very little apparatus. The standard of software and associated apparatus used for the CV measurements described in this thesis caused the cost of the equipment to increase dramatically, although it is considerably cheaper than thermal analytical equipment. However the electrochemical technique requires a larger sample and more extensive sample preparation than the calorimetric technique.

Both techniques are used for quality assurance. The thermal analytical technique is used primarily as a screening test for an oil formulation before full engine testing, as well as a route to monitoring antioxidative behaviour. DSC experiments may be used

to simulate the thermal environment of an engine because the thin films of oil are saturated with oxygen. The electrochemical method can be used to determine whether the oil has had the correct inhibitor package added or whether any additives remain in an oil formulation that is already in service. It has been shown that DSC cannot be used to discriminate between different antioxidants. Cyclic voltammetry can be employed for the quantitative determinations of two antioxidants in the same sample. The use of DSC or CV individually could not be used to distinguish between Topanol 'O' and Topanol 'A'. Both methods gave an indication that an antioxidant had been added to an oil when the two component system was analysed. The Topanol 'A' had a deleterious effect on the antioxidant performance of Topanol 'O', so thermal analysis indicated that the blend possessed a low oxidative stability (suggesting that very little additive was present). The electrochemical technique indicated that the oil contained 1.1% antioxidant, four times the quantity estimated from the analysis by DSC. Combining the results of the two techniques may enable the analysis of the mixed phenolic antioxidant system to be possible.

'Kinetic' data can be obtained using isothermal and dynamic DSC techniques. The 'kinetic' measurements obtained from DSC give an indication of the global 'activation energy' associated with the oxidation processes of an oil. The isothermal technique is used to measure the induction time before the onset of rapid oil oxidation. It has been assumed that the overall activation energy measured is related to the initiation of oil oxidation (by hydrocarbon cleavage and peroxide decomposition) and the consumption of the antioxidant [2-5]. The dynamic technique for obtaining 'kinetic' data measures the difference in peak maximum temperature as a function of the heating rate. The activation energy measured is a global activation energy of the oil degradation processes. In general, the overall order of a reaction can be determined from 'kinetic' data using DSC measurements. The kinetic methods employed in this thesis provide an empirical relationship between the reaction rate and the temperature or heating rate. From these relationships the activation energies associated with the oil oxidation processes may be estimated.

The kinetic data from the electrochemical technique give an indication of the facility of the electron transfer processes and the chemical reactions associated with the electrode reaction. The kinetic parameters associated with the degradation of the electrochemically oxidised species may also be extracted from electrochemical data. The decomposition of the electrochemically oxidised species is assumed to be first (or

pseudo first) order. The kinetic data obtained from DSC experiments are more realistic, with regard to an indication of the oxidation stability of an oil blend, despite the reservations mentioned in this thesis (sections 4.2.3 and 5.2.3).

DSC is an experimental technique where the results obtained rely on the calibration of the apparatus because the mathematical theory of the apparatus is too complex. The mathematical theory is related to the equipment design and the heat fluxes within the cell. The electrochemical technique does not need calibration with standards in this manner. The electrochemical technique is well founded in mathematical description, as shown in chapter 3 (and appendix 1). Mathematical relationships are used to relate the signal response to the concentration and diffusion coefficient of the electro-active species in solution. The cyclic voltammogram can be modelled very precisely using the program Condesim (developed by Dr N. Taylor in the School of Chemistry at Leeds), from which the rate of the electrode reaction is obtained, which is a route to the activation energy of the electron transfer process.

6.2 A Comparison Between the Base Oils

The physical properties of the base oils were given in chapter 1. The volatility of the oils in an atmosphere of nitrogen have been compared using the Stanton Redcroft STA-781, described in appendix 3. Two experimental techniques were employed, first a scanning method in which a 15 mg sample was heated at a rate of 10°C min^{-1}. The volatility of the oils was determined from the extrapolated onset and the peak temperature of the DTA curve. An alternative route to determining the volatility of a sample was to measure the extrapolated onset and finish temperatures of the TG curve (table 6.1).

Table 6.1

The Volatility of the Base Oils by the Dynamic DTA-TG Method

Base Oil	TG Onset /°C	TG Finish /°C	DTA Onset /°C	DTA Peak /°C
Oligomer	260	333	237	306
Mineral	258	316	217	303
Ester	302	365	271	341

The second method was an isothermal technique in which 10 mg of oil was heated to a fixed temperature (200°C) at a rate of 10°C min^{-1}. The volatility of the sample over

a 30 minute isothermal period was compared to that of a squalane standard (table 6.2).

Table 6.2
The Volatility of the Base Oils by the Isothermal TG Method

Base Oil	Mass Loss /mg	Relative Volatility
Squalane (standard)	1.28	1.00
Oligomer	1.76	1.38
Mineral	1.84	1.44
Ester	0.24	0.19

Both techniques illustrate that the ester oil has a volatility considerably lower than that of the oligomer and mineral oils, with the mineral oil being the most volatile. The average molecular weight of the ester oil is 564 and that of the oligomer oil is 423. The high volatility of the mineral oil may be due to the presence of low molecular weight fractions. This may account for the relative volatility of the samples (squalane has a molecular weight of 425).

The oxidation stabilities of the base oils were also measured using the STA-781. The experimental conditions used were identical to those employed for the dynamic volatility measurements, apart from the use of an atmosphere of oxygen instead of nitrogen. The oil samples all showed a small mass loss before the onset of the DTA curve. The oxidation stabilities, given in table 6.3, were found to be ester > mineral > oligomer. The difference in the ranking of the oil volatility and oxidation stability could be due to the highly branched nature of the oligomer oil. Hydrogen atoms attached to a tertiary carbon atom are preferentially abstracted from the molecule in initiation and propagation reactions. The mineral oil contains approximately 5% aromatic hydrocarbons and 0.15% sulphur, which as explained in chapter 1 can lead to an enhanced stability of the oil blend [6,7]. It may be assumed that the aromatic hydrocarbons exhibit some degree of antioxidant character which is enhanced by the presence of sulphur compounds. The study of oxidative stabilities by the isothermal method required the use of an elevated pressure. The isothermal analysis performed using the Du-Pont DSC-990, ranked the oils in the same order as the dynamic method performed on the Stanton Redcroft STA-781. There is no reason to believe that the use of different equipment for the analysis of oil samples would give different rankings, although the precise values (of the volatility or oxidative stability) may change.

Table 6.3
The Oxidative Stability of the Base Oils Using the STA-781

Base Oil	TG Onset /°C	TG Finish /°C	DTA Onset /°C	DTA Peak /°C
Oligomer	229	279	216	263
Mineral	244	303	pre-peak 192	pre-peak 214
			peak 238	peak 308
Ester	269	316	249	312

The analysis of the oil samples using high pressure DSC highlighted further differences in the base oils. The thermal analysis curves of mineral oil samples showed pre-peaks and shoulders which were absent with the oligomer and ester oil samples. This may indicate the presence of fractions with different oxidation stabilities. Tong [8] also found that the analysis of mineral oil samples was complicated by erratic peak shapes. A further difference between the oils is the different responses of the base oils to the two antioxidants. The increase in oxidation stability of oil blends containing the amine antioxidant was the greatest for the ester oil and least for the oligomer oil. The oil blends containing the Topanol 'O' behaved in the opposite manner. The greatest increase in oxidation stability occurred with the oligomer oil and the least for the ester oil. The reversal of the response of the base oils to the phenolic antioxidant (compared to DODPA) may be due to the temperatures used for the analysis'. The ester oil was analysed at a higher temperature than the oligomer oil.

A further difference between the base oils may be observed when the respective 'activation energies' associated with the initiation of oil oxidation are compared. Table 6.4 contains data obtained from the isothermal DSC technique. The activation energy obtained for the mineral oil is of a magnitude expected for the reaction rate governed by peroxide decomposition. The activation energies obtained for the ester and oligomer oils are lower than expected for either initiation by hydrocarbon oxidation or peroxide decomposition and may even relate to a square root dependence on the rate constant of either of these types of sets. The square root dependence on the rate constant assumes a steady state theory, where the rate of chain initiation equals the rate of termination. The termination of the chain may occur by the combination of peroxy radicals, a second order process. The initiation of the chain to produce the peroxy radicals is then considered to be a half order process, hence the observed activation energy being half the expected value. The oxidation potential of the three base oils

(table 6.4) using the current-potential data of a cyclic voltammogram may reflect the ease of the initiation reactions. The relationship between the oxidation potentials and the activation energies obtained by DSC may be fortuitous. Further base oils will need to be studied to ascertain whether any correlation exists.

Table 6.4
A Comparison of the Base Oils

Base Oil	Activation Energy /kJ mol^{-1}	Oxidation Potential /V
Oligomer	70 ± 10	1.58
Mineral	171 ± 12	2.00
Ester	103 ± 11	1.75

6.3 A Comparison of the Antioxidants

As mentioned earlier in this thesis, DODPA is believed to capture four hydroperoxide radicals per antioxidant molecule whilst Topanol 'O' is thought to capture two. From this statement alone it might be inferred that Topanol 'O' would be less effective than DODPA at inhibiting the free radical oxidation of lubricating oils. Massey and Wilson [9] supported the theory that amine antioxidants are superior to the phenolic compounds. Warne and Vienna [10] compared the antioxidant characteristics of various phenolic hydrocarbons concluded that Topanol 'O' is the most effective phenolic inhibitor. It can be seen from the calibration curves illustrated in chapters 4 and 5 that the amine antioxidant is the more effective additive. This difference is even more marked when the antioxidants are compared on a molar basis, i.e. in mol kg^{-1} of oil rather than mass percent (figure 6.1). Instead of the induction time of the blend being recorded, the percentage increase of induction time above that of the base oil may also be used to illustrate the superiority of the amine inhibitor (figure 6.2). For the DSC investigations the amine antioxidant was analysed at higher temperatures than the phenol, yet the amine still provided superior induction times for comparable concentrations. Ford [11] stated that phenolic antioxidants are usually only employed in situations where the temperature will not exceed 180°C whilst amine antioxidants can be used at temperatures in excess of 200°C. The results of the DSC experiments are supported by Tong [8] who concluded that DODPA is a more effective antioxidant than Topanol 'O', which in turn is superior to Topanol 'A'.

When oil samples were partially oxidised, the analysis of the blends containing the

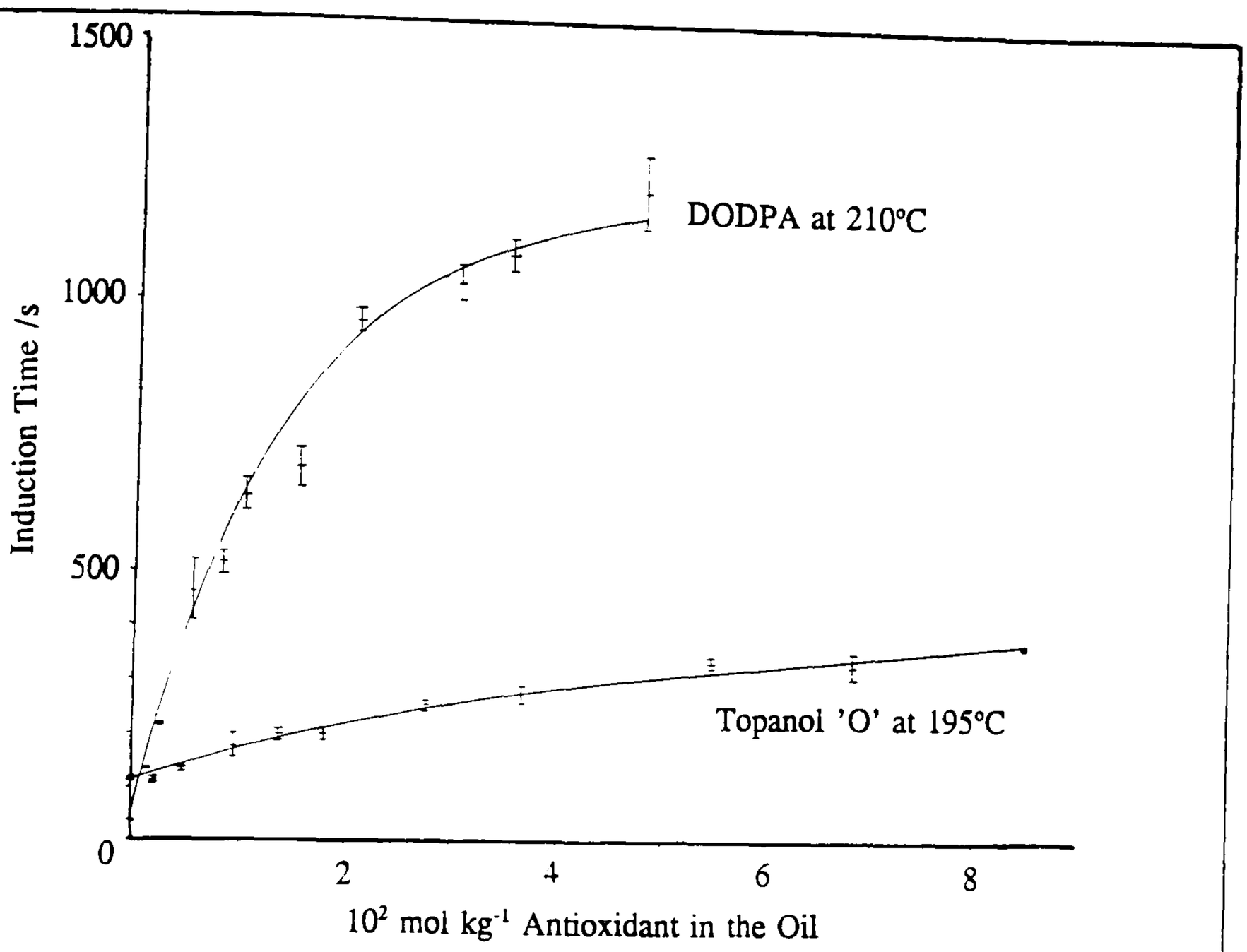

Figure 6.1

A Comparison Between the Calibration Curves of DODPA and Topanol 'O' in the Mineral Oil

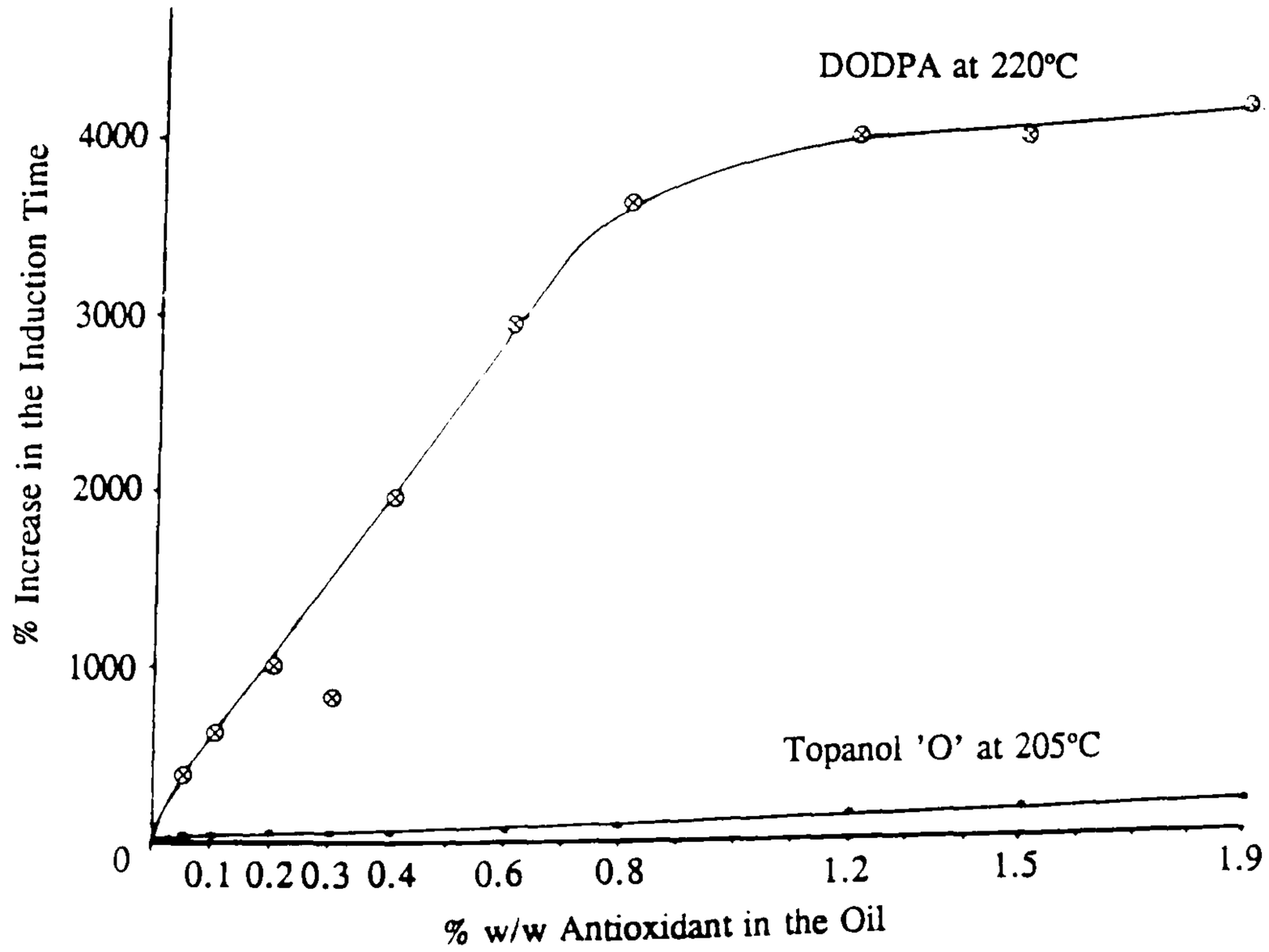

Figure 6.2

A Comparison of the Response of the Ester Oil to DODPA and Topanol 'O'

phenolic antioxidant showed an instant decrease in oxidative stability that virtually parallelled the decrease in antioxidant concentration. Blends containing the amine initially displayed a retention of the oxidative stability of the fresh oil before the stability decreased. This suggests that the oxidation products of the amine antioxidant (unlike those of the Topanol) possess antioxidant properties. This may be due to the polymerisation of the oxidised products of DODPA. The delay before the reduction in oxidative stability varied with the blends. It was the shortest for the ester oil and longest for the oligomer oil, which may be a reflection of the temperature of analysis used for each blend and not of the individual base oils. The shape of the isothermal DSC curves may also indicate that the oxidation products of the amine antioxidant possess antioxidant properties. The shape of the DSC curves for the oil mixtures containing different quantities of Topanol 'O' were essentially the same. The peak height and width of the curves were no different for the basestock and the fully formulated oil. The shape of the DSC curves containing DODPA changed with inhibitor concentration. As the DODPA concentration increased the peak height reduced and the peak width became larger. The change in peak shape suggests that an oil blend oxidises more slowly than the base oil.

The 'activation energy' associated with the initiation of oil oxidation may enable a comparison between the antioxidants to be made. The data given in table 6.5 show the 'activation energies' obtained from isothermal DSC analyses. For mixtures in two base oils the activation energy required for the initiation of oil oxidation is greater in the presence of DODPA than Topanol 'O'. This may imply that DODPA is the more effective antioxidant, but the pre-exponential factors associated with the initiation processes are not given. The oxidation potentials of the antioxidants obtained by cyclic voltammetry may illustrate their relative efficiencies. The implication is that the more easily oxidised antioxidant will be more effective at inhibiting oil degradation. The potential of the maximum of the current-potential peak is given in table 6.5.

Table 6.5
A Comparison of the Antioxidants

	Oxidation	E_a /kJ mol^{-1}		
Antioxidant	Potential /V	Oligomer Oil	Mineral Oil	Ester Oil
DODPA	0.91	134 ± 10	131 ± 11	108 ± 16
Topanol 'O'	1.75	103 ± 11	116 ± 5	147 ± 7

6.4 The Modelling of the Analytical Curves

In this section the varying success obtained with modelling DSC and CV curves will be described. The modelling of electrochemical data has proved to be very successful using the "Condesim" program developed by Mr. R. Luo and Dr. N. Taylor at the University of Leeds. Experimental peak shapes can be modelled very closely. From the model a value of the rate constant of the electrode reaction can be obtained. The shape of the DSC curves have been modelled less successfully. It was not possible to ascribe any kinetic parameters to a specific reaction for a real oil sample from the model. The model was unable to make allowances for the response time, heat capacities or thermal resistances of the apparatus.

6.4.1 Cyclic Voltammetry

The modelling of an electrochemical reaction involves the solution of the mass transfer problem to allow concentration profiles to be converted into current-potential-time data. The calculated current-potential history is then compared with experimental results. The numerical solution of the diffusional problems involves the solution of Fick's law of diffusion for a three dimensional process which is a very complicated analysis. The mathematical problems under investigation are simplified to enable treatment by a relatively simple model. For a planar electrode with a large surface area in an unstirred solution, the diffusional processes can be assumed to be only in the direction perpendicular to the electrode surface. The diffusional problem to be solved is therefore greatly simplified. Even so the diffusional processes can be complicated by convection and migration effects, the electrode geometry or heterogeneous chemical kinetics. The solution of the diffusional problem can be performed using Laplace transforms, the conversion of the boundary problems into integral equations or direct numerical solution using finite difference techniques [12]. The third method has the advantage over the others in that the concentrations of the species at different positions in the solution at any given time can be followed by the construction of a three dimensional graph. The mathematical problems associated with the digital simulation of electrochemical systems has been described in detail by Luo [12] who, as already mentioned, developed the 'Condesim' software package with Dr. N. Taylor.

For the simulation of a current-potential-time curve, the experimental parameters are inserted into the program. These parameters are the sweep rate, starting and reversal potentials, the temperature, electrode area and the concentration of the electroactive species in the bulk solution. The sample variables inserted into the

program are the half-wave potential, the diffusion coefficient of the electroactive species, the number of electrons transferred in the electrode reaction, the rate constant of the associated chemical reaction (if there is one). The value of k_o is an unknown quantity and has to be estimated, therefore its value can be obtained by the use of the 'Condesim' simulation program. Insertion of the correct value of k_o (and other parameters) permits the experimental curve to be modelled very closely (figure 6.3). The process for evaluating k_o is as follows. The separation between the oxidation and reduction peaks of an experimental curve are measured at different sweep rates. Different values of k_o are then inserted into the simulation program until the separation of the peaks for the simulated data matches that obtained experimentally. This process is repeated for simulations performed using different sweep rates and temperatures. The calculation of k_o in this manner enables the activation energy for the electron transfer process to be obtained (see section 4.3.3).

6.4.2 Differential Scanning Calorimetry

The use of a kinetic model in DSC is designed to interpret the thermal analysis curve in terms of simple reaction kinetics. Such a process is fraught with difficulty but it is possible to account for changes in the curve shape. It would be optimistic to expect a great deal of success in modelling curve shapes precisely because the theoretical basis for DSC is extremely complicated. The first attempt at such a model was made by Brown et al. [2]. The authors used the following reaction mechanism to represent base oils with and without the presence of an antioxidant.

$$A \rightarrow B \qquad 1$$

$$A + B \rightarrow B + C \qquad 2$$

$$B + B \rightarrow D \qquad 3$$

$$B + E \rightarrow F \qquad 4$$

where A represents the parent hydrocarbon, B a free radical and E an inhibitor. C, D and F are reaction products. Step 4 was used to represent the natural resistance of the oil towards oxidation, as well as the addition of a commercial antioxidant. In the absence of this step, no induction time (corresponding to oxidative resistance) was recorded before the simulated isothermal DSC peaks. The presence of the inhibition step (4) had to be included to represent the natural resistance of the oil towards oxidation.

Our approach is very similar to that used by Brown et al [2]. An attempt was made to interpret the shape and induction time of isothermal DSC curves using a kinetics

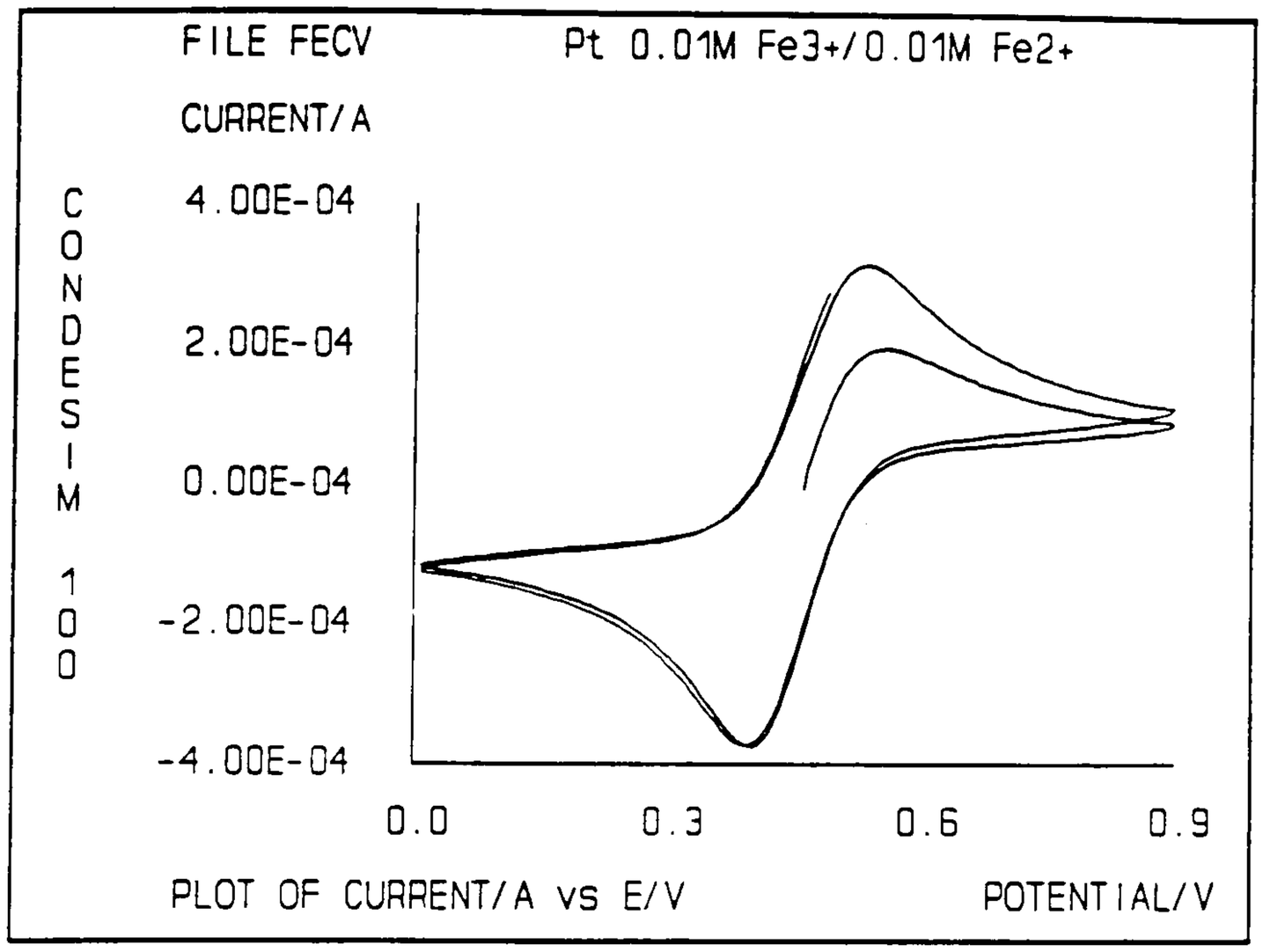

Cyclic voltammogram for the Fe^{3+}/Fe^{2+} couple on a platinum electrode in 1M $HClO_4$ solution.

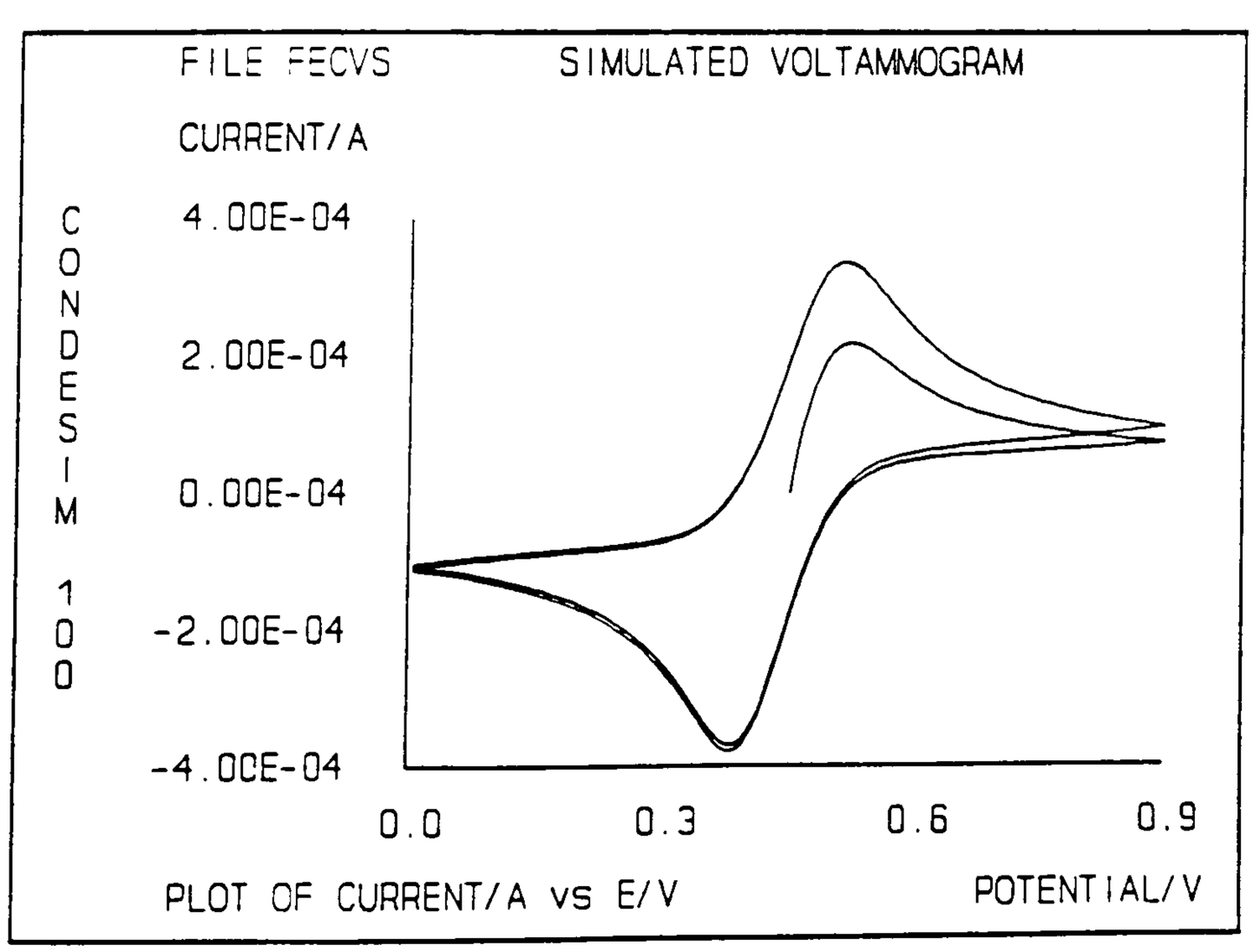

Simulated cyclic voltammogram using experimental determined parameters for the Fe^{3+}/Fe^{2+} couple.

Figure 6.3

A Comparison Between an Experimental and Simulated Cyclic Voltammogram [12]

simulation computer program developed at Leeds University by Ayscough and Mansfield [13]. The program calculated the concentration of each individual species from the reaction rates and reactant concentrations inserted into it. The program plotted the concentration of selected species using Gear's method of stepwise integration [14]. The program was written in BBC basic and enabled calculations to be performed for a maximum of 12 reactions containing 8 different species.

The program written by Ayscough and Mansfield was modified to open a file to store the time and species concentration data. The program was investigated to determine whether the output data was smoothed with no anomalies. When it had been established that the data was smoothed, a program was written to calculate the time derivatives of the concentration data. The program simply calculated d[conc]/dt and tabulated the results to enable a hard copy to be printed if required. Another program was written to read the output data from the time derivative program and plot the data. It was these plots that were used as simulated isothermal DSC peaks. The heat release that is the cause of the DSC peaks was assumed to originate from the propagation reaction only, enabling the plot of the rate of formation C to represent the DSC curve. The simulated peaks were compared to those obtained experimentally within the laboratory. It was intended that the reaction scheme tested should be as simple as possible to reduce the computer run time of each simulation. The BBC microcomputer was not a particularly fast machine which meant the simulation run times could easily exceed 30 minutes. It was our desire to observe the effect of the individual reaction rates (propagation, branching etc) on the peak shape.

Using the same kinetic parameters as employed by Brown et al. [2], our calculations obtained from the reaction simulation program were in agreement with those reported. The authors commented that the kinetic parameters needed to reproduce the experimental curves were unacceptable from a physical standpoint. Our concern was to modify the reaction scheme and the values of the kinetic parameters in order to reproduce the experimental induction times for the base oil and a formulated oil. It was considered important to employ realistic kinetic parameters for the calculation of the individual rate constants.

We also confirm that in the absence of an inhibition step we do not obtain an induction period for a base oil when realistic kinetic parameters are employed. The rate constants for each reaction step were altered to investigate the possibility of obtaining

an induction period, but with no success. The initiation step was changed from A → B to A → 2B to represent the formation of a peroxide radical in addition to the alkyl radical. The alteration of the initiation step had little effect on the overall reaction scheme apart from accelerating the rate of hydrocarbon consumption to form products. The initiation step was then restored to the original A → B representation because it was the simpler of the two processes.

At all temperatures investigated, the simulated peak widths were considerably narrower than those obtained experimentally. A tenfold increase in the inhibitor concentration afforded a tenfold increase in the simulated induction period, whereas only a fivefold increase was obtained experimentally. An increase in the rate constant of the termination step had the same effect on the induction time and peak shape as increasing the simulated inhibitor concentration. This led to the increase in the induction period obtained, with a widening of the peak width and a decrease in the overall maximum rate of reaction. This phenomena was supported experimentally during the course of the research when the DSC peak shapes were observed at different antioxidant concentrations. The increase in induction period and the associated changes in peak shape could be accounted for by the free radical concentration being lowered within the reaction scheme. A decrease in free radical concentration subsequently reduced the rate of hydrocarbon consumption in step 2, which was taken to be the cause of the DSC peak. A reduction in the rate of the initiation step was found to have the same effect as increasing the rate of the termination step, because it also led to a reduction in the concentration of the free radical species. An increase in the rate of the propagation reaction reduced the induction period dramatically and consequently the thermal analysis peaks became sharper, because the rate of consumption of the hydrocarbon to form product C was increased.

The values of the rate constants at different temperatures were inserted into the program to enable a plot of the natural logarithm of the induction time verses the reciprocal of the temperature to be performed. This was to enable an estimate of the temperature dependence of the system to be made. The temperature dependence may be represented by the term 'activation energy'. The 'activation energy' thus measured is a global parameter for the sum of the initiation processes and it cannot be ascribed to any particular reaction. The simulated activation energy of the base oil was found to be 145 kJ mol^{-1} compared to an experimental value of 127 kJ mol^{-1}.

There were three inherent shortcomings associated with the model, namely the inability to predict the oxidation stability of the base oil without incorporating an inhibition step; the inability to predict the correct increase in oxidation stability and the unrealistic peak widths obtained. The best fit of experimental data obtained resulted in an acceptable peak width at low temperatures with a peak width corresponding to 5 seconds of run time (far too narrow) at high temperatures.

The next step was to ascertain whether the DSC curve could be reproduced by incorporating a chain branching step (B → 2B) in the mechanism and by omitting the inhibition step. The kinetic parameters for chain branching via an organic hydroperoxide were obtained from the literature [15-18]. These were found to be in the range A = 2×10^{10} to 7×10^{15} s^{-1} and E_a = 96 to 188 kJ mol^{-1}. The overall reaction scheme at this point was

$$A \rightarrow B \qquad 1$$

$$A + B \rightarrow B + C \qquad 2$$

$$B \rightarrow 2B \qquad 5$$

$$B + B \rightarrow D \qquad 3$$

It was found that this mechanism gave no induction period using realistic values for the kinetic parameters, so the inhibition step B + E → F was reinstated to account for the oxidation stability of the base oil. This shortcoming of the model was the only way the natural oxidation resistance of the oil could be represented. Below 500 K the model was found to provide similar results to that without the branching step. The effect of the branching step on the induction time of the simulated DSC curve increased with temperature. The alteration of the rate constants of the initiation and termination reactions permitted the experimentally obtained induction times to be matched at high and low temperatures. The peak widths were again found to be too narrow. In an attempt to improve the fit of the modelled data to the experimental data, the overall 'activation energy' of the reaction model was reduced. An improved fit was obtained when the modelled 'activation energy' was reduced to 130 kJ mol^{-1}.

The addition of a commercial antioxidant was represented by a second inhibition step. The main features of the experimental curves were reproduced when the kinetic parameters given in table 6.6 were used.

The effect of each parameter on the induction time and peak width can be seen in table 6.7. From experimental data, the peak width for oils containing an antioxidant

can vary from one to fifteen minutes. The peak width depends on the temperature of analysis, the base oil and the antioxidant concentration.

Table 6.6
The Kinetic Parameters Inserted into the Simulation Program

	REACTION	A/*	E_a/kJ mol^{-1}
1	A → B	1 x 10^{11}	140
2	A + B → B + C	2 x 10^{9}	35
5	B → 2B	1 x 10^{9}	95
4	B + E → F	1 x 10^{9}	16
3	B + B → D	2 x 10^{9}	0
6	B + G → F	4 x 10^{9}	25

* Units are s^{-1} for first order reactions and dm^3 mol^{-1} s^{-1} for second order reactions.

Table 6.7
The Effect of the Reaction Rates on the Simulated DSC Curves

	Run							
	1	2	3	4	5	6	7	8
10^{6} k_1 *	5.61	5.61	5.61	5.61	5.61	5.61	5.61	5.61
10^{-2} k_2 *	8.66	8660	866	866	866	866	1732	1732
10^{-8} k_3 *	1.00	1.00	1.00	1.00	10.0	1.00	10.0	1.00
10_2 k_5 *	1.18	1.18	1.18	1.18	1.18	1.18	1.18	1.18
10^{-5} k_6 *	6.91	6.91	6.91	6.91	69.1	34.6	69.1	139
T /K	450	450	450	450	450	450	450	450
t_{ind} /s (expt)	150	150	150	150	150	150	150	150
t_{ind} /s (comp)	207	0	207	___	220	218	228	217
Comment	peak width too large	peak width 720 s	peak width 480 s	slow ind	peak width 900 s	peak width 360 s	peak width 420 s	peak width 350 s

* Units are s^{-1} for first order reactions and dm^3 mol^{-1} s^{-1} for second order reactions.

The overall 'activation energy' calculated from simulated data for the base oil was 138 kJ mol^{-1} compared to the experimentally obtained 127 kJ mol^{-1} (figure 6.4). The

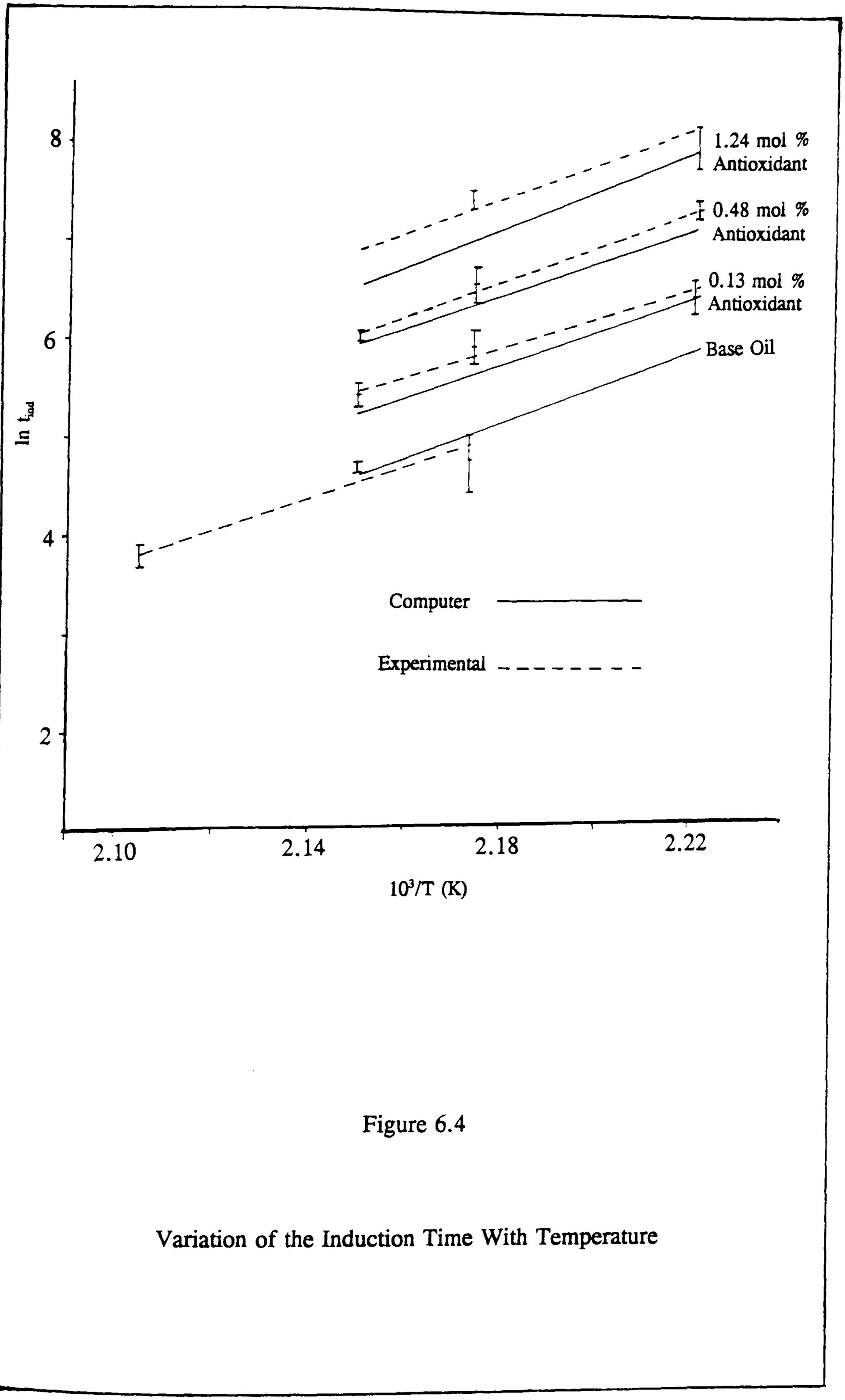

Figure 6.4

Variation of the Induction Time With Temperature

inhibited oil was found to have an 'activation energy' ranging from 128 to 145 kJ mol^{-1} while the simulated results gave values ranging from 144 to 161 kJ mol^{-1} for the same blends. This shows that the model provides us with a reasonable representation of the reaction mechanism for the oxidation of an oil at low temperatures.

The model can be used to reproduce the induction periods of the oil for inhibitor concentrations up to 1.25 molar percent at 450 and 465 K (figure 6.5), but it is unable to faithfully replicate the peak shape. The simulated data match the initial rise of the experimental curve, but the peak shape itself is too sharp. This may be due to the small number of steps used to represent the vast number of reactions that occur when an oil oxidises. For isothermal DSC curves, the peak shape is found to be independent of the heat capacity of the sample. However the thermal resistances and gradients between the sample and the temperature sensors, which contribute to the response time of the apparatus will cause a broadening of the body of the peak. The model of Brown et al. [2] provided a closer representation of the DSC curve shape at the expense of realistic kinetic parameters, but it could not be used to match the variation of peak height with temperature. The concentrations of the various species plotted as a function of time are illustrated in figure 6.6. The simulated DSC curve is superimposed onto the concentration-time figure. The rapid oxidation of the oil following the depletion of the antioxidant is also shown. It is apparent from figure 6.6 that the concentration of the free radical species increases as the oxidation process begins and decays as the reaction slows. This disproves the steady state assumption (at least for the computer model) assumed by Brown et al. [2] insofar that [B] does not remain in a constant ratio to [A]. Until very late stages in the oxidation reaction it would appear that the steady state theory is not valid. Assuming the steady state theory to be valid, the authors provided the following relationship to determine the rate of the initiation process, k_i, from the induction period t_{ind}.

$$t_{ind} = [G]_o/(k_i[A]_o)$$

Despite having reservations as to the validity of this calculation, because of the assumption of a steady state, the rate constants for the initiation processes were determined. Knowing the values of the initial concentration of the hydrocarbon, A, and the antioxidant, G, the initiation rate calculated from experimental data was found to be only marginally smaller than that obtained from simulated data. The agreement between the initiation rates calculated from experimental and simulated data is a further indication of the close fit of the model to the experimental data.

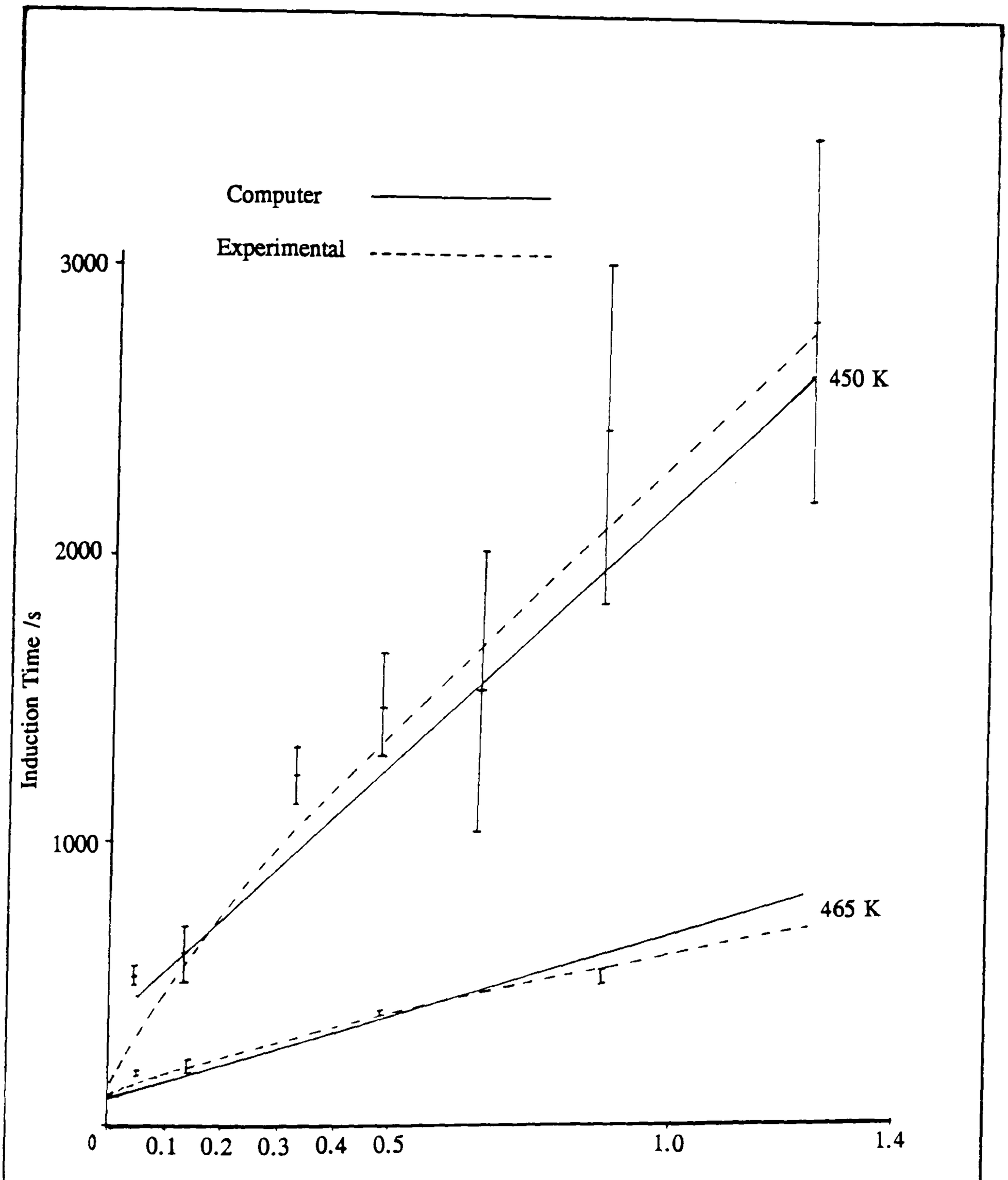

Figure 6.5

Variation of the Induction Time With the Inhibitor Concentration

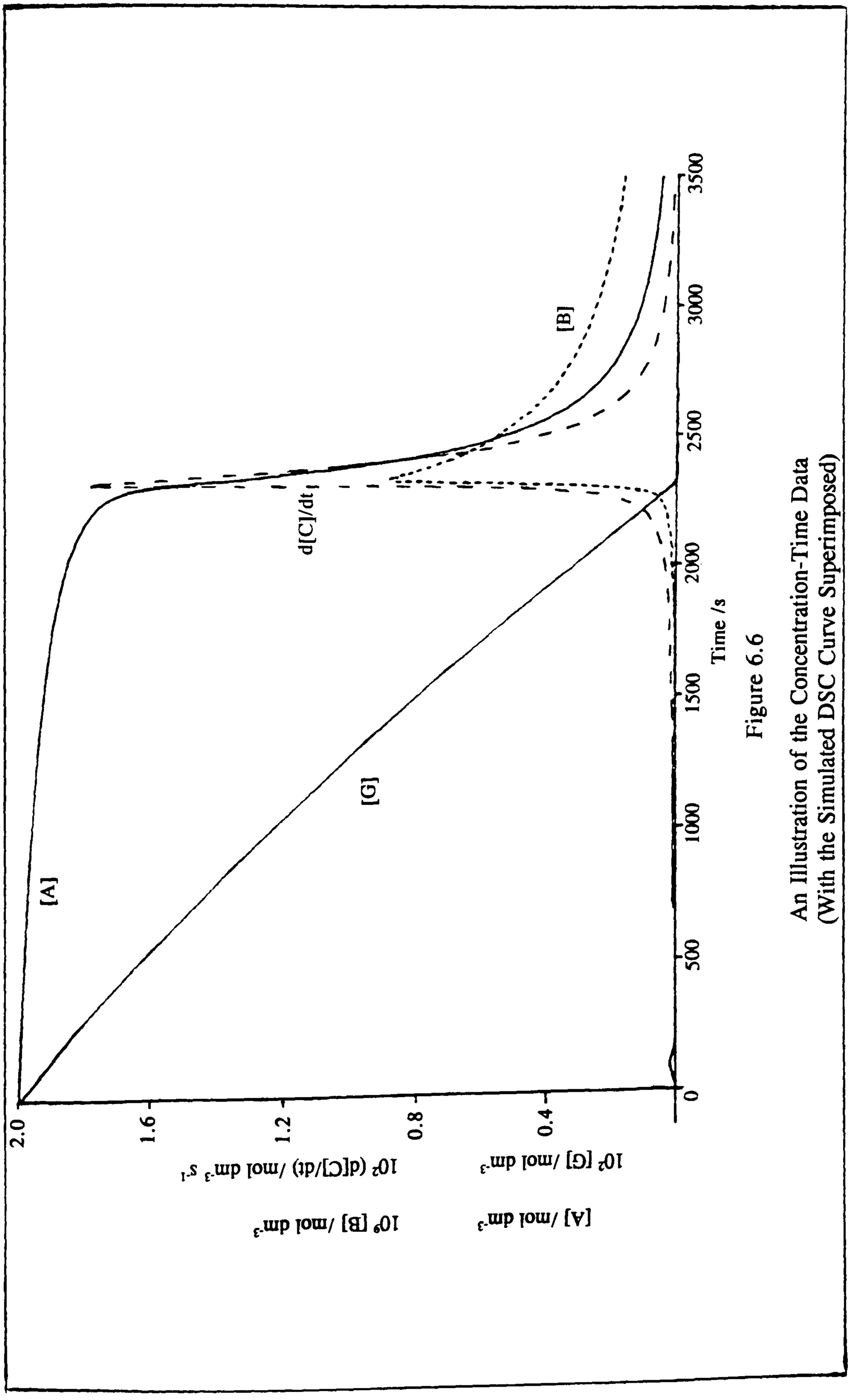

Figure 6.6

An Illustration of the Concentration-Time Data
(With the Simulated DSC Curve Superimposed)

6.5 Future Work

The continuing study of antioxidant behaviour in lubricating oil may be split into three different sections.

1. The electrode reactions of DODPA and Topanol 'O' could be studied in the $MeCl_2$/TBAP solvent system. A knowledge of the electrode reaction of Topanol 'O' exists in methanol with a potassium hydroxide electrolyte but not in methylene chloride with TBAP electrolyte. This study will need to involve the use of different investigative techniques that may analyse reaction intermediates and products. The different techniques may include GC separation followed by UV or mass spectrometric techniques. The electrochemical study of zinc dialkyl(aryl)dithio phosphate (ZDDP) to enable calibration curves to be constructed in a manner similar to that employed for DODPA and Topanol 'O' could be useful to the petrochemical industry. A tentative study of this group of antioxidants has already been made in an antioxidant blend supplied by DQA-TS. The ZDDP constituted only 10% of the antioxidant blend supplied, thus hampering analysis, but despite solubility problems the early results were promising. The lifetime of the additives in a commercial engine oil is not well known. Oil and engine manufacturers state that an oil should be changed at preset mileages, without providing any indication towards how long the additives last. British Rail monitor oil quality during service using a variety of analytical techniques and have saved a considerable amount of money in doing so. In his thesis Cash [19] monitored the oxidation stability of an engine oil at stated mileages. In a study of antioxidant levels in oils, the concentration of the antioxidants could be observed using CV prior the depletion of the lubricating efficiency of the oil to a standard below acceptable values. The samples could be analysed in parallel by DSC and HPLC to extract further information about the lifetime of a commercial engine oil.

2. The analysis of oil samples by an oxygen absorption technique contained in a heat flux calorimeter may provide further information as to what stage in the oxidation process (and how much) oxygen is absorbed by the oil. The atmosphere above the oil sample may be linked up to a mass spectrometer to analyse any volatile matter evolved. Oil samples may be extracted during various stages of the oxidation process for analysis to help identify the breakdown products of the oil and the antioxidants themselves. The results obtained in this thesis suggest that the breakdown products of DODPA possess antioxidant activity. If these products could be separated they could be tested for these properties using a conventional DSC experiment.

The study of oxidised oil blends to which further antioxidant is added may also be important in further understanding the behaviour of antioxidants in lubricating oils. This study should include the addition of different quantities of antioxidant to the oil to discover whether there is any relationship between the quantity of antioxidant added and the increase in oxidation stability. Another route to investigate is to add antioxidant to oil samples that have been oxidised for different durations. This will allow the determination of the extent of oil degradation required, before a greatly enhanced oxidative stability occurs, upon the addition of a small quantity of antioxidant. This second route may be the key to understanding with which oxidation product the fresh antioxidant may react synergistically.

The synergism and antagonistic behaviour obtained for different antioxidant blends should be the subject of further study. The antagonism noted when Topanol 'O' and Topanol 'A' were blended is a cause for concern. Warne and Vienna [10] also recorded an antagonism between phenolic antioxidants, as did Massey and Wilson [9] who also recorded a dilution effect when antioxidants were mixed. The dilution effect noted when DODPA and Topanol 'O' were blended is interesting, but it is more important to discover antioxidants which when blended display a marked synergism. The investigation of blended antioxidants requires further study to realise the optimum ratios of the component additives and a better understanding of the underlying chemistry. It is also important to determine whether calibration curves for different antioxidant blends can be made for DSC and CV analysis. This can be used to differentiate between blends containing different ratios of the same two antioxidants at varying concentrations.

3. The final area of future work relevant to the work performed in this thesis is the relationship of the DSC peak shape to the concentration of the antioxidant in the oil. The experimental work conducted in this thesis led to the realisation that a trend exists between peak shape and the oil composition. For the isothermal experiments it was realised that with increasing antioxidant concentration the DSC peaks tended to become broader, with a lower peak maximum height ($d\Delta Q/dt$). The widths of the DSC curves were also dependent on the base oil and would probably alter with the extent of sample oxidation (engine mileage). There was no relationship found between the peak area (exothermicity), or sample mass loss during analysis, and the composition of the oil. A general trend was observed between the antioxidant concentration and the peak shape for oligomer oil samples. The analysis involved the measurement of the peak height,

the peak width at half height and the gradient of the leading edge of the peak. The parameters used for this analysis could not be measured with enough precision to determine any definite relationship. The DSC peak shapes obtained for mineral oil samples were too varied to lend themselves for this type of analysis.

References

1. R. L. Blaine, *American Lab.*, 1974.
2. R. L. Brown, J. A. Walker and W. Tsang, *Proc 11th NATAS*, New Orleans, Louisianna, Oct 18-21, 1981, Vol 11, (Ed J. P. Schelz), p 507.
3. J. R. Barnes and J. C. Bell, *Lubr. Eng.*, 45, 1989, p 549.
4. A. Zeman, *J. Synth. Lubr.*, 5, 1988, p 133.
5. S. M. Hsu, A. L. Cummings and D. B. Clark, *SAE Technical Paper No 821252*, 1982.
6. A. J. Burn and G. Greig, *J.I.P.*, 58, 1972, p 346.
7. S. J. Leonardi, E. A. Oberright, B. A. Orkin and R. V. White, *A.C.S. Meeting, Div. Petroleum Chemistry, General Papers, Miami*, April 1957, p 35.
8. A. Tong, "Determination of the Oxidation Stability of Several Antioxidant/Base Oil Mixtures by Pressure DSC", Technical Report, DQA/TS Harefield.
9. L. Massey and A. C. M. Wilson, *J.I.P.*, 44, 1958, p 336.
10. T. M. Warne and P. C. Vienna, *Lubr. Eng.*, 40, 1984, p 211.
11. J. F. Ford, *J.I.P.*, 54, 1968, p 198.
12. R. Luo, *Ph.D Thesis*, Dept. of Mining and Min. Eng., Leeds Univ., 1990.
13. P. B. Ayscough and A. J. Mansfield, "Complex Reaction Mechanisms", Lib. of Phys. Chem. Software, Oxford Univ. Press, 1988.
14. C. W. Gear, "Numerical Initial Value Problems in Ordinary Differential Equations", Prentice Hall, New Jersey, 1971.
15. M. P. Halstead, L. J. Kirsch, A. Prothero and C. P. Quinn, *Proc. Roy. Soc.*, London, 346, 1975, p 515.
16. R. Walker, *Chem. Soc. (spec. Period. Rept.)*, 1, 1975, p 297.
17. R. A. Cox and J. A. Cole, *Combust. and Flame*, 60, 1985, p 109.
18. R. R. Baldwin and R. A. Walker, *J. Chem. Soc. Faraday Trans.*, 1, 1979, p
19. A. A. J. Cash, *Ph.D Thesis*, Dept. of Phys. Chem., Leeds Univ., 1988.

Appendix 1

An Expansion of the Basic Principles of Electrochemistry

A 1.1 Introduction

In this section, the work of other authors discussed in Chapter 3 is given in further detail. The theories explained below are employed in the data capture program 'Condecon', which was developed by Dr N. Taylor and Mr R. Luo at The School of Chemistry, Leeds University.

The mathematical notation for the concentration of a given species will be given by the term '[A]' instead of 'Ca', owing to the need for special symbols in the mathematical formulae.

A 1.2 The Solution of Fick's Second Law

The laplace transform $f(S)$ of a function f(t) is defined by

$$f(S) = \int_0^\infty \exp -[St)f(t)].dt, \qquad A.1$$

where S is assumed to be a real variable. The notation L{f(t)} also represents the operation of the transform. This is a linear transform (because $L\{f_1 + f_2\} = Lf_1 + Lf_2$). The application of Laplace transforms is almost entirely restricted to linear equations on $0 \leq x < \infty$. Equation A.1 is rarely used directly to obtain the transform of an equation because tables of the functions and their corresponding transforms are widely available. The function $f(S)$ is never evaluated because it is lost in the process of the inverse transformation.

In order to obtain the solution of Fick's second law, we shall assume a particularly simple experimental arrangement, ie. the application of a potential step function to the electrode. Two boundary and an initial condition have to be set. The first boundary condition is that if an extreme potential is applied to the electrode, the surface concentration of species A is driven to zero, therefore the problem is entirely diffusion controlled. The other condition is that at distances far enough away from the electrode this phenomena will pass unnoticed. Therefore

$$[A]_{(0,t)} = 0 \text{ for } t>0 \text{ and}$$

$\lim_{x\to\infty}[A]_{(x,t)} = [A]^*$ for all values of t,

where $[A]^*$ is the bulk concentration of the electrolyte. The initial condition is a simple one, providing that the solution is homogeneous (and therefore that no mass transport occurs).

$$[A]_{(x,0)} = [A]^* \text{ for } t=0.$$

The equation to be solved is

$$\frac{\delta[A]_{(x,t)}}{\delta t} = Da.\frac{\delta^2[A]_{(x,t)}}{\delta x^2}. \qquad A.2$$

By transforming this equation with respect to variable t we find

$$S[\bar{A}]_{(x,S)} - [A]_{(x,0)} = Da.\delta^2[\bar{A}]_{(x,S)}/\delta x^2. \qquad A.3$$

By introducing the initial boundary condition and
rearranging we obtain

$$\frac{\delta^2[\bar{A}]_{(x,S)}}{\delta x^2} - \frac{S[\bar{A}]_{(x,S)}}{Da} = -\frac{[A]^*}{Da}. \qquad A.4$$

The rearrangement gives an ordinary differential equation that can be solved by the application of a Laplace transformation again, this time on the variable x. The Laplace transform $f(p)$ of the function f(x) is defined by

$$f(p) = \int \exp-[(px)\, f(x)]\, dx \qquad A.5$$

over the limits 0 to ∞.

$$p^2[\tilde{A}]_{(p,S)} - p[\bar{A}]_{(x=0)} - [d\bar{A}/dx]_{(0,S)} - \frac{S[\tilde{A}]_{(p,s)}}{Da} = -\frac{[A]^*}{pDa}. \qquad A.6$$

$[A]_{(0,S)}$ and $[dA/dx]_{(0,S)}$ are dependent on the boundary conditions.
Rearrangement gives

$$[\bar{A}]_{(p,S)} = \frac{-[A]^*/Da + p^2[\bar{A}]_{(0,S)} + p[d\bar{A}/dx]_{(0,S)}}{p[p - (S/Da)^{1/2}][p + (S/Da)^{1/2}]}. \qquad A.7$$

Equation A.7 can be written in the following form, involving three constants L, M, and N

$$[\bar{A}]_{(p,S)} = \frac{L}{[p - (S/Da)^{1/2}]} + \frac{M}{[p + (S/Da)^{1/2}]} + \frac{N}{S}. \qquad A.8$$

Multiplying equation A.8 by p and then setting $p = 0$ we obtain

$$N = [A]^*/S. \qquad A.9$$

When the inverse transformation of equation A.8 is performed the variable x is reintroduced:

$$[\bar{A}]_{(x,S)} = L \exp -([S/Da]^{1/2}.x) + M \exp ([S/Da]^{1/2}.x) + [A]^*. \qquad A.10$$

Constants L and M can be determined by employing the boundary condition at infinity:

$$\lim_{x\to\infty} [\bar{A}]_{(x,t)} = [A]^*/S, \qquad A.11$$

which to be true means that the first two terms of equation A.10 must be zero. The value of constant M must be zero because exp $(-\infty) = 0$ and exp $(+\infty) = \infty$. Transforming the final boundary condition we obtain

$$[\bar{A}]_{(0,t)} = 0. \qquad A.12$$

Setting $x = 0$ and applying this to equation A.10 we have

$$[\bar{A}]_{(x,S)} = 0 = L + 0 + [A]^*/S. \qquad A.13$$

Therefore $$L = -[A]^*/S.$$

Hence $$[\bar{A}]_{(x,S)} = [A]^*/S - ([A]^*/S) \exp[-(S/Da)^{½}.x]. \qquad A.14$$

The inverse transformation of the equation above reintroduces the time dependence and gives

$$[A]_{(x,t)} = [A]^* - [A]^* \operatorname{erfc}(x/2[Da.t]^{½}) = [A]^*(1 - \operatorname{erfc}[x/2(Da.t)^{½}]) \qquad A.15$$

The term erfc is the compliment of the normal error function. This is defined by the expression erfc $= (2/\pi) \int \exp -x^2$, between the limits x and infinity. Equation A.14 provides us with the concentration profile in terms of space and time.

A 1.3 The Convolution with the Function $(\pi t)^{-½}$

Cyclic voltammetry employs a triangular ramp on the applied potential, the apex being referred to as the switching or reversal potential. Up to the point of the reversal potential the potential is a readily defined function of time, which for a reduction process is defined as

$$E_{(t)} = E_i - vt. \qquad A.16$$

The potential at time $t=0$ is E_i and v is the sweep rate dE/dt. In the case of an electron transfer system in which the rate of transfer is fast, the electrode surface concentrations are effectively determined by the Nernst equation. In this example the electrode boundary condition is time dependent, therefore for the reaction

$$O + ne^- \rightleftharpoons R \qquad A.17$$

the boundary condition at the electrode is

$$[O]_{(0,t)}/[R]_{(0,t)} = \exp nF(E - E^{\theta})/RT. \qquad A.18$$

Substituting the potential in from equation A.16 we obtain

$$[O]_{(0,t)}/[R]_{(0,t)} = \exp nF(E_i - vt - E^{\theta})/RT. \qquad A.19$$

It is impossible to solve the above equation to obtain the current function by the use of Laplace transformations. A Laplace transformation can only be performed if the relationship is not a function of time, a condition not met by equation A.19. Nicholson and Shain however, have given a most comprehensive numerical treatment [1]. Their work is summarised below.

The diffusion equations under consideration are:

$$\delta[O]/\delta t = Do(\delta^2[O]/\delta x^2) \qquad A.20$$

$$\delta[R]/\delta t = Dr(\delta^2[R]/\delta x^2) \qquad A.21$$

The two equations are limited by the following conditions

1/ The ratio at the interface of the concentrations of the oxidised and the reduced species is governed by the Nernst equation, A.18

2/ The solution initially consists of a homogeneous distribution of the oxidised species, with the reduced species absent:

$$[O] = [O]^* \text{ and } [R] = 0 \text{ for } t = 0, x > 0.$$

3/ We are considering a planar electrode in an infinite solution.

$$[O] \rightarrow [O]^* \text{ and } [R] \rightarrow 0 \text{ for } t > 0, x < \infty$$

4/ At the electrode boundary the fluxes of the oxidised species are equal and opposite

$$Do(\delta[O]/\delta x)_{x=0} + Dr(\delta[R]/\delta x)_{x=0} = 0 \text{ for } t > 0, x = 0$$

5/ The current is given by the flux of one species at the electrode surface,ie.

$$Do(\delta[O]/\delta x)_{x=0} = i/nFA.$$

Using Laplace transforms, the diffusion equations A.20 and A.21 can be rewritten as

$$[\bar{O}] = [O]^*/S + ([\bar{O}]_{x=0} - [O]^*/S) \exp -Sx/Do^{1/2} \qquad A.22$$

and

$$[\bar{R}] = [R]_{x=0} \exp -Sx/Dr^{1/2} \qquad A.23$$

The two equations can be differentiated, then the balance of the flux and the definition of the current conditions can be implemented. The Laplace transform for the concentration of the oxidised and the reduced species at the electrode surface are expressed as

$$[\bar{O}]_{x=0} = ([O]^*/S) - [(\bar{i}/nFA)/(Do.S)^{1/2}] \qquad A.24$$

$$\text{and } [R]_{x=0} = [(\bar{i}/nFA)/(Dr.S)^{1/2}] \qquad A.25$$

The terms in the brackets do not have a known inverse transformation, therefore to proceed further the convolution theorem is employed. This theorem is used to obtain the inverse transformation if the function can be separated into further functions, each with a known inverse transformation. The convolution theorem gives

$$L^{-1}[\bar{f}(S)\bar{g}(S)] = \int_0^t G(u)F(t-u)\,du. \qquad A.26$$

where $\bar{f}$ and $\bar{g}$ are the Laplace transforms of the functions F and G respectively. The variable u is a dummy variable (it is lost in the evaluation of the definite integral).

The term $[(\bar{\imath}/nFA)/(Do.S)^{½}$ can be expressed as the product of two functions, $\bar{\imath}/nFA$ and $1/(Do.S)^{½}$.

Thus
$$L^{-1}\{\bar{\imath}/nFA\} = i/nFA \qquad A.27$$

and
$$L^{-1}\{1/(Do.S)^{½} = 1/(Do.\pi.t)^{½}. \qquad A.28$$

Thus the expressions for the concentrations at the electrode surface can be illustrated in terms of convolution integrals

$$[O]_{(0,t)} = [O]^* - \frac{1}{(\pi.Do)^{½}} \int_0^t \frac{i(u)}{nFA} \cdot \frac{1}{(t-u)^{½}} \cdot du, \qquad A.29$$

$$[R]_{(0,t)} = \frac{1}{(\pi.Dr)^{½}} \int_0^t \frac{i(u)}{nFA} \cdot \frac{1}{(t-u)^{½}} \cdot du. \qquad A.30$$

Equation A.19 has not been used in the derivation of the above equations, which means that there are no restrictions on the kinetics of electron transfer or the form of perturbation used. These limitations must be introduced if the current is to be expressed in terms of a function of the potential. Thus dividing equation A.29 by equation A.30 and equating this to the right hand side of the boundary condition, A.19 we obtain

$$\frac{[O]_{(0,t)}}{[R]_{(0,t)}} = \exp \frac{nF(E_i-E^{\theta}-vt)}{RT} = \frac{[O]^* - (\pi.Do)^{-½} \int_0^t i(u)/nFA \,.\, (t-u)^{-½}.du}{(\pi.Dr)^{-½} \int_0^t i(u)/nFA \,.\, (t-u)^{-½}.du} \qquad A.31$$

On rearrangement an integral equation is obtained:

$$\int_0^t \frac{i(u)}{nFA} \cdot \frac{1}{(t-u)^{½}} .du = \frac{[O]^*.(\pi.Do)^{½}}{1+(Do/Dr)^{½} \exp nF(E_i-vt-E^{\theta})/RT}. \qquad A.32$$

This equation can be solved numerically to give the current as a function of potential. Nicholson and Shain [1] give the solution to the equation in terms of a dimensionless current function $\varkappa$:

$$i = nFA[O]^*(\pi.Do.nFv/RT)^{½}\varkappa, \qquad A.33$$

where $$\varkappa = [\sum (-1)^{J+1} J^{½} \exp[-JnF(E-E^{\theta})/RT]]/\pi^{½}. \quad \text{A.34}$$

The range of the summation is from J+1 to infinity. The term E^{θ} can be replaced by the polarographic half-wave potential $E_{½}$, or in this example the potential at which the oxidised and reduced species are present at the electrode in equal concentrations. These two potentials are related by the expression

$$E_{½} = E^{\theta} - (RT/nF) \ln (Do/Dr). \quad \text{A.35}$$

$E_{½}$ is equal to E^{θ} when the diffusion coefficients of the oxidised and reduced species are the same. From equation A.33 it can be seen that the size of the peak current is dependent on $v^{½}$ and the bulk concentration of the starting species. In a similar manner equation A.34 shows that the potential of the maximum current is independent of the sweep rate and the starting concentration.

A 1.4 The Analysis of the CEC System

The advantage of using the I_1 convolution for the analysis of a simple electrochemical reaction, where it is applied in a quantitative manner, has already been outlined. If the outward sweep of the I_1 function reaches a plateau but the reverse sweep fails to return to zero, the implication is that a following chemical reaction is consuming the product of the electron transfer step. If there is a rising plateau value or a sweep rate dependency of the limiting value of the I_1 convolution, a regenerating scheme may be involved.

One of the most frequently encountered and simplest electrode processes is the EC scheme, in which the chemical reaction is considered as uni-directional, ie.

$$O + ne^{-} \leftrightharpoons R \xrightarrow{k_c} C. \quad \text{A.36}$$

This represents an extreme of the system

$$O + ne^{-} \rightleftharpoons R \rightleftharpoons C, \quad \text{A.37}$$
$$\qquad\qquad\quad k_b$$

of which A.36 is only a particular example, where $k_c >> k_b$. A solution of A.37 is therefore a solution of A.36.

A further example of a chemical reaction complicating the electrochemical system is the CE case where the reaction involves the first species. When this effect is combined with the former we have the CEC scheme:

$$A \underset{k_b}{\overset{k_f}{\rightleftharpoons}} B \overset{ET}{\rightleftharpoons} C \underset{k_b'}{\overset{k_f'}{\rightleftharpoons}} D. \qquad \text{A.38}$$

If scheme A.38 can be solved then a solution for any combination of chemical reaction with the electrode reaction can be obtained. Scheme A.38 can be solved using the convolution theorem and Laplace transforms [2]. For the general CEC scheme the surface concentrations of the four species are given by

$$[A]_{x=0} = [A]_0 + \frac{k_b}{k_f+k_b}\,\beta.D^{1/2}(I_1-I_2) \qquad \text{A.39}$$

$$[B]_{x=0} = [B]_0 + \beta.D^{1/2}\left(\frac{k_f}{k_f+k_b}.I_1 + \frac{k_b}{k_f+k_b}.I_2\right) \qquad \text{A.40}$$

$$[C]_{x=0} = [C]_0 - \beta.D^{1/2}\left(\frac{k_b'}{k_f+k_b}.I_1 + \frac{k_f'}{k_f+k_b}.I_3\right) \qquad \text{A.41}$$

$$[D]_{x=0} = [D]_0 - \frac{k_f'}{k_f+k_b}\,\beta.D^{1/2}\,(I_1-I_3) \qquad \text{A.42}$$

where $\beta = 1/nFA.D^{1/2}$, $[A]_0$, $[B]_0$, $[C]_0$ and $[D]_0$ are the starting concentrations of the component species. The values of the individual convolution functions are

$$I_1 = I_1(t) = \frac{1}{\pi^{1/2}}\int_0^t \frac{i(u)}{(t-u)^{1/2}}.du \qquad \text{A.43}$$

$$I_2 = I_2(t) = \frac{1}{\pi^{1/2}}\int_0^t \frac{i(u)\,\exp -(k_f+k_b)(t-u)}{(t-u)^{1/2}}.du \qquad \text{A.44}$$

$$I_3 = I_3(t) = \frac{1}{\pi^{1/2}}\int_0^t \frac{i(u)\,\exp -(k_f'+k_b')(t-u)}{(t-u)^{1/2}}.du \qquad \text{A.45}$$

The terms I_2 and I_3 represent the convolution functions. They are dependent on the current response and the chemical rate constants. The equations A.39 to A.42 and A.44 and A.45, are general expressions encompassing all variants of the CEC system, having been derived without recourse to any model for the electron transfer process.

When the coupled chemical reactions are negligible (E), $k_f >> k_b$ and $k_b' >> k_f'$ therefore from equations A.39 and A.40 we have

$$[A]_{x=0} = [A]_0 \qquad \text{A.46}$$

and

$$[B]_{x=0} = [B]_0 - \beta.D^{1/2}.I_1, \qquad \text{A.47}$$

when k_f/k_f+k_b tends to unity and k_b/k_f+k_b tends to zero. Similarly when $k_f'/k_f'+k_b'$

tends to zero and $k_b'/k_f'+k_b'$ tends to unity from equations A.41 and A.42 we have

$$[C]_{x=0} = [C]_0 + \beta.D^{½}.I_1 \qquad A.48$$

and

$$[D]_{x=0} = [D]_0. \qquad A.49$$

It has been shown that species A and D play no part in the electrochemical response. As expected for a simple electron transfer process, the concentration of species B and C alter by equal and opposite amounts. Due to the fact that $[C]_0 = 0$ when $t = 0$ we can write

$$I_1 = \frac{[B]_0 - [B]_{x=0}}{\beta.D^{½}} - \frac{[C]_{x=0}}{\beta.D^{½}}, \qquad A.50$$

as demonstrated earlier for a simple electron transfer process.

For the EC system ($k_f >> k_b$) equations A.46 and A.47 apply, but the concentrations of C and D at the electrode depend on the values of k_f' and k_b'. Equation A.47 shows that there will be a limiting value for the I_1 convolution given by

$$I_L = [B]_0/\beta.D^{½}. \qquad A.51$$

In a cyclic voltammetric experiment this maximum value is attained on the forward sweep and the values of k_f' and k_b' dictate the shape of the I_1 curve on the return sweep. If $k_f' > k_b'$ the I_1 convolution will return to zero at a rate dependent on k_f'/k_b' and the timescale of the experiment. However when $k_f' >> k_b'$ the I_1 function will not return to zero. This phenomena can be explained by examining the concentrations of B, C and D on the outward sweep of the voltammogram. At the limit of the voltammogram $I_1 = I_L$ and $[B]_{x=0} = 0$. Therefore

$$[B]_0 = [C]_{x=0} + [D]_{x=0} = \beta.D^{½}.I_L. \qquad A.52$$

Species D is essentially electroinactive and unable to form species C at any appreciable rate, therefore the I_1 convolution will remain displaced from zero on the return sweep by an amount proportional to the D formed during the experiment. This system is known as the EC_{irrev} scheme because the chemical reaction is essentially uni-directional.

For the EC_{irrev} scheme it is assumed that $k_f >> k_b$, $k_f' >> k_b'$ and $[A]_0 = [D]_0 = 0$. Based on these assumptions the surface concentrations of the component species can be written as

$$[A]_{x=0} = [A]_0 = 0, \qquad \text{A.53}$$

$$[B]_{x=0} = [B]_0 - \beta.D^{½}.I_1, \qquad \text{A.54}$$

$$[C]_{x=0} = [C]_0 + \beta.D^{½}.I_3 = \beta.D^{½}.I_3, \qquad \text{A.55}$$

$$[D]_{x=0} = [D]_0 + \beta.D^{½}.(I_1-I_3) = \beta.D^{½}(I_1-I_3). \qquad \text{A.56}$$

The expression for the value of the convolution integral I_3 (A.45) can be simplified on the assumption that $k_f'+k_b'$ is virtually the same as k_f'.The simplified form of I_3, given by I_3', is

$$I_3 = \frac{1}{\pi^{½}} \int_0^t \frac{i(u) \exp [- k_f'(t-u)]}{(t-u)^{½}} .du. \qquad \text{A.57}$$

Equations A.55 and A.56 can now be rewritten as

$$[C]_{x=0} = \beta.D^{½}.I_3' \qquad \text{A.58}$$

and

$$[D]_{x=0} = \beta.D^{½}.(I_1-I_3'). \qquad \text{A.59}$$

As a result of this treatment equations A.53, A.54, A.58 and A.59 are easier to handle than the complete versions (A.38 - A.42) due to the reduction in the number of variables.

Introducing the Butler-Volmer equation into the model demonstrates that the use of the convolution integrals allows the same conclusions to be drawn as Imbeaux and Saveant [3] for a scheme where the rate constant k_f' is large enough to prevent an appreciable amount of diffusion of species C away from the electrode. Saveant and Tessier [4] have denoted this scheme as the "pure kinetic" regime whereby a steady state for species C is arrived at by the balance of the homogeneous reaction rate and diffusion. The Butler-Volmer model can be summarized as

$$i = \frac{i_0}{[B]_0}. ([B]_{x=0} - [C]_{x=0} \exp -\epsilon) \exp \alpha\epsilon. \qquad \text{A.60}$$

where $\epsilon = (E - E_{½})F/RT$ and $i_0 = i_{t=0} = nFAk^{\theta}[B]_0$. Replacing the concentration terms in equation A.60 we obtain

$$\frac{i}{i_0} \beta D^{½} I_L \exp -\alpha\epsilon = \beta D^{½}(I_L - I_1 - I_3' \exp -\epsilon). \qquad \text{A.61}$$

Through cancelling the common terms and factorising the exponentials

$$\left(\frac{i}{i_0} (I_L \exp (1-\alpha)\epsilon) + I_3'\right) \exp -\epsilon = I_L - I_1. \qquad \text{A.62}$$

Therefore

$$-\epsilon = \ln \frac{I_L - I_1}{\left(\frac{i}{i_0}\left[I_L \exp\left(1-\alpha\right)\epsilon\right] + I_3'\right)} . \qquad \text{A.63}$$

The large value of k_f' means that the exponential term in the convolution integral I_3' becomes very small, which in turn forces the I_3' term to zero. These conditions can be expressed as

$$-\epsilon = \ln\left(\frac{I_L - I_1}{i}\right) - \ln\left(\frac{I_L \exp\left(1-\alpha\right)\epsilon}{i_0}\right), \qquad \text{A.64}$$

which is in agreement with Saveant. The above equation is only applicable under the extreme conditions of the "pure kinetic" regime therefore for more general conditions equations A.54, A.58 and A.59 are appropriate. The three equations previously stated are used for the study of electron transfer systems followed by a first-order chemical reaction whereby the convolution integral I_3' can be assessed knowing the value of k_f'.

References

1. R. S. Nicholson and I. Shain, *Anal. Chem.*, 36, 1964, p 706.
2. N. K. Blackwell, *Ph.D Thesis*, The Dept. of Physical Chemistry, The Univ. of Leeds, 1988.
3. J. C. Imbeaux and J. M. Saveant, *J. Electroanal. Chem. and Interfac. Electrochem.*, 44, 1973, p 169.
4. J. M. Saveant and D. Tessier, *J. Electroanal. Chem. and Interfac. Electrochem.*, 65, 1975, p 57.

Appendix 2

The Stanton Redcroft DSC-700

A 2.1 Introduction

A prototype DSC-700 assembly, consisting of the furnace and thermocouple assembly, was supplied by Stanton Redcroft. In its original form the DSC-700 was designed to work under atmospheric pressure. The purpose of the present project was twofold, the assessment of its performance under elevated pressure and the attempted electrical calibration of the apparatus. The assembly was incorporated into a purpose built pressure vessel and calibrated using electrical heaters, both of which were designed and constructed in the department.

Some work had already been performed in the attempt to obtain a direct calibration of the DSC-700, using two electrical heaters, placed on both the reference and sample thermocouples. The aim was to use electrical calibration in conjunction with, and eventually to replace calibration by means of chemical standards.

A 2.2 Apparatus: Description and Development

The prototype Stanton Redcroft heat flux DSC-700 consisted of a moveable Ni/Cr thermocouple assembly, mounted in an asymmetric cobalt alloy furnace, surrounded by radiation shielding (figure A 2.1). To optimise a flat signal baseline over the working range of the apparatus (-150 to +700°C), the thermocouple assembly could be rotated in the furnace. The thermocouple plate possessed three locating ears each, for both the sample and reference pans. This method of positive sample location was to help in obtaining reproducible results. The allowed pan size was, an outside diameter of 6 mm, with straight sides 4 mm in height. These pans retained a maximum volume of 0.1 cm^3, which in terms of sample mass equates to 100 mg of indium.

The instrument signal of the prototype had not been linearised which meant that the differential temperature signal was examined directly. The apparatus displayed the expected decrease in sensitivity as the temperature increased.

The calorimeter assembly was mounted in a pressure vessel similar to that described by Levy [1]. The pressure vessel, furnace and radiation shield were mounted on a base plate, which also contained inlet and outlet ports for the purge gas and an 11 way electrical lead through. The electrical connections were for the thermocouples (3), the platinum resistance element (2), the furnace power supply (2), and the electrical calibration heaters (4). The gas supply was identical to that used for the Du-Pont DSC 990 (described in chapter 2).

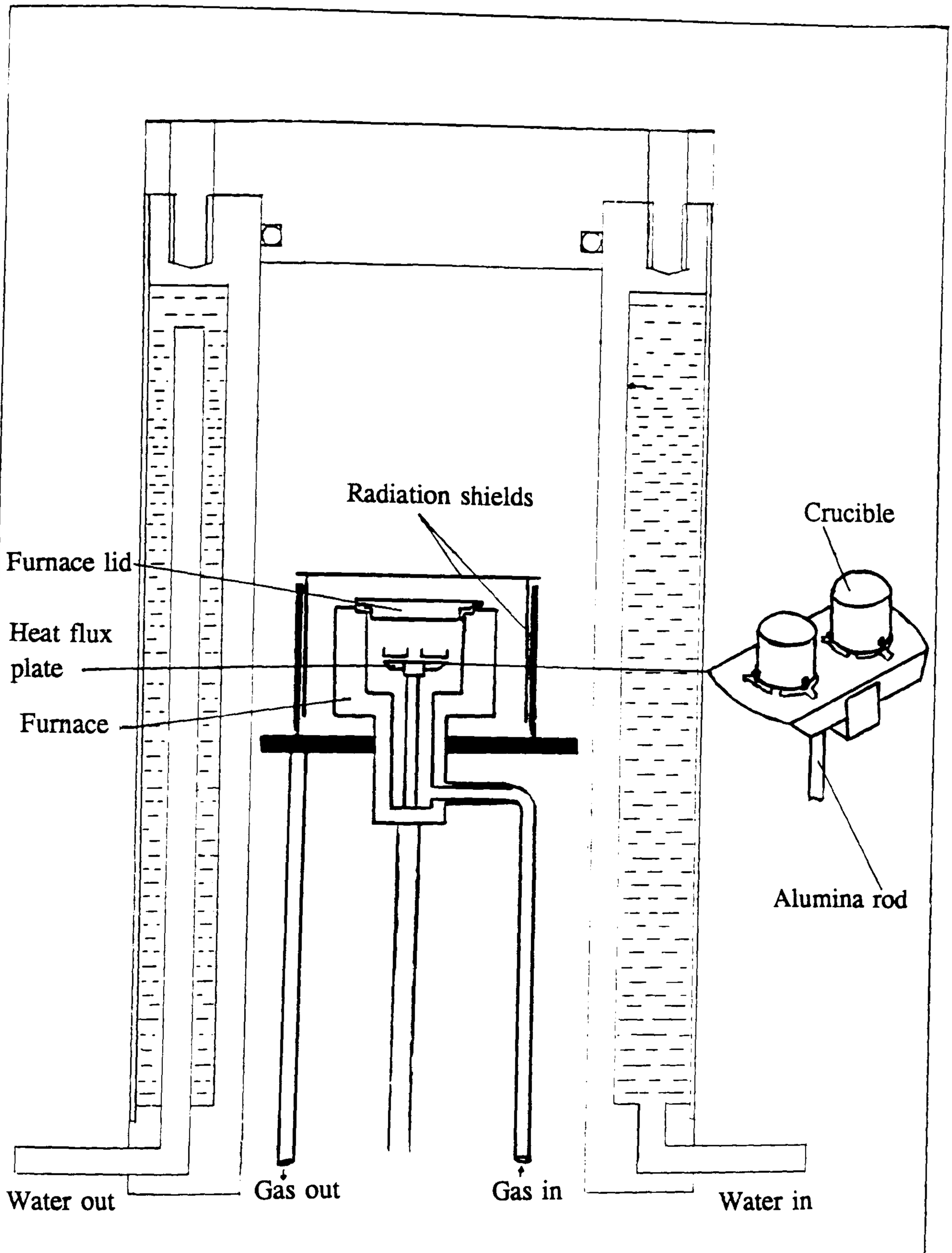

Figure A 2.1

Illustration of the DSC-700 Thermocouple /Furnace
Assembly in the Water-cooled Pressure Jacket

The furnace temperature was controlled by a Stanton Redcroft CPC-706 temperature programmer, operating from a Platinum resistance element mounted in the furnace windings. The furnace was powered by a custom built AC/DC transformer controlled by the CPC-706 programmer. The furnace could be heated at any rate between 0.1 and 150°C min^{-1}. The temperature of the chromel heat flux plate was monitored by chromel-alumel thermocouples, via an ice/water cold junction, to a BBC Goerz Metrawatt SE120 chart recorder and a BBC model B (latterly an Amstrad PC 1640 HD-20) microcomputer. The thermocouples were formed by spot welding alumel wires to the centres of the underside of the crucible platforms. The DSC head was mounted on an alumina rod, through which the thermocouple wires passed to the base of the apparatus. The differential temperature signal passed to the chart recorder and microcomputer via a Stanton Redcroft DC amplifier with a resolution of 10 to 1,000 μV per 10 mV output.

Where the thermocouple wires departed from the support of the overall calorimeter assembly, the insulating ceramic between the wires disintegrated. The wires thus exposed were prone to short circuit causing spurious results. This was overcome by encapsulating both the wires and the end of the alumina rod in Araldite two part adhesive to support and isolate each wire.

When experiments were performed at high temperatures and under elevated pressures, the pressure jacket became hot to touch. The increase in temperature of the jacket affected the experimental results during the course of the day. For isothermal experiments the set temperature would vary by as much as 6°C and the calibration constant of the apparatus could decrease by as much as 30 W V^{-1}. This change in sensitivity was illustrated by the irreproducible calibration coefficients obtained at elevated pressures. The reduction of the temperature rise of the pressure jacket, by wrapping it in a copper coil through which water was passed, proved to have limited success. To overcome the heating problem completely a larger diameter stainless steel pressure vessel with an integral water cooled jacket was constructed (figure A 2.1). The vessel was described in Chapter 2 of the thesis.

A 2.3 Electrical Calibration

The basis of the work was to develop a system of electrical calibration for thermal analysis apparatus, to provide a quick and reproducible method of calibration, for use at all temperatures. It was intended that the method should eliminate the need for the

individual chemical standards currently in use. For pressurised systems, the extra advantage incurred would be that all the measurements could be performed without the need of venting and repressurising the apparatus, as is the case when chemical standards are employed.

The prototype heaters were constructed from nichrome wire (0.025 mm in diameter) wound on thin mica discs and then pressed into the flat base of standard aluminium pans. Attempts at electrical calibration using these heaters were hampered by them lifting off the plate thermocouples, owing to the weight of the connecting cable, which pulled them out of the furnace.

The final design of heaters (figure A 2.2), again consisted of nichrome wire (0.025 mm in diameter) wound on thin mica discs. The discs and heater elements were encapsulated in a long slender machinable ceramic body (Macor machinable ceramic). The heaters were spot welded to copper cable which passed from the top of the heater assembly and down to the lead through at the bottom of the cell base. The copper cables which connected the heaters in series, had a total resistance 3% of that of the heater elements. The cables were shrouded in thermal insulation where they left the protection of the heater assembly. The resistances of the heaters were approximately 0.6 and 7.0 Ω, for the reference and sample heaters respectively. To maintain the heaters on the thermocouples, a new non magnetic stainless steel lid was constructed, which contained two chamfered holes to accommodate two collars. The collars, made of the same metal, were designed to secure the heaters and prevent them lifting off the thermocouples under the weight of the cable.

The heaters were connected in a circuit (figure A 2.3) with a purpose built integral current regulator-programmer, which acted as a constant current source. The programmer triggered a digital timer (also constructed in the department) which measured the duration of the experiment in hundredths of seconds. The current passing through the circuit was measured by a digital multimeter (Keithley model 175 Autoranging Multimeter). To determine whether the resistances of the heaters altered during the course of an experiment, a second digital voltmeter (Keithley model 175 autoranging Multimeter) was placed across the circuit between the DSC cell and the regulator and ammeter. Throughout the duration of an experiment the voltage across the high resistance heater changed by 0.015% and the current by 0.036%. Thus the maximum possible variation in the resistance was 0.045%. The procedure was repeated

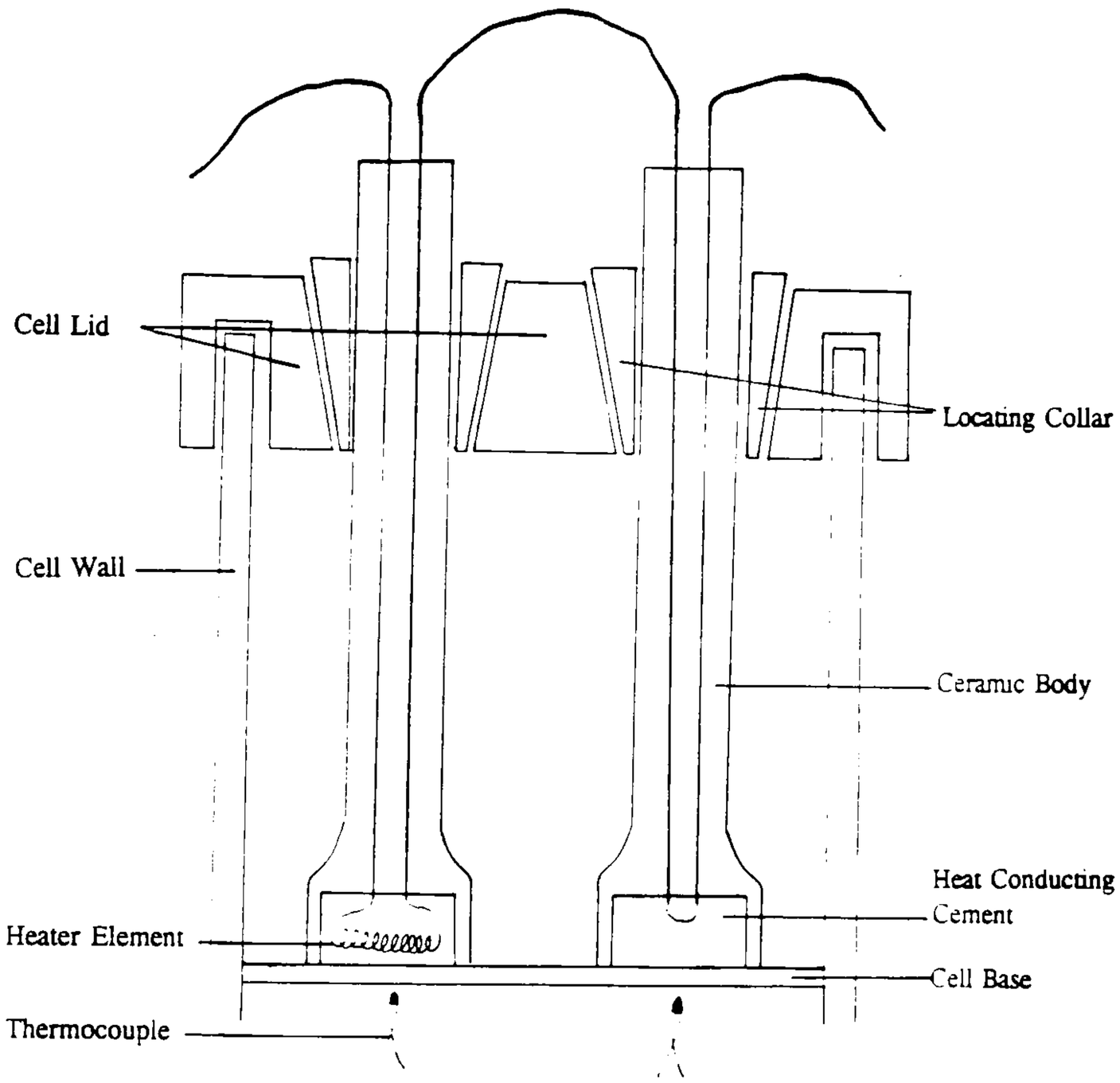

Figure A 2.2
Schematic Representation of the Electrical Heaters

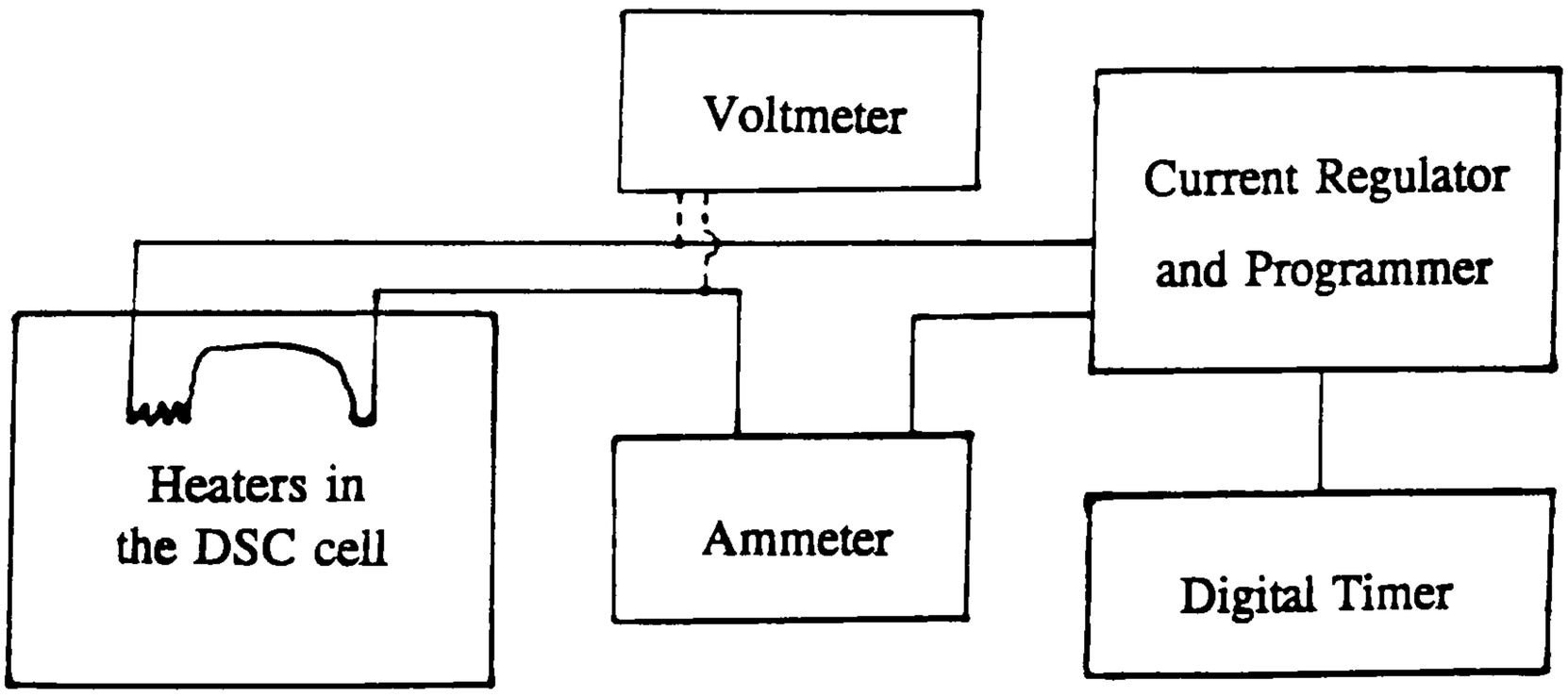

Figure A 2.3

The Electrical Circuit Employed For Electrical Calibration of a DSC

for the low resistance heater and the two heaters in series. The changes in resistance measured were all minimal, and well within experimental error. In the calibration experiments the variation in heater resistance, due to their heating, was found to be a maximum of 0.002 Ω or less (0.33% for the low resistance heater), and could therefore be ignored. The leads to the heaters had a resistance of less than 0.1 ohm compared to 7 Ω.

The area of the peak caused by the electrical heating was calculated in V s^{-1}. The energy, Q (Watts), supplied to the heaters was calculated from the equation

$$Q=I^2Rt$$

where I was the current passing through the circuit (amps), R the difference in resistance between the two heaters (ohms), and t was the duration of the experiment in seconds. The peak area when divided into the energy supplied to the heaters gave the calibration coefficient of the apparatus in W V^{-1}, at the temperature measured during the experiment.

The calibration coefficient thus obtained was approximately two orders of magnitude greater than that obtained by means of chemical standards. The discrepancy was ascribed to poor thermal contact between the heater and the plate thermocouples. To overcome this, and to simulate more closely the conditions experienced when using chemical standards, the heaters were placed in aluminium pans. A marginal improvement was obtained, but the location of the heaters themselves on the thermocouples was found to be of more importance. If the heaters were not thoroughly pressed down on the thermocouples, a calibration coefficient considerably greater than expected was not uncommon. When aluminium pan lids were placed between the heater and the thermocouple a further improvement in the calibration coefficient was observed. The reason for the improvement was that the pan lids had a lower mass than the pans themselves.

The heaters had a large mass in comparison with the chemical standards and heat could flow away from the heating elements up the neck of the heaters and pass into the lid of the cell via the locating collars. The heat dissipated could also pass along the wires attached to the elements away from the thermocouples. To improve the thermal contact between the heater and the aluminium pan lid, heat sink grease could be used. The main disadvantage with using grease is that it has a maximum working temperature of 200°C which is very limiting with regards to high temperature calibration work.

The DSC cell produced a linear response to the power supplied by the heaters over the range 0 to 4.9 J, equivalent to a mass range of 0 to 172 mg of indium. Calibration of the apparatus using electrical heaters was an excellent method for displaying the relative sensitivity of the DSC at any given temperature and pressure. The method illustrated the dynamic range of the apparatus (figure A 2.4), but the calibration coefficient obtained differed from that obtained when chemical standards were employed,due to either poor thermal contact or heat loss by conduction. For this reason the work was not pursued, despite the reproducibility of the results (in the dynamic range at different temperatures and pressures).

A 2.4 Chemical Calibration

The apparatus was calibrated using the fusion peaks of the usual chemical standards, indium, tin, lead and zinc. The temperature and enthalpy of fusion of the metals are given in Chapter 2. Experiments were carried out using approximately 2 mg samples of the metal powder placed in aluminium pans whose bases had been previously flattened between two metal presses. The pans were then sealed with a lid and placed on the sample thermocouple. A similar pan containing an equal mass of alumina was placed on the reference thermocouple.

Calibration experiments performed under elevated pressures employed a static atmosphere of nitrogen, but at atmospheric pressure a flow rate of 50 cc min^{-1} was used. During each experiment the sample was heated at a rate of 5°C min^{-1}, until the fusion peak returned to the baseline. The peak of the first fusion was ignored if it had a poor shape and melting temperature. The experimental procedure has been described in further detail in Chapter 4 of this thesis.

Heat capacity measurements were also used to determine the calibration coefficient of the DSC cell. The thermal analysis curves for a 61 mg sapphire disc were recorded in an aluminium crucible over temperature intervals of 20 to 50°C at a heating rate of 2°C min^{-1}. The calibration coefficient, ϵ, was calculated from the equation

$$\epsilon = C\beta m/S$$

where C is the heat capacity of sapphire at the average temperature of the experiment (J g^{-1} K^{-1}). β is the heating rate (K s^{-1}), m the mass of the sapphire disc (g) and S the difference in signal response between the sample and the blank (V).

The results of the calibration experiments are shown in figure A 2.5. The

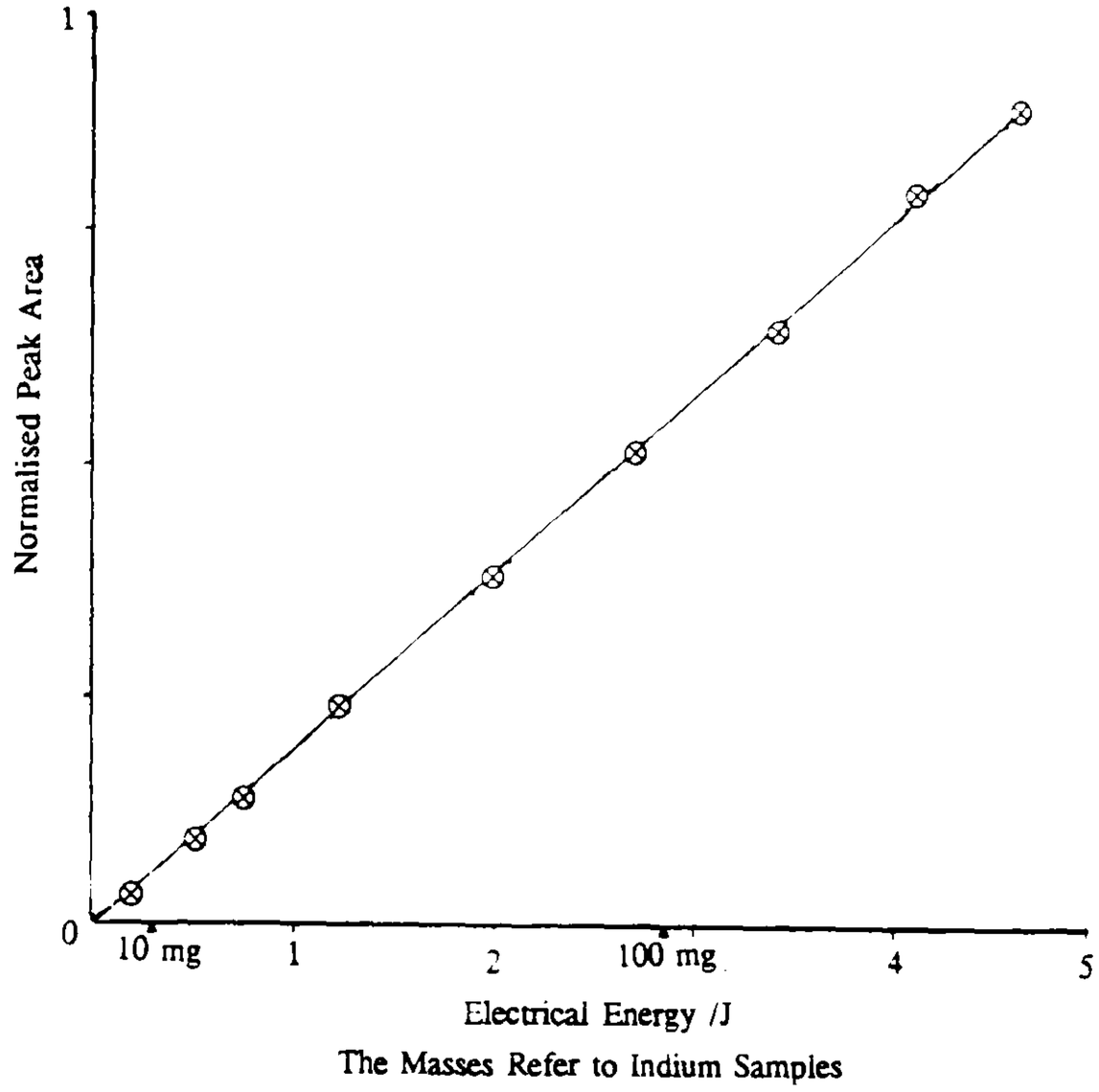

Figure A 2.4

Dynamic Range of the Stanton Redcroft DSC-700
at Atmospheric Pressure and 380°C

Figure A 2.5
The Calibration Curves of the DSC-700

magnitude of the error bars illustrates the standard deviations of the data. The results lie on smooth curves, with the expected decrease in sensitivity, illustrated by the increase in the value of the calibration coefficient with increasing temperature and pressure. The curves are for calibrations at atmospheric pressure, 3,450 kPa (500 lbf in^{-2}) and 6,900 kPa (1,000 lbf in^{-2}) respectively. There was a decrease in sensitivity of approximately 10% between each pressure increase and a mean error of 5% in best fitting the data to each of the curves given above.

A 2.5 The Thermal Analysis of Lubricating Oils

The analysis of oil samples supplied by the Ministry of Defence and the Institute of Petroleum STG-9 panel, was conducted using the pressure vessel described by Levy [1]. Analysis for the Ministry of Defence incorporated 1 mg samples of oil which were compared to an empty reference crucible. The experimental parameters for dynamic experiments were; atmospheric pressure oxygen with a flow rate of 50 cc min^{-1} and a heating rate of 10°C min^{-1}. The isothermal experiments employed a heating rate of 99°C min^{-1} up to the set temperature and a static atmosphere of 3,450 kPa oxygen. The furnace was maintained at that temperature until the oil oxidized. The scanning experiments were repeated using the Du-Pont DSC 990 to provide a correlation between the results obtained using the DSC-700. The onset temperatures obtained using the Stanton Redcroft DSC-700 were higher than those from the Du-Pont owing to differences in the furnace design and sample geometry. The dynamic experiments performed for the Institute of Petroleum STG-9 panel employed identical test parameters (except for a sample size of 2.00 +/- 0.01 mg).

The apparatus displayed poor temperature control during the isothermal period of an experiment, despite a linear heating rate. The poor control was due to the temperature programmer being unable to control the furnace. Although the settings of the programmer were altered the deviations from linearity could only be reduced and not eliminated. When blends of DODPA in RTS-9745 were analysed under isothermal conditions to construct a calibration curve, the temperature rose linearly with time after reaching the set temperature. The longer the induction period before oil oxidation, the greater the temperature rise of the sample. The temperature rise was much as 17° C in one instant. Compounded with the slow rise in temperature the sample temperature signal displayed a distinct ripple which often exceeded 1°C, figure A 2.6. The non-systematic interference of the furnace temperature was caused by the coupling of the DSC-700 with the Stanton Redcroft CPC-706 temperature programmer. The

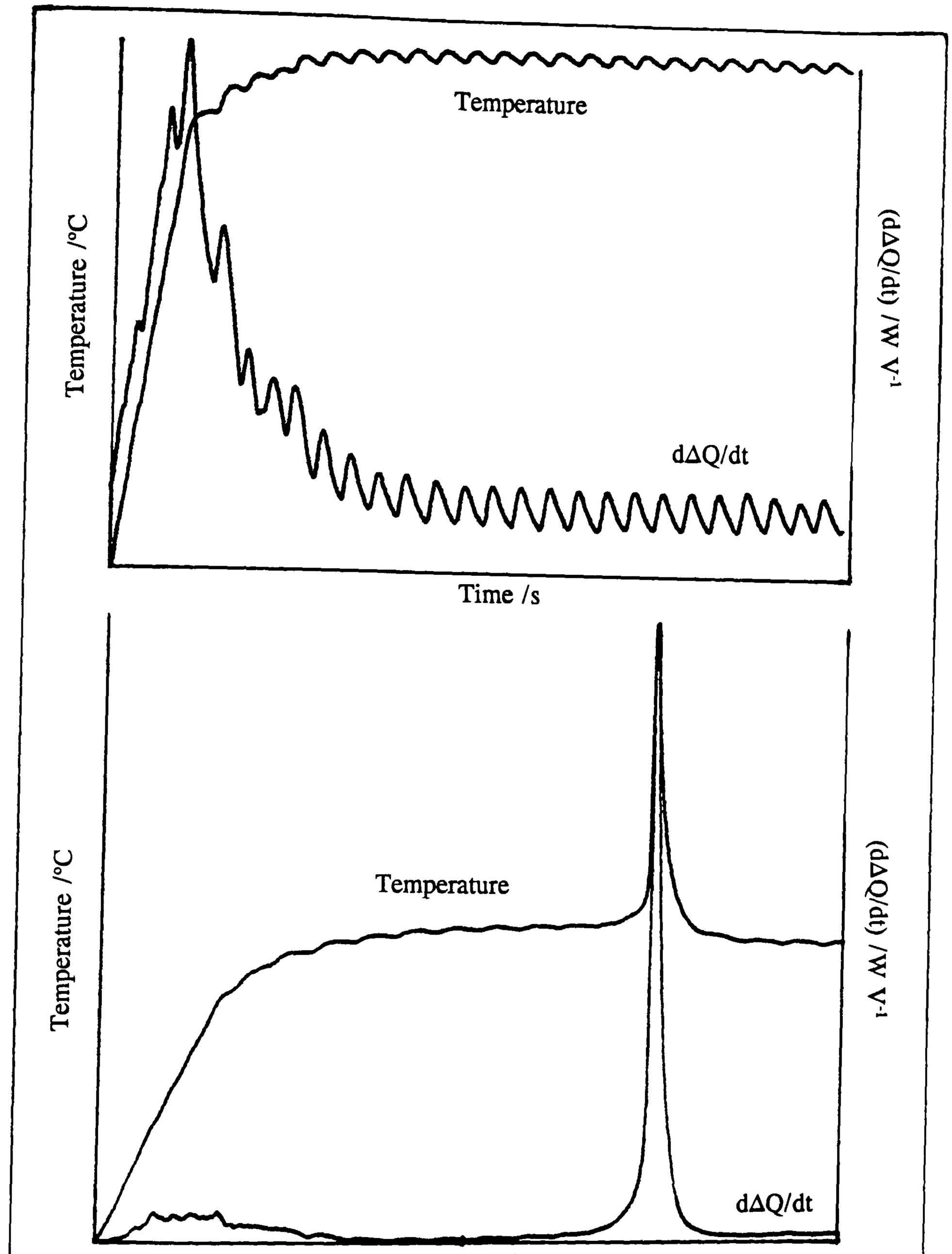

Figure A 2.6

An Illustration of the Temperature Control of the DSC-700

temperature ripple was caused by the programmer switching the furnace heater on and off. The new programmer produced by Stanton Redcroft (PL Thermal Science) is computer controlled, therefore to overcome the low thermal inertia of the oven, the programmer can be continuously reprogrammed to maintain the optimum settings required.

In conclusion, the electrical calibration can be used to display the relative sensitivity of the apparatus at different temperatures and pressures. It can also be used to illustrate the dynamic range of the DSC assembly, although it is unable to provide an absolute method for energy calibration. The dynamic range of the DSC was tested using indium, as a 'double check'. The calibration coefficient of the apparatus remained unaltered over a sample mass range of 0.5 to 100 mg. For the analysis of lubricating oils the Stanton Redcroft DSC-700 was best suited to the dynamic or scanning method. It is no fault of the apparatus that this technique is not as discriminating between samples as the isothermal method. The apparatus was unable to reproduce experimental conditions in the 'isothermal mode', thus it was deemed to be unsuitable for the work contained in this thesis.

REFERENCE

1. P. F. Levy, G. Nieuweboer and L. C. Semanski, *Thermochim. Acta*, 1, 1970, p 429.

Appendix 3

The Development of Standard Test Methods

A 3.1 Introduction

The work discussed in this appendix consists of the experiments conducted for the Institute of Petroleum thermal analysis panel STG-9 in connection with the development of standard test methods. In addition some measurements are reported which have been carried out for other laboratories, including those for MOD/DQA-TS. The ability to compare the relative merits of different experimental procedures has been gained from the work performed in this appendix. Furthermore, a comparison has been made of the results obtained in this laboratory with those of other laboratories. This is particularly difficult when the different furnace geometries (instrumentation) used by the panel members of the STG-9 committee are considered.

The apparatus used to was the Du-Pont DSC-990, described in Chapter 2, the Stanton Redcroft DSC-700, (for one series of experiments) described in Appendix 2 and the Stanton Redcroft STA-781 simultaneous DTA-TG apparatus. The STA-781 was used for volatility measurements and the configuration of the apparatus will be described in the following section of this appendix. Prior to any measurements being made, the apparatus was calibrated in the usual fashion, using the fusion peaks of pure metals under similar conditions to the test method employed for the analysis of the oil samples.

A 3.2 The Stanton Redcroft STA-781

The STA-781 apparatus consists of a simultaneous DTA-TG assembly incorporated in a moderately fast response furnace, with a maximum working temperature of 1500°C. The balance is situated directly above the furnace and has a maximum working capacity of 5 g. Two hangdowns are supplied, one for only TG measurements and the other for simultaneous DTA-TG work, which can accommodate samples up to 200 mg. The hangdown is suspended from an arm of a counter balance beam, which is pivoted at the centre. When the beam is horizontal light is reflected onto a splitter lens to divert it onto two photoelectric cells. The difference in the signal strength from these cells is used to operate a coil, which maintains the balance at equilibrium. The signal that passes through the coil is also passed onto the balance control unit. This has two operating ranges, 0 to 20 mg and 0 to 200 mg, with resolutions of 1 and 10 μg respectively. The mass of the sample is displayed on a digital readout and an output is provided to a 10 mV full scale deflection chart recorder. A derivative of the TG signal can also be obtained.

The sample hangdown assembly and furnace design are illustrated in figure A 3.1. The thermocouple assembly consists of two Pt/Pt-13% Rh plate thermocouples, the wires from which pass up a four bore alumina tube. The assembly is encased in a ceramic micro-environmental cup inside the furnace by three ceramic baffles on the hangdown. The micro-environmental cup reduces the swept volume of the environment immediate to the thermocouple assembly to 4 cm^3, which helps to reduce the temperature gradients around the sample. The passage of purge and exhaust gases into the balance assembly are minimised by the use of a cold finger. The thermocouple circuitry incorporates an electrical 'ice point' located in the rear of the instrument, before the signal is passed to a chart recorder. The ΔT signal is amplified before being displayed on a second channel of the chart recorder.

The cylindrical furnace is constructed from an alumina liner surrounded by a non-inductively wound coil of Pt-20% Rh wire, with a maximum working temperature of 1500°C. The heating element is surrounded by a water cooled jacket, to homogenise the temperature of the furnace and permit rapid cooling at the end of each experiment. The heating rate below 100°C is limited to 10°C min^{-1}, to avoid damage to the heater, but above this temperature the maximum recommended heating rate is 50°C min^{-1}.

The reproducible positioning of the furnace for each experiment is obtained from a motorised lifting mechanism, on which the furnace is mounted by means of a spring loaded clamp. The gas atmosphere within the micro-environmental cup is controlled by a needle valve and monitored by a flow meter. The purge gas enters the bottom of the micro-environmental cup, flows over the hangdown assembly, past the baffles and out of the furnace at the bottom. The recommended gas flow rate is 50 cm^3 min^{-1}. A heated capillary tube can be mounted in the system through small holes in the baffles to sample the gas environment above the sample crucible, for evolved gas analysis.

The instrument temperature programmer was a Stanton Redcroft universal temperature programmer (UTP). The selectable heating rates ranged from 0 to a maximum of 50°C min^{-1} for this apparatus, available from thumbwheel switches. The minimum and maximum temperature set points were -200 and 1999°C, also selected by thumbwheel switches. The programmer could be set to heat, cool, or cycle between two temperatures. It was also possible to isotherm at any given temperature. The UTP had various output ports at the rear, which enabled extra facilities to be used. The programme temperature could be output as a signal of 0.01 mV $°C^{-1}$ and an add on

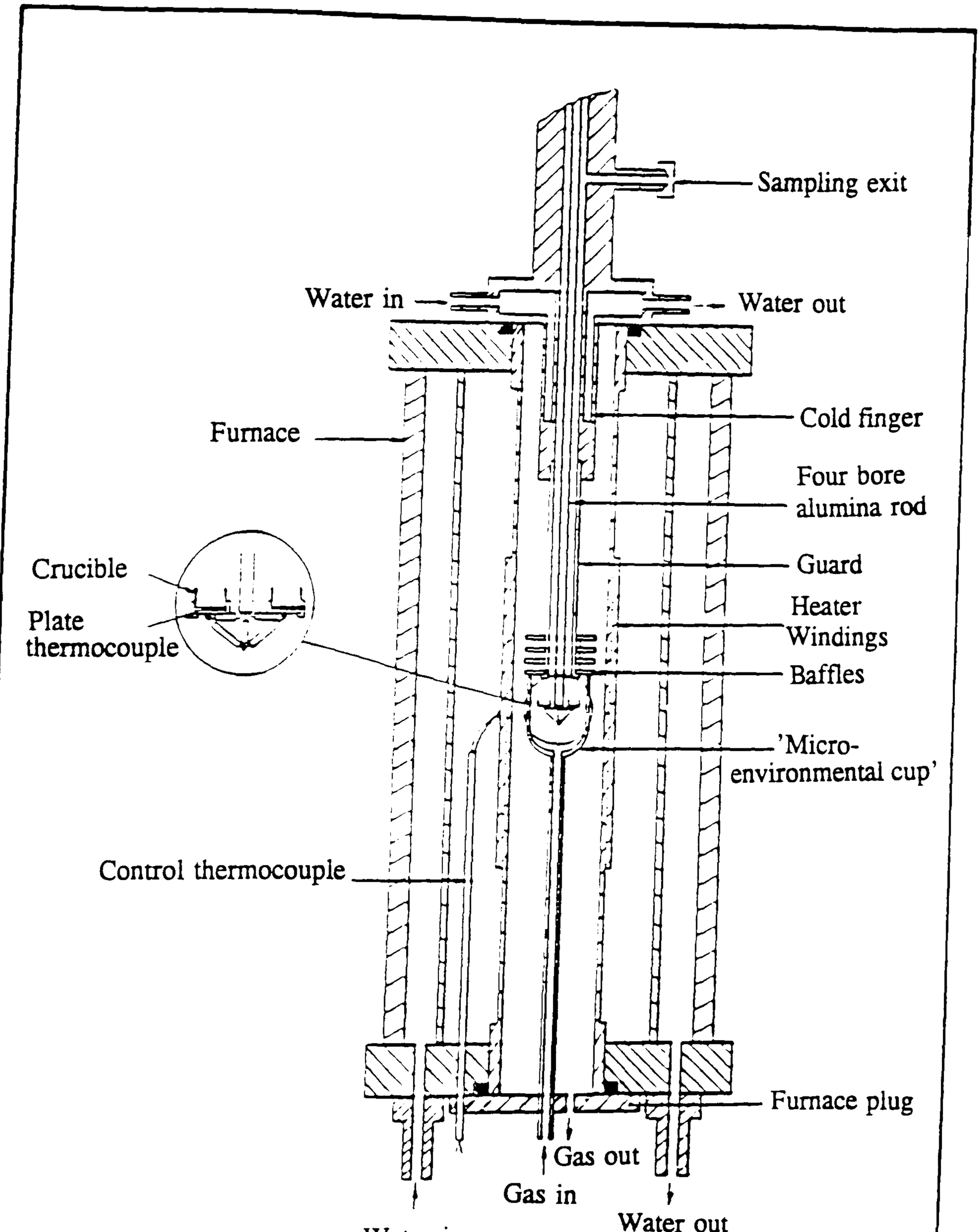

Figure A 3.1

The Stanton Redcroft STA-781 DTA-TG

timer was available if multiple stage programming was required. The UTP could also be employed to operate gas valves, solenoids or status signals and could itself be controlled by a computer through an IEEE interface.

To enable the use of the UTP in conjunction with different furnaces the proportional, integral and differential band settings of the programmer could be altered. These settings controlled the linearity of the heating rate, the rapidity with which the isothermal temperature was attained and the linearity of the isothermal temperature-time trace. If they were poorly adjusted, the temperature ramp was not linear, the sample took a long time to reach (or overshot) the set temperature and the isothermal portion of a programme displayed a distinct ripple. For a correctly set programmer, the accuracy of the heating rate and set temperature was 0.5%, with a stability better than 0.1%. The furnace temperature could be controlled by either the furnace thermocouple, or the sample temperature thermocouple.

The DC amplifier used to magnify the ΔT signal was made by Croydon Precision Instruments. The amplifier had eleven ranges to provide a 10 mV output, corresponding to a full scale deflection. The ranges varied from 10 to 1000 μV and the ΔT sensitivity ranged from 0.005 to 0.25°C mm^{-1} depending on the range employed. The noise level was claimed to be better than 0.05 μV and the drift less than 0.2 μV hr^{-1} $°C^{-1}$.

A more complete description of the apparatus is given in the operations manual that accompanies the STA-781 [1].

A 3.3 Analysis for the Institute of Petroleum

A 3.3.1 The Oxidative Stability of Oils

The oxidation stability of two standard oils were examined using the Stanton Redcroft DSC-700, as part of a programme to establish a new test procedure. A 2 mg sample was heated at a rate of 10°C min^{-1}, under a flowing atmosphere of oxygen (50 cm^3 min^{-1}) at ambient pressure. All participating panel members found the method to give poor results for the oxidation stability of the more volatile standard. The repeatability was found to be very poor and the method was considered to be impossible to discriminate between two samples with sufficient confidence. In a second method the sample mass was reduced to 0.5 mg. The method also employed elevated

pressures and a heating rate reduced to 5°C min^{-1}. The experiments were conducted on the Du-Pont DSC-990. The method was found to give excellent repeatability and reproducibility. The members who participated in the round-robin all ranked the oils in the same order. At the last meeting of the IP thermal analysis panel STG-9, it was decided to make the method relative, whereby the oxidation results are compared to a standard (squalane). It is hoped that this new approach will eliminate the variables introduced when the results obtained from different instruments are compared.

A 3.3.2 Volatility Measurements

The volatility of lubricating oils was studied, using the Stanton Redcroft STA-781 simultaneous DTA-TG apparatus. A sample mass of 15 mg was used in the method under investigation. The sample was isothermed at 40°C for 5 minutes before being heated at a rate of 10°C min^{-1}, under an atmosphere of nitrogen flowing at 50 cm^3 min^{-1}. The STA-781 does not permit the use of elevated pressures. The temperatures at specified weight losses (10, 15, 20, 30, 40, 50, 60, 70, 80, and 90%) were recorded. The method was found to be unrepeatable owing to the large mass losses employed, because condensation products collected within the furnace and hangdown assemblies, only to revolatilise when a subsequent sample was studied. Furthermore the large sample masses used, led to large quantities of condensates being retained within the furnace, necessitating regular cleaning of the furnace by baking in oxygen at 1000°C.

A subsequent test procedure employed an isothermal method. A 10 mg sample was heated to the isothermal temperature, at a rate of 10°C min^{-1}. The isothermal temperature was chosen to provide a mass loss of 3.5 to 4.5 mg of a tetracosane standard over a 30 minute interval, after the isothermal period of the programme had begun. The gaseous environment was nitrogen at a flow rate of 50 cm^3 min^{-1}. The method used the comparison of the mass loss of the oil samples over the half hour period to that of the standard. However the results obtained for the tetracosane proved to be unrepeatable, owing to its condensation on the furnace wall and hangdown assembly. The results obtained for the oil samples themselves showed excellent repeatability and reproducibility amongst the panel members, but once again the furnace was discovered to require regular cleaning.

Squalane was chosen as the next standard because it was a liquid at room temperature, thus facilitating handling, and because it does not condense in the apparatus so readily. The mass losses obtained for the oil samples were very

repeatable, but the squalane standard again proved to be unreliable. The squalane was found to creep over the pan walls, sometimes out over the edge, therefore inconsistent sample surface areas were obtained between each experiment, which had the effect of altering the recorded sample volatility. When the experiments were repeated using platinum pans, the volatility measurements performed on the squalane were repeatable. The squalane was found to be sensitive to the surface of the pans. The aluminium pans used in this laboratory are 'home made' and unlike some commercial pans are not anodised. When alumina pans were used for the analysis of squalane the results from individual experiments were not repeatable. It was decided that only commercially made aluminium pans should be employed for the tests. The problems encountered with squalane, when alumina and 'home made' aluminium pans were used illustrates the care required to chose the optimum experimental conditions. The interaction of the sample with the pan surface rendered the method useless. For the comparison of the results obtained by different laboratories, the sample pan material must be specified in order to avoid discrepancies such as the one just mentioned. The choice of a standard purge gas and heating rate are also necessary to enable these comparisons to be made.

A 3.3.3 Temperature Calibration of the STA-781

An investigation into the calibration of DTA-TG apparatus was conducted for the thermal analysis panel using the boiling and sublimation points of pure materials. The first set of experiments concerned the boiling point of tetracosane, using a heating rate of 10°C min^{-1}. The samples were weighed into aluminium pans, which were sealed with a lid punctured using a syringe needle. The hole size in the pan lid varied from 0.15 to 0.3 mm in diameter. The lids were pierced using a syringe needle, because no drill bit small enough could be located. The results of the calibration were found to be inconclusive because a dependence of the apparent boiling point to the hole size was discovered. The second set of experiments employed the boiling and sublimation temperatures of adamantane and 2-adamantantanone, using crimped pans with holes in the lids less than 0.1 mm in diameter. A correlation between the boiling and sublimation temperatures with the DTA peak and end temperatures or the TG onset and end temperatures was attempted. Once again no relationship could be discovered because the temperatures were again dependent on the size of the hole in the pan lid. A dependence on the initial mass of the sample was also found. It was decided that calibration of DTA-TG apparatus was unreliable using this method. The holes in the lids were of an irregular shape, due to their being made by puncturing with a syringe. This made the area measurements difficult and the size of the hole was found not to

be repeatable. If pan lids could be pierced using lasers (or another method that would provide a reproducible hole size) it would be worthwhile considering this procedure for the calibration of simultaneous DTA-TG equipment once more.

A 3.4 Analysis for Other Laboratories

A series of seven samples was received from MOD/DQA-TS, consisting of blended ester oil basestocks, inhibited by amine antioxidants. Four samples were fresh oils and three had been oxidised. They were analysed using the Stanton Redcroft DSC-700 (see Appendix 2) using both isothermal and dynamic methods. The results of the dynamic experiments were compared using the Du-Pont DSC-990. The experimental conditions for the dynamic tests were, a sample mass of 1.00 $\pm$ 0.05 mg, heated under an atmosphere of oxygen (atmospheric pressure, flow rate 15 cm^3 min^{-1}) at a heating rate of 10°C min^{-1}. For the isothermal experiments an atmosphere of 500 lbf in^{-2} static oxygen was employed and the sample (again a mass of 1 mg) was heated to the set temperature at a rate of 99°C min^{-1}. The set temperature was chosen to give an induction time of approximately 200 s.

Acceptable agreement between the results for the samples obtained using the two pieces of apparatus is shown in figure A 3.2, despite the differences in furnace geometry. The main problem was encountered during the isothermal experiments, when the poor temperature control of the DSC-700 was highlighted. For identical test conditions, the isothermal temperature attained for the samples varied by 14°C, which obviously rendered the results obtained for isothermal experiments questionable. These results illustrate that the Stanton Redcroft DSC-700 could only be used for the analysis of samples in the dynamic or scanning mode, and most certainly not in the isothermal mode.

The procedure developed by Barnes and Bell [2] was used to analyse samples that had been provided by another laboratory. For this procedure the reference sample (2.00 $\pm$ 0.05 mg) was analysed using a dynamic method, with a heating rate of 20°C min^{-1} and a flowing atmosphere of oxygen (60 cm^3 min^{-1}) at 15 lbf in^{-2}. The isothermal experiments were conducted at a temperature 40 to 50°C below the onset temperature of the reference oil during the dynamic test. For the isothermal experiments, an oxygen atmosphere at 500 lbf in^{-2} (3,500 kPa), flowing at 60 cm^3 min^{-1} was chosen. The sample was heated to the isothermal temperature at a heating rate of 100°C min^{-1}, and during the heating period the pressure increase within the cell was purged cautiously.

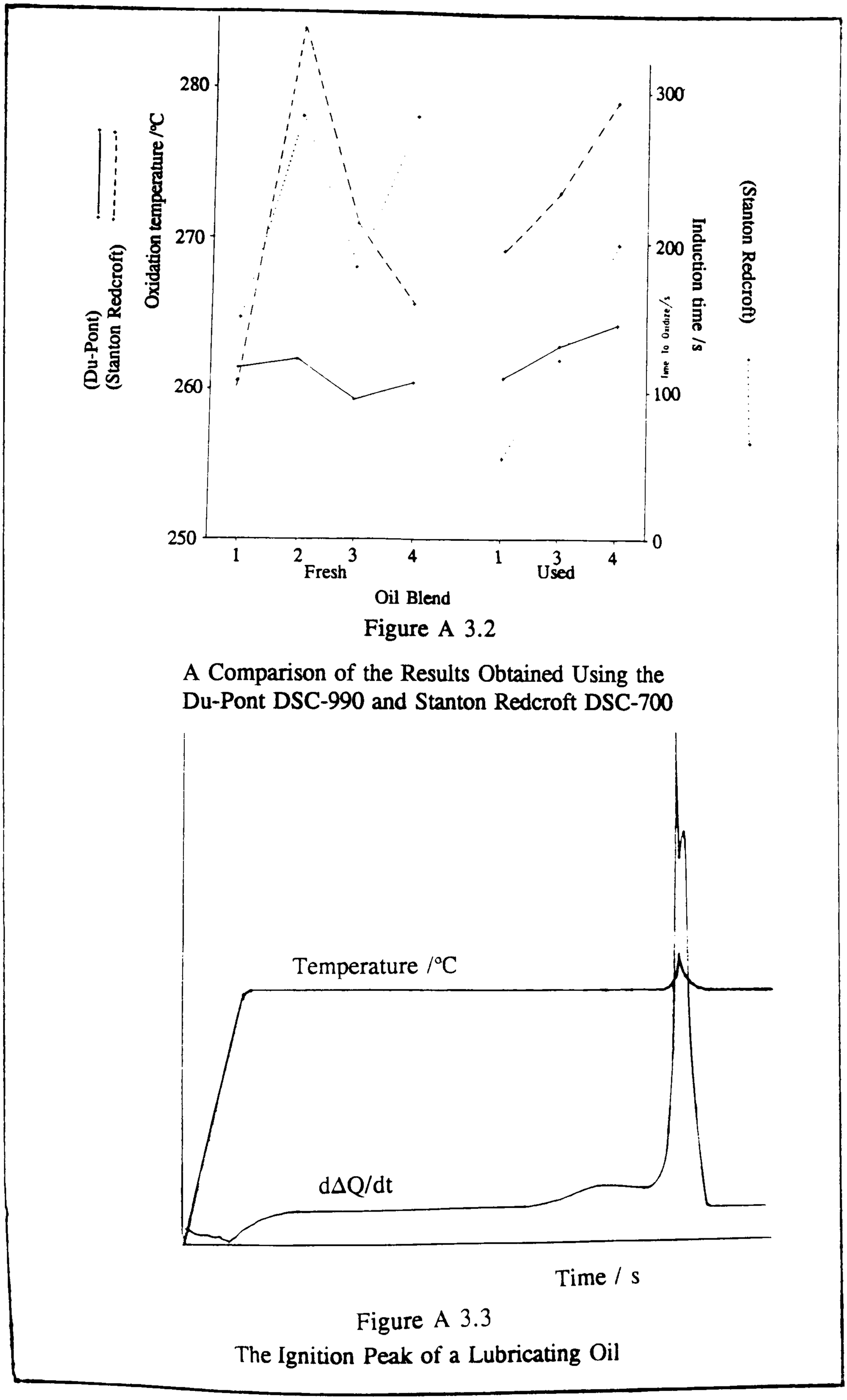

Figure A 3.2

A Comparison of the Results Obtained Using the Du-Pont DSC-990 and Stanton Redcroft DSC-700

Figure A 3.3

The Ignition Peak of a Lubricating Oil

The repeatability of the method was good, nominally ± 2 or 3%, even with samples that tended to ignite. The samples that ignited were subjected to the same experimental conditions as the other samples. Therefore if replicate analyses ignited the induction times were recorded and their ignition noted. The method provided the operator with a simple procedure to choose the isothermal temperature for sample analysis. The induction times recorded were slightly shorter than those obtained using the isothermal experiments in this thesis. This was also reflected in the tendency of some samples to ignite readily. The choice of a flowing atmosphere complicated the experimental procedure to some extent insofar that a stable gas flow had to be established and maintained. The use of a flowing atmosphere sweeps out volatile components from the cell prior to the auto-oxidation of the oil and the oxidation products during the course of the reaction. The removal of hot purge gases may be expected to reduce the sensitivity of the DSC, but it allows the access of oxygen to the oil surface leading to a faster reaction rate and therefore a stronger signal. The main disadvantage of the method is the short induction times obtained (therefore an inability to distinguish adequately between some samples) and the tendency of some samples to ignite, owing to the high temperatures employed. It was discovered that the analysis of one group of samples was impossible because the induction times were immeasurably short or non-existent. Moreover, the performance of the reference provided was incompatible with that of the samples, insofar that its induction time was much longer. To overcome this, and therefore make it possible to distinguish between samples, a temperature 65°C below the onset temperature of the reference oil was chosen for the analysis of these samples.

When a sample ignited, the sharp ignition peak was followed by a second peak (figure A 3.3). The sudden decrease in the signal prior to the second peak was thought to be due to the sample pan being blown off the sample platform by the power of the reaction or to the melting of the aluminium pans by the heat of the reaction. The peak shape was essentially the same when the sample pan was not blown off the platform. When a platinum pan was used for an ignition experiment, it did not melt in the heat caused by the reaction. Therefore it was concluded that the second peak was due to a second reaction mechanism.

REFERENCES

1. The Stanton Redcroft 780 Series Portfolio, Operations manual for the STA-781.
2. J. R. Barnes and J. C. Bell, *Lubr. Eng.*, 45, 1989, p 549.